Numerical Analysis of Surge Performances in Power Systems(Dissertation_全文)

AUTHOR(S):

Hara, Takehisa

CITATION:

Hara, Takehisa. Numerical Analysis of Surge Performances in Power Systems. 京都大学, 1972, 工学博士

ISSUE DATE:

1972-01-24

URL:

https://doi.org/10.14989/doctor.k1162

NUMERICAL ANALYSIS OF SURGE PERFORMANCES IN POWER SYSTEMS

TAKEHISA HARA

NUMERICAL ANALYSIS OF SURGE PERFORMANCES IN POWER SYSTEMS

TAKEHISA HARA

NUMERICAL ANALYSIS OF SURGE PERFORMANCES IN POWER SYSTEMS

By

TAKEHISA HARA

DEPARTMENT OF ELECTRICAL ENGINEERING

KYOTO UNIVERSITY, KYOTO, JAPAN

JUNE 1971

ABSTRACT

Surge performances on single- and multi-conductor systems have been studied theoretically and experimentally by many pioneers over about one century. The achievements of the seniors of Kyoto University in this field have been very noticeable and they have always fulfiled the leading part of this field. Whereas the new research field has spread out with the remarkable advance of the digital computer, and so the author, too, has made a great effort to analyze the surge problems by using the digital computer. This thesis is concerned with the author's research achievements, and consists of seven chapters.

In Chapter 1, as the model case of the transmission system of overhead line-submarine cable, the author picks out the 22kV Tonosho Transmission Line of the Chyugoku Electric Power Company, which has suffered the insulation breakdown fault in the submarine cables by the abnormal voltage due to the lightning stroke at the tower in 1964. First the author introduces a new digital calculation considering wave distortion on the line or cable due to skin effect for the traveling waves along the single-conductor systems and the symmetric three-conductor systems. Next he investigates numerically the problem of the transient voltage rises of the rubber and paper insulated

cable, which are used in the above-mentioned actual systems, due to the lightning stroke at the transmission line towers near the junction point of the line and cable. Then he makes sure of possibility of the insulation breakdown fault, which has been occurred on the above-mentioned cable.

Furthermore he studies on the effect of the impedance of the tower and tower foot with counterpoises, on the surges along the overhead line-cable systems.

In Chapter 2, he introduces a new digital analysis of the surge problems in power networks, which utitizes the computation principle of the low speed electronic surge analyzer. Hitherto the digital analysis of the traveling waves in the networks, which have many transition points containing the lumped inductance and capacitance, has been very difficult. However it is made possible that we can easily calculate the refracted and reflected voltages at the transition points by using the above-mentioned analyzing method. Accordingly we can calculate the required transient voltage at a specified point in the network, approximately but with high accuracy.

In Chapter 3, the above-mentioned new method is applied to the analysis of the surge performances on the four examples of practical systems. Namely the surge performances on a overhead distribution system having distributed pole transformers, a transmission system whose overhead ground wire is struck by lightning, a overhead line-cable system which has been discussed in Chapter 1 and a overhead line-cable system with whose junction point a lightning arrester is fitted up, are analyzed.

Then the author shows that his method can be applied simply, and usefully to these examples.

In Chapter 4 he tries the numerical analysis of the nonlinear surge equations including the effect of corona losses for traveling waves on single-conductor systems. He proposes two methods (Methods 1 and 2) of numerical calculation, which are obtained by piecewise linearizing the nonlinear surge equations and each of which is employed to facilitate comparison with the experimental results made on an artificial transmission line by other researchers. From the numerical investigations by these methods he estimates the optimum values of corona loss constants of traveling waves.

In Chapter 5 the author originated the other numerical calculating method (Method 3), which can digitally solve the original nonlinear equations without piecewise linearization, and by using Method 3, he solves the same problems as in the preceding chapter, and again he estimates the optimum values of corona loss constants and corrects the ones obtained by Method 1 or 2. And by the numerical calculation using these values he shows that the results agree with the experimental ones fairly well. Next he compares the Methods 1, 2 and 3, and shows that Methods 3 is the best among these methods.

In Chapter 6, the author applies the numerical calculation of the line equations for the single-conductor systems to the ones for the two-conductor systems as one example of the multiconductor systems. Namely by Method 3 he analyzes the surges along the two-conductor system with the aid of the values of

the corona loss constants, that have been obtained in Chapter 5 for the single-conductor systems. Next he compares the computed results with the experimental ones under the various sending end and final end conditions.

Lastly in Chapter 7, he summarizes the main results of his investigation in Chapter 1 to 6.

ACKNOWLEDGMENTS

This doctoral thesis has been studied under the guidance of Professor Dr. Juro Umoto of Kyoto University. The author thanks him from the bottom of his heart for his kind guidance and encouragements that enable the author to complete the work. He also critically read the manuscript of the thesis and gave accurate comments which were sincerely appreciated.

The author is also very much indebted to the staffs of Professor J. Umoto's Laboratory, especially Assistant Tsuguo Ando and graduate student Mr. Koji Fukumori for their valuable discussions and excellent cooperation.

The author wishes to express his thanks to Emetitus Professor Dr. Shigenori Hayashi, Professor Dr. Masaya Yamaguchi of Kyoto University and Mr. Eishi Nakamura of Sumitomo Electric Works for discussions and criticism concerning the work of Chapters 4 and 5.

Last, but not least, the author must thank to Miss Junko Tomita, the Secretary of Professor J. Umoto, for her self-sacrificing efforts in typing the entire manuscript. Without her devoted help, this work would have been unable to be completed.

CONTENTS

CHAPTER 1

NUMERICAL ANALYSIS OF SURGES ON TRANSMISSION SYSTEMS OF OVERHEAD LINE-CABLE CONSIDERING THE DISTORTION DUE TO SKIN EFFECT

1.1 Introduction

For the lightning-proof design of transmission systems consisting of overhead lines and cables, it is one of the very important problems to investigate the abnormal surge voltages, which appears on the overhead line or on the cable, by analyzing propagation, reflection and refraction of traveling waves on the transmission line systems containing cable. As such systems, we can think of the transmission line consisting of overhead line-submarine cable, the system containing the incoming cable in the power station or the substation, which is connected with the line, and so on.

The surge performances on the system containing the incoming cable in the power station or the substation have been analyzed by means of the surge computing boards[1],[2] or the

electronic surge simulators[1] and recently the digital computer.[4] Though the analyses by the surge computing board or the simulator have many merits, they have the demerits that the values of the system constants cannot be changed simply, the computation results are not so accurate, etc. Moreover, in digital computer analyses up to now, the influence of skin effect on surge distortion has been neglected or considered only approximately. Thus in this chapter, as the model case of the transmission system of overhead line-submarine cable,[5] the author picks out the 22kV Tonosho Transmission Line of the Chyugoku Electric Power Company, which has suffered the insulation breakdown fault in the submarine cables by the abnormal voltage due to the lightning stroke at the tower in 1964. The insulation test of this system and the investigation of the results of the test have been done by the researching staffs of the Chyugoku Electric Power Company.[6] However, they have done only the rough approximate analysis of the surge performances on the system and have not obtained the satisfactory results. Therefore, first the author introduces a new digital calculation[7],[8] considering wave distortion on the line or cable due to skin effect for the traveling waves along the single-conductor systems and the symmetric three-conductor systems. Next he investigates numerically the problem of the transient voltage rises of the rubber and paper insulated cable, which are used in the above-mentioned actual systems, due to the lightning stroke at the transmission line towers near the junction point of the line and cable. Then he discusses the influences of

skin effect, line length or cable length on the transient voltage rises of the cables and the difference of the voltage rises between rubber and paper insulated cable, and moreover he makes sure of possibility of the insulation breakdown fault, which has been occurred on the above-mentioned cable.

Next, he studies on the effect of the tower foot impedance with counterpoises, which are often used for the purpose of decreasing the grounding resistance of the tower to prevent the insulators at the tower from the back flashover due to lightning stroke, and the tower impedance, on the surges along the overhead line-cable system. Namely, he performs the digital analyses of the voltage rises of the cables due to the lightning stroke against the towers by the use of the equivalent circuit of the tower[9],[10] considering the tower impedance and the tower foot impedance containing counterpoise, and he gives the many available data for the lightning proof design of transmission systems of the overhead line-cable.

1.2 Numerical Calculation of Surge Distortion by Skin Effect

When the impulse voltage is impressed on the beginning end of a semi-infinite line, the approximate operational solution[11] of the line voltage considering the wave front distortion by the skin effect of the line conductor and the ground return is given by

$$V(p) = \varepsilon^{-\frac{x}{g}p}\ \varepsilon^{-\sigma x\sqrt{p}}\ E(p), \tag{1.1}$$

where

$$\left.\begin{aligned}
&E(p) = \mathcal{L}\{e(t)\} \text{ : input impulse voltage,}\\
&V(p) = \mathcal{L}\{v(t)\} \text{ : line voltage at distant } x \text{ from initial point,}\\
&\sigma = (\alpha+\beta)/2z \text{ : distortion constant } (\sqrt{s}/m),\\
&\alpha = \sqrt{(\mu\rho/\pi)10^{-9}}/r \quad (\Omega\sqrt{s}/m),\\
&\beta = \sqrt{(2\mu_g\rho_g/\pi)10^{-9}}/h \quad (\Omega\sqrt{s}/m),\\
&z \text{ : surge impedance } (\Omega),\\
&g \text{ : surge propagation velocity } (m/s),\\
&\mu \text{ : relative permeability of conductor,}\\
&\mu_g \text{ : relative permeability of ground,}
\end{aligned}\right\} \tag{1.2}$$

ρ : intrinsic resistance of conductor (Ωm),

ρ_g : intrinsic resistance of ground (Ωm),

r : conductor radius (m),

h : conductor hight (m),

The t-function of Eq. (1.1) is

$$v(t) = e(t) \circledast erfc\left(\frac{\sigma x}{2\sqrt{t}}\right) \circledast H(t - x/g) \,, \tag{1.3}$$

where the symbol $\circledast$ represents the convolution integral and

$$H(t - x/g) = \begin{cases} 0 \,, & t \le x/g \,, \\ 1 \,, & t > x/g \,, \end{cases} \quad : \text{unit function} \tag{1.4}$$

$$erfc(\xi) = 1 - \frac{2}{\pi}\int_0^{\xi} \varepsilon^{-u^2} du \,. \quad : \text{conplementary error function} \tag{1.5}$$

The integral form of Eq. (1.3) is expressed as follows:

$$v(t) = H(t - x/g)\int_{x/g}^{t} e(t-\tau)\left\{\frac{d}{d\tau}\, erfc\left(\frac{\sigma x}{2\sqrt{\tau - x/g}}\right)\right\} d\tau \,, \tag{1.6}$$

Here we give the applied impulse voltage by the following form

$$e(t) = E_0\, \varepsilon^{-a_0 t} \,, \tag{1.7}$$

Putting Eq. (1.7) into Eq. (1.6) yields

$$v(t) = H(t - x/g)E_0 \frac{\sigma x}{2\sqrt{\pi}} \int_0^{t-x/g} F(\tau')\,d\tau', \tag{1.8}$$

where

$$\left.\begin{aligned} \tau' &= \tau - x/g \ , \\ F(\tau') &= \tau'^{-\frac{3}{2}} \varepsilon^{-\frac{(\sigma x)^2}{4\tau'} - a_0(t - x/g - \tau')} \end{aligned}\right\} \tag{1.9}$$

With respect to σx which is used practically in this chapter, $(\sigma x)^2 \geqq 10^{-9}$, and in such case $F(\tau')$ in Eq. (1.9) satisfies the next equation

$$\int_0^{10^{-11}} F(\tau')\,d\tau' \simeq 0 \ , \tag{1.10}$$

where the upper limit 10^{-11} is decided from the graph of $F(\tau')$ which is shown in Fig. 1.1.

$$v(t) = H(t - x/g)E_0 \frac{\sigma x}{2\sqrt{\pi}} \int_{10^{-11}}^{t-x/g} F(\tau')\,d\tau', \tag{1.11}$$

The value of the voltage $v(t)$ at an arbitrary time t can be obtained by calculating the definite integral given in Eq. (1.11). However since the Simpson integral formula, which is

fast and accurate for digital computation, devides equally the integral region, the formula is not appropriate for the numerical integration of $F(\tau')$ which is shown in Fig. 1.1. Therefore let us consider the next transformation

$$\tau' = 10^{\tau''}, \qquad d\tau' = \log 10 \cdot 10^{\tau''} d\tau'', \tag{1.12}$$

then Eq. (1.11) becomes

$$v(t) = H(t - x/g) E_0 \log 10 \frac{\sigma x}{2\sqrt{\pi}} \int_{-11}^{\log_{10}(t-x/g)} F(10^{\tau''}) 10^{\tau''} d\tau''. \tag{1.13}$$

To the digital computation of Eq. (1.13), we can apply the Simpson integral formula and determine numerically the value of $v(t)$.

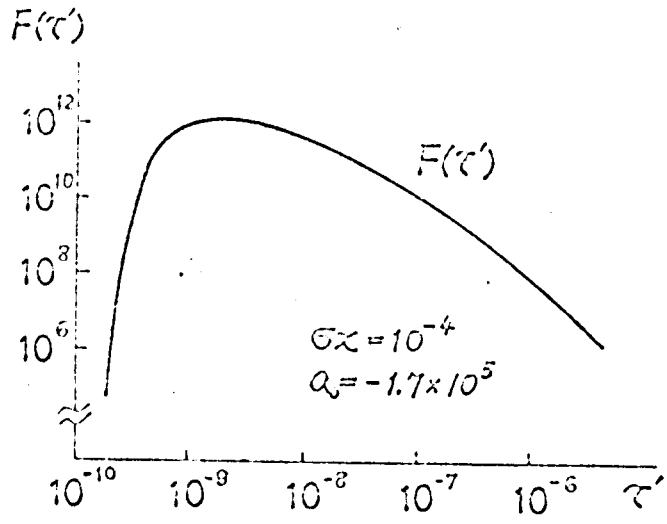

Fig. 1.1 Graph of $F(\tau')$.

1.3 Numerical Analysis of Surges on Transmission Systems of Overhead Line-Cable

1.3.1 Numerical Calculation for Single-Conductor Systems

In Fig. 1.2 the author shows the model system which has been chosen as the subject of the study. In this section he intends to analyze the transient voltage rises of the both ends of the cable shown in Fig. 1.2 considering the successive refraction and reflection of surges on overhead line and cable in the case where it is assumed that the lightning strikes at the tower near the junction point of overhead line and cable and then immediately the back flashover along the insulator chain occurs. In Fig. 1.2

l_1 and l_2 : lengths of overhead line and cable,

g_1 and g_2 : surge propagation velocities on overhead line and cable,

σ_1 and σ_2 : distortion constants of overhead line and cable,

z_1 and z_2 : surge impedances of overhead line and cable,

Z_0 : stroke channel impedance,

R_G : grounding resistance of tower.

Next if we assume that the wave form of the lightning stroke current is expressed by the following form

$$i(t) = I_0 \varepsilon^{-a_0 t} \quad , \tag{1.14}$$

the wave form of the voltage which penetrates into overhead line is given by

$$e(t) = Z\, i(t) = \frac{\mathfrak{z}_1 R_G}{\mathfrak{z}_1 + 2R_G} I_0 \varepsilon^{-a_0 t} \quad , \tag{1.15}$$

where Z is the input impedance of the transmission system viewed from the lightning stroke point.

Next the reflection coefficients F_{I1}, F_{I2}, F_{I3} and F_{I4} and the refraction coefficients F_{r1}, F_{r2}, F_{r3} and F_{r4} at the tower and both ends of the cable of Fig. 1.2 are given by the following equations

$$\left.\begin{aligned}
F_{r1} &= \frac{2Z_0 R_G}{\mathfrak{z}_1 Z_0 + (\mathfrak{z}_1 + 2Z_0) R_G} \quad , \\
F_{I1} &= F_{r1} - 1 \quad , \\
F_{r2} &= \frac{2\mathfrak{z}_2}{\mathfrak{z}_1 + \mathfrak{z}_2} \quad , \\
F_{I2} &= F_{r2} - 1 \quad , \\
F_{r3} &= F_{r4} = \frac{2\mathfrak{z}_1}{\mathfrak{z}_1 + \mathfrak{z}_2} \quad , \\
F_{I3} &= F_{I4} = F_{r3} - 1 \quad .
\end{aligned}\right\} \tag{1.16}$$

Until now the lattice diagram method is usually used for the numerical calculation of successive reflection and refraction of surges. This method has the merit that its calculation process is simple and easy to understand intuitively, but on the other hand it has the demerit that the calculation with figures is very troublesome. Here we apply the lattice diagram method to the digital calculation and enable the calculation of the surge distortion due to the skin effect.

The author's digital calculating method is given below. First by the number whose element in each figure is composed of 1 or 2, let us express all the waves, which start from the lightning stroke point and arrive at the beginning end of the cable after passing through the various pathes. And we make the figure whose element is 1 correspond to the wave which once goes and comes back along the overhead line section from the beginning end of the cable, and the figure whose element is 2 corresponds to the wave which goes and comes back along the cable. For example, the number 121 represents the wave which starts from the lightning stroke point, arrives at the beginning end of the cable, once goes and comes back along the overhead line section, once goes and comes back along the cable, again goes and comes back along overhead line section and lastly arrives at the beginning end of the cable.

Now let us consider the wave which is expressed by the number composed of n_1-1's and n_2-2's. The voltage of our wave is expressed by the following equation,

$$v(t) = F Z\, i(t) \otimes \operatorname{erfc}\left(\frac{S}{2\sqrt{t}}\right) \otimes H(t-T)\,, \tag{1.17}$$

where

$$\left.\begin{aligned} S &= (2n_1+1)\sigma_1 l_1 + 2n_2\sigma_2 l_2\,, \\ T &= (2n_1+1) l_1/g_1 + 2n_2 l_2/g_2\,, \end{aligned}\right\} \tag{1.18}$$

F is the product of the reflection and refraction coefficients at every transition point, at which our wave reflects or refracts, where the refraction coefficients contain the one corresponding to the last refraction at the beginning end of the cable.

We can obtain the value of $v(t)$ in Eq. (1.17) at an arbitrary time t by evaluating the convolution integral with the method, which has been described in the preceding section. And so we can get the value of the transient voltage at the beginning end of the cable by performing the above mentioned digital calculation about all waves which arrive at that end. Moreover the value of the voltage at the final end of the cable or at the lightning stroke point can be obtained by the same procedure after correcting Eq.s (1.18) a little. The digital flow chart used in our calculation is shown in Fig. 1.3.

1.3.2 Numerical Calculation for Symmetrical Three-Conductor Systems

In this article we will consider the case where the lightning strikes at the tower and then instantly the three-phase back flashover along the insulator chain occurs. If it is assumed that the model system is the symmetrical three-conductor systems for simplicity, we can carry out the surge calculation by the method described in the preceding article, where the zero-phase-sequence surge inpedance of the system must be used instead of the surge impedance of the single line used in the preceding article.

Namely in the similar manner to the preceding article, the voltage wave, which is expressed by the number consisting of n_1-1's and n_2-2's, is given by the following equation.

$$[v(t)] = F_0 Z_{10}\, i(t) \otimes \operatorname{erfc}\left(\frac{S_0}{2\sqrt{t-T}}\right) H(t-T) \begin{bmatrix} 1 \\ 1 \\ 1 \end{bmatrix}, \qquad (1.19)$$

where

$$\begin{aligned} S_0 &= (2n_1+1)\sigma_{10} l_1 + 2n_2 \sigma_{20} l_2 , \\ T &= (2n_1+1) l_1/g_1 + 2n_2 l_2/g_2 , \end{aligned}$$

σ_{10} : zero-phase-sequence component of distortion constant of overhead line,

σ_{20} : zero-phase-sequence component of distortion constant of cable, (1.20)

Z_{l0} : zero-phase-sequence component of input impedance,

F_0 : product of zero-phase-sequence component of reflection and refraction coefficients at every transition point.

Using Eq. (1.19) we can obtain the values of the voltages of both end of the cable in the case of three-phase back flashover.

1.3.3 Calculated Results and Discussions

The model system, which is chosen as the object of the study, is the overhead line-submarine cable system of the Tonosho Transmission Line of the Chyugoku Electric Power Company. In practice it is the 22kV double circuits of three-phase transmission system and *provided with* the three-core rubber and paper insulated cable for the submarine cable and so in order to investigate the system regorously we must treat it as a six-conductor system. However such a treatment makes the calculation complicate and we are apt to miss the general situation. Therefore in this article first we perform the digital calculation to see the rough influence of skin effect

on the surge distortion by assuming that the model system is a single-conductor one. Next assuming that it is symmetrical three-conductor systems, we carry out the digital calculation for the case that the three-phase back flashover occurs at the tower struck by lightning.

(1) Single conductor system:

Table 1.1 shows the values of the system constants used in calculation. These values are quoted from the Reference (6). For the wave form of the lightning stroke current we pick out the $0 \times 40\,\mu s$ wave and assume that the crest value is 1, since our system is a linear one. Namely

$$i(t) = I_0 \varepsilon^{-a_0 t} = 1 \cdot \varepsilon^{-1.733 \times 10^{4} t} \quad . \tag{1.21}$$

Fig.s 1.4(a) and 1.5 show the calculated transient voltage at the beginning and final ends of the rubber insulated cable. In Fig.s 1.6 and 1.7 are plotted those of the paper insulated cable. In these figures, in order to facilitate comparison the transient voltage in the case that the skin effect is not considered are also drawn. In order to coinside the calculating condition with the practical one, we choose the lengthes of the overhead line section, rubber and paper insulated cables $75m$, $1739m$ and $1794m$ respectively.

Fig. 1.4(b) shows the magnified forms of the transient voltages of Fig. 1.4(a) from 0 to $10\,\mu s$ and from this figure we can see the influence of the skin effect on the voltage wave

form, namely it makes its appearance in the roundish step of the voltage wave form and the gradual reduction of the value of each step voltage. Moreover in Fig.s 1.4 to 1.7, the voltage wave forms in the case considering skin effect change more smoothly compared with the ones in the case of no loss line, which change violently and notchy.

The values of the maximum voltages of the rubber insulated cable in the case considering skin effect are about 76% and 79% of the ones in the case no considering that at the beginning and final ends respectively. And in the case of the paper insulated cable, those are about 88% and 94% at the beginning and final ends respectively. As above described the voltage wave forms and maximum values fairly differ from each other in the two cases where the skin effect is considered and not considered. Since the distortion constant of the paper insulated cable is fairly small compared with the one of the rubber insulated cable, it is thought to be natural that the maximum values of the voltages in the former are higher than the ones of the latter.

(ii) Symmetrical three-conductor system:

Here we assume that the model system given in the preceding article is a symmetrical three-conductor system and the three-phase back flashover occurs along the insulator chain as soon as the lightning strikes at the tower. In Reference (6) it is indicated that the three-phase back flashover fault may be concluded to have occurred in the Tonosho Line by supposing the breakdown situation of the insulator chain. Therefore the

calculated results in this term (11) are considered to be able to explain the practical surge performances fairly well.

In this connection we use the digital calculation introduced in Article 1.3.2 the values of constants of the overhead line, rubber and paper insulated cables used in the computation are shown in Table 1.2, which are also quoted from the Reference (6), where the self- and mutual-impedance of the overhead line are calculated from the situation of the lines. We give the wave form of the lightning stroke current by Eq. (1.21) in the same manner as the case of single-conductor system.

The computed voltage wave forms at the beginning and final end of the rubber insulated cable are shown in Fig. 1.8 and those of the paper insulated cable are plotted in Fig. 1.9. The voltage wave form in the case of three-phase back flashover is fairly different from that in the case of the back flashover in single-conductor system.

Reference (6) shows that the insulation breakdown has occurred within the rubber insulated cable and the insulator chain of the neighboring tower of the final end of the paper insulated cable is broken. According to our calculated results the maximum voltages of the final ends of the two cables become higher than that of those beginning ends and $V_{max}/I_o = 10.6$ for rubber insulated cable and $V_{max}/I_o = 15.0$ for the paper insulated cable. The 50% flashover voltage of the chain of two insulators, which is practically used, is 255kV, and so the value of I_o which makes the tower voltage exceed the flashover voltage in the case of $R_G = 15\Omega$ is about 17kA. And in the case

of I_o = 17kA the maximum voltage of the rubber insulated cable reaches 17 × 10.6 = 180kV and that of paper insulated cable reaches 17 × 15.0 = 255kV. In Reference (6) it is guessed that the impulsive breakdown voltage of the rubber insulated cable becomes about 175kV. Consequently it may be thought to be natural that the insulation breakdown has occurred in the rubber insulated cable and that the flashover has occurred at the neighboring tower of the final end of the paper insulated cable before the insulation breakdown would occur in the paper insulated cable because the insulating strength of this cable was fairly strong. The above stated consideration is considered to explain the practical surge phenomena fairly well.

(iii) The maximum voltage rises:

In the foregoing term the calculation has been executed in the case of l_1 = 75m and l_2 = 1739 or 1794m in order to calculate under the same conditions as the practical ones. Here we will investigate how the maximum voltage of the model system varies when the overhead line or cable length varies. As the final end voltages of both cables become higher than the beginning end ones, we obtain the maximum voltages at the final ends of both cables. Fig.s 1.10 and 1.11 show a series of the calculated values of the maximum voltages of the rubber and paper insulated cables respectively. From the figures we can see the rough tendency that the shorter the overhead line or cable length become, the higher the maximum voltage rises and vice versa. Moreover these results are considered to give the useful data for the lightning proof design of overhead-submarine cable system.

Table 1.1 Values of system constants used in computations.

(Single-conductor systems)

		Overhead line	Rubber insulated cable	Paper insulated cable
Surge impedance	Z (Ω)	538	50.6	58.0
Distortion constant	σ ($\sqrt{s/m}$)	1.64×10^{-7}	4.48×10^{-7}	0.745×10^{-7}
Surge propagation velocity	g (m/s)	300×10^{6}	160×10^{6}	130×10^{6}
Stroke channel impedance	Z_0 (Ω)	400		
Grounding resistance of tower	R_G (Ω)	15		

Table 1.2 Values of system constants used in computations.

(Symmetric three-conductor systems)

	Overhead line	Rubber insulated cable	Paper insulated cable
Zero-phase surge impedane $Z_0(\Omega)$	280	20.0	43.7
Zero-phase distortion constant $\sigma_0(\sqrt{s}/m)$	2.68×10^{-7}	7.24×10^{-7}	1.70×10^{-7}
Surge propagation verocity v (m/s)	300×10^6	160×10^6	130×10^6

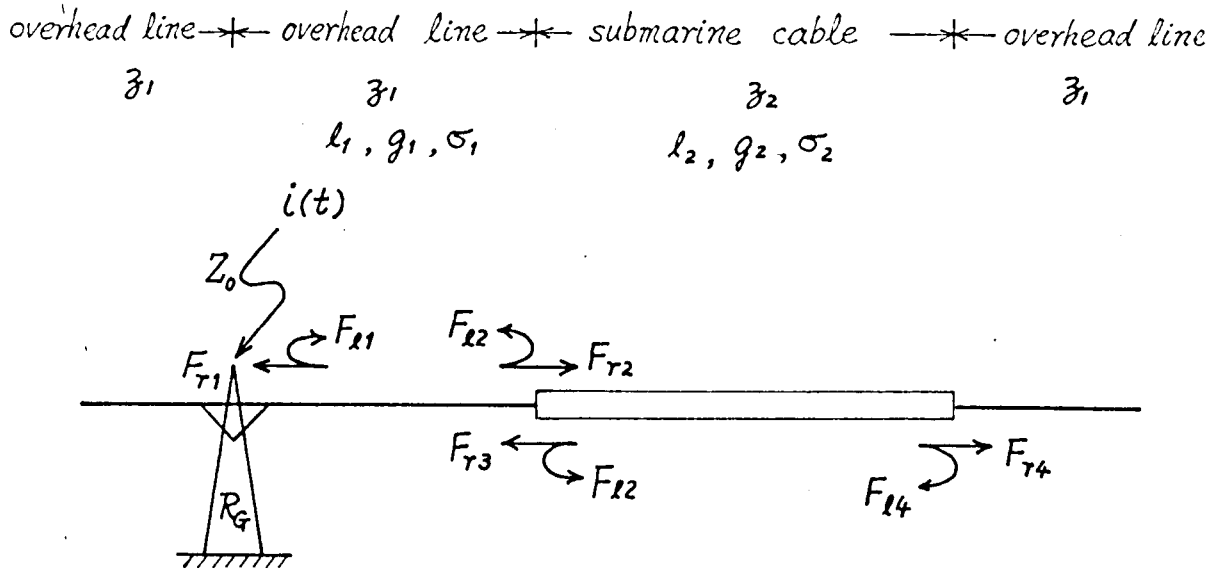

Fig. 1.2 A transmission system of overhead line-submarine cable.

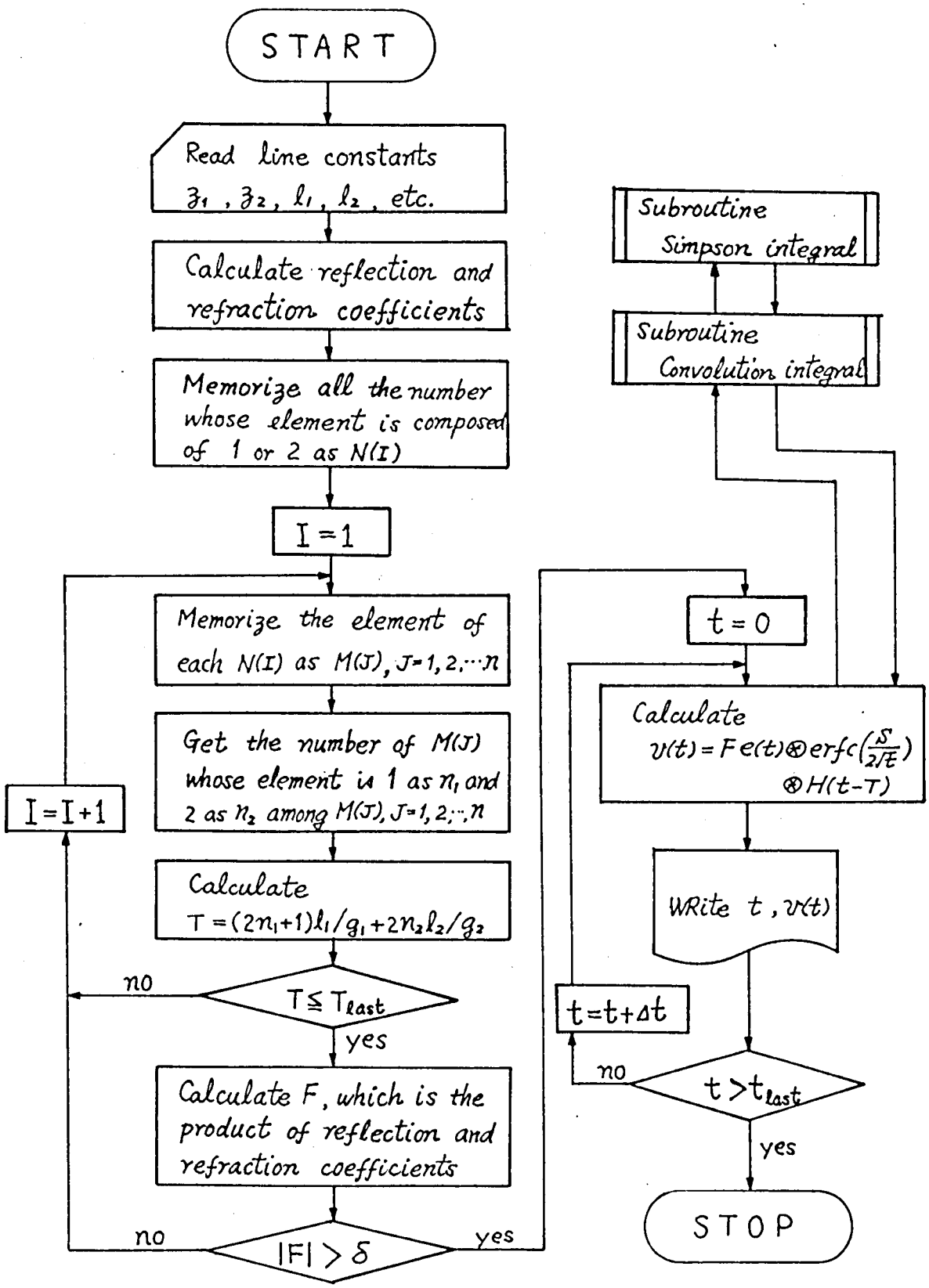

Fig. 1.3 Digital computer flow-chart.

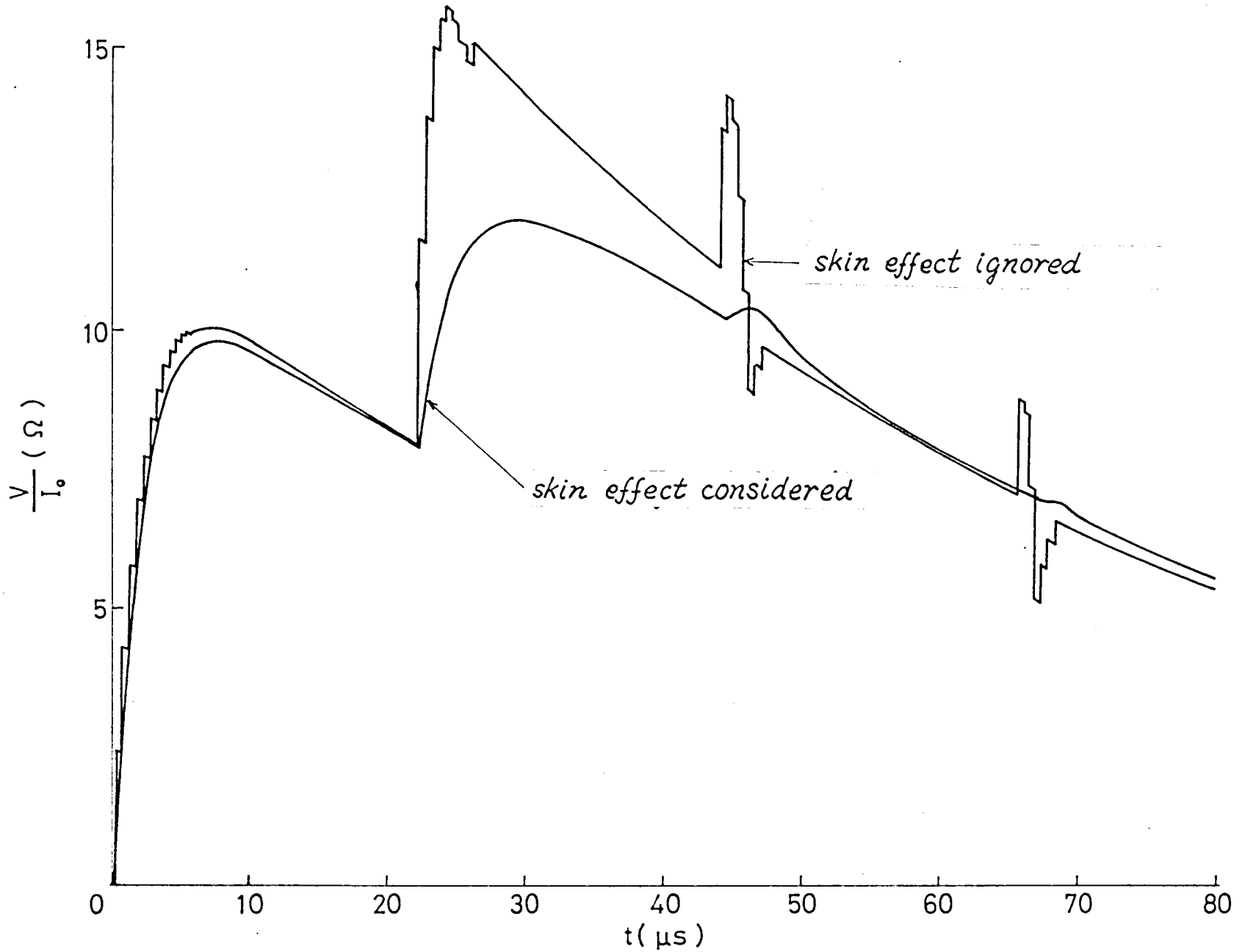

Fig. 1.4(a) Transient voltages at beginning end of rubber insulated cable.

(Single-conductor systems)

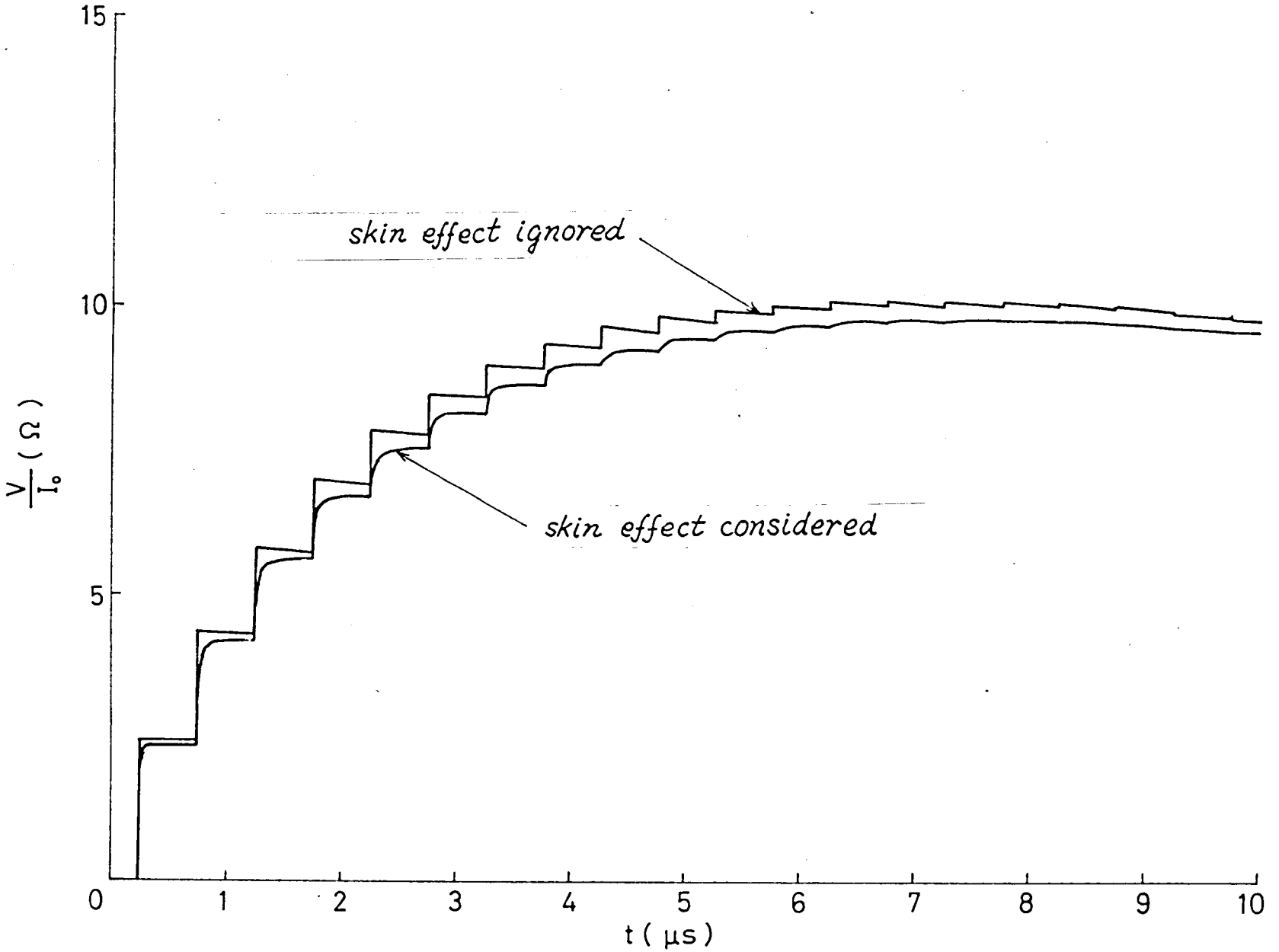

Fig. 1.4(b) Transient voltages at beginning end of rubber insulated cable.

(Single-conductor systems)

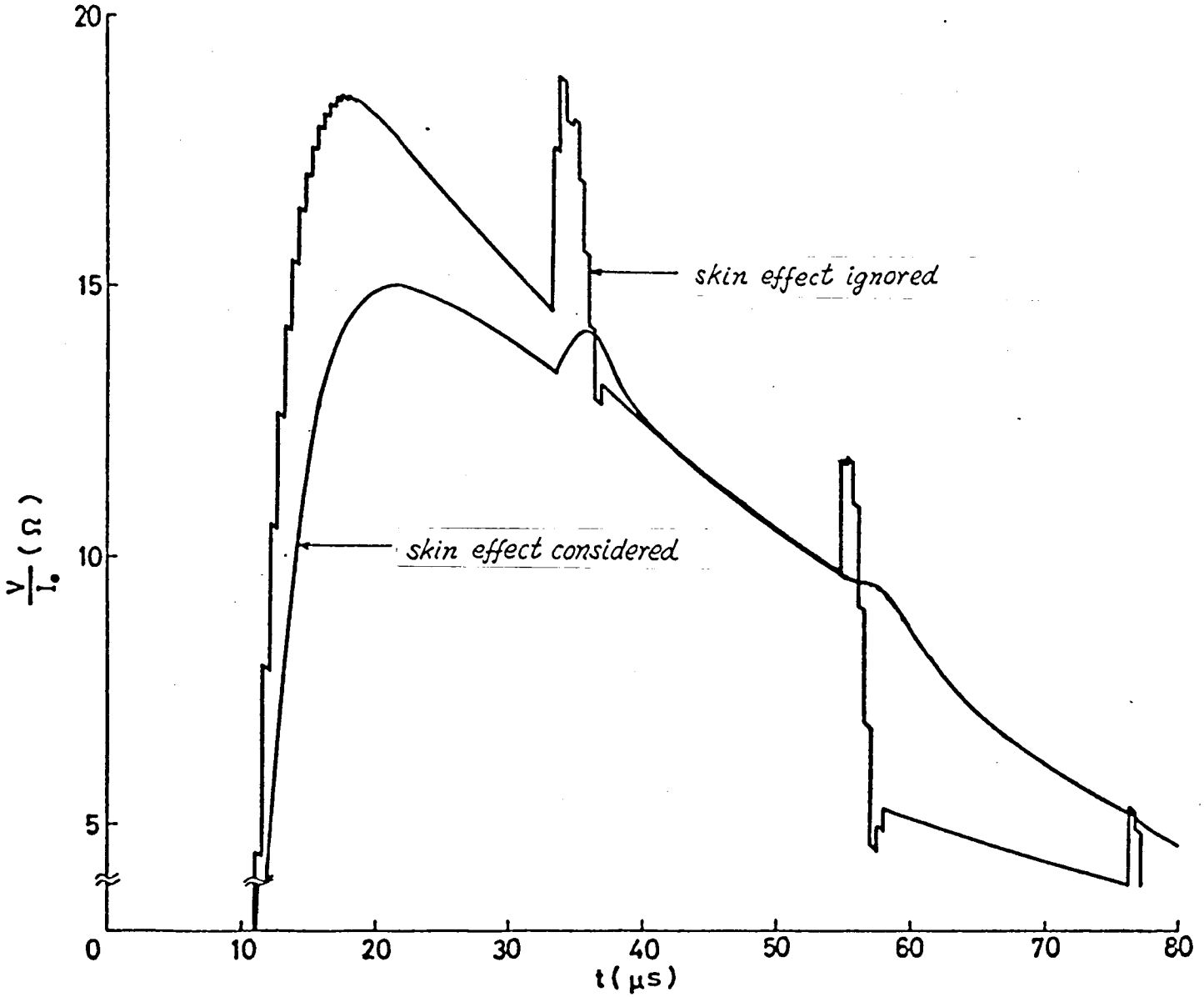

Fig. 1.5 Transient voltages at final end of rubber insulated cable.
(Single-conductor systems)

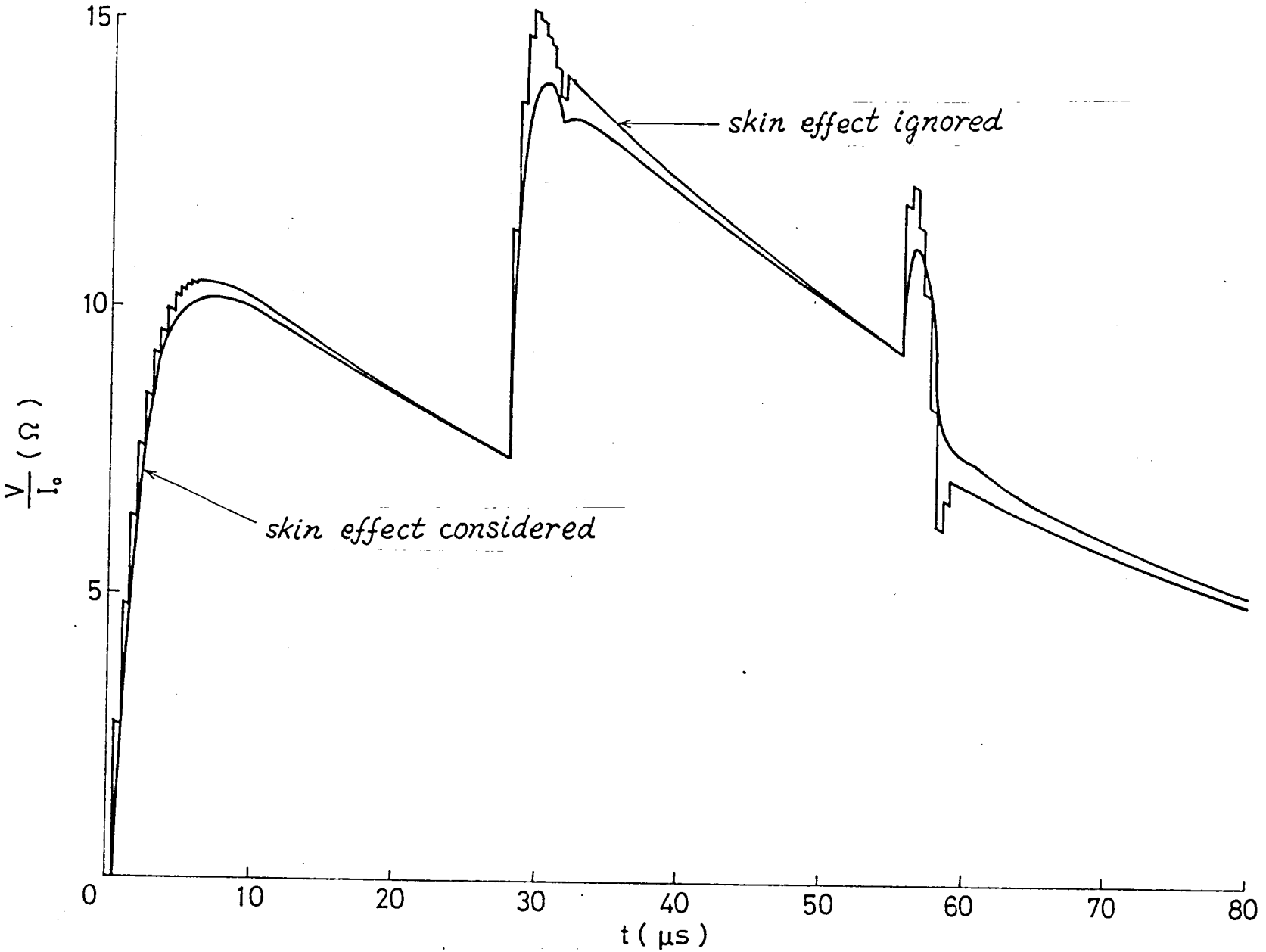

Fig. 1.6 Transient voltages at beginning end of paper insulated cable.

(Single-conductor systems)

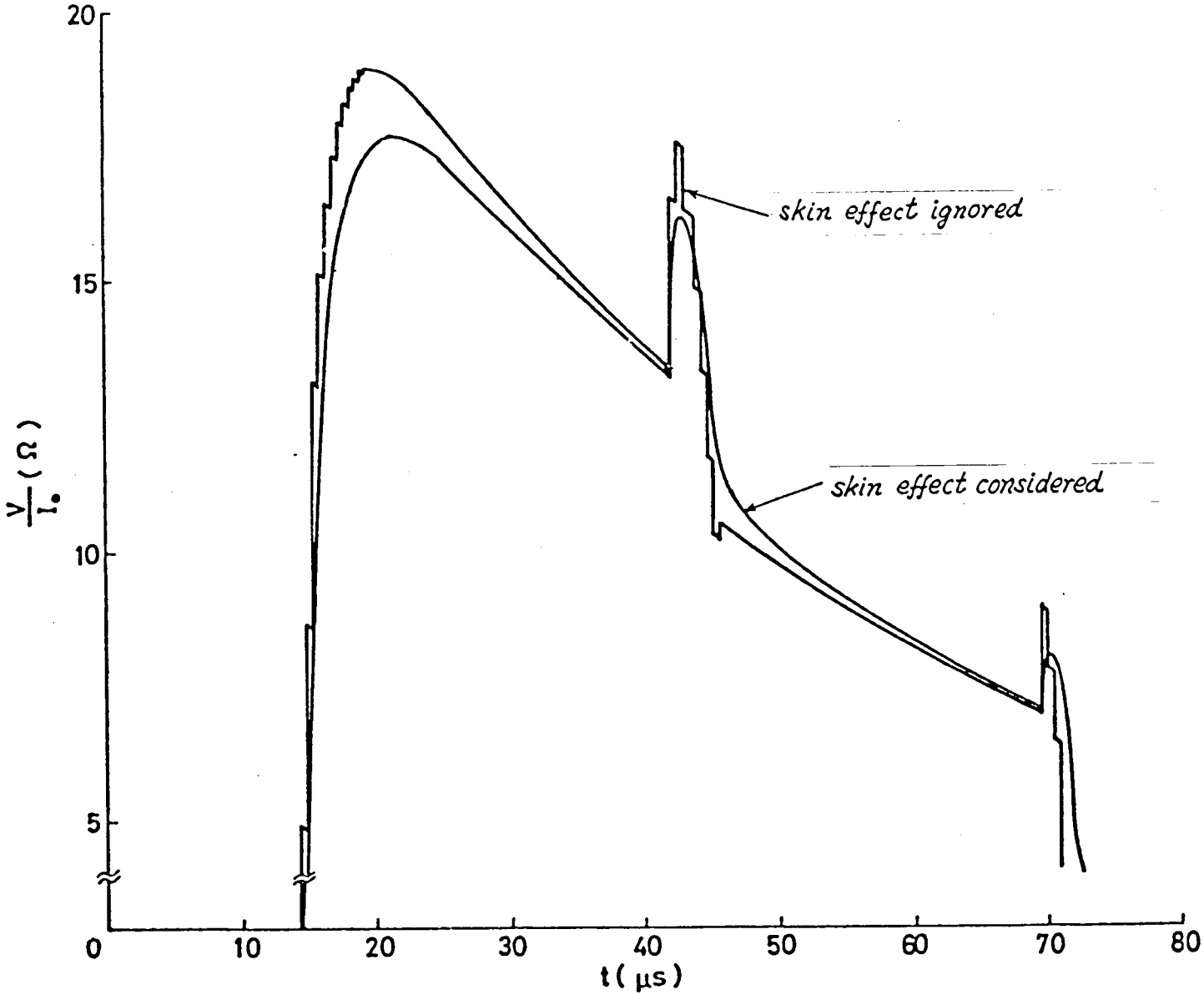

Fig. 1.7 Transient voltages at final end of paper insulated cable.
(Single-conductor systems)

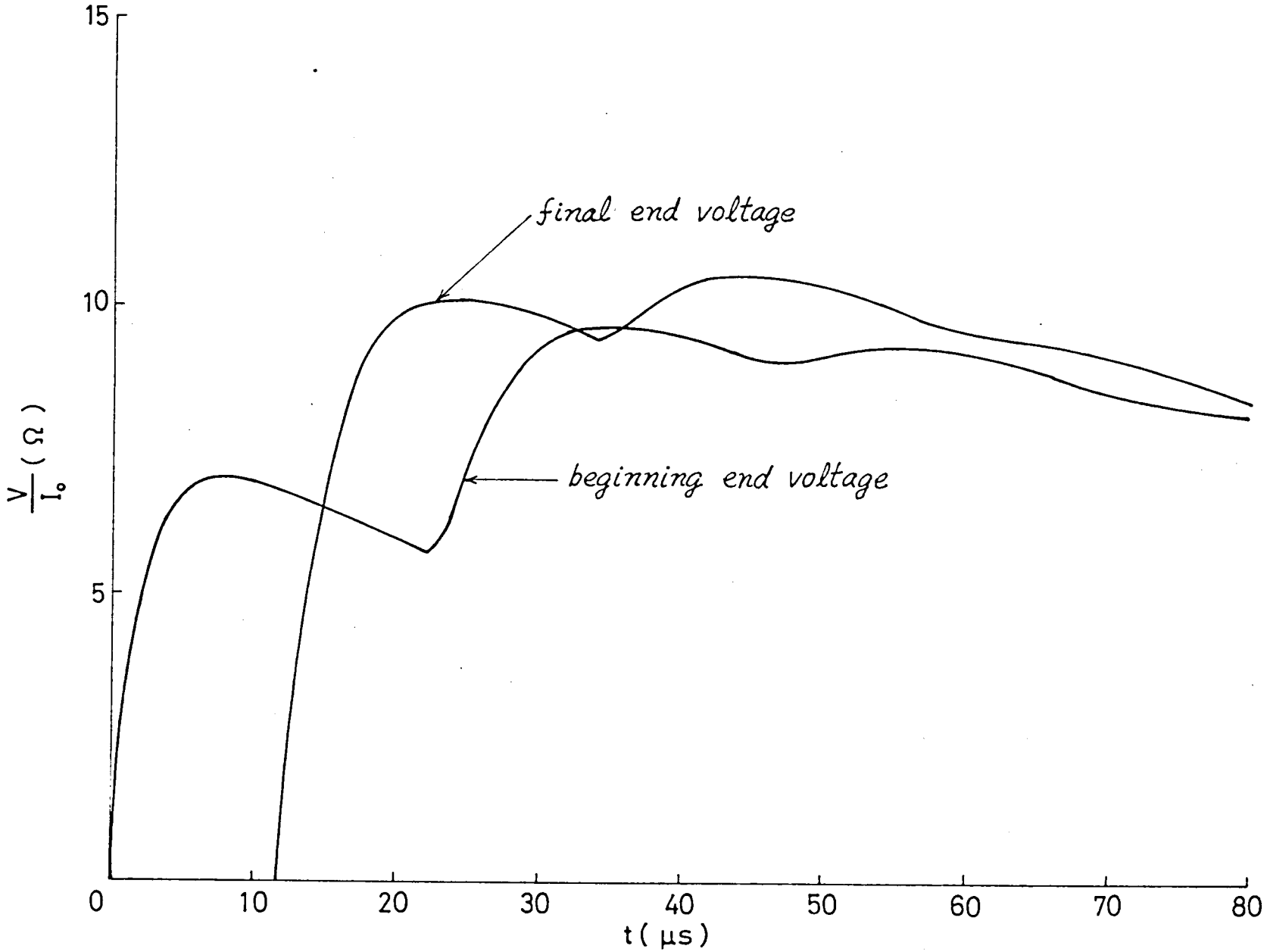

Fig. 1.8 Transient voltages at beginning and final ends of rubber insulated cable.
(Symmetric three-conductor systems)

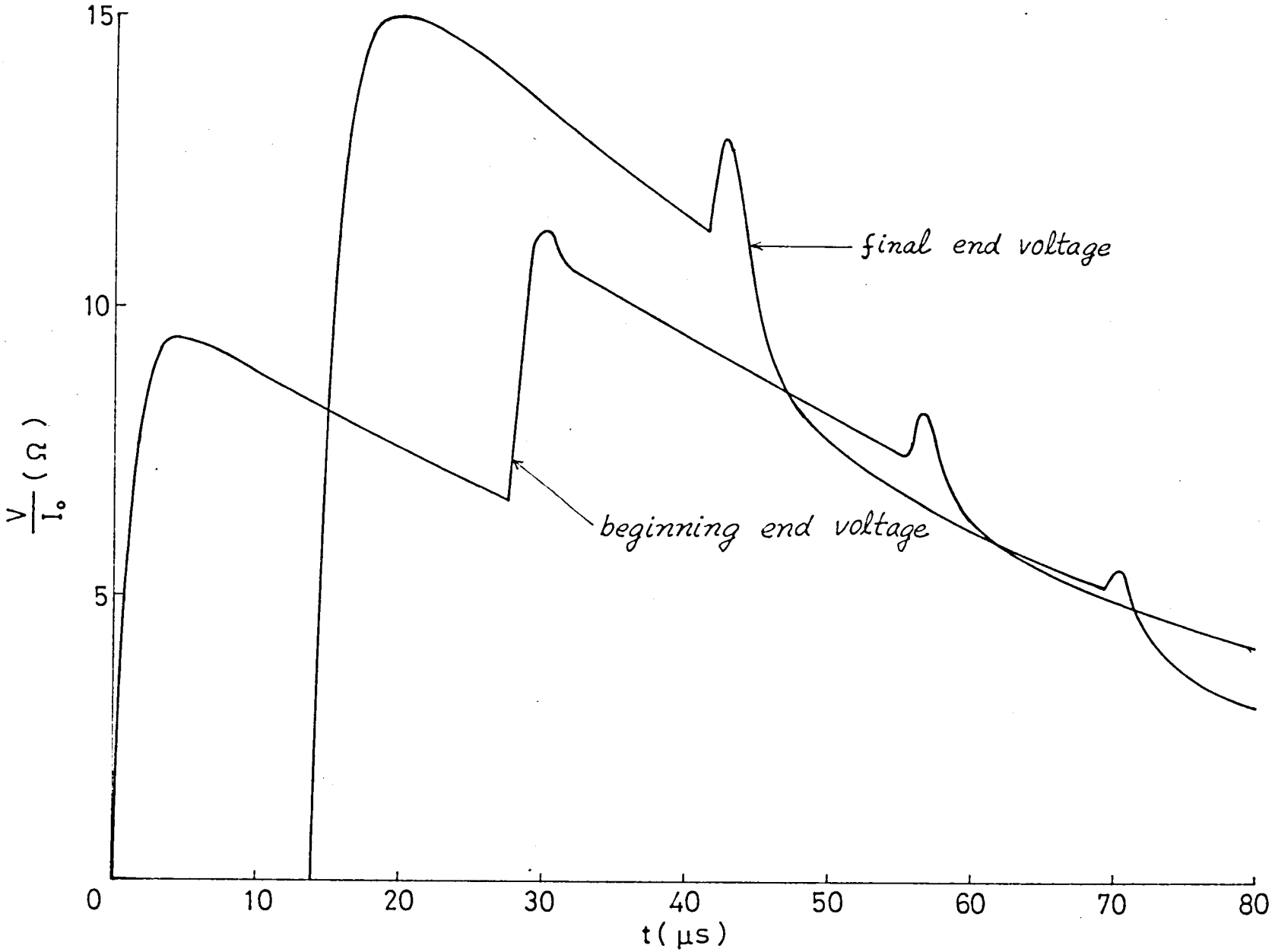

Fig. 1.9 Transient voltages at beginning and final ends of paper insulated cable.
(Symmetric three-conductor systems)

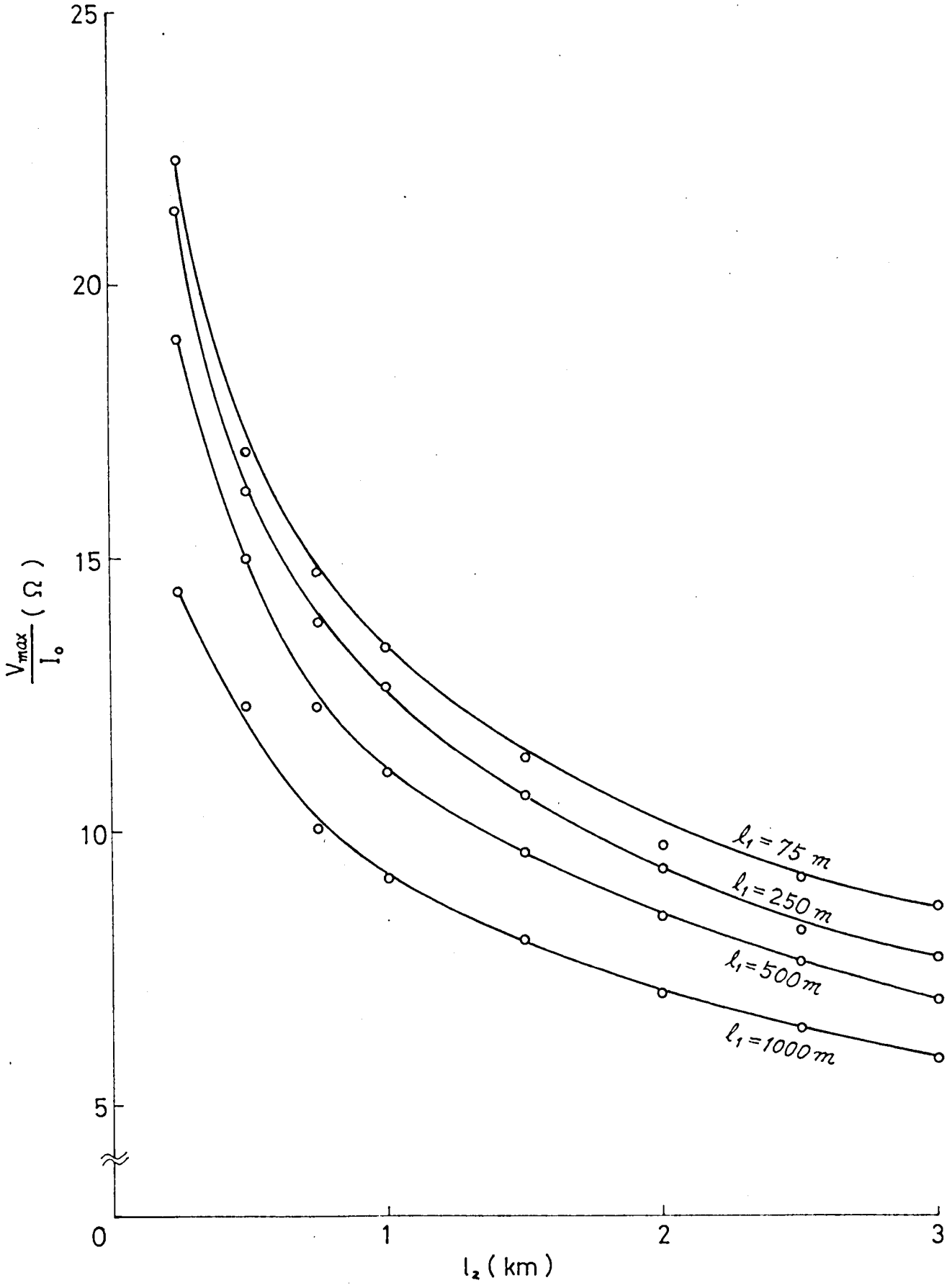

Fig. 1.10 Maximum voltages at final end of rubber insulated cable. (Symmetric three-conductor systems)

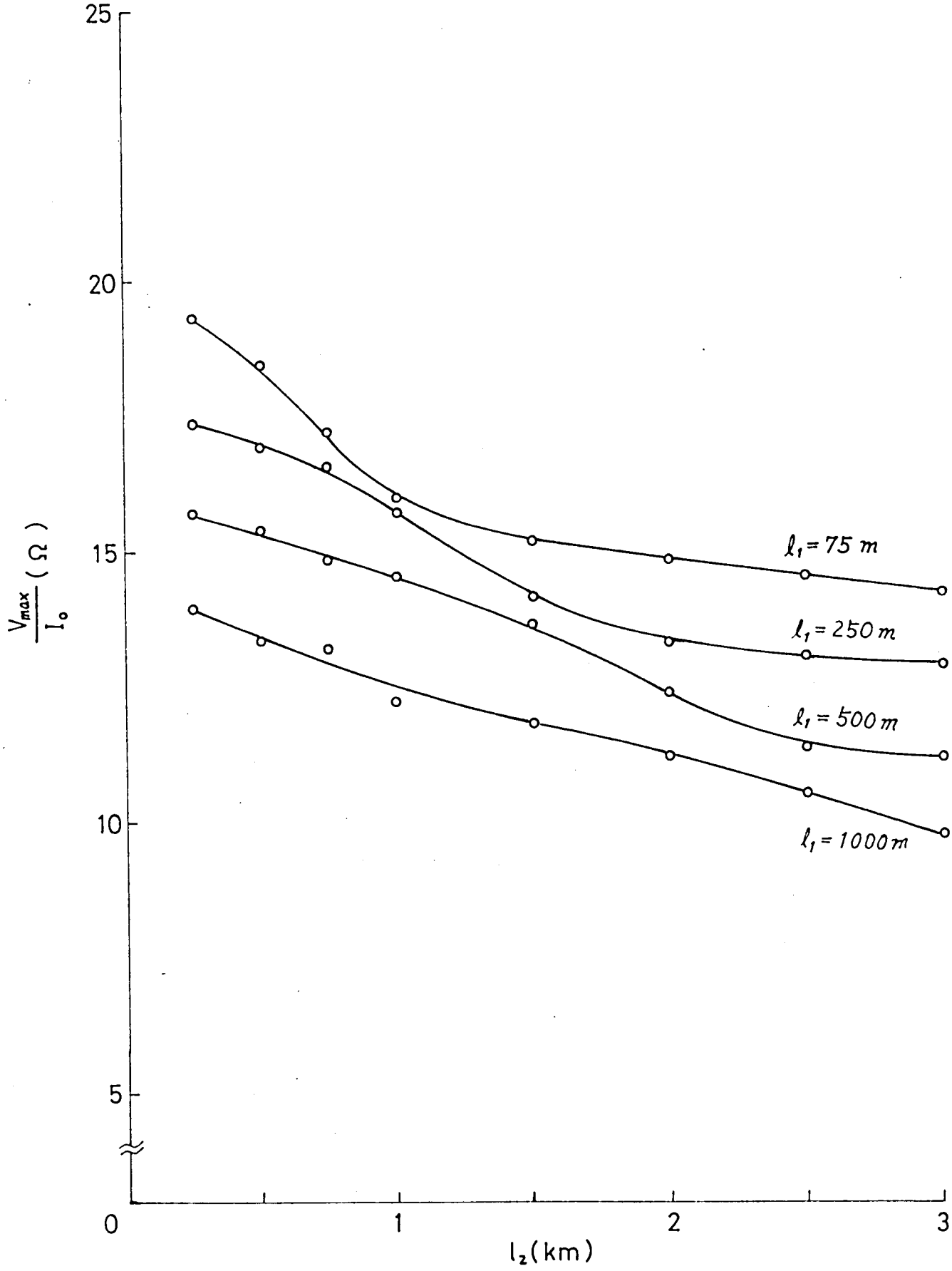

Fig. 1.11 Maximum voltages at final end of paper insulated cable.

(Symmetric three-conductor systems)

1.4 Numerical Analysis of Surges on Transmission Systems

1.4.1 Numerical Calculation on Transmission Systems Considering Tower Impedance

In this section let us investigate the surge performance on a transmission systems in the case where the counterpoise is set up for the purpose of reducing the grounding resistance of the transmission tower. As the model system, we use the one in the preceding section. As the equivalent circuit of tower which the counterpoise is provided with, let us adopt the circuit shown in Fig. 1.12. In this figure,

R_T : resistance to decide initial value of tower impedance,

L_T : equivalent tower inductance,

R_E : resistance to decide initial value of surge impedance of tower foot with counterpoise,

L_E : equivalent inductance of tower foot with counterpoise,

R_G : grounding resistance.

In this section we will discuss the case where it is assumed that the value of R_G is constant and also the impedance of the tower foot with the counterpoise is inductive. In Chapter 3 we will refer to the case where the tower foot impedance is capacitive.

In the present case the constant coefficients F and Z in Eq. (1.17) are changed for p-function as shown in Eq.s (1.22) and (1.23). Namely

$$v(t) = F' e_n(t) \otimes erfc\left(\frac{\delta}{2\sqrt{t}}\right) \odot H(t-T) \quad , \tag{1.22}$$

where

$$\left.\begin{aligned} F' &: \text{product of reflection and refraction coefficients at every transition point except tower,} \\ e_n(t) &= \mathcal{L}^{-1}\{F_{11}(p)^n Z(p) I(p)\} \quad , \\ F_{11}(p) &: \text{reflection coefficient at tower,} \\ Z(p) &: \text{input impedance at tower,} \\ I(p) &: \text{lightning stroke current.} \end{aligned}\right\} \tag{1.23}$$

We can obtain the numerical value of $v(t)$ from Eq. (1.22) by deciding the functional formula of $e_n(t)$ in Eq.s (1.23). In order to do so, let us determine the functional formulas of $F_{11}(p)$, $Z(p)$ and $I(p)$ as follows:

(i) Total tower impedance: Z_t

The total tower impedance Z_t which is given by the equivalent circuit as shown in Fig. 1.12, is expressed as follows:

$$Z_t = Z_T + Z_E + R_G \ ,$$

where

$$Z_T = pL_TR_T/(pL_T + R_T) \quad : \text{equivalent tower impedance,}$$

$$Z_E = pL_ER_E/(pL_E + R_E) \quad : \text{equivalent surge impedance of tower foot with counterpoise.}$$

(1.24)

Then Z_t is expressed by the following fractional formula:

$$Z_t = \frac{A_t p^2 + B_t p + C_t}{p^2 + D_t p + E_t} \ ,$$

where

$$A_t = R_T + R_E + R_G \ ,$$

$$B_t = (R_TR_E/L_E + R_TR_E/L_T + R_ER_G/L_E + R_TR_G/L_T) \ ,$$

$$C_t = R_TR_ER_G/L_TL_E \ ,$$

$$D_t = R_E/L_E + R_T/L_T \ ,$$

$$E_t = R_TR_E/L_TL_E \ .$$

(1.25)

(ii) Input impedance at tower: $Z(p)$

Using Eq. (1.25), the input impedance $Z(p)$ at tower is expressed as follows:

$$Z(p) = M_1 \frac{p^2 + a_1 p + a_2}{p^2 + b_1 p + b_2} = M_1 \left(\frac{p + \beta_1}{p + \alpha_1} \right) \left(\frac{p + \beta_2}{p + \alpha_2} \right) , \tag{1.26}$$

where

$$\left.\begin{aligned} M_1 &= z_1 A_t / (z_1 + 2A_t) , \\ a_1 &= B_t / A_t , \\ a_2 &= C_t / A_t , \\ b_1 &= (z_1 D_t + 2B_t) / (z_1 + 2A_t) , \\ b_2 &= (z_1 E_t + 2C_t) / (z_1 + 2A_t) , \\ \left.\begin{matrix} \alpha_1 \\ \alpha_2 \end{matrix}\right\} &= \frac{b_1 \pm \sqrt{b_1^2 - 4b_2}}{2} , \\ \left.\begin{matrix} \beta_1 \\ \beta_2 \end{matrix}\right\} &= \frac{a_1 \pm \sqrt{a_1^2 - 4a_2}}{2} . \end{aligned}\right\} \tag{1.27}$$

(iii) Reflection coefficient at tower: $F_{II}(p)$

Also using Eq. (1.25), the reflection coefficient $F_{II}(p)$ at tower is got as follows:

$$F_{II}(p) = M_2 \frac{p^2 + c_1 p + c_2}{p^2 + d_1 p + d_2} = M_2 \left(\frac{p + \delta_1}{p + \gamma_1} \right) \left(\frac{p + \delta_2}{p + \gamma_2} \right) , \tag{1.28}$$

where

$$
\left.
\begin{aligned}
M_2 &= -\beta_1(A_t + Z_0)/\{(2Z_0+\beta_1)A_t + Z_0\beta_1\}, \\
C_1 &= (B_t + Z_0 D_t)/(A_t + Z_0), \\
C_2 &= (C_t + Z_0 E_t)/(A_t + Z_0), \\
d_1 &= \{(2Z_0+\beta_1)B_t + Z_0\beta_1 D_t\}/\{(2Z_0+\beta_1)A_t + Z_0\beta_1\}, \\
d_2 &= \{(2Z_0+\beta_1)C_t + Z_0\beta_1 E_t\}/\{(2Z_0+\beta_1)A_t + Z_0\beta_1\}, \\
\left.\begin{matrix}\beta_1 \\ \gamma_2\end{matrix}\right\} &= \frac{d_1 \pm \sqrt{d_1^2 - 4d_2}}{2}, \\
\left.\begin{matrix}\delta_1 \\ \delta_2\end{matrix}\right\} &= \frac{C_1 \pm \sqrt{C_1^2 - 4C_2}}{2}.
\end{aligned}
\right\} \qquad (1.29)
$$

(iv) Derivation of $e_n(t)$:

Here let us give the lightning stroke current the same functional formula as Eq. (1.21), namely

$$i(t) = I_0 \varepsilon^{-\alpha_0 t} . \qquad (1.30)$$

Then the p-function of this equation becomes

$$I(p) = I_0 \frac{p}{p+\alpha_0} . \qquad (1.31)$$

Putting Eq.s (1.26), (1.28) and (1.31) into Eq.s (1.23) yields

$$e_n(t) = I_0 M_1 M_2^n \mathcal{L}^{-1}\left\{ \frac{p}{p+\alpha_0} \frac{p+\beta_1}{p+\alpha_1} \frac{p+\beta_2}{p+\alpha_2} \left(\frac{p+\delta_1}{p+\gamma_1}\right)^n \left(\frac{p+\delta_2}{p+\gamma_2}\right)^n \right\} . \qquad (1.32)$$

With respect to Eq. (1.32), we have the following relation

$$\frac{p}{p+a_0}\,\frac{p+\beta_1}{p+\alpha_1}\,\frac{p+\beta_2}{p+\alpha_2} = \frac{Ap}{p+a_0} + \frac{Bp}{p+\alpha_1} + \frac{Cp}{p+\alpha_2}\ , \tag{1.33}$$

where

$$\begin{bmatrix} A \\ B \\ C \end{bmatrix} = \begin{bmatrix} 1 & 1 & 1 \\ \alpha_1+\alpha_2 & a_0+\alpha_2 & a_0+\alpha_1 \\ \alpha_1\alpha_2 & a_0\alpha_2 & a_0\alpha_1 \end{bmatrix}^{-1} \begin{bmatrix} 1 \\ \beta_1+\beta_2 \\ \beta_1\beta_2 \end{bmatrix} \tag{1.34}$$

Next substituting Eq. (1.33) into Eq.(1.32) yields

$$e_n(t) = I_0 M_1 M_2^n \mathcal{L}^{-1}\{A f_n(t,a_0) + B f_n(t,\alpha_1) + C f_n(t,\alpha_2)\}\ , \tag{1.35}$$

where

$$f_n(t,\alpha) = \mathcal{L}^{-1}\left\{\frac{p}{p+\alpha}\left(\frac{p+\delta_1}{p+\gamma_1}\right)^n\left(\frac{p+\delta_2}{p+\gamma_2}\right)^n\right\}. \tag{1.36}$$

By applying Heaviside Expansion Theorem to Eq. (1.36), we get

$$f_n(t,\alpha) = \varepsilon^{-\alpha t}\left[1 + \sum_{j=1}^{n}\binom{n}{j}\left(\frac{\delta_1}{\gamma_1}\right)^j \frac{\Gamma_{j-1}(\gamma_1 t)}{(j-1)!}\right.$$

$$\left. + \sum_{j=1}^{n}\binom{n}{j}\left(\frac{\delta_2}{\gamma_2}\right)^j \frac{\Gamma_{j-1}(\gamma_2 t)}{(j-1)!}\right.$$

$$+\sum_{j=1}^{n}\sum_{k=1}^{n}\binom{n}{j}\binom{n}{k}\left(\frac{\rho_1}{\eta_1}\right)^{j}\left(-\frac{\rho_2}{\eta_2}\right)^{k}$$
$$\left\{\frac{\Gamma_{k-1}(\eta_2 t)}{(k-1)!}-\frac{\varepsilon^{-\eta_1 t}}{(k-1)!}\left(\frac{\eta_2}{\eta_2-\eta_1}\right)^{k}\sum_{\mu=0}^{j-1}\frac{(\eta_1 t)^{\mu}}{\mu!}\right.$$
$$\left.\sum_{\nu=0}^{\mu}(-1)^{\nu}\binom{\mu}{\nu}\frac{\Gamma_{k+\nu-1}(\eta_2-\eta_1 t)}{(\eta_2-\eta_1 t)^{\nu}}\right\}\Bigg], \qquad (1.37)$$

where

$$\left.\begin{aligned}&\begin{cases}\rho_1=\delta_1-\gamma_1,\\ \rho_2=\delta_2-\gamma_2,\end{cases}\qquad\qquad \begin{cases}\eta_1=\gamma_1-\alpha,\\ \eta_2=\gamma_2-\alpha,\end{cases}\\ &\Gamma_K(x)=K!\int_0^x\frac{\xi^K}{K!}\varepsilon^{-\xi}\,d\xi=K!\left(1-\varepsilon^{-x}\sum_{\mu=0}^{K}\frac{x^{\mu}}{\mu!}\right)\\ &\qquad\qquad\text{: incomplete Gamma function.}\end{aligned}\right\} \qquad (1.38)$$

Therefore the digital calculation by the same method as described in Section 1.2 is possible, and so in our case we can obtain the value of the voltage of each transition point.

1.4.2 Numerical Results and Discussions

In this article we perform the surge calculation in the case where the total tower impedance is considered and the three-phase back flashover at the tower struck by lightning is

assumed using the method described in the foregoing article. And then we investigate the influences of the impedance of tower and tower foot with counterpoise on surge voltage.

The computed transient voltage at the beginning end of the rubber insulated cable in the case where only the grounding resistance of the tower is considered, is shown in Fig. 1.13. In this case we assume $Z_t = R_G$ as follows:

$$Z_t = R_G = 10,\ 15,\ 20,\ 30\ \Omega .$$

From the figures it can be seen that the larger the value of R_G is, the higher the cable end voltages are.

Next as the values of R_T and L_T we adopt the following values

$$R_T = 100\ \Omega , \qquad L_T = 10\ \mu H .$$

Also we assume the next value for R_E and L_E

$$R_E = 50\ \Omega , \qquad L_E = 50\ \mu H .$$

And we use the value of the following grounding resistance

$$R_G = 15\ \Omega .$$

Moreover in order to investigate the effects of the tower impedance on the surge performances we perform the calculation in the case without counterpoise, namely

$$R_T = 100\ \Omega, \qquad L_T = 10\ \mu H,$$
$$R_E = 0, \qquad L_E = 0,$$
$$R_G = 15\ \Omega.$$

Next to clarify the effects of the counterpoise we perform the calculation about the following case

$$R_T = 0, \qquad L_T = 0,$$
$$R_E = 50\ \Omega, \qquad L_E = 50\ \mu H,$$
$$R_G = 15\ \Omega.$$

In this connection, as the values of the other system constant, we adopt the same values as used in Section 1.3.

The computed transient voltage at the beginning end of the rubber insulated cable in the above-mentioned several cases are plotted in Fig. 1.14(a) and the magnified voltage wave forms from 0 to 10 μs are shown in Fig. 1.14(b). And the voltage wave forms at the final end of the paper insulated cable are also shown in Fig. 1.15.

From Fig. 1.14(b) or Fig. 1.15, it is seen that the transient voltage in the case, where the tower foot with counter-

poise is considered, is considerably different from that in the case where only the grounding resistance is considered. Especially in Fig. 1.15 the maximum value of the former is about 1.5 times high as that of the latter.

The influences of the tower impedance on the surge performances is considerably great while the effect of the skin effect is small, and on the contrary, the ones of tower impedance is not so great while the effect of the skin effect is great as seen in Fig. 1.14(a). Thus we must consider the effects of both tower impedance and the skin effect in the analysis of surge performances on the system as adopted in this section.

The influence of impedance of tower foot with counterpoise on the cable end voltage is larger than that of only the tower impedance as seen in Fig.s 1.14(b) and 1.15. Hence it may be concluded that the value of the transient impedance of tower foot with the counterpoise should be reduced when the counterpoise is provided.

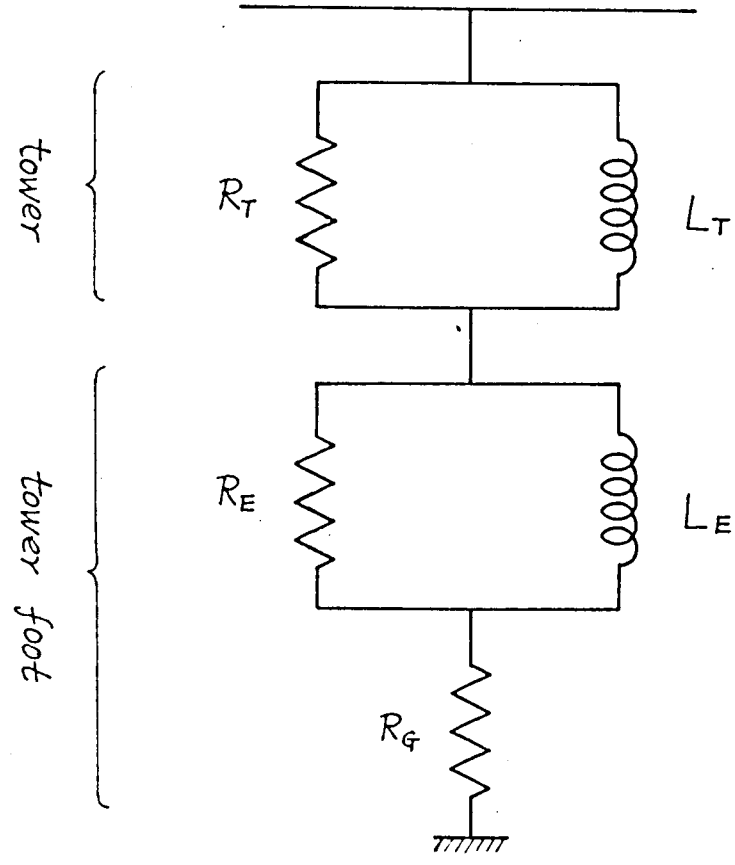

Fig. 1.12 Equivalent circuit of tower.

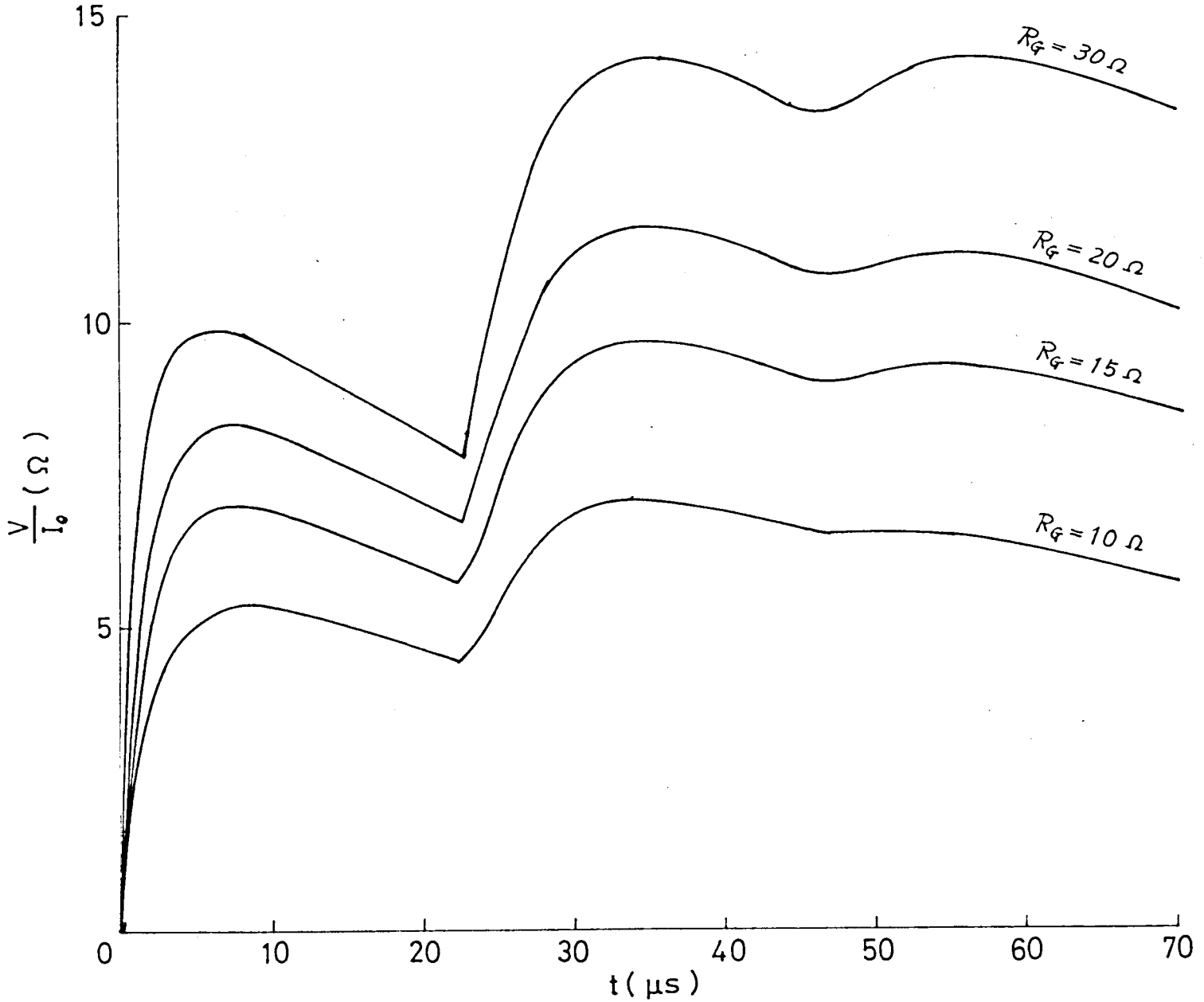

Fig. 1.13 Transient voltages at beginning end of rubber insulated cable for various values of R_G. (Symmetric three-conductor systems)

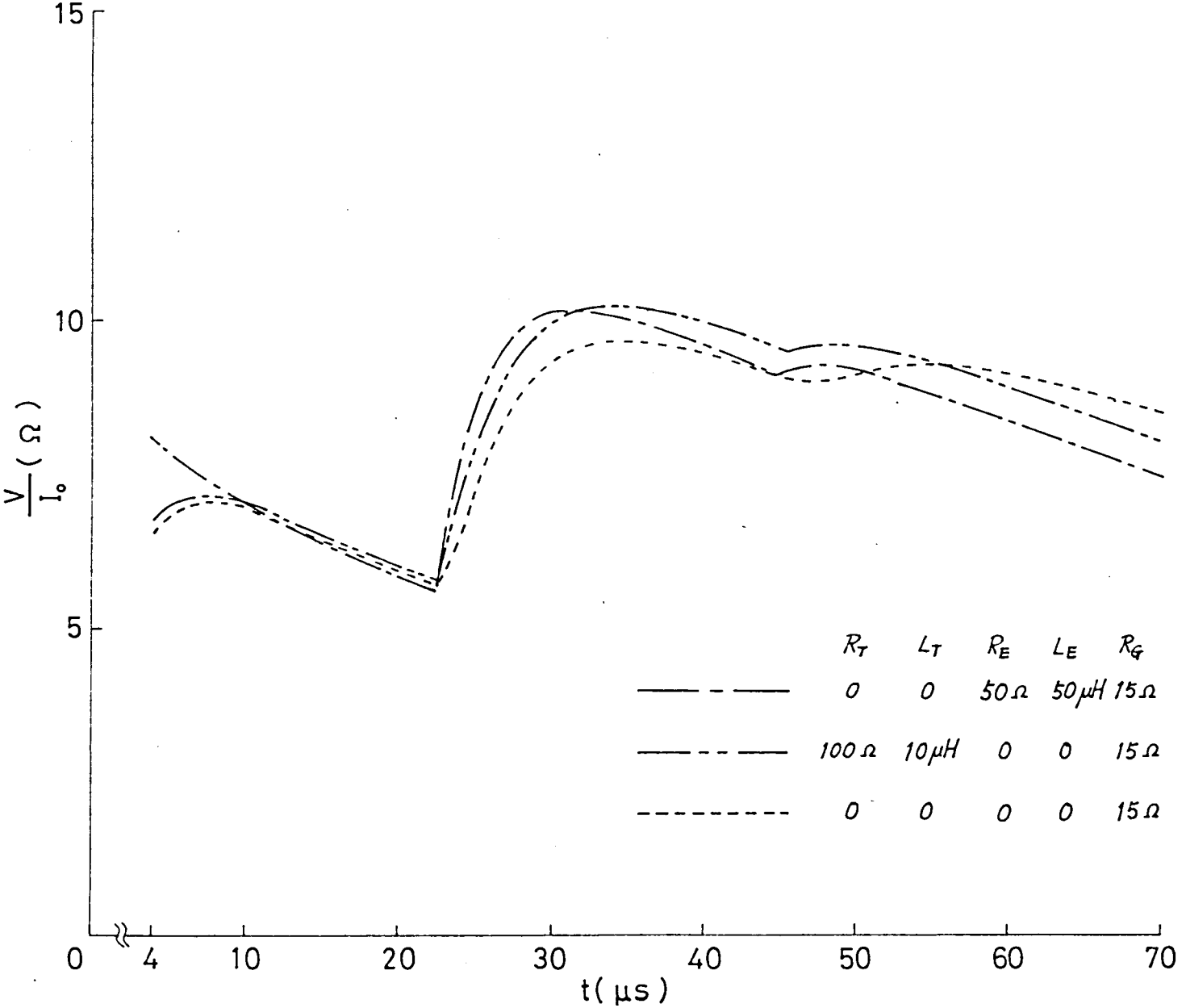

Fig. 1.14(a) Transient voltages at beginning end of rubber insulated cable considering tower impedance. (Symmetric three-conductor systems)

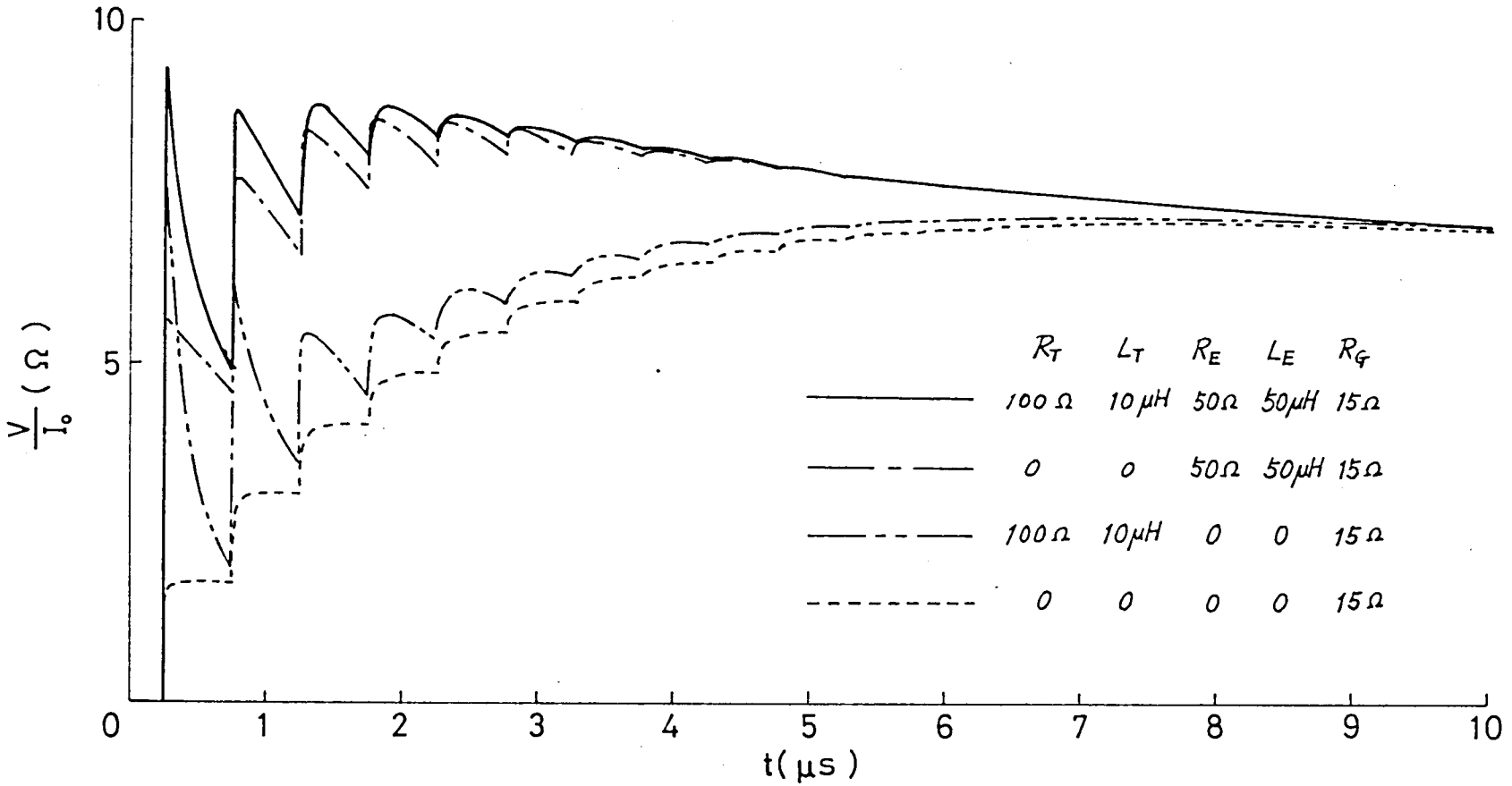

Fig. 1.14(b) Transient voltages at beginning end of rubber insulated cable considering tower impedance. (Symmetric three-conductor systems)

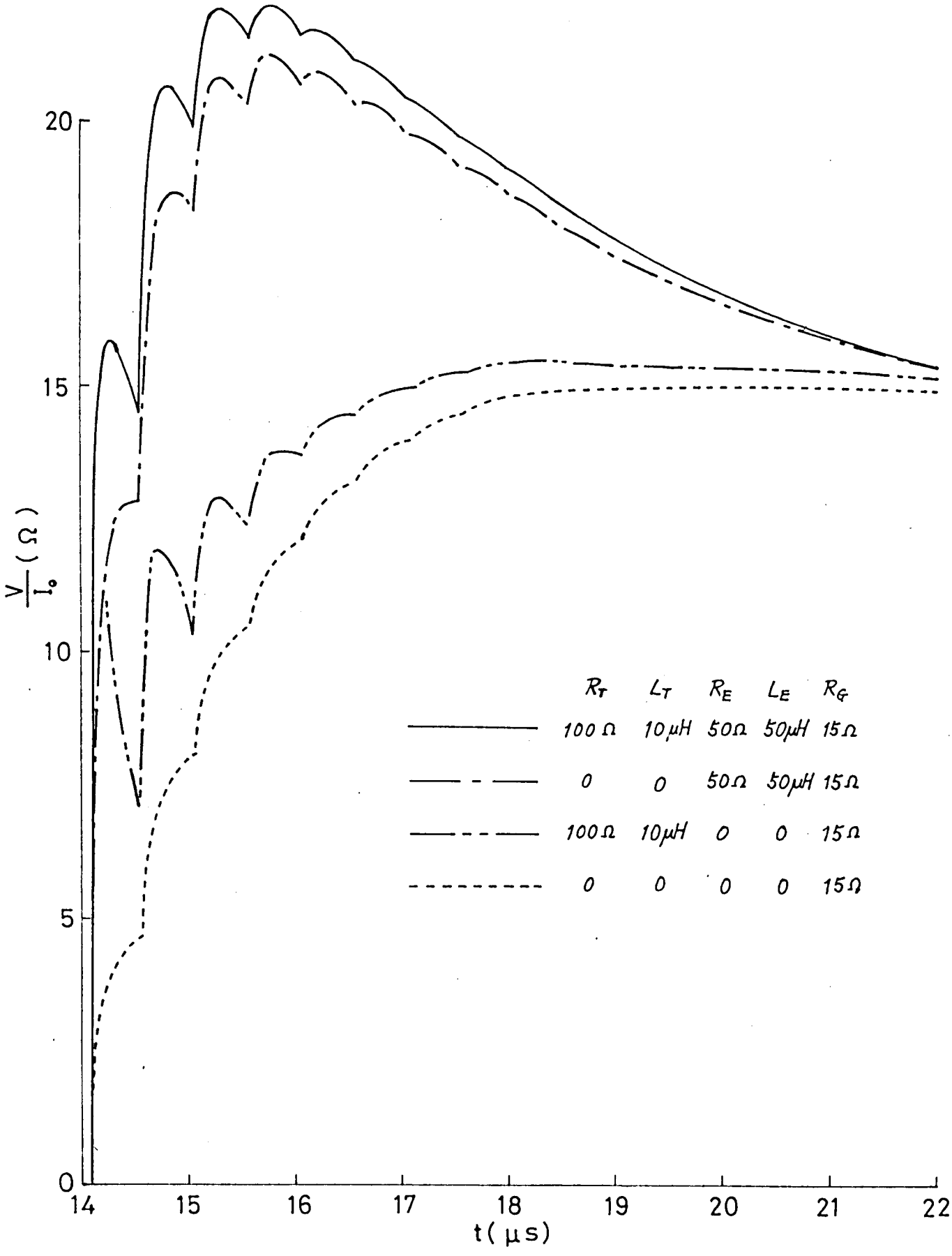

Fig. 1.15 Transient voltages at final end of paper insulated cable considering tower impedance.

CHAPTER 2

NUMERICAL CALCULATION OF SURGE PERFORMANCES IN ELECTRIC POWER NETWORKS UTILIZING CONVOLUTION INTEGRAL

2.1 Introduction

The lightning surge problems on electric power systems have been analyzed by means of numerical calculation with figures applying the lattice diagram method[12],[13] or analog computer.[3],[14] Recently, digital computer analysis of such problems are attempted by several researchers.[15]~[17]

In this chapter the author introduces a new digital analysis[18]~[21] of surge performances in power networks, which utilizes the principle of the low speed electronic surge analyzer[16] which has been already developed in the author's laboratory. In the surge analyzer, the delay of traveling waves along the line is simulated by the special electronic delay circuit, and the computation of the refracted and reflected voltages at the transition points is carried out by analog computer circuit.

And in analog computer, the computing circuits of the refracted and reflected voltages are constituted by means of resolving the equations of the refraction and reflection coefficients, which are generally the higher order fractional functions of p, into partial fractions.

Thus we derive the digital calculating method that . obtain the t-function of each p-function, which is resolved into the above-mentioned partial fractions, and calculate the convolution integral of the t-function and the values of incoming voltages, which can be numerically obtained, approximately but with high accuracy, and seek for the numerical values of the refracted and reflected voltages at the transition points.

This new analyzing method can be applied to the calculations of the surge performances in the complicated and large scale power networks with not only linear circuit elements, which give the higher order fractional functions at the transition points, but also the nonlinear one as lightning arrester. Moreover, by the new method we can treat the surge attenuation and distortion due to skin effect, though approximate. And the process of surge calculation programing is standardized, simple and plain for any networks, and we can get the numerical solutions in short computation time and in high accuracy.

Moreover in the next chapter the author will describe the application of his method to the problems of the surge performances on some practical systems, viz. a distribution line system having distributed pole transformers, an overhead transmission line-cable system, a transmission one with overhead

ground wire, and a system containing one arrester.

Though a calculating method utilizing Z-transformation was derived by Ishihara[15] for the digital analysis of the surge problems, it is thought that the author's method is superior to Ishihara's one in points of simplicity of the surge flow graph, simplicity and convenience of calculating process, when especially the inductances and capacitances are connected with the transition points, and numbers of the memories required for computation.

2.2 Numerical Calculation of Surge Performances in Power Networks

2.2.1 Surge Flow Graph

In this article, the author will introduce the numerical calculation of traveling waves which he thinks out for the case, where the lightning strikes at a point of an arbitrary power network. Briefly speaking, it is the method by which first we make up the surge flow graph of a given power network and next set up a voltage equation at each node by means of the flow graph and finally solve numerically the voltage equation by adopting an approximate calculating method of the convolution integral, which will be explained later.

The finite transmission line conductor of Fig. 2.1(a), which is connected with two infinite ones at the both ends, can be represented by the fundamental graph of Fig. 2.1(b). In the figures v_1 and v_2 are two transition point voltages, F_1 and F_2 are refraction coefficients at two transition points when surges penetrate in the direction of the arrow, and T is the propagation time of traveling wave on the finite line. And in Fig. 2.1(b), the path beside which 1, -1, F_1 or F_2 is written is the one whose beginning point voltage should be multiplied by these coefficients and the result should be the final point voltage. On the other hand, the path beside which T is written represents the time delay path.

Next in the case where lightning strikes at any point in

a power network as shown in Fig. 2.2(a), where it is assumed that the conductor expressed by the dotted line extends infinitely, the network can be displaced by the flow graph in Fig. 2.2(b) by applying the fundamental graph of Fig. 2.1(b) to each branch of the network. In the figures F_1, F_2, ·····, F_8 are refraction coefficients at each transition point, T_1, T_2, T_3 and T_4 are surge propagation time on each branch, and $i(t)$ is the lightning stroke current.

Next when we assign numbers to all node according to the following rule, we can calculate the node voltages in numerical order by the method introduced in the next articles. First we number arbitrarily the nodes, which are the final ends of the time delay paths, from 1 onward. We number the rest nodes in such a way that for a certain node the number of the several nodes directed towards it are always smaller than the number of the node itself. For example, in Fig. 2.2(b), node 19 has a larger number than the nodes 5 and 12 that are directed towards it. The nodes can be numbered with the various ways satisfying the above-mentioned rule. We should number the nodes in such way that the equations for surge analysis can be handled as conveniently as possible.

2.2.2 Approximate Calculation of Convolution Integral

Using the surge graph of Fig. 2.2(b), we can write the following set of equations.

$$
\left.
\begin{aligned}
&\left.
\begin{aligned}
&v_{2r-1}(t) = v_{2r+12}(t-T_r), \\
&v_{2r}(t) = v_{2r+13}(t-T_r),
\end{aligned}
\right\} \quad r = 1, 2, 3, 4 \\
&v_9(t) = F_1 v_2(t) + F_3 v_4(t) + F_5 v_6(t) + F_7 v_8(t) + Z i(t), \\
&v_{r+9}(t) = F_{2r} v_{2r-1}(t), \qquad r = 1, 2, 3, 4 \\
&\left.
\begin{aligned}
&v_{2r+12}(t) = v_9(t) - v_{2r}(t), \\
&v_{2r+13}(t) = v_{r+9}(t) - v_{2r-1}(t),
\end{aligned}
\right\} \quad r = 1, 2, 3, 4
\end{aligned}
\right\} \qquad (2.1)
$$

where $v_r(t)$ is the r-th node voltage and Z is the input impedance viewed from the lightning stroke point. We define $v_{2r+12}(t-T_r) = 0$ and $v_{2r+13}(t-T_r) = 0$ when $t < T_r$.

Then in Eq.s (2.1), since $i(t)$ is a given function and the values of $F_1, F_2, \cdots, F_8$, T and Z are known, we can compute the values of $v_\nu(\Delta t)$, $(\nu = 1, 2, \cdots, 21)$ numerical order from Eq.s (2.1) by selecting appropriately time interval Δt. Next, similary we can evaluate the values of $v_\nu(2\Delta t)$, $(\nu = 1, 2, \cdots, 21)$.

After repeating the same processes as above-mentioned, we can calculate the values of $v_\nu(t)$, $(\nu = 1, 2, \cdots, 21,\ t = 3\Delta t, 4\Delta t, \cdots)$. However, in order to compute numerically the values of $v_{2r+12}(t-T_r)$ and $v_{2r+13}(t-T_r)$, we must choose the values of Δt a common measure of T_r.

However, only in the case where the refraction coefficient $F = F_1, F_2, \cdots, F_8$ and the input impedance Z are constant, we

can perform the numerical calculation with Eq.s (2.1). And when F and Z are the functions of p, the terms $Fv(t)$ and $Zi(t)$ in Eq.s (2.1) must be changed as follows:

$$\mathcal{L}^{-1}\{F(p)\} \odot v(t)H(t),$$
$$\mathcal{L}^{-1}\{Z(p)\} \odot i(t)H(t),$$

where $\mathcal{L}^{-1}$ is the symbol of inverse Laplace transformation, and $\odot$ is the one of convolution integral. Now as $F(p)$ and $Z(p)$ are usually some fractional functions of p, whose numerator and denominator are homogeneous, or the former is less than the latter by one dimension, they can be resolved into the partial fraction as follows:

$$F(p) = A_0 + \frac{A_1}{p+\alpha_1} + \frac{A_2}{p+\alpha_2} + \cdots\cdots\cdots + \frac{A_m}{p+\alpha_m}, \qquad (2.2)$$

where A_0, A_1, ---, A_m are the constant multipliers and α_1, α_2, ---, α_m are the characteristic roots, which are assumed to be all distinct. Then we have

$$\mathcal{L}^{-1}\{F(p)\} \odot v(t)H(t) = A_0 v(t)H(t) + \sum_{j=1}^{m} A_j g_j(t), \qquad (2.3)$$

where

$$\left.\begin{aligned} g_j(t) &\simeq \frac{1}{2}\{v(t)+v(t-\Delta t)\varepsilon^{-\alpha_j\Delta t}\}\Delta t + g_j(t-\Delta t)\varepsilon^{-\alpha_j\Delta t}, \\ g_j(0) &= 0 . \end{aligned}\right\} \qquad (2.4)$$

These approximate relations will be proved in the next article. Therefore, in the case where F is a function of p, $Fv(t)$ in Eq.s (2.1) should be displaced by the recurrence formula of Eq.s (2.3) and (2.4). Through the similar process $Zi(t)$ can be calculated.

As previously described, resolving the function $F(p)$ into the partial fractions as shown in Eq. (2.2), we can calculate approximately the values of $\mathcal{L}^{-1}\{F(p)\} \odot v(t)H(t)$ by Eq.s (2.3) and (2.4), if only we could obtain the numerical values of $v(t)$ at $t = \Delta t, 2\Delta t, \cdots\cdots$ admitting that we don't know the functional form of $v(t)$.

Next $A_1, A_2, \cdots\cdots, A_m$ and $\alpha_1, \alpha_2, \cdots\cdots, \alpha_m$ in Eq. (2.2) are not always real numbers, and generally those consist of some real numbers and some groups of coordinate complex numbers. Supposing A_1, A_2 and α_1, α_2 are coordinate complex numbers respectively and each other, these can be expressed as follows:

$$A_1 = A + jA', \qquad A_2 = A - jA', \qquad (A, A' : \text{real})$$

$$\alpha_1 = \alpha + j\alpha', \qquad \alpha_2 = \alpha - j\alpha'. \qquad (\alpha, \alpha' : \text{real})$$

Next, $g_1(t)$ and $g_2(t)$ which are reduced from Eq.s (2.4), using the coordinate complex numbers α_1 and α_2, become also coordinate

complex functions. Then we have

$$g_1(t) = g(t) + jg'(t), \qquad g_2(t) = g(t) - jg'(t).$$

($g(t)$, $g'(t)$: real functions)

Hence the function $A_1 g_1(t) + A_2 g_2(t)$ can be modified as follows:

$$\begin{aligned} A_1 g_1(t) + A_2 g_2(t) &= (A + jA')\{g(t) + jg'(t)\} + (A - jA')\{g(t) - jg'(t)\}, \\ &= Ag(t) - A'g'(t) + j\{A'g(t) + Ag'(t)\} \\ &\quad + Ag(t) - A'g'(t) - j\{A'g(t) + Ag'(t)\}, \\ &= 2\{Ag(t) - A'g'(t)\}. \end{aligned} \tag{2.5}$$

Apparently since this function is a real one, $\sum_{j=1}^{m} A_j g_j(t)$ becomes a real function, and so the convolution integral $\mathcal{L}^{-1}\{F(p)\} \odot v(t)H(t)$ of Eq. (2.3) also becomes a real function. Accordingly in digital computation we should compose programs so as to treat of A_j, α_j and $g_j(t)$, $(j = 1, 2, \cdots\cdots, m)$ as complex numbers. Then the values of voltages at each node becomes real number automatically.

The above-stated is effective for the case where α_j is a simple root. So next the author will show the numerical calculation in the case where $F(p)$ has the multiple roots which is thought to be very rare case. When α_j is the k_j-ple root, $F(p)$ can be represented as follows:

$$F(p) = A_0 + \left\{ \frac{A_{11}}{p+\alpha_1} + \frac{A_{12}}{(p+\alpha_1)^2} + \cdots\cdots + \frac{A_{1k_1}}{(p+\alpha_1)^{k_1}} \right\}$$
$$+ \left\{ \frac{A_{21}}{p+\alpha_2} + \frac{A_{22}}{(p+\alpha_2)^2} + \cdots\cdots + \frac{A_{2k_2}}{(p+\alpha_2)^{k_2}} \right\}$$
$$+ \cdots\cdots\cdots\cdots\cdots\cdots\cdots\cdots$$
$$+ \left\{ \frac{A_{m1}}{p+\alpha_m} + \frac{A_{m2}}{(p+\alpha_m)^2} + \cdots\cdots + \frac{A_{mk_m}}{(p+\alpha_m)^{k_m}} \right\} . \qquad (2.6)$$

The convolution integral of this case is given by

$$\mathcal{L}^{-1}\{F(p)\} \circledast v(t)H(t) = A_0 v(t)H(t) + \sum_{j=1}^{m} \sum_{k=1}^{k_j} A_{jk}\, g_{jk}(t) , \qquad (2.7)$$

where, $g_{jk}(t)$ satisfies the next recurrence formula,

$$g_{jk}(t) \simeq \begin{cases} \text{given by Eq. (2.4)}, \ k=1 , \\ \frac{(\Delta t)^k}{(k-1)!} \sum_{\lambda=1}^{k-1} D_k(\lambda)\, v(t-\lambda\Delta t)\, \varepsilon^{-\alpha_j \lambda \Delta t} \\ + \sum_{l=1}^{k} (-1)^{l-1}\, {}_kC_m\, g_{jk}(t-l\Delta t)\, \varepsilon^{-\alpha_j l \Delta t} , \quad k \geq 2 , \end{cases} \qquad (2.8)$$

and $D_k(\lambda)$ is a constant given by

$$D_k(\lambda) = \sum_{\gamma=0}^{\lambda} {}_kC_\gamma\, (-1)^\gamma (\lambda-\gamma)^{k-1} , \qquad (2.9)$$

but in order to evaluate $g_{jk}(t)$ in Eq. (2.8), the following values of $g_{jk}(t)$, viz.

$$g_{jk}(l\Delta t) = \frac{(\Delta t)^k}{(k-1)!}\left\{\sum_{s=0}^{l-1}(l-s)^k v(s\Delta t)\varepsilon^{-\alpha_j(m-s)\Delta t} - \frac{1}{2}v(0)l^k\varepsilon^{-\alpha_j l\Delta t}\right\}. \tag{2.10}$$

$(l = 0,1,\cdots\cdots,k)$

must be known. Moreover for example, when $k=2$

$$\left.\begin{aligned} g_{j2}(t) &\simeq (\Delta t)^2 v(t-\Delta t)\varepsilon^{-\alpha_j\Delta t} \\ &\quad + 2g_{j2}(t-\Delta t)\varepsilon^{-\alpha_j\Delta t} - g_{j2}(t-2\Delta t)\varepsilon^{-\alpha_j 2\Delta t}, \\ g_{j2}(0) &= 0, \\ g_{j2}(t) &\simeq \frac{1}{2}(\Delta t)^2 v(0)\varepsilon^{-\alpha_j\Delta t}. \end{aligned}\right\} \tag{2.11}$$

when $k=3$

$$\left.\begin{aligned} g_{j3}(t) &\simeq \frac{1}{2}(\Delta t)^3\{v(t-\Delta t)\varepsilon^{-\alpha_j\Delta t} + 4v(t-2\Delta t)\varepsilon^{-\alpha_j 2\Delta t} \\ &\quad + 3g_{j3}(t-\Delta t)\varepsilon^{-\alpha_j\Delta t} - 3g_{j3}(t-2\Delta t)\varepsilon^{-\alpha_j 2\Delta t} \\ &\quad + g_{j3}(t-3\Delta t)\varepsilon^{-\alpha_j 3\Delta t}, \\ g_{j3}(0) &= 0, \\ g_{j3}(\Delta t) &\simeq \frac{1}{4}(\Delta t)^3 v(0)\varepsilon^{-\alpha_j\Delta t}, \\ g_{j3}(2\Delta t) &\simeq \frac{1}{2}(\Delta t)^3\{v(\Delta t)\varepsilon^{-\alpha_j\Delta t} + 4v(0)\varepsilon^{-\alpha_j 2\Delta t}\}. \end{aligned}\right\} \tag{2.12}$$

Finally when α_j is a complex number, we can apply the same procedure as in the case where α_j is a simple root to Eq.s (2.7) to (2.10).

2.2.3 Proof of Approximate Calculation of Convolution Integral

Here we will prove Eq.s (2.3) and (2.4) which are used in the preceding article. First putting

$$q_j(t) = \mathcal{L}^{-1}\left\{\frac{1}{p+\alpha_j}\right\} \circledast v(t)H(t), \tag{2.13}$$

into Eq. (2.2), we can introduce Eq. (2.3). Next we will show that $q_j(t)$ given in Eq. (2.13) satisfies recurrence Eq.s (2.4). Applying Duhamel's theorem to Eq. (2.13), we get

$$\begin{aligned} q_j(t) &= \frac{1}{\alpha_j}(1-\varepsilon^{-\alpha_j t}) \circledast v(t)H(t), \\ &= \frac{d}{dt}\int_0^t \frac{1}{\alpha_j}(1-\varepsilon^{-\alpha_j \tau})\, v(t-\tau)H(t-\tau)\,d\tau, \\ &= \int_0^t \varepsilon^{-\alpha_j \tau} v(t-\tau)\,d\tau. \end{aligned} \tag{2.14}$$

Substituting $t = n\Delta t$ above equation, we have

$$q_j(n\Delta t)=\int_0^{n\Delta t} f(\tau)d\tau \quad ; \quad n=1,2,\text{------}, \tag{2.15}$$

where

$$f(\tau)=\varepsilon^{-\alpha_j\tau}v(n\Delta t-\tau). \tag{2.16}$$

Now, Eq. (2.15) can be transformed to

$$\begin{aligned} q_j(n\Delta t) &= \int_0^{\Delta t} f(\tau)d\tau+\int_{\Delta t}^{2\Delta t} f(\tau)d\tau+\text{-----}+\int_{(n-1)\Delta t}^{n\Delta t} f(\tau)d\tau, \\ &\simeq \frac{f(0)+f(\Delta t)}{2}\Delta t+\frac{f(\Delta t)+f(2\Delta t)}{2}\Delta t+\text{-----} \\ &\qquad \text{----------}+\frac{f(\overline{n-1}\Delta t)+f(n\Delta t)}{2}\Delta t, \\ &= \left\{\tfrac{1}{2}f(0)+f(\Delta t)+\text{----}+f(\overline{n-1}\Delta t)+\tfrac{1}{2}f(n\Delta t)\right\}\Delta t. \end{aligned}$$

Substituting Eq. (2.16) into the above equation gives

$$\begin{aligned} q_j(n\Delta t)\simeq\Big\{&\tfrac{1}{2}v(n\Delta t)+v(\overline{n-1}\Delta t)\varepsilon^{-\alpha_j\Delta t}+\text{-----} \\ &\text{-----}+v(\Delta t)\varepsilon^{-\alpha_j(n-1)\Delta t}+\tfrac{1}{2}v(0)\varepsilon^{-\alpha_j n\Delta t}\Big\}\Delta t \end{aligned} \tag{2.17}$$

Similarly for the case of $t=(n-1)\Delta t$ Eq. (2.17) becomes

$$q_j(\overline{n-1}\Delta t)\simeq\Big\{\tfrac{1}{2}v(\overline{n-1}\Delta t)+v(\overline{n-2}\Delta t)\varepsilon^{-\alpha_j\Delta t}+\text{-----}$$

$$----- + v(\Delta t)\varepsilon^{-\alpha_j \overline{n-2}\Delta t} + \frac{1}{2}v(0)\varepsilon^{-\alpha_j \overline{n-1}\Delta t}\Big\}\Delta t \qquad (2.18)$$

Hence $q_j(t)$ satisfies the next recurrence formula,

$$q_j(n\Delta t) \simeq \frac{1}{2}\{v(n\Delta t) + v(\overline{n-1}\Delta t)\varepsilon^{-\alpha_j \Delta t}\}\Delta t + q_j(\overline{n-1}\Delta t)\varepsilon^{-\alpha_j \Delta t}.$$

Substituting $t = n\Delta t$, $t - \Delta t = (n-1)\Delta t$ into the above equation yields

$$\left.\begin{aligned} q_j(t) &\simeq \frac{1}{2}\{v(t) + v(t-\Delta t)\varepsilon^{-\alpha_j \Delta t}\}\Delta t + q_j(t-\Delta t)\varepsilon^{-\alpha_j \Delta t}, \\ q_j(0) &= 0. \end{aligned}\right\} \qquad (2.19)$$

Eq.s (2.19) are the same as Eq.s (2.4). By the above description Eq.s (2.3) and (2.4) in the foregoing article are proved to come into existence.

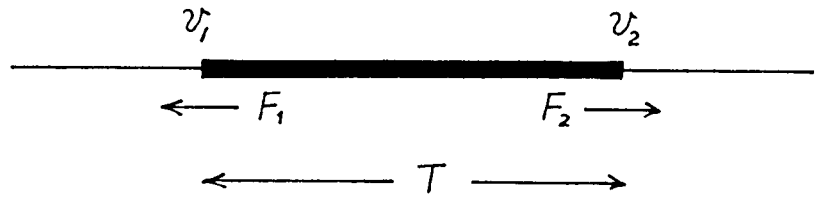

(a) Line of finite length.

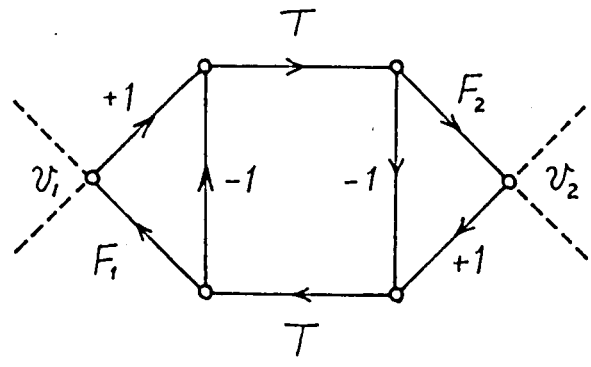

(b) Fundamental flow graph.

Fig. 2.1 Fundamental flow graph of line of finite length.

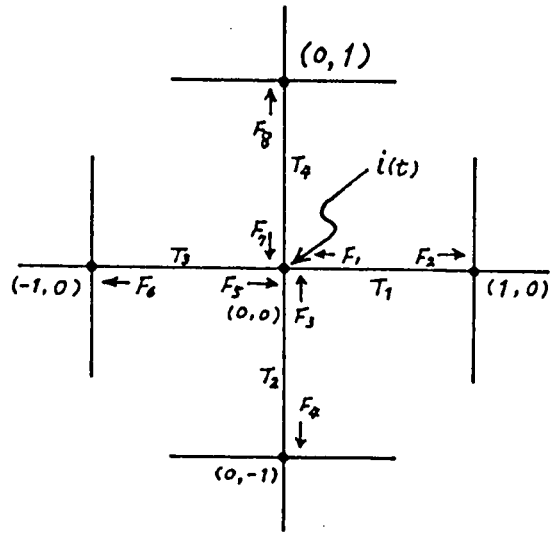

(a) Network.

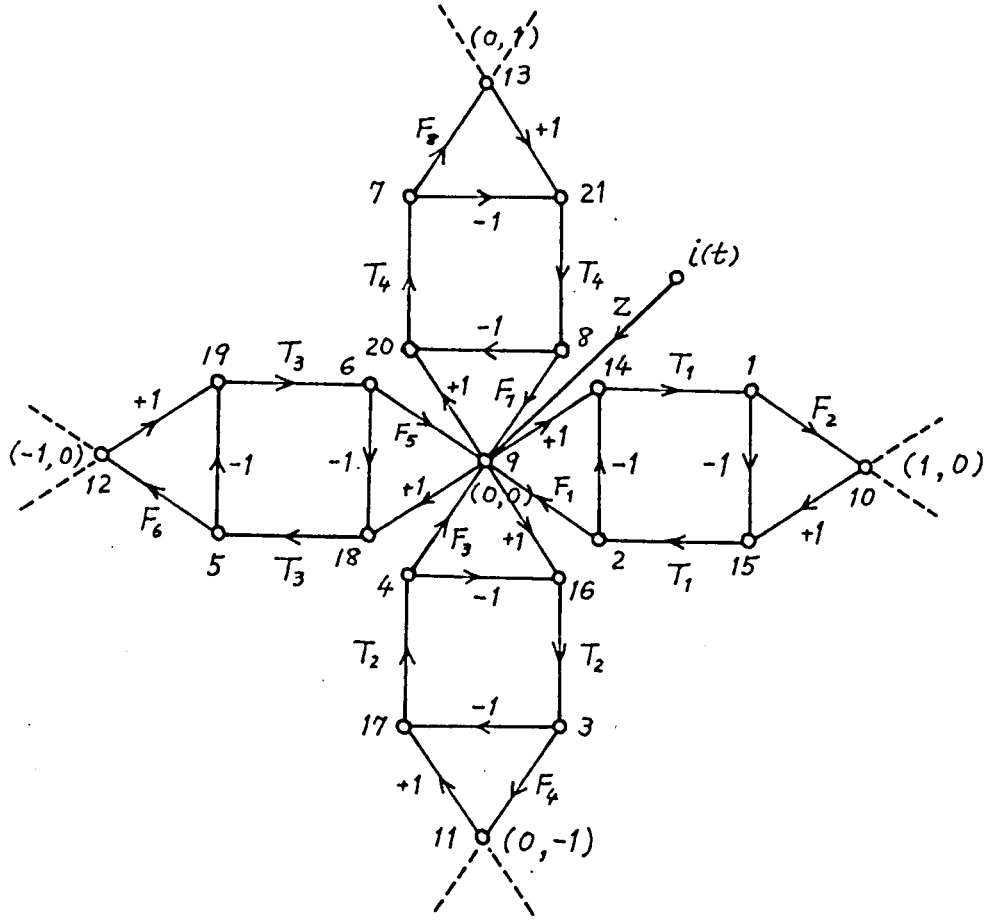

(b) Flow graph.

Fig. 2.2 A network and it's flow graph.

2.3 Approximate Calculation of Distortion of Surges Due to Skin Effect

Here a numerical calculation of surge performances considering skin effect along the line is presented. Now let us approximate the error function, which expresses the distortion of surges due to skin effect, by an exponential function as follows:

$$erfc\left(\frac{\sigma x}{2\sqrt{t}}\right) \simeq K(1-\varepsilon^{-\gamma t}), \tag{2.20}$$

where σ is the distortion constant and K and γ are constants. In Eq. (2.20) K must be 1 so that the right term may agree with the left term at $t=\infty$. But as the practical range of t for us to use for calculation is a finite value, it is advantageous that we decide the values of K and γ so that the exponential function may give the good approximation to the error function within a finite range of t.

In the case where the skin effect is considered, $v_{2r+12}(t-T_r)$ or $v_{2r+13}(t-T_r)$ in Eq.s (2.1) must be displaced by the following convolution integral

$$\mathcal{L}^{-1}\{\varepsilon^{-Tp-\sigma x\sqrt{p}}\} \otimes v(t)H(t).$$

Substituting Eq. (2.20) into the above equation and modifying the result with the same procedure as in the Article 2.2.2 give

$$
\begin{aligned}
&\mathcal{L}^{-1}\{\varepsilon^{-Tp-\sigma x\sqrt{p}}\} \circledast v(t)H(t) \\
&= \operatorname{erfc}\left(\frac{\sigma x}{2\sqrt{t-T}}\right) H(t-T) \circledast v(t)H(t), \\
&\simeq K\{1-\varepsilon^{-\gamma(t-T)}\} H(t-T) \circledast v(t)H(t), \\
&= \frac{d}{dt}\int_T^t K\{1-\varepsilon^{-\gamma(\tau-T)}\} v(t-\tau)\,d\tau, \\
&= K\gamma\int_T^t \varepsilon^{-\gamma(\tau-T)} v(t-\tau)\,d\tau, \\
&= K\gamma\int_0^{t-T} \varepsilon^{-\gamma\tau'} v(t-T-\tau')\,d\tau', \quad (\tau'=\tau-T), \\
&= K\gamma h(t), \qquad (2.21)
\end{aligned}
$$

where

$$
h(t) = \int_0^{t-T} \varepsilon^{-\gamma\tau'} v(t-T-\tau')\,d\tau'. \qquad (2.22)
$$

Since this integral has the same form as Eq. (2.14), the following recurrence formulas are obtained.

$$
\mathcal{L}^{-1}\{\varepsilon^{-Tp-\sigma x\sqrt{p}}\} \circledast v(t)H(t) \simeq K\gamma h(t), \qquad (2.23)
$$

where

$$\left.\begin{aligned} h(t) &= \frac{1}{2}\{v(t-T) + v(t-T-\Delta t)\varepsilon^{-\gamma\Delta t}\}\Delta t \\ &\quad + h(t-\Delta t)\varepsilon^{-\gamma\Delta t}, \qquad (t>T), \\ h(t) &= 0\ , \qquad (0 \leq t \leq T). \end{aligned}\right\} \tag{2.24}$$

Accordingly in the case where the skin effect is considered, we should use this recurrence Eq.s (2.23) and (2.24) instead of the first two equations of Eq.s (2.1).

2.4 Treatment of the Circuit Composition Changes in Progress of Transient Phenomena

In this article we will introduce the calculating method for the case where the circuit composition changes in progress of the transient phenomena, for example, the case where the back flashover occurs after some time lag from the instant when the lightning strikes at a transmission tower.

Assuming that lightning stroke current $i(t)$ penetrates the tower at $t=0$ and the back flashover along a insulator chain occurs at $t=t_0$, this is the case where the input impedance of the circuit changes $Z(p)$ to $Z'(p)$ at $t=t_0$. And such a problem is equal to the one of solving the transient phenomena of the circuit given in Fig. 2.3. The terminal voltage $v_1(t)$ of the impedance Z, untill t reaches t_0 after closing the switch S_1 at $t=0$, is

$$v_1(t) = \mathcal{L}^{-1}\{Z(p)\} \circledast i(t)H(t), \qquad 0 \leq t \leq t_0 . \tag{2.25}$$

Next when the switch S_2 is closed at $t=t_0$, the current $i_1(t)$ shown in Fig. 2.3 becomes

$$i_1(t) = \mathcal{L}^{-1}\left\{\frac{1}{Z(p)+Z_0(p)}\right\} \circledast v_1(t)H(t-t_0), \qquad t \geq t_0 . \tag{2.26}$$

And the terminal voltages $v_2(t)$ of the impedance Z_o is given by

$$v_2(t) = \mathcal{L}^{-1}\{Z_o(p)\} \circledcirc i_1(t), \quad t \geq t_o .$$

Putting Eq.s (2.26) and (2.25) in the above equation yields

$$v_2(t) = \mathcal{L}^{-1}\left\{\frac{Z_o(p)}{Z(p)+Z_o(p)}\right\} \circledcirc v_1(t)H(t-t_o), \quad t \geq t_o ,$$

$$= \mathcal{L}^{-1}\left\{\frac{Z(p)Z_o(p)}{Z(p)+Z_o(p)}\right\} \circledcirc i(t)H(t-t_o), \quad t \geq t_o .$$

Supposing $Z'(p)$ is the impedance of parallel connection of $Z(p)$ and $Z_o'(p)$, the above equation becomes

$$v_2(t) = \mathcal{L}^{-1}\{Z'(p)\} \circledcirc i(t)H(t-t_o), \quad t \geq t_o . \tag{2.27}$$

Therefore, the terminal voltage of the impedance which changes from $Z(p)$ to $Z'(p)$ at $t=t_o$ is given by

$$v(t) = \begin{cases} \mathcal{L}^{-1}\{Z(p)\} \circledcirc i(t)H(t), & 0 \leq t < t_o , \\ \mathcal{L}^{-1}\{Z'(p)\} \circledcirc i(t)H(t-t_o), & t \geq t_o . \end{cases} \tag{2.28}$$

Similarly in the network whose refraction coefficient of the transition point changes from $F(p)$ to $F'(p)$, the refracted voltage at this point is given by the following equations

$$v(t)=\begin{cases}\mathcal{L}^{-1}\{F(p)\}\circledast v(t)H(t), & 0\le t<t_0\ ,\\ \mathcal{L}^{-1}\{F(p)\}\circledast v(t)H(t-t_0), & t\ge t_0\ .\end{cases}\qquad(2.29)$$

Now, for the first equation of Eq.s (2.28) or (2.29), the author has already derived the digital calculating method in the preceding article, and so let us introduce the numerical calculation of the second equation of Eq.s (2.28) or (2.29).

Here, we will adopt Eq.s (2.29) as an example, provided that $F(p)$ can be resolved into partial fractions as shown in Eq. (2.2) like $F(p)$, the second equation of Eq.s (2.29) is represented as follows:

$$\mathcal{L}^{-1}\{F(p)\}\circledast v(t)H(t-t_0)=A_0v(t)H(t-t_0)+\sum_{j=1}^{m}A_jg_j(t)\ ,\qquad(2.30)$$

where

$$\begin{aligned}g_j(t)&=\mathcal{L}^{-1}\left\{\frac{1}{p+\alpha_j}\right\}\circledast v(t)H(t-t_0)\ ,\\&=\frac{d}{dt}\int_0^t\frac{1}{\alpha_j}(1-\varepsilon^{-\alpha_j\tau})v(t-\tau)H(t-t_0-\tau)\,d\tau\ ,\\&=\int_0^{t}\varepsilon^{-\alpha_j\tau}v(t-\tau)H(t-t_0-\tau)\,d\tau\ ,\\&=\int_0^{t-t_0}\varepsilon^{-\alpha_j\tau}v(t-\tau)\,d\tau\ ,\end{aligned}$$

and putting $t=n\Delta t$ in the above equation, gives

$$q_j'(n\Delta t) = \int_0^{n\Delta t - t_0} \varepsilon^{-\alpha_j \tau} v(n\Delta t - \tau)\, d\tau .$$

By utilizing the procidure deriving Eq. (2.17) from Eq. (2.14) the above equation is transformed to

$$q_j'(n\Delta t) = \{ \tfrac{1}{2} v(n\Delta t) + v(\overline{n-1}\Delta t)\varepsilon^{-\alpha_j \Delta t} + \cdots\cdots\cdots + v(\Delta t + t_0)\varepsilon^{-\alpha_j (n-1)\Delta t} + \tfrac{1}{2} v(t_0)\varepsilon^{-\alpha_j n\Delta t} \}\Delta t . \qquad (2.31)$$

Similarly when $t = (n-1)\Delta t$, Eq. (2.31) is changed to

$$q_j'(\overline{n-1}\Delta t) = \{ \tfrac{1}{2} v(\overline{n-1}\Delta t) + v(\overline{n-2}\Delta t)\varepsilon^{-\alpha_j \Delta t} + \cdots\cdots\cdots + v(\Delta t + t_0)\varepsilon^{-\alpha_j (n-2)\Delta t} + \tfrac{1}{2} v(t_0)\varepsilon^{-\alpha_j \overline{n-1}\Delta t} \}\Delta t . \qquad (2.32)$$

From Eq.s (2.31) and (2.32) we can obtain the next recurrence formula of $q_j'(t)$,

$$q_j'(n\Delta t) = \tfrac{1}{2}\{ v(n\Delta t) + v(\overline{n-1}\Delta t)\varepsilon^{-\alpha_j \Delta t} \}\Delta t + q_j'(\overline{n-1}\Delta t)\varepsilon^{-\alpha_j \Delta t} .$$

Substituting $t = n\Delta t$ and $t - \Delta t = (n-1)\Delta t$ into above equation yields

$$q_j'(t) \simeq \tfrac{1}{2}\{ v(t) + v(t-\Delta t)\varepsilon^{-\alpha_j \Delta t} \}\Delta t + q_j'(t-\Delta t)\varepsilon^{-\alpha_j \Delta t}, \quad t > t_0 , \qquad (2.33)$$

$$q_j'(t) = 0, \quad 0 \le t \le t_o . \qquad \Big\rfloor$$

And with the same way $\mathcal{L}^{-1}\{Z(p)\} \circledast i(t)H(t-t_o)$ can be transformed to the similar equations to Eq.s (2.23).

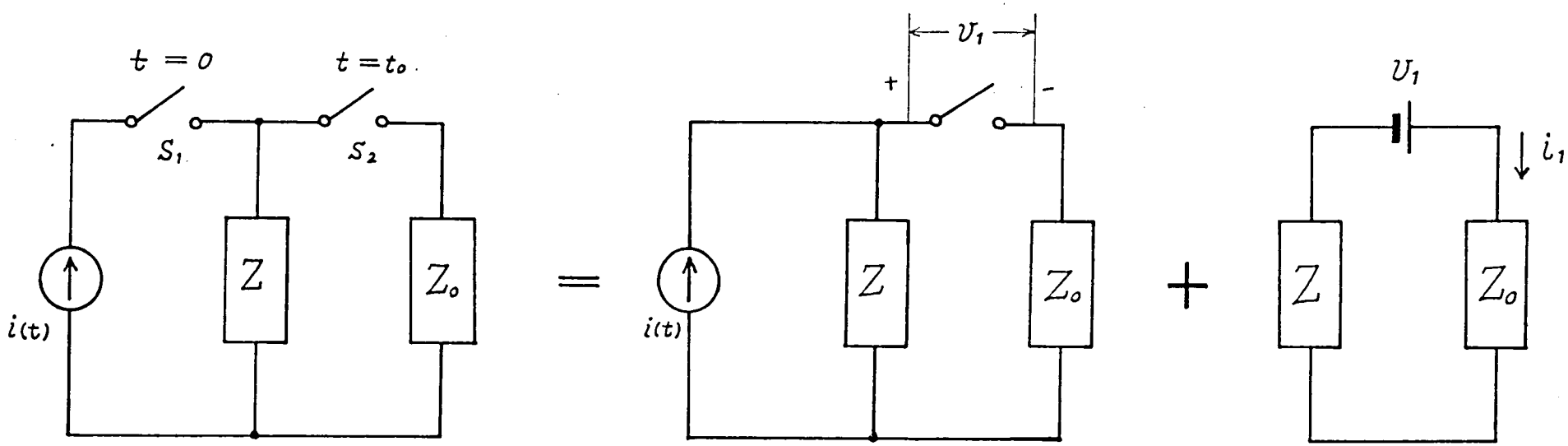

Fig. 2.3 The circuit whose composition changes in progress of transient phenomena.

2.5 Treatment of Transition Point Having Arrester

The method calculating the node voltage at the transition point having arrester as shown in Fig. 2.4 is investigated here. Now, in this figure the node voltage v_a, when the surge voltage e arrives at the node from left side of the line, is given by

$$v_a = v_{ao} - W i_a \tag{2.34}$$

where

$v_{ao} = F e$: the node voltage when the line has no arrester,

$F = \frac{2Z_2}{Z_1 + Z_2}$: refraction coefficient,

$W = \frac{Z_1 Z_2}{Z_1 + Z_2}$

i_a : arrester current.

On the other hand, from the arrester voltage-current characteristics, we have

$$v_a = C_0 i_a^m , \tag{2.35}$$

where C_0 and m are constants. Then from Eq.s (2.34) and (2.35), we have

$$C_0 i_a^m + W i_a - v_{a0} = 0 \tag{2.36}$$

Hence the voltage of the node having arrester can be calculated as illustrated in Fig. 2.5. Namely we can calculate the current i_a by Eq. (2.36), and using the value of this current i_a, we can do the node voltage by Eq. (2.34) or (2.35). And since m in Eq. (2.36) is not an integer generally, we use Regula Falsi Method in Scientific Subroutine Library of FACOM 230-60, in order to obtain the root of the equation.

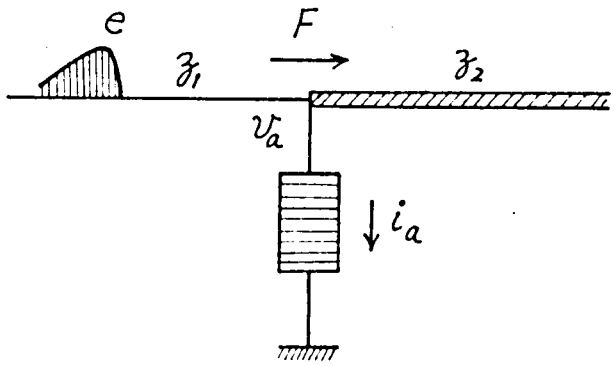

Fig. 2.4 Transition point having arrester.

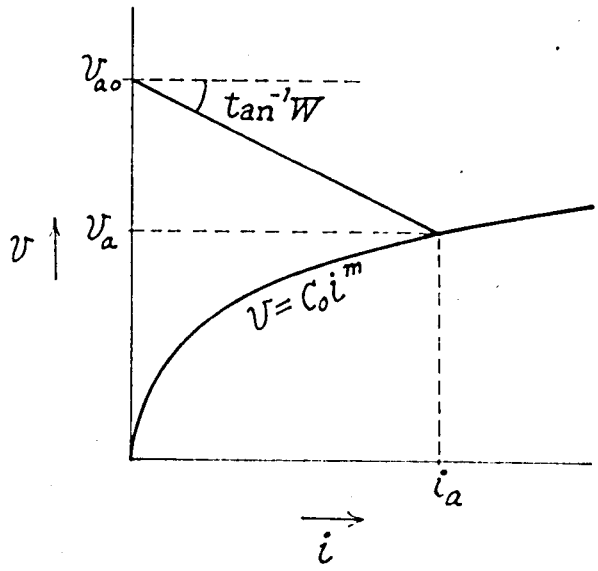

Fig. 2.5 Graphical analysis for arrester circuit.

CHAPTER 3

APPLICATION OF NUMERICAL CALCULATION DERIVED IN CHAPTER 2 TO SURGE PERFORMANCES IN VARIOUS ELECTRIC POWER NETWORKS

3.1 Introduction

In the preceding chapter the author has presented a new numerical calculation of surge performances in electric power networks utilizing convolution integral, so in this chapter he applies this method to the analysis of the surge performances on the four examples of practical systems.

First, he analyzes the surges on the overhead distribution system having the distributed pole transformers. The simple theoritical analyses of surge performances on such a system can be seen in the L.V.Bewley's writings[12] and others.[22] However they have calculated the values of the transient voltages at the primary terminals of the transformers by means of only the successive refracted voltage waves in the case, where the so-called equivalent capacitances of the transformers is considered, which are decided by the distributed capacitances in

the transformers own. And they have ignored the grounding resistances of the transformers, the various reflected waves which are arisen at the transformer terminals and so forth.

So he investigates the influences of equivalent capacitance and grounding resistance of pole transformer and the front duration of the incident wave on the primary terminal voltages of the transformers.

Next the surge performances on the transmission systems due to lightning stroke against the overhead ground wire are analyzed. This problem has been studied by many researchers[9],[11],[23] for a long time, and mainly they have tried to make clear the surge performances on the overhead ground wire including transmission towers and their analytical investigations have been done with the theoretical expressions or the surge simulator, etc. However the analysis considering the effects of the tower and tower foot on surges is very troublesome and so generally the analysis is carried out by using the equivalent circuit method, for example, by replacing the tower with a proper constant resistance determined by the tower impedance, the tower inductance or the parallel circuit of the resistance and inductance. The author also introduces the theoretical expressions and the digital calculation[18] of the surge for our system.

Then after calculating the voltage rise of the lightning stroke point and the 1st tower which is nearest to the point, he investigates the effects the values of the equivalent tower impedances, the duration of the wave front of lightning stroke current and the length of span on the tower voltage rises.

And he discusses when back flashover at the line or the tower will happen.

Thirdly by the new calculation presented in Chapter 2 he analyzes again the surge performances on overhead line-cable system[5] which has been discussed in Chapter 1 and compares the results with the ones calculated by the accurate solutions which have been got in Chapter 1. Moreover he performs the numerical calculation in the case where the skin effect of the cable is considerd by using the method which has been introduced in Section 2.3.

Lastly as the fourth example, one application of the method which has been introduced in Section 2.5 is described. Now, in order to protect the insulation of the machines and apparatuses in the station or the substation from the abnormal voltages caused by the outer or inner lightning surges which occur in the power system, the arrester is used usually and widely. For the abnormal voltage counterplan at the station and the substation, the problem of insulation coordination[24],[25] with the protective devices, for example the arrester and the grounding wire, etc. becomes very important. Especially the problems, which are concerned with the protection against the overvoltages in the substation connected to overhead lines by a length of cable and the fitted place of the arresters, have been investigated by many pioneers.[1]~[4],[26] Also recently the 140kV cables have been newly laid under the city center with the expansion of the power system within the big city.

So here the author investigates the effect of the arrester

on the abnormal voltage rises of the overhead line-cable system simulating the substation one due to the lightning stroke at the tower near the cable end, which is one of the important problems to be clarified for the lightning proof design of the substation system. Namely he persues the surge performances in the case when one tower of the overhead line-cable system, with whose junction point a lightning arrester is fitted up, is struck by lightning. In this case, he assumes that the back flashover happenes as soon as the tower voltage exceedes the insulator breakdown voltage. In this connect, for the case where the circuit composition changes in progress of transient phenomena, the method which has been introduced in Section 2.4 is utilized. With the calculated results, the effect of the lightning arrester and the possibility of insulation breakdown of the cable are discussed.

As mentioned above the author picks up the four examples, and shows that the calculation, which has been introduced in the preceding chapter, can be applied simply and usefully to those. It is thought that these computation results give many available data for the lightning-proof design of transmission or distribution systems.

3.2 Surges on Overhead Distribution Line Having Distributed Pole Transformers

3.2.1 Numerical Calculation

It is very important to investigate the surge performances on overhead distribution line having the distributed pole transformers for the lightning protection of pole transformers. Therefore in this article we will analyze the surges on the systems shown in Fig. 3.1(a) and it is assumed that the primary terminals of a transformer are connected to the overhead three-phase distribution line in the lump and the secondery terminals are grounded with the tank. In the figure

$e(t)$: voltage of a incoming wave,

$\mathcal{Z}_0$: zero-phase impedance of the three-phase distribution line,

C_0 and R_0 : equivalent capacitance and grounding resistance of the transformer,

ℓ : line length between two transformers,

T : propagation time of traveling waves between two transformers.

Fig. 3.1(b) is a flow graph of this system in the case

where the $(n+1)$ transformers are distributed along the line of a finite length.

The numbering rule in the flow graph dosen't satisfy the rule explained in Chapter 2, but for convenience we use the special numbering rule, which decreases the number of equations and makes the repeating calculation easy.

The refraction coefficient at the junction point of every transformer is given by

$$F = M\left(1 + \frac{\beta - \alpha}{\beta + \alpha}\right), \tag{3.1}$$

where

$$M = \frac{2R_0}{2R_0 + Z_0}, \quad \alpha = \frac{2}{C_0(2R_0 + Z_0)}, \quad \beta = \frac{1}{C_0 R_0}. \tag{3.2}$$

The voltage equations at the nodes in the flow graph are given by the following ones

$$\left.\begin{aligned} &e(t) = E_0(1 - \varepsilon^{-\alpha_0 t}), \\ &v_{2r-1}(t) = v_{2n+2r-1}(t-T), \\ &v_{2r}(t) = v_{2n+2r}(t-T), \\ &q_0(t) = \frac{1}{2}\{e(t) + e(t-\Delta t)\varepsilon^{-\alpha\Delta t}\}\Delta t \\ &\qquad + q_0(t-\Delta t)\varepsilon^{-\alpha\Delta t}, \end{aligned}\right\} \quad r = 1, 2, \cdots, n$$

$$
\left.
\begin{aligned}
&g_2(t) = \frac{1}{2}\{v_2(t) + v_2(t-\Delta t)\varepsilon^{-\alpha\Delta t}\}\Delta t \\
&\qquad + g_2(t-\Delta t)\varepsilon^{-\alpha\Delta t}, \\
&v_{4n+1}(t) = M[e(t) + v_2(t) + (\beta-\alpha)\{g_0(t) + g_2(t)\}], \\
&\left.
\begin{aligned}
&g_{2r-1}(t) = \frac{1}{2}\{v_{2r-1}(t) + v_{2r-1}(t-\Delta t)\varepsilon^{-\alpha\Delta t}\}\Delta t \\
&\qquad + g_{2r-1}(t-\Delta t)\varepsilon^{-\alpha\Delta t}, \\
&g_{2r+2}(t) = \frac{1}{2}\{v_{2r+2}(t) + v_{2r+2}(t-\Delta t)\varepsilon^{-\alpha\Delta t}\}\Delta t \\
&\qquad + g_{2r+2}(t-\Delta t)\varepsilon^{-\alpha\Delta t}, \\
&v_{4n+r+1}(t) = M[v_{2r-1}(t) + v_{2r+2}(t) \\
&\qquad + (\beta-\alpha)\{g_{2r-1}(t) + g_{2r+2}(t)\}],
\end{aligned}
\right\} r = 1, 2, \cdots, n-1 \\
&g_{2n-1}(t) = \frac{1}{2}\{v_{2n-1}(t) + v_{2n-1}(t-\Delta t)\varepsilon^{-\alpha\Delta t}\}\Delta t \\
&\qquad + g_{2n-1}(t-\Delta t)\varepsilon^{-\alpha\Delta t}, \\
&v_{5n+1}(t) = M\{v_{2n-1}(t) + (\beta-\alpha)g_{2n-1}(t)\}, \\
&\left.
\begin{aligned}
&v_{2n+2r-1}(t) = v_{4n+r}(t) - v_{2r}(t), \\
&v_{2n+2r}(t) = v_{4n+r+1}(t) - v_{2r-1}(t).
\end{aligned}
\right\} r = 1, 2, \cdots, n
\end{aligned}
\right\} \quad (3.3)
$$

Then we can calculate each node voltage by the above equations in order.

3.2.2 Calculated Results and Discussions

In this article, by using the equations obtained in Article 3.2.1 the author solves the various numerical examples and investigates the influences of the equivalent capacitance C_0 and the grounding resistance R_0 of the transformer on the primary terminal voltages. The values of system constants used in the numerical computation are got from the experimental results of the Okubo Distribution Line[27] of the Kansai Electric Power Company and are presented in Table 3.1.

Fig. 3.2 shows the wave forms of the primary terminal voltages of the 1st, 5th and 10th transformers for the four cases where

$$R_0 = 25\ \Omega,\quad C_0 = 1000\ pF,\quad e : E_0 = 1\,(1 \times \infty\,\mu s),$$

$$R_0 = 25\ \Omega,\quad C_0 = 1500\ pF,\quad e : E_0 = 1\,(1 \times \infty\,\mu s),$$

$$R_0 = 25\ \Omega,\quad C_0 = 1000\ pF,\quad e : E_0 = 1\,(2 \times \infty\,\mu s),$$

$$R_0 = 25\ \Omega,\quad C_0 = 1500\ pF,\quad e : E_0 = 1\,(2 \times \infty\,\mu s).$$

From the figure we can see that the more the transformers are away from the sending end the more slowly the primary terminal voltages of the transformers rise in every case. However we see that the final values of the voltages finally becomes the same ones judging from the character of equivalent circuit of a transformer. With respect to the influence of the front duration of incoming wave on primary terminal voltage of each transformer, the shorter the front duration is, the sharper the

initial slope of the voltage wave form becomes, but the values of the final voltages are the same in any case as previously described.

Next let us investigate the influence of equivalent capacitance C_0 on the primary terminal voltages. The initial slopes of the voltage wave forms in the case, where the value of C_0 is small are sharper than the ones in the case where it is large and the final values of the voltages in the former case are higher than the ones in the latter case. Thus since the value of C_0 give a great influence on the terminal voltage of transformer, we must know the value of the equivalent capacitance of the transformer as accurately as possible in practical problems.

Fig. 3.3 shows the primary terminal voltages of the 1st, 5th and 10th transformers in three cases where

$$R_0 = 5\ \Omega, \quad C_0 = 1000\ pF, \quad e : E_0 = 1\ (1 \times \infty\ \mu s),$$

$$R_0 = 25\ \Omega, \quad C_0 = 1000\ pF, \quad e : E_0 = 1\ (1 \times \infty\ \mu s),$$

$$R_0 = 100\ \Omega, \quad C_0 = 1000\ pF, \quad e : E_0 = 1\ (1 \times \infty\ \mu s).$$

From the figure we can see that the initial slopes of the voltages become a little more gentle when the value of the grounding resistance R_0 becomes larger, and so this value has not so much influences on wave forms.

Next the author compares the result of numerical calculation of the first refracted voltage wave form at the 10th

transformer with the one calculated from the accurate analytical solution of the voltage. These two wave forms coincide with each other very well, for example the value of the former voltage at $t=4.0\,\mu s$ is 0.766 and that of the latter is 0.765. From this fact, we can see that the author's method of calculation has a high accuracy. Moreover already Umoto[27] has introduced the theoretical analysis of the surges on the overhead distribution line having the distributed pole transformers by using the lattice diagram method. The numerical calculation by the method is very troublesome and needs a lot of calculating time. This weakness could have been settled by the origination of the author's method.

Table 3.1 Values of constants used in computations in Section 3.2.

Incoming voltage wave	$e(t): E_0 = 1 (1\times\infty\mu s, 2\times\infty\mu s)$
Zero-phase surge impedance of overhead line	$z_0 = 355\ \Omega$
Equivalent capacitance of transformer	$C_0 = 1000\,pF, 1500\,pF$
Grounding resistance of transformer	$R_0 = 5\Omega, 25\Omega, 100\Omega$
Span length	$\ell = 45\ m$
Propagation time	$T = 0.15\ \mu s$
Number of transformers	$n+1 = 21$
Time interval	$\Delta t = 0.01\ \mu s$

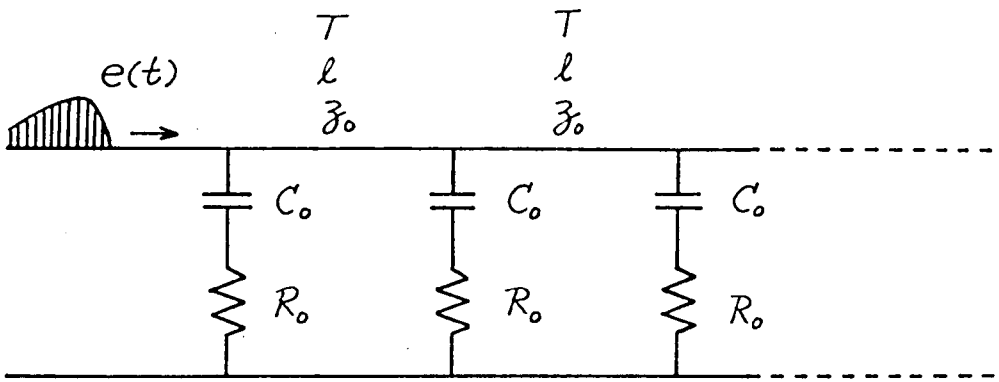

(a) Power system.

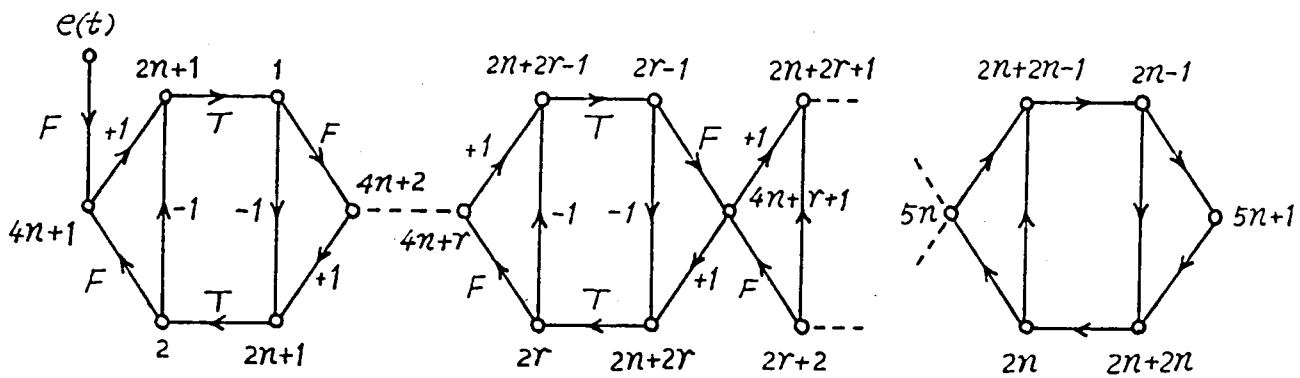

(b) Flow graph.

Fig. 3.1 Illustration of overhead distribution line system having distributed transformers.

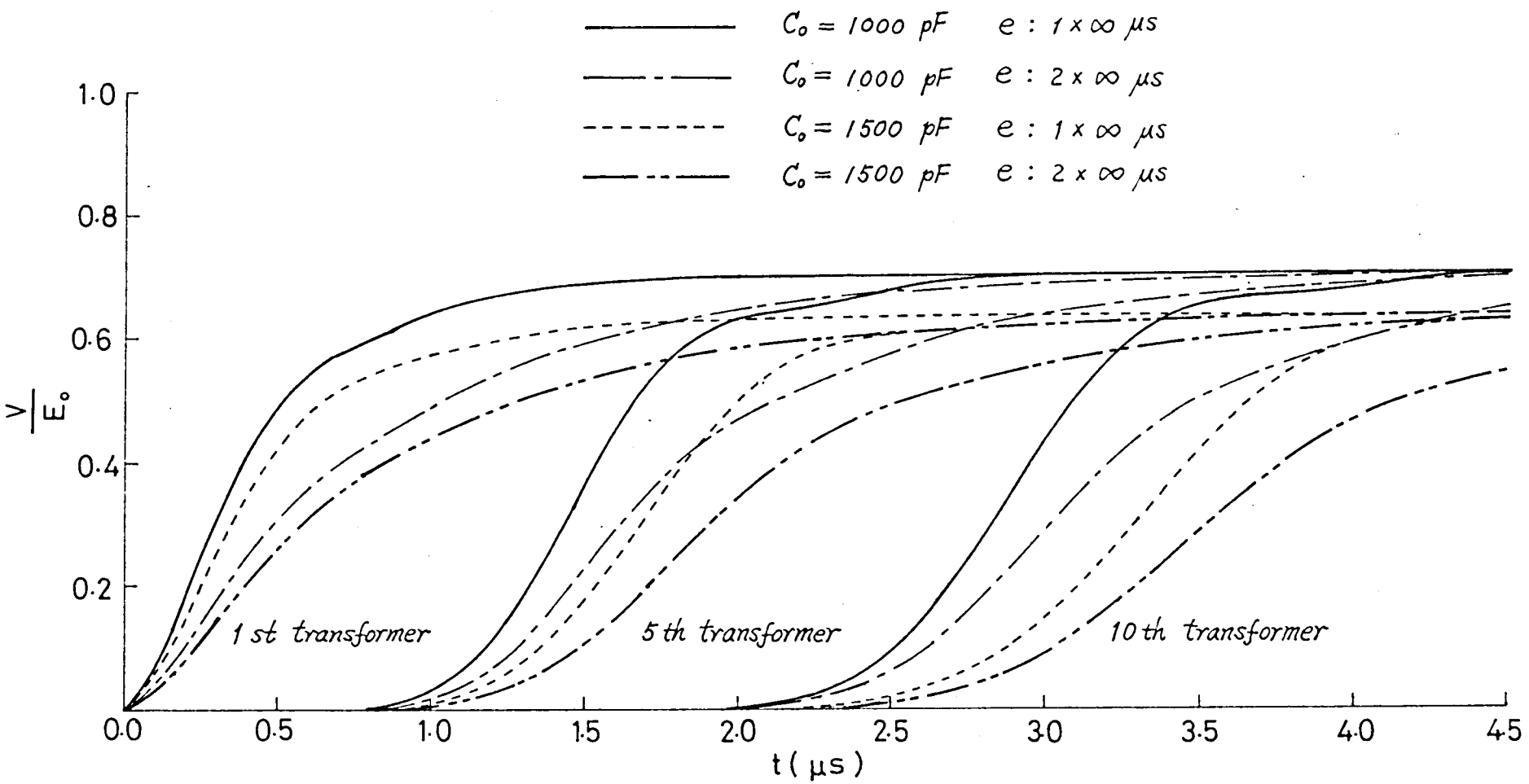

Fig. 3.2 Primary transient voltages of 1st, 5th and 10th transformers.

(C_o, e : variable, R_o= 25Ω)

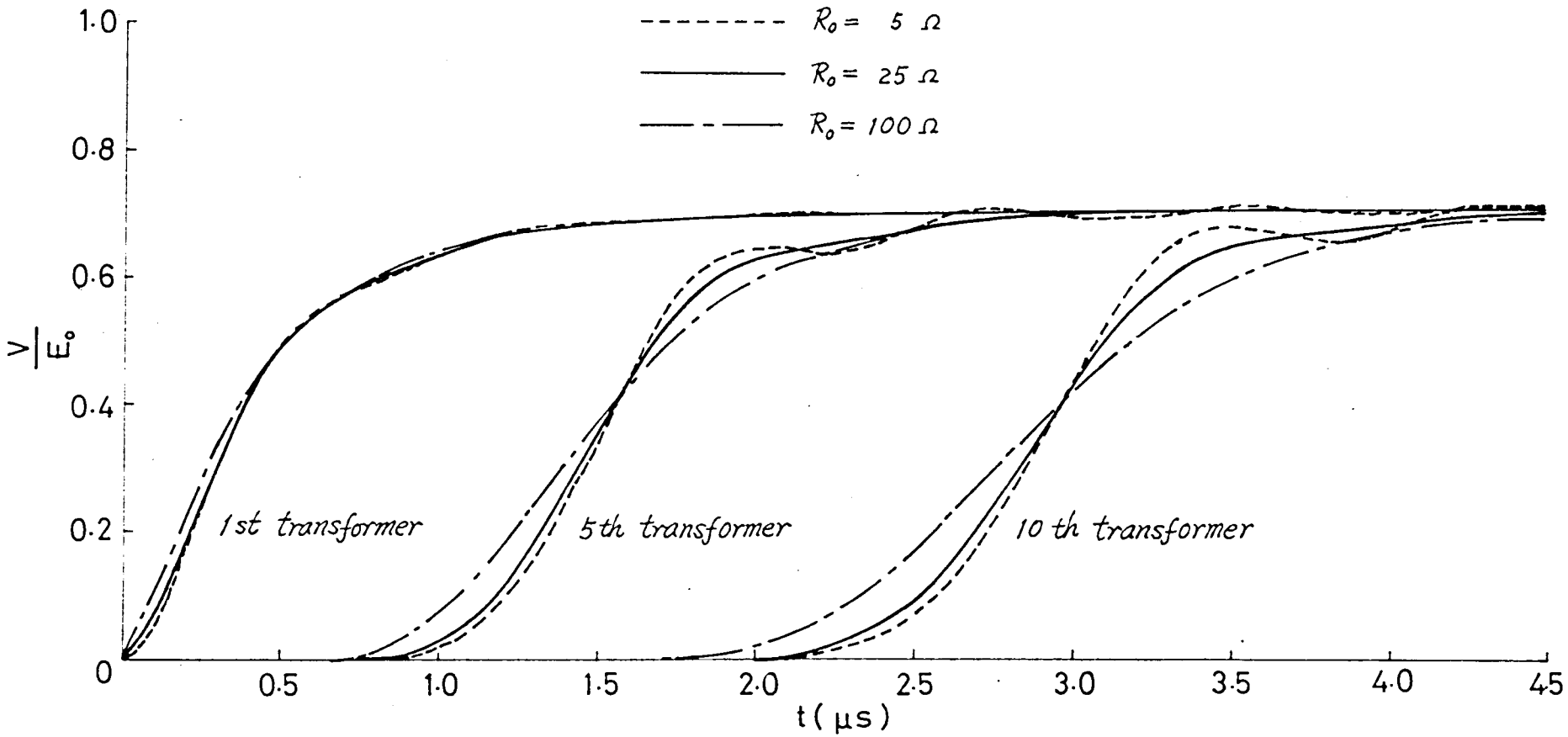

Fig. 3.3 Primary transient voltages of 1st, 5th and 10th transformers.

(R_0 : variable, $C_0 = 1000\ pF$, $e(t): E_0 = 1\ (1 \times \infty \mu s)$)

3.3 Surges on Transmission Systems Due to Lightning Stroke on Overhead Ground Wire

3.3.1 Numerical Calculation

In this section let us analyze the transient voltage rises of the lightning stroke point and tower in the case where the lightning strikes at overhead ground wire of the transmission systems as shown in Fig. 3.4(a). We adopt the equivalent circuit of a tower as shown in Fig. 3.4(c), which has been decided experimentally and theoretically for the tower of some 140kV transmission systems by Tanaka[28] and Okamura.[29] In Fig.s (3.4) (a) and (c)

$i(t)$: lightning stroke current,

Z_g : surge impedance of ground wire,

Z_0 : stroke channel impedance,

l : span length,

τ : propagation time of traveling waves on one span,

R_T : resistance to decide initial value of tower impedance,

L_T : equivalent tower inductance,

R_E : resistance to decide initial value of surge impedance of tower foot with counterpoise,

L_E : equivalent inductance of tower foot with counterpoise,

R_G : grounding resistance.

Now let us assume that the lightning strikes at the center of the span on the ground wire. The flow graph of right half side of the system in the case where n towers line up on both sides of the lightning stroke point is presented in Fig. 3.4(b).

Now the input impedance Z and refraction coefficients F_0 and $F(p)$ in this figure are given by following equations

$$\left.\begin{aligned} Z &= \frac{Z_0}{2}\ , \\ F_0 &= \frac{2Z_0}{Z_0 + 2Z_0}\ , \\ F(p) &= M\left(1 + \frac{A_1}{p+\alpha_1} + \frac{A_2}{p+\alpha_2} + \frac{A_3}{p+\alpha_3}\right)\ . \end{aligned}\right\} \qquad (3.4)$$

In the above equations M, A_j, α_j $(j = 1,2,3)$ are the constants whose values are deriven from the next equations

$$\left.\begin{aligned} F(p) &= \frac{a_0p^3 + a_1p^2 + a_2p + a_3}{b_0p^3 + b_1p^2 + b_2p + b_3}\ , \\ &\text{where} \\ a_0 &= 2R_G L_T L_E C(R_T + R_E)\ , \end{aligned}\right\} \qquad (3.5)$$

$$
\begin{aligned}
a_1 &= 2l_T L_E(R_T + R_E + R_G) + 2R_T R_E R_G C(L_T + L_E),\\
a_2 &= 2R_E l_T(R_T + R_G) + 2R_T R_E(R_E + R_G),\\
a_3 &= 2R_T R_E R_G,\\
b_0 &= R_G L_T L_E C(2R_T + 2R_E + \beta_g),\\
b_1 &= L_T L_E(2R_T + 2R_E + 2R_G + \beta_g)\\
&\quad + R_T R_G L_E C(2R_E + \beta_g) + R_E R_G L_T C(2R_T + \beta_g),\\
b_2 &= R_E L_T(2R_T + 2R_G + \beta_g)\\
&\quad + R_T L_E(2R_E + 2R_G + \beta_g) + R_T R_E R_G C\beta_g,\\
b_3 &= R_T R_E(2R_G + \beta_g).
\end{aligned}
$$

The voltage equation for each node of the flow graph in Fig. 3.4(b) is given as follows:

$$
\begin{aligned}
&i(t) = I_0(1 - \varepsilon^{-\alpha_0 t})\\
&v_1(t) = v_{2n+1}(t - T/2)\\
&v_2(t) = v_{2n+2}(t - T/2)\\
&v_{2r-1}(t) = v_{2n+2r-1}(t - T)\\
&v_{2r}(t) = v_{2n+2r}(t - T)\\
&v_{4n+1}(t) = Z\,i(t) + 2F_0 v_2(t)\\
&q_{j,2r-1}(t) = \frac{1}{2}\{v_{2r-1}(t) + v_{2r-1}(t-\Delta t)\varepsilon^{-\alpha_j \Delta t}\}\Delta t\\
&\qquad\qquad + q_{j,2r-1}(t-\Delta t)\varepsilon^{-\alpha_j \Delta t}, \qquad r = 1, 2, \cdots, n-1
\end{aligned}
\tag{3.6}
$$

$$
\left.
\begin{aligned}
g_{j,2r+2}(t) &= \frac{1}{2}\{v_{2r+2}(t) + v_{2r+2}(t-\Delta t)\varepsilon^{-\alpha_j \Delta t}\}\Delta t \\
&\quad + g_{j,2r+2}(t-\Delta t)\varepsilon^{-\alpha_j \Delta t}, \\
v_{4n+2r+1}(t) &= M\{v_{2r-1}(t) + v_{2r+2}(t) \\
&\quad + \sum_{j=1}^{3} A_j \{g_{j,2r-1}(t) + g_{j,2r+2}(t)\}\},
\end{aligned}
\right\} j=1,2,3
$$

$$
\left.
\begin{aligned}
g_{j,2n-1}(t) &= \frac{1}{2}\{v_{2n-1}(t) + v_{2n-1}(t-\Delta t)\varepsilon^{-\alpha_j \Delta t}\}\Delta t \\
&\quad + g_{j,2n-1}(t-\Delta t)\varepsilon^{-\alpha_j \Delta t}, \\
v_{5n+1}(t) &= M\{v_{2n-1}(t) + \sum_{j=1}^{3} A_j\, g_{j,2n-1}(t)\},
\end{aligned}
\right\} j=1,2,3
$$

$$
\left.
\begin{aligned}
v_{2n+2r-1}(t) &= v_{4n+r}(t) - v_{2r}(t), \\
v_{2n+2r}(t) &= v_{4n+r+1}(t) - v_{2r-1}(t).
\end{aligned}
\right\} r=1,2,\cdots,n
$$

Since the flow graph shown in Fig. 3.4(b) is concerned with only the right half side of the system shown in Fig. 3.4 (a), $v_2(t)$ is multiplied by 2 as shown in the above 6th equation in order to get the net value of $v_{4n+1}(t)$, considering the both side of the system.

3.3.2 Calculated Results and Discussions

Next Table 3.2 shows the values of constants used in

digital computation. We use the values which had been obtained by Okamura[77] for the values of the equivalent circuit elements of tower and these are devided into two groups, i.e., the one is the group containing $R_E = 10\,\Omega$ (A group) and the other is that doing $R_E = 20\,\Omega$ (B group). And these values are presented in Table 3.3. Fig. 3.5(a) and (b) show the transient impedances of tower foots with counterpoise belonging to each group. Moreover in the case of B group the values of α_1, α_2, A_1 and A_2 in Eq.s (3.4) become complex number.

Fig. 3.6 and Fig. 3.7 show the transient voltages at the lightning stroke point and the 1st tower, viz. either of the towers which stand on both side of the lightning stroke point respectively, in the case where A group is used for the equivalent circuit of tower, the span length $\ell = 300m$ and the lightning stroke current is the $1\times 50\,\mu s$ wave. In the case where B group is used for the equivalent circuit of tower, span length $\ell = 200m$ and the lightning stroke current is the $2\times 50\,\mu s$ wave, the similar transient voltages are shown in Fig. 3.8 and Fig. 3.9. Next in Table 3.4 the maximum voltages at the lightning stroke point and the 1st tower in each case are shown.

Next let us discuss the influences of the tower-foot impedance with counterpoise, span length and the wave form of lightning stroke current on the lightning stroke point and tower voltage rises.

(i) Tower impedance with counterpoise:

In Fig. 3.6 we plot the transient voltage at the lightning stroke point in the case, where only the equivalent tower

impedance is considered, by the dotted line. From Fig.s 3.6 and 3.8 we can see that the rising portions of the voltages at the lightning stroke point are scarcely influenced by the tower foot impedance with counterpoise, and hence the possibility of back flashover between ground wire and line conductors is same in any case. And we can see from Fig.s 3.7 and 3.9 that the larger the tower foot impedance becomes the higher the voltage rise of the 1st tower and consequently the possibility of back flashover at tower do.

Conjecturing from these results, in order to decrease the possibility, we should reduce the values of not only the stationary grounding resistance but also the transient impedance of tower foot with counterpoise.

(ii) Span length:

In Fig.s 3.10 and 3.11, we plot the transient voltages at the lightning stroke point and the first tower, respectively, in the two cases where the span length ℓ= 200m and ℓ= 300m. We can see from Fig. 3.10 that the maximum values of the voltages at the lightning stroke point increase when span length does, and accordingly the possibility of the back flashover between ground wire and line conductors is guessed to become large, if the span length becomes longer. On the contrary, Fig. 3.11 shows that the transient voltages at the 1st tower suffer little influences of the span length.

(iii) Wave form of lightning stroke current:

In Fig. 3.12 we compare the transient voltages at the lightning stroke point in two cases where the lightning stroke

currents have the wave forms of $1\times\infty\ \mu s$ and $2\times\infty\ \mu s$. Next in Fig. 3.13 we make the same comparison of the transient voltages at the first tower. From Fig. 3.12 we can see that the sharper the initial slope of the lightning stroke current becomes, the higher the maximum value of the lightning stroke point voltage becomes. Therefore the shorter the duration of the wave front of the lightning stroke current becomes, the larger the possibility of the back flashover between tower and line conductors becomes. Next Fig. 3.13 indicates that the initial part of the 1st tower voltage is fairly affected by the duration of the wave front of the lightning stroke current but the subsequent part of the 1st tower voltage is little influenced by it, and therefore the possibility of back flashover at tower is almost identical for any duration of the wave front of the lightning stroke current unless it is occurred at the above-mentioned initial part.

Summarizing the above (i), (ii) and (iii), it is considered that the larger the tower foot impedance with counterpoise becomes, the longer the wave front duration of lightning stroke current becomes or the shorter the span length becomes, the larger the possibility of back flashover at the 1st tower becomes. And in the case of the opposite tendency it is considered that the back flashover may occur at lightning stroke point and if it does not occur at this point it will not occur at the tower too.

Table 3.2 Values of constants used in computations in Section 3.3.

Lightning stroke current	$i(t): I_o = 1$ ($1 \times \infty \mu s$, $2 \times \infty \mu s$)
Stroke channel impedance	$Z_o = 400\ \Omega$
Surge impedance of overhead ground wire	$Z_g = 550\ \Omega$
Span length	$\ell = 200\ m$, $300\ m$
Surge propagation time between span	$T = 0.68\ \mu s$, $1.0\ \mu s$
Time interval	$\Delta t = 0.02\ \mu s$

Table 3.3 Values of equivalent circuit constants of tower.

		R_T (Ω)	L_T (μH)	R_E (Ω)	L_E (μH)	R_G (Ω)	C ($\times 10^{-4}$ pF)
A	1	100	10	10	3	10	10.0
	2	100	10	10	27	20	6.4
	3	100	10	10	27	30	4.2
	4	100	10	10	27	40	3.2
B	1′	100	10	20	25	30	4.2
	2′	100	10	20	25	40	3.2
	3′	100	10	20	25	50	2.5
	4′	100	10	20	25	70	1.8

Table 3.4 Maximum voltages at lightning point and first tower.

Span length (m)			300	300	200	200
Lightning stroke current wave form (μs)			1×∞	2×∞	1×∞	2×∞
Maximum voltages at lightning point (V/I_0)			254	198	227	160
Maximum voltages at first tower (V/I_0)	A	1	8.0	7.8	7.8	7.5
		2	16.2	15.7	15.7	15.1
		3	22.2	21.5	21.3	20.5
		4	27.8	27.3	26.5	25.5
	B	1′	21.0	20.7	20.4	19.7
		2′	26.5	26.2	25.5	24.4
		3′	31.9	31.6	30.6	29.1
		4′	41.7	41.0	39.8	37.7

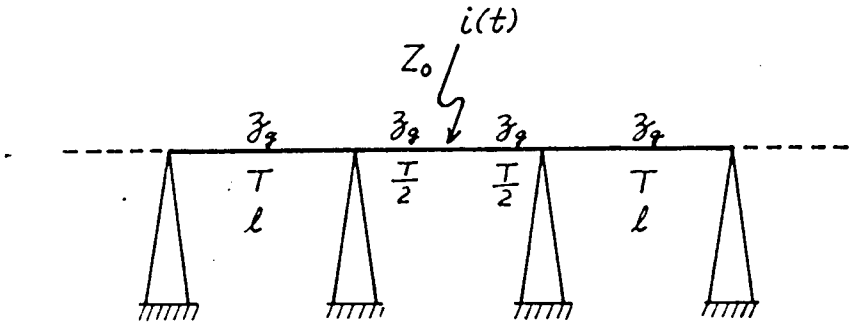

(a) Power system.

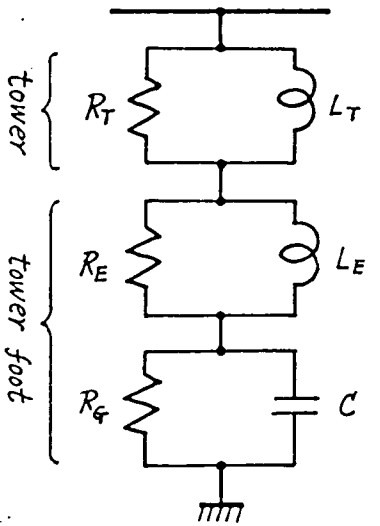

(c) Equivalent circuit of tower.

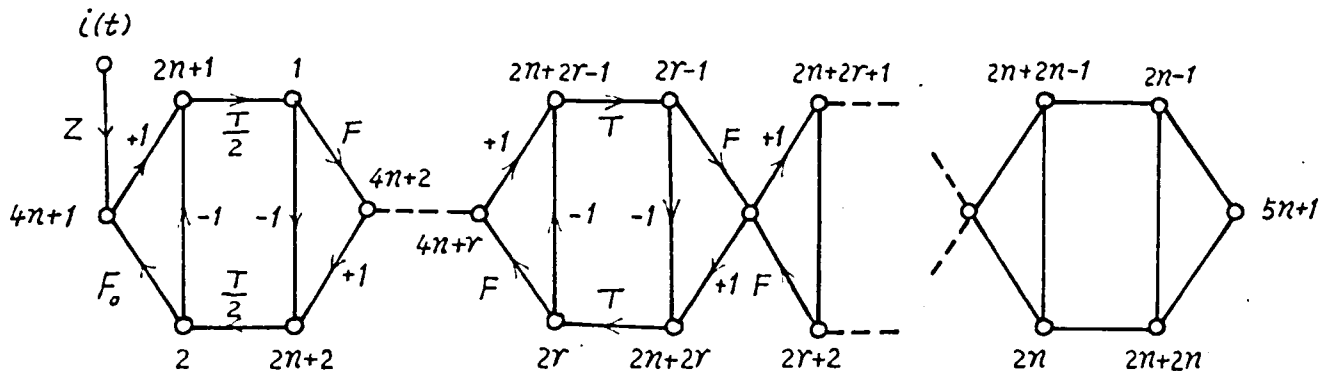

(b) Flow graph.

Fig. 3.4 Illustration of lightning stroke against overhead ground wire.

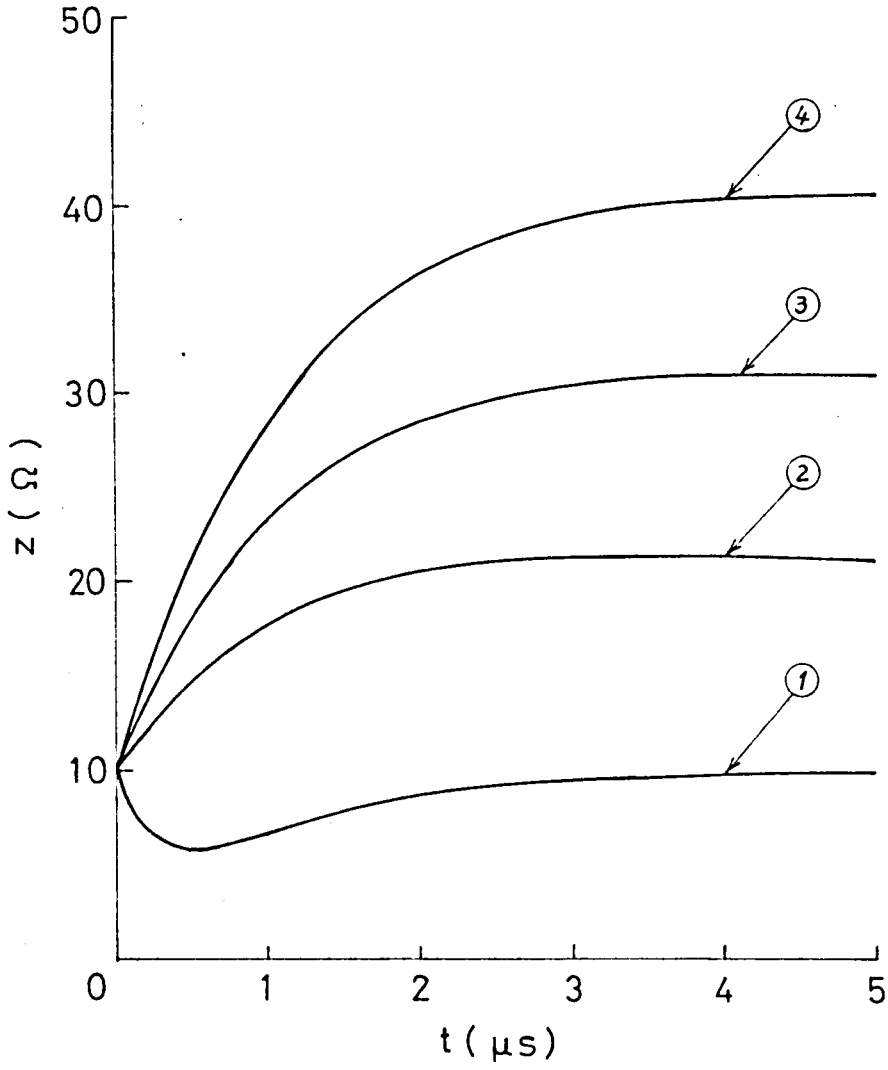

Fig. 3.5(a) Transient impedances of tower foots with counterpoise belonging to A group.

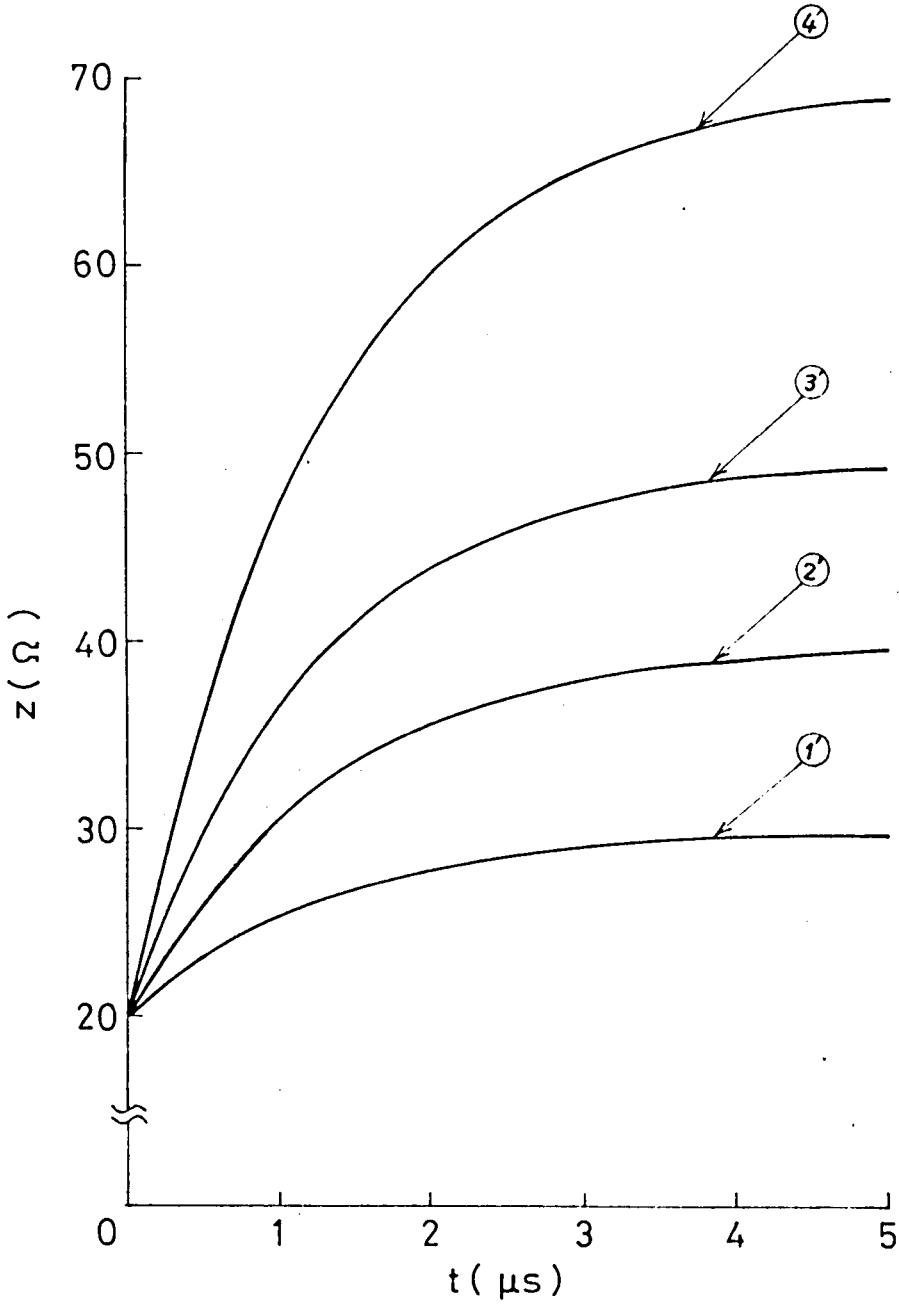

Fig. 3.5(b) Transient impedances of tower foots with counterpoise belonging to B group.

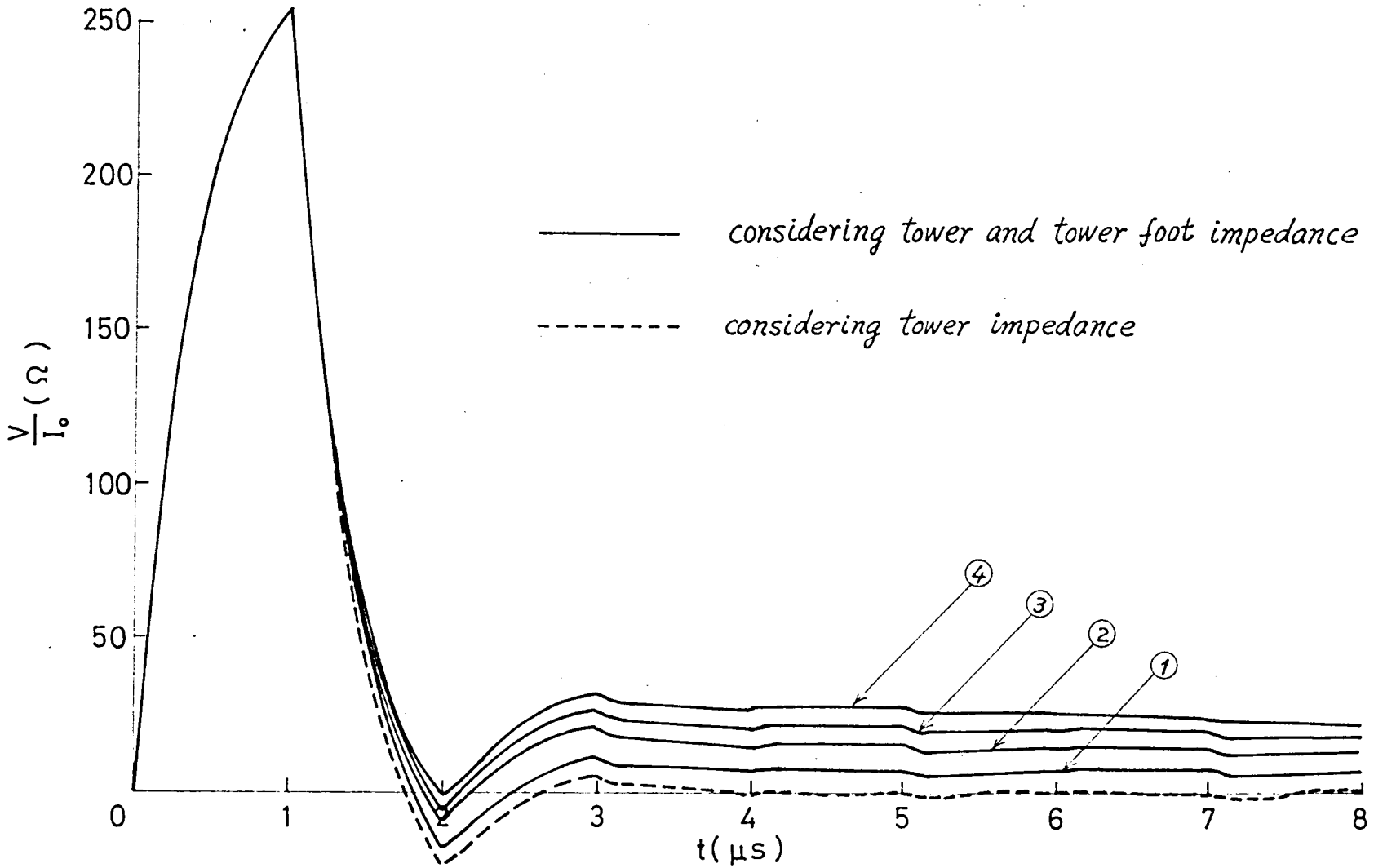

Fig. 3.6 Transient voltages at the lightning stroke point.

(Equivalent circuit of tower : A, $\ell = 300\,m$, $i(t)$: $I_0 = 1\,(1 \times \infty\,\mu s)$)

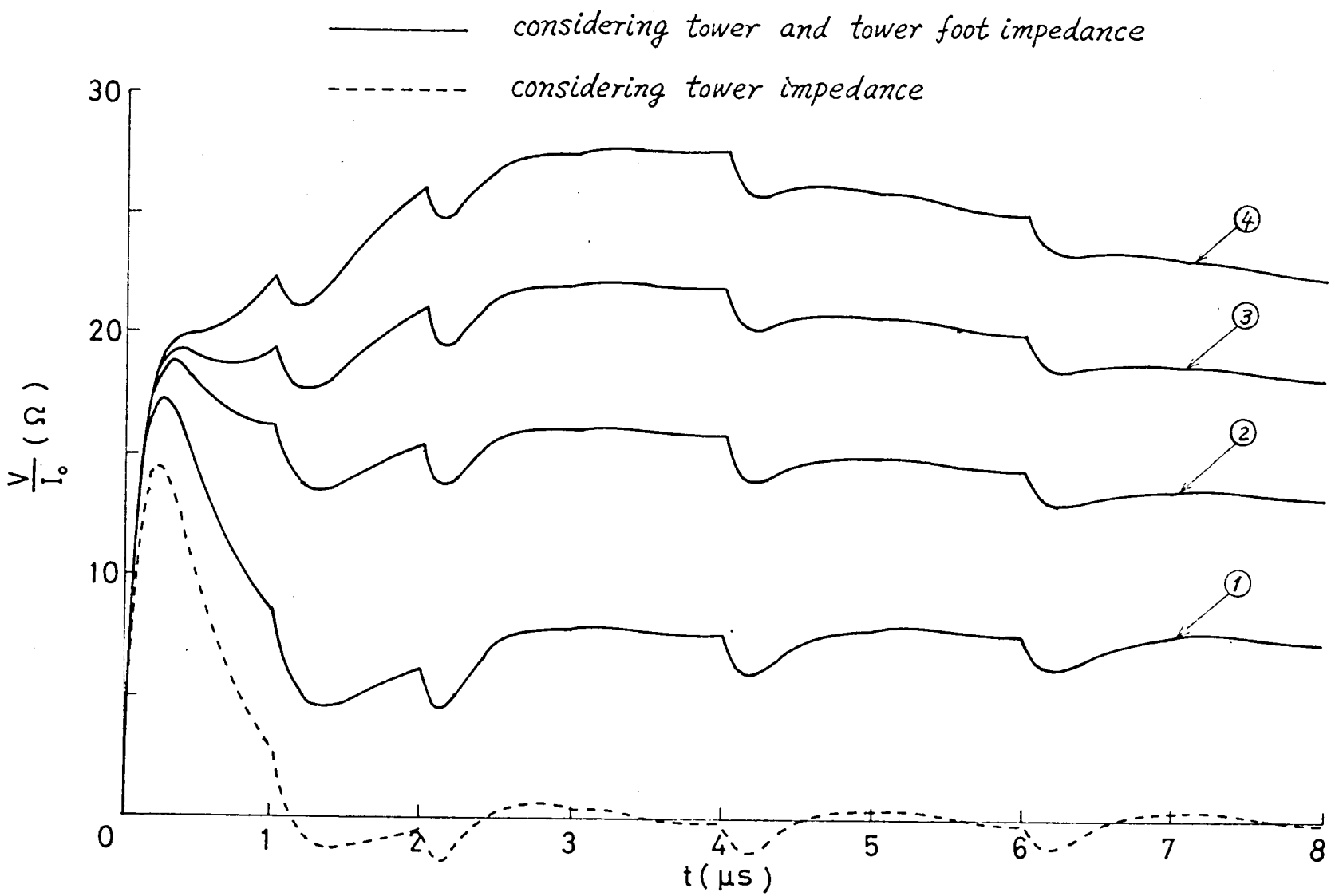

Fig. 3.7 Transient voltages at the 1st tower.

(Equivalent circuit of tower : A, $\ell = 300\,m$, $i(t): I_0 = 1\,(1 \times \infty\,\mu s)$)

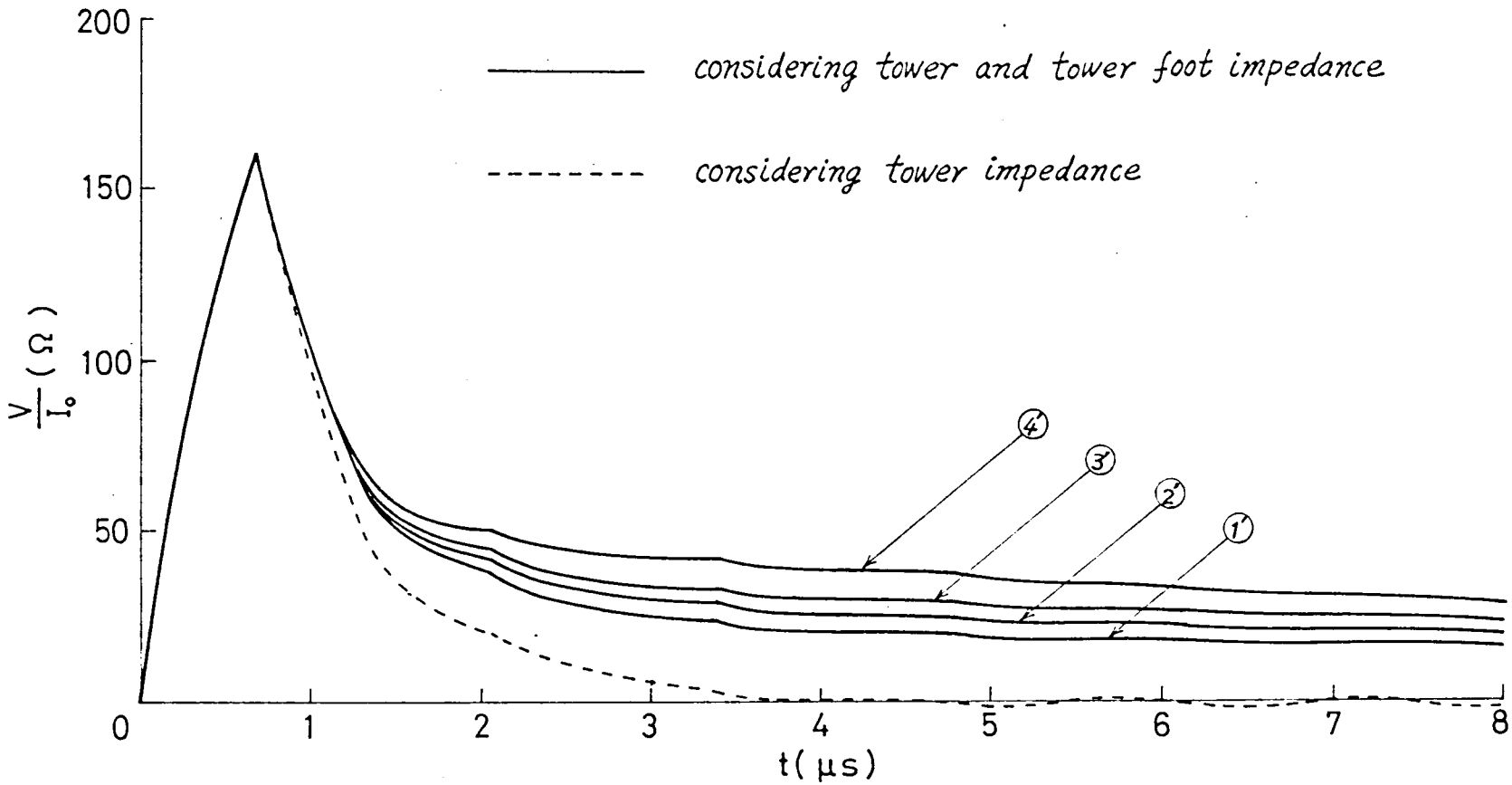

Fig. 3.8 Transient voltages at the lightning stroke point.

(Equivalent circuit of tower : B, $\ell = 200m$, $i(t): I_0 = 1(2\times\infty\mu s)$)

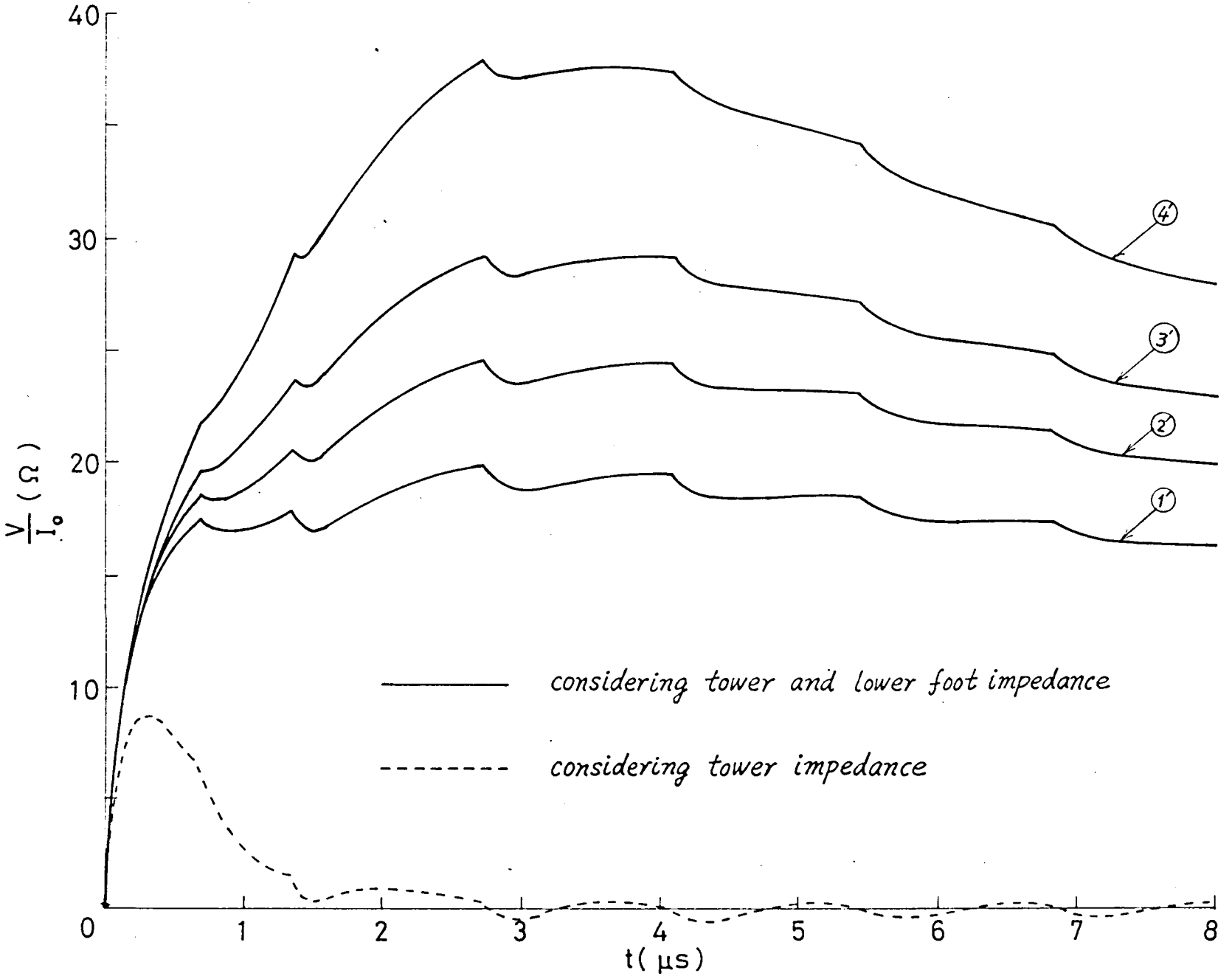

Fig. 3.9 Transient voltages at the 1st tower.

(Equivalent circuit of tower : B, $\ell = 200\,m$, $i(t): I_0 = 1(2\times\infty\mu s)$)

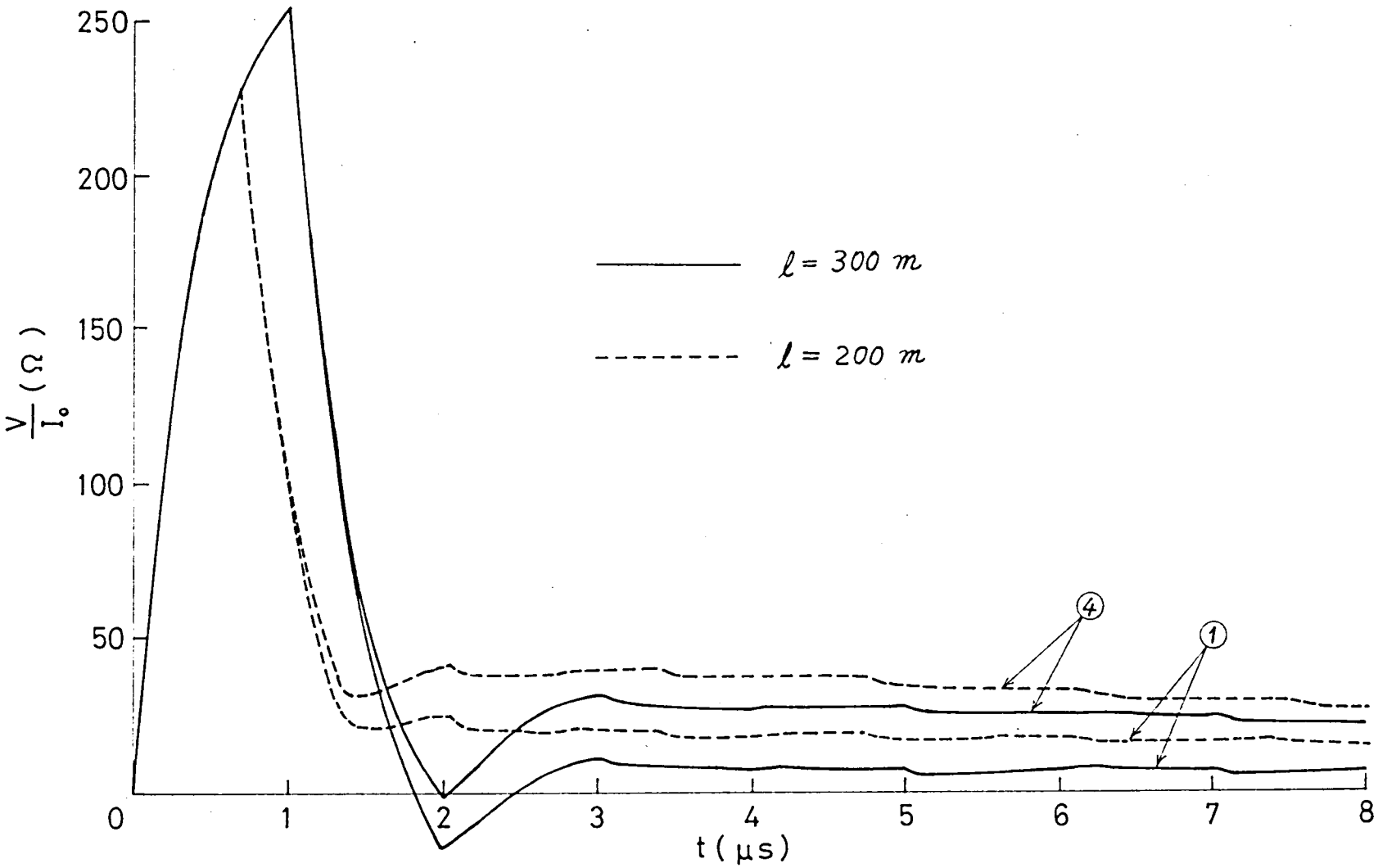

Fig. 3.10 Transient voltages at the lightning stroke point.

(Equivalent circuit of tower : A, $i(t): I_0 = 1 (1 \times \infty \mu s)$)

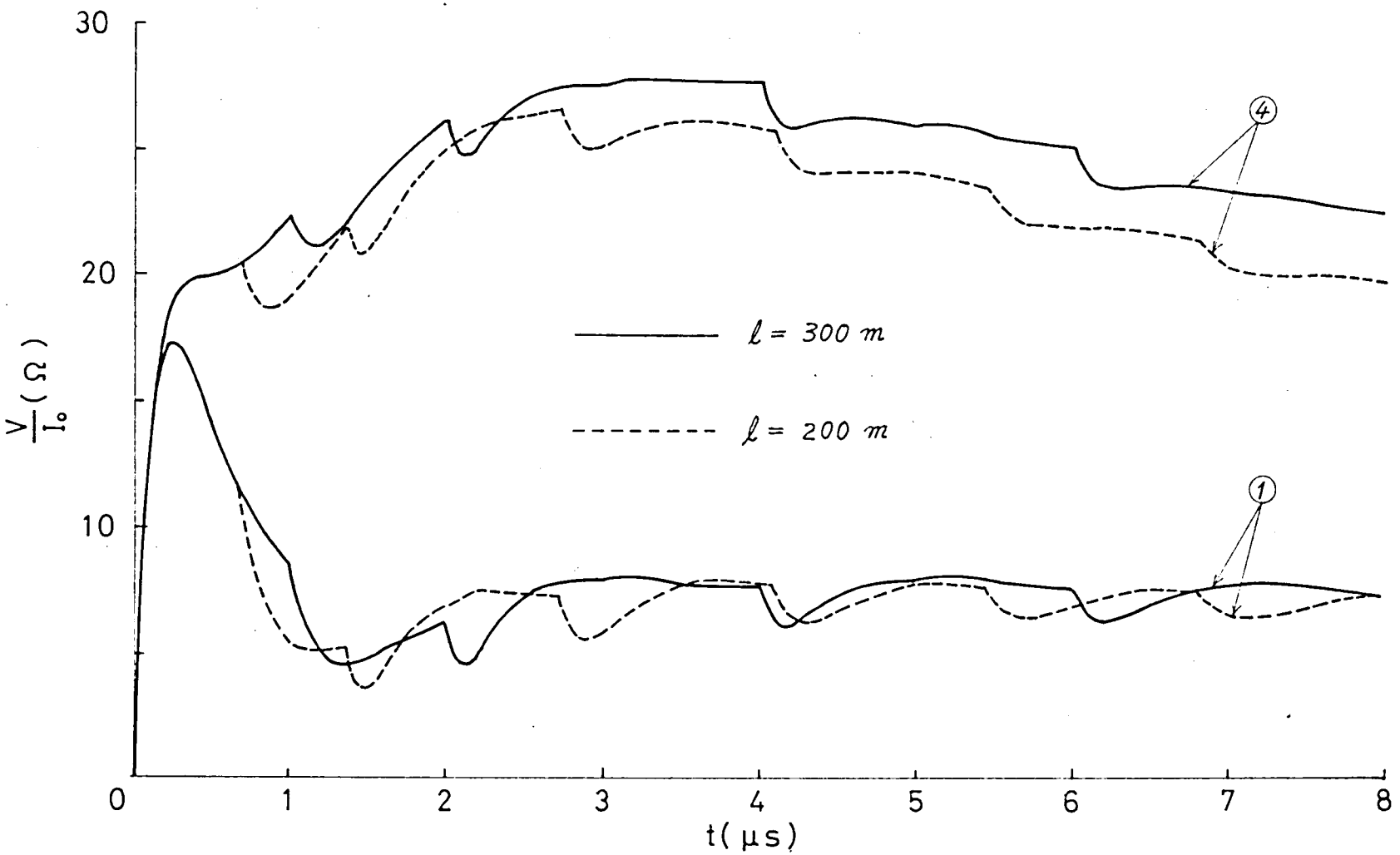

Fig. 3.11 Transient voltages at the 1st tower.

(Equivalent circuit of tower : A, $i(t): I_0 = 1(1\times\infty\mu s)$)

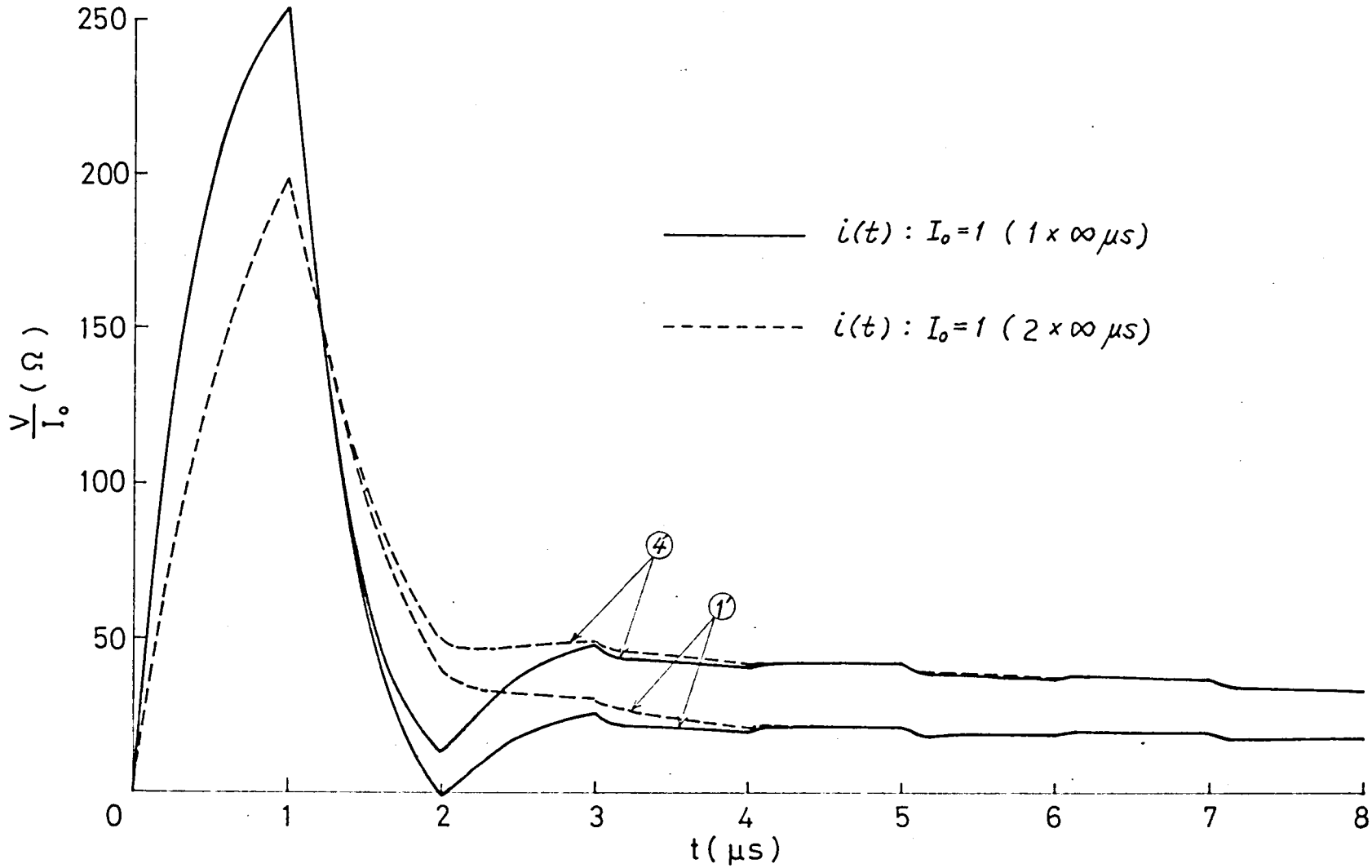

Fig. 3.12 Transient voltages at the lightning stroke point.

(Equivalent circuit of tower : B, $\ell = 300\ m$)

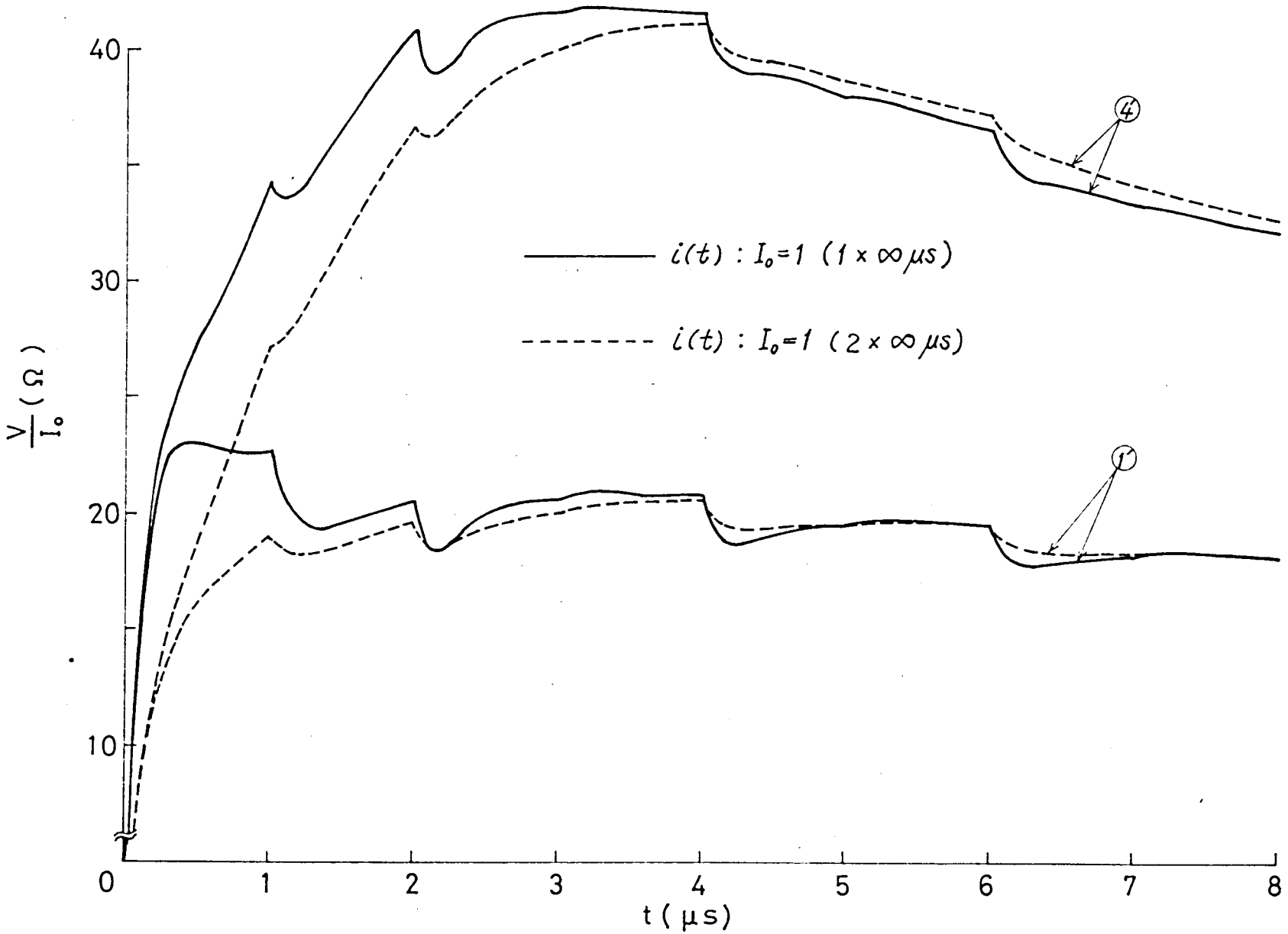

Fig. 3.13 Transient voltages at the 1st tower.

(Equivalent circuit of tower : B, $\ell = 300\,m$)

3.4 Surges on Overhead Line-Cable Transmission System

3.4.1 Numerical Calculation

In this section, let us discuss the transient voltages at the junction point of overhead line and cable in the case where the lightning strikes at the neighbouring tower of junction point on overhead line-cable transmission system as shown in Fig. 3.14(a). In this figure

$i(t)$: lightning stroke current,

Z_0 : stroke channel impedance,

β_1 and β_2 : surge impedances of line conductor and cable,

ℓ_1 and ℓ_2 : lengthes of line conductor and cable,

T_1 and T_2 : propagation time of surge on line conductor- and cable-sections,

F_1, F_2, F_3 and F_4 : refraction coefficients of each point.

As the equivalent circuit of tower, we use the one shown in Fig. 3.14(c), which is thought to be appropriate for the tower of the high voltage transmission systems. In this figure the constants of equivalent circuit of tower R_T, L_T, R_E, L_E and R_f

are the same constants as described in Article 3.3.1. Let us consider the distortion of surges by the skin effect of the cable, which is far longer and has the larger values of distortion constant than the overhead line between the junction point and the neighbouring tower.

The flow graph of the system as illustrated in Fig. 3.14 (a) becomes as Fig. 3.14(b). The imput impedance $Z(p)$ and refraction coefficients $F_1(p)$, F_2, F_3 and F_4 in Fig. 3.14(b) is obtained as follows:

$$\left.\begin{aligned} Z(p) &= M_1\left(1+\frac{A_{11}}{p+\alpha_{11}}+\frac{A_{12}}{p+\alpha_{12}}\right), \\ F_1(p) &= M_2\left(1+\frac{A_{21}}{p+\alpha_{21}}+\frac{A_{22}}{p+\alpha_{22}}\right), \\ F_2 &= \frac{2\beta_2}{\beta_1+\beta_2}, \\ F_3 &= F_4 = \frac{2\beta_1}{\beta_1+\beta_2}. \end{aligned}\right\} \qquad (3.7)$$

In Eq.s (3.7), M_i, A_{ij}, α_{ij} ($i = 1,2$ and $j = 1,2$) are the constants, whose values can be decided by the next equations

$$\left.\begin{aligned} Z(p) &= M_1\,\frac{p^2+a_1p+a_2}{p^2+b_1p+b_2}, \\ F_1(p) &= M_2\,\frac{p^2+c_1p+c_2}{p^2+d_1p+d_2}, \end{aligned}\right.$$

where

$$
\left.
\begin{aligned}
&M_1 = z_1 A_t / (z_1 + 2A_t), \\
&a_1 = B_t / A_t, \\
&a_2 = C_t / A_t, \\
&b_1 = (z_1 D_t + 2B_t) / (z_1 + 2A_t), \\
&b_2 = (z_1 E_t + 2C_t) / (z_1 + 2A_t), \\
&M_2 = 2Z_0 A_t / \{(z_1 + 2Z_0)A_t + z_1 Z_0\}, \\
&c_1 = B_t / A_t, \\
&c_2 = C_t / A_t, \\
&d_1 = \{(z_1 + 2Z_0)B_t + z_1 Z_0 D_t\} / \{(z_1 + 2Z_0)A_t + z_1 Z_0\}, \\
&d_2 = \{(z_1 + 2Z_0)C_t + z_1 Z_0 E_t\} / \{(z_1 + 2Z_0)A_t + z_1 Z_0\}, \\
&A_t = R_T + R_E + R_G, \\
&B_t = (R_T R_E / L_E + R_T R_E / L_T + R_E R_G / L_E + R_T R_G / L_T), \\
&C_t = R_T R_E R_G / L_T L_E, \\
&D_t = R_E / L_E + R_T / L_T, \\
&E_t = R_T R_E / L_T L_E .
\end{aligned}
\right\} \qquad (3.8)
$$

Moreover we approximate the error function, which expresses the distortion of surges due to the skin effect of the cable, by the same next equation as Eq. (2.20).

$$erfc\left(\frac{\sigma l_2}{2\sqrt{t}}\right) \simeq K(1-\varepsilon^{-\gamma t}), \tag{3.9}$$

where σ is the distortion constant of the cable.

Next we can obtain the voltage equations for each node of the flow graph shown in Fig. 3.14(b) by using the method which was explained in the preceding chapter as follows:

$$\left.\begin{aligned}
&i(t) = I_0 \varepsilon^{-\alpha_0 t},\\
&v_1(t) = v_8(t-T_1),\\
&v_2(t) = v_9(t-T_1),\\
&h_1(t) = \tfrac{1}{2}\{v_{10}(t-T_2) + v_{10}(t-T_2-\Delta t)\varepsilon^{-\gamma\Delta t}\}\Delta t\\
&\qquad\qquad + h_1(t-\Delta t)\varepsilon^{-\gamma\Delta t},\\
&h_2(t) = \tfrac{1}{2}\{v_{11}(t-T_2) + v_{11}(t-T_2-\Delta t)\varepsilon^{-\gamma\Delta t}\}\Delta t\\
&\qquad\qquad + h_2(t-\Delta t)\varepsilon^{-\gamma\Delta t},\\
&v_3(t) = K\gamma h_1(t),\\
&v_4(t) = K\gamma h_2(t),\\
&g_{1j}(t) = \tfrac{1}{2}\{i(t) + i(t-\Delta t)\varepsilon^{-\alpha_{1j}\Delta t}\}\Delta t\\
&\qquad\qquad + g_{1j}(t-\Delta t)\varepsilon^{-\alpha_{1j}\Delta t},\\
&g_{2j}(t) = \tfrac{1}{2}\{v_2(t) + v_2(t-\Delta t)\varepsilon^{-\alpha_{2j}\Delta t}\}\Delta t\\
&\qquad\qquad + g_{2j}(t-\Delta t)\varepsilon^{-\alpha_{2j}\Delta t},
\end{aligned}\right\} \quad j = 1, 2 \tag{3.10}$$

$$v_5(t) = M_1\{i(t) + A_{11}g_{11}(t) + A_{12}g_{12}(t)\}$$
$$+ M_2\{v_2(t) + A_{21}g_{21}(t) + A_{22}g_{22}(t)\},$$
$$v_6(t) = F_2 v_1(t) + F_3 v_4(t),$$
$$v_7(t) = F_4 v_3(t),$$
$$v_8(t) = v_5(t) - v_2(t),$$
$$v_9(t) = v_6(t) - v_1(t),$$
$$v_{10}(t) = v_6(t) - v_4(t),$$
$$v_{11}(t) = v_7(t) - v_3(t).$$

By using the above equations, we can evaluated each node voltage $v_r(t)$ (from $r = 1$ to 11) at $t = \Delta t$, $2\Delta t$, ... successively.

3.4.2 Calculated Results and Discussions

In the author's digital calculation, we choose the Tonosho Overhead Line-Cable System[4] of the Chugoku Electric Power Company as the model system. The line constants and another constants used in the calculation are exhibited in Table 3.5. Since it is very important to carry out the calculation including the effect of counterpoise though the towers on the Tonosho Line System have no counterpoise in practice, we per-

form the calculation using the value of the tower foot impedance with counterpoise, which had been obtained for the tower on the Yubara Transmission Line[30] of the Chugoku Electric Power Company previously. Moreover, though this system is a double circuit of three-phase transmission line, we assume that this system is a symmetric three-phase transmission line for simplicity, and occurs three-phase back flashover at the instant when the tower is struck by lightning. Next if we choose

$$K = 0.9, \qquad \gamma = 0.381. \tag{3.11}$$

in Eq. (3.9), the exponential function can coincide fairly good with the error function in the case of $\xi = 0$ to 50 as shown in Fig. 3.15. From $\xi = 50$ in this figure, we get the real time as follows:

$$t = (\sigma l_2)^2 \xi = (7.24 \times 10^{-7} \times 1740)^2 \times 50 = 79.34 \times 10^{-6} \ (s) \ . \tag{3.12}$$

Therefore we may use Eq. (3.9) as a fairly good approximate equation from $t = 0$ to about 80μs, if we adopt the values of K and γ given in Eq.s (3.11). In this connection the value of γ in Eq.s (3.11) is determined so as to coincide the area between the curve of the error function and ξ axis with the one between the curve of the exponential function and ξ axis in the range of $\xi = 0$ to 50 under the condition of $K = 0.9$.

Fig. 3.16(a) shows the computed transient voltages at the

junction point on the above-mentioned transmission system of overhead line-cable in the case where $l_1 = 75$m and $l_2 = 1740$m. In the figure the calculated result by the above described method is plotted by the solid line and the exact one by the theoretical solution which has been introduced in Chapter 1 is done by the dotted line. We choose the value of time interval $\Delta t = 0.05\,\mu s$ in the former case, and we can see that the approximate solution by the new method agree with the exact one very good. Although it takes about one hour to calculate the exact solution using the digital computer FACOM 230-60 in Data Processing Center, Kyoto University, it does only ten seconds to calculate the approximate one by the new method using the same digital computer.

Next Fig. 3.16(b) shows the same transient voltages as Fig. 3.16(a) from $t = 0$ and $80\mu s$. Here we show only the calculated results by the new method and compare the transient voltages in the case, where the skin effect is considered, with the one that the skin effect is not considered. We can see that it is necessary to consider the skin effect in the case where the propagation distance of surges become fairly long.

Though the transient voltage in the case where the skin effect is not considered really oscillates very finely, we show it by a smooth envelope as it is very difficult to illustrate the oscillation.

Next we show the calculated results in the case where the value of l_1 is assumed to be 200m instead of 75m in our system in Fig. 3.17(a) and (b). From these two figures we can see

the same facts as mentioned above.

Table 3.5 Values of constants used in computations in Section 3.4.

Lightning stroke current	$i(t)$: $I_0 = 1$ ($0 \times 40\,\mu s$)
Stroke channel impedance	$Z_0 = 400\ \Omega$
Zero-phase surge impedance of overhead line	$Z_1 = 280\ \Omega$
Zero-phase surge impedance of cable	$Z_2 = 20\ \Omega$
Overhead line length	$l_1 = 75\ m$, $200\ m$
Cable length	$l_2 = 1740\ m$
Surge propagation time on line conductor	$T_1 = 0.25\,\mu s$, $0.67\,\mu s$
Surge propagation time on cable	$T_2 = 10.85\,\mu s$
Zero-phase distortion constant of cable	$\sigma = 7.24 \times 10^{-7}\ \sqrt{s}/m$
Time interval	$\Delta t = 0.05\,\mu s$, $0.067\,\mu s$
Equivalent circuit constant of tower	$R_T = 100\,\Omega$, $R_E = 50\,\Omega$, $R_F = 15\,\Omega$ $L_T = 10\,\mu H$, $L_E = 50\,\mu H$

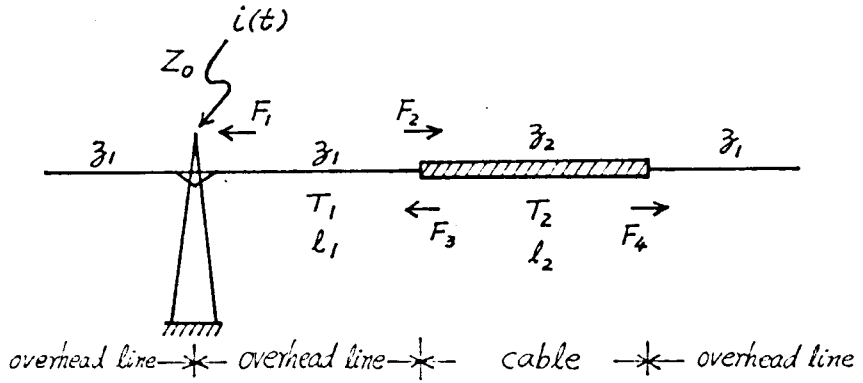

(a) Power system.

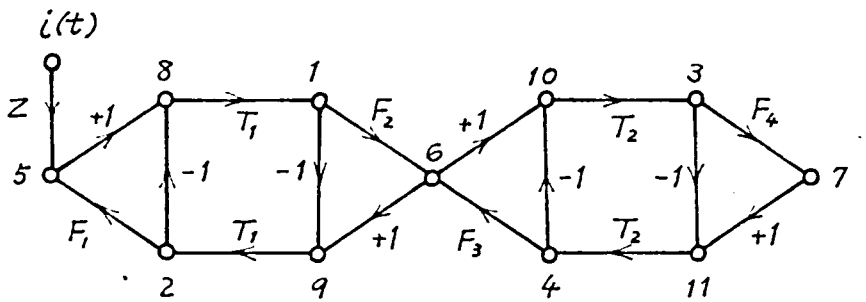

(b) Flow graph.

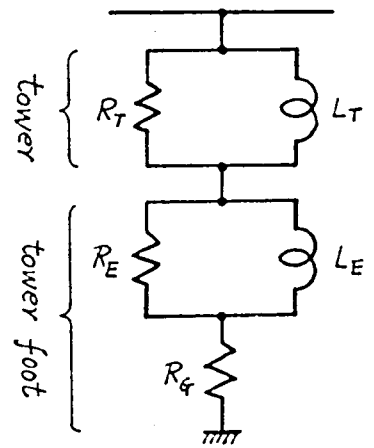

(c) Equivalent circuit of tower.

Fig. 3.14 Illustration of overhead line-cable transmission system.

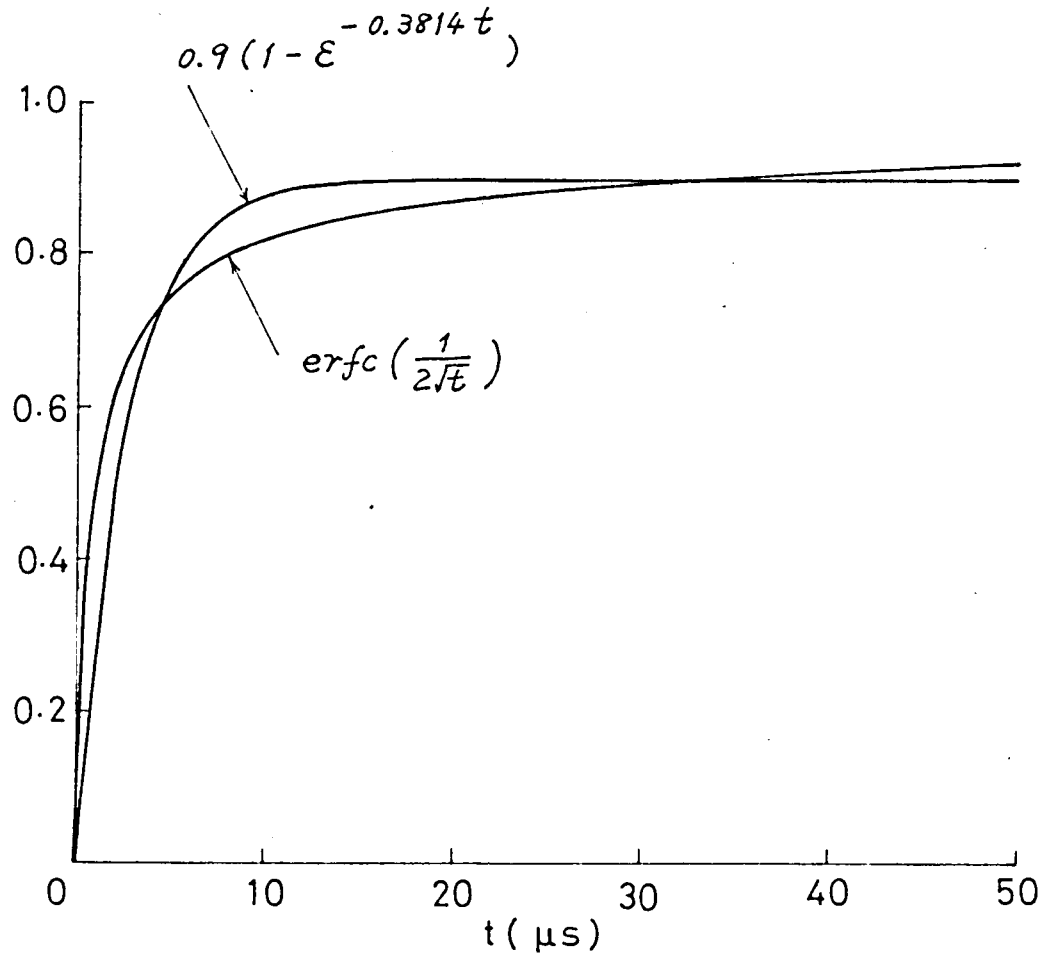

Fig. 3.15 An approximation of error function by exponential function.

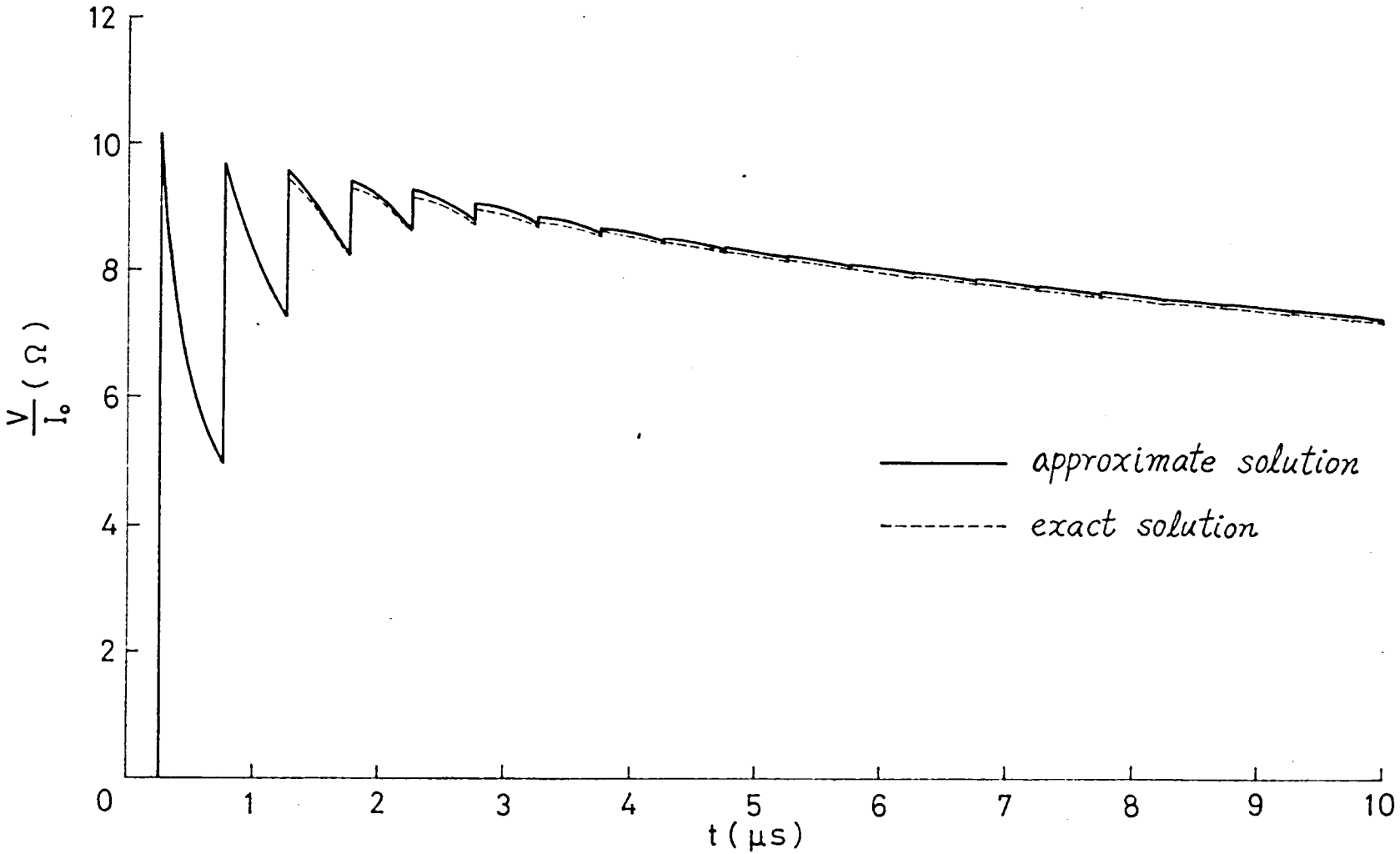

Fig. 3.16(a) Transient voltages at junction point of overhead line and cable.

($l_1 = 75\,m$, $l_2 = 1740\,m$, $\Delta t = 0.05\,\mu s$)

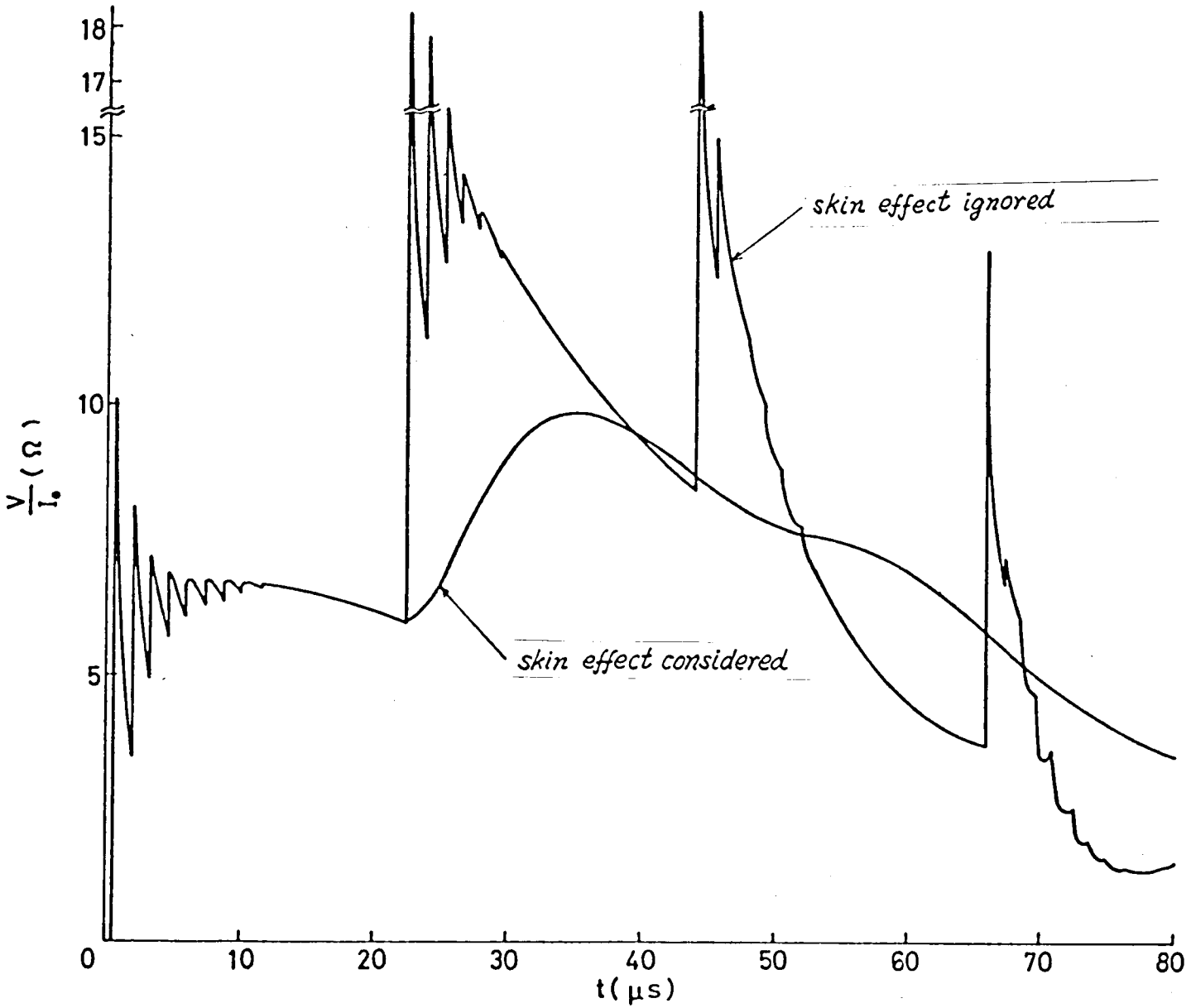

Fig. 3.16(b) Transient voltages at junction point of overhead line and cable.
($l_1 = 75\,m$, $l_2 = 1740\,m$, $\Delta t = 0.05\,\mu s$)

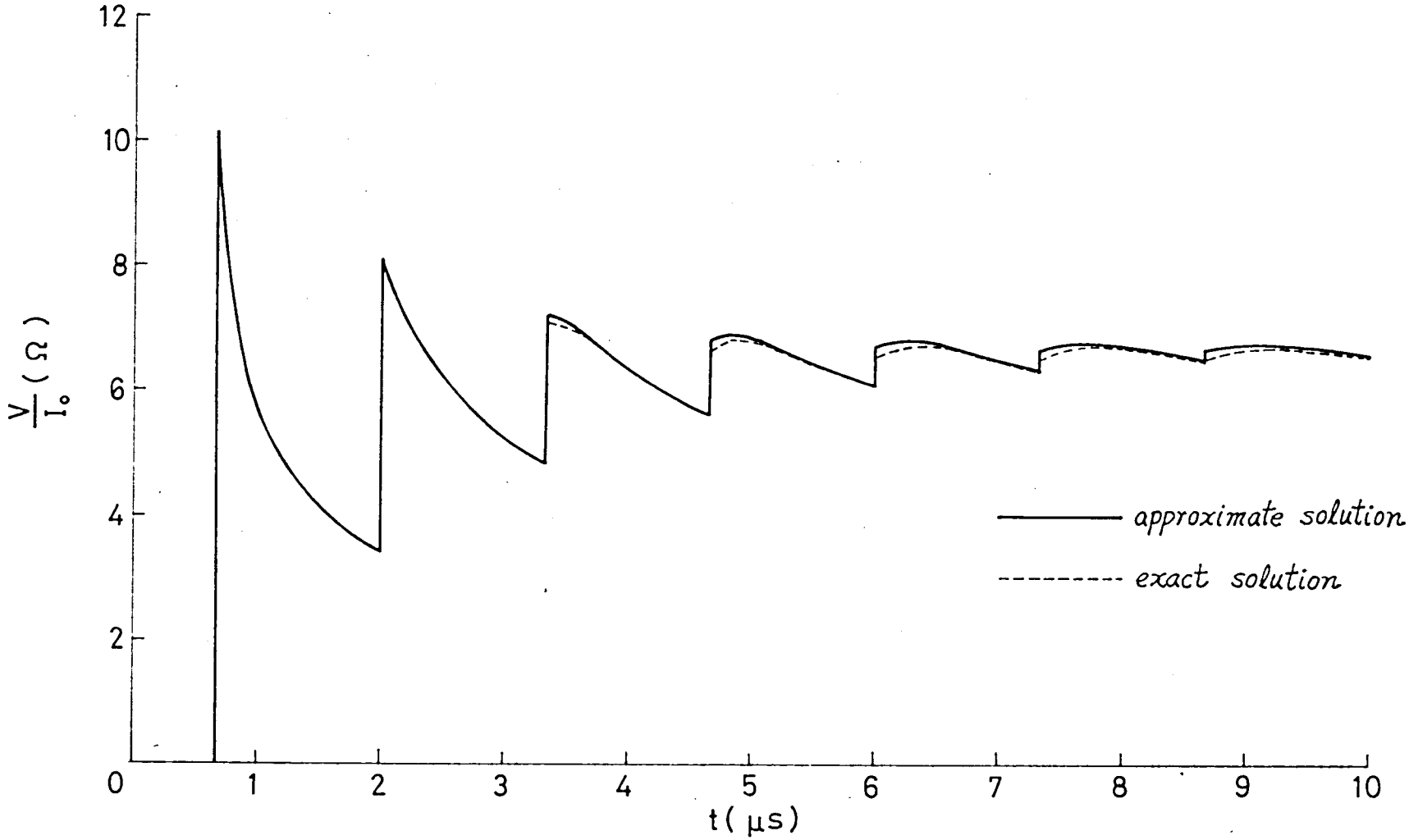

Fig. 3.17(a) Transient voltages at junction point of overhead line and cable.

($\ell_1 = 200\,m$, $\ell_2 = 1740\,m$, $\Delta t = 0.067\,\mu s$)

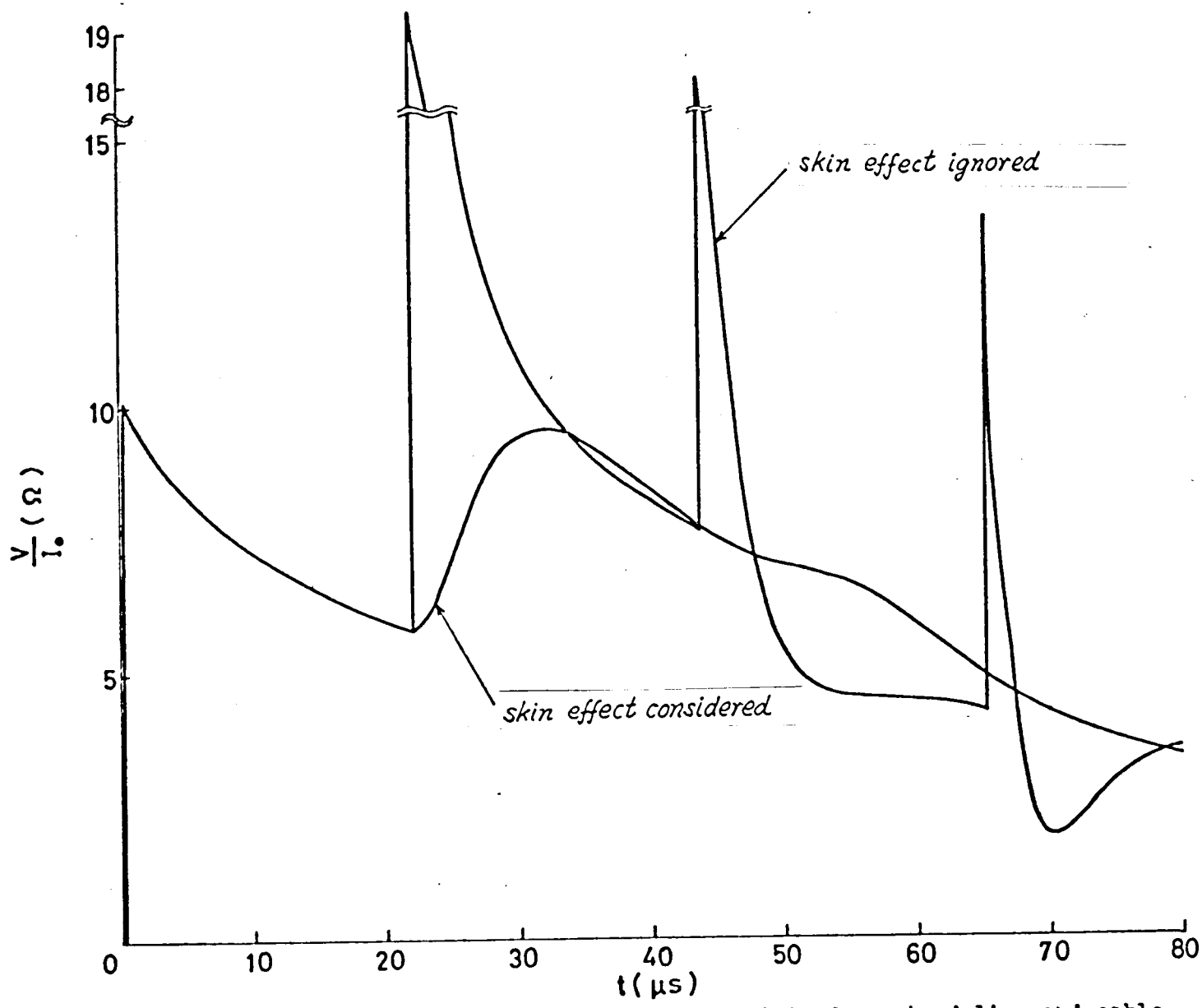

Fig. 3.17(b) Transient voltages at junction point of overhead line and cable.

($l_1 = 200\,m$, $l_2 = 1740\,m$, $\Delta t = 0.067\,\mu s$)

3.5 Surges on Overhead Line-Cable Systems with Arrester at Junction Point

3.5.1 Numerical Calculation

In this Section, let us analyze the surge performances on the overhead line-cable systems which an arrester is connected to the junction point and the final end of the cable is connected to the main transformer within the substation which is represented by a equivalent capacitance of the substation as shown in Fig. 3.18(a). The system is the one which Ishihara[3] has already adopted as the model systems. Now we shall calculate the transient voltages at the tower, which is struck by lightning, the neighborhood tower, and the both ends of the cable, where it is assumed that the tower nearest the junction point of line and cable is struck by lightning. In Fig. 3.18 (a)

$i(t)$: lightning stroke current,

Z_o : stroke channel impedance,

C : equivalent capacitance of a main transformer of the substation,

$\mathcal{Z}$, $\mathcal{Z}_j$ and $\mathcal{Z}_c$: surge impedances of overhead line conductor, overhead ground wire and cable,

T, T_g and T_c : propagation time of surge on overhead line conductor-, overhead ground wire- and cable-sections.

Here we will use the circuit shown in Fig. 3.18(c) as the equivalent circuit of the tower in the case where the grounding resistance is small, and show the values of the system constants in Table 3.6. And though in Section 3.4 we have assumed that the back flashover occurs at the instant when the lightning strikes at the tower, here we assume that the back flashover occurs at the instant when the tower voltage exceeds the flashover one given by the v-t characteristic curve of the insulator chain. Moreover we assume that the arrester bigins to discharge at the instant when the junction point voltage surpasses the discharge voltage given by the v-t characteristic curve of the arrester gap.

Fig. 3.18(b) shows the flow graph of the present systems. In this figure

Z_1 and Z_2 : input impedances before and after the back flashover,

F_1 and F_2 : refraction coefficients at node before and after the back flashover,

F_3, F_4, ----- and F_7 : refraction coefficients at each node.

These coefficients are given by the following equations

$$
\left.
\begin{aligned}
&F_i'(p) = M_i\left(1 + \frac{A_{i1}}{p+\alpha_{i1}} + \frac{A_{i2}}{p+\alpha_{i2}}\right), \quad (i = 1, 2, \cdots, 5), \\
&F_5(p) = \frac{2\zeta_c}{\zeta + \zeta_c}, \\
&F_6(p) = \frac{2\zeta}{\zeta + \zeta_c}, \\
&F_7(p) = M_6 \frac{1}{p + \alpha_6}, \\
&F_1'(p) = Z_1(p), \qquad F_2'(p) = Z_2(p), \qquad F_3'(p) = F_1(p), \\
&F_4'(p) = F_2(p) = F_3(p), \qquad F_5'(p) = F_4(p).
\end{aligned}
\right\} \tag{3.13}
$$

where

M_i, A_{ij} and α_{ij} $(i, j = 1, 2, \ldots, 5)$ in the above equations can be obtained by the next equations

$$
\left.
\begin{aligned}
&F_i'(p) = \frac{X_i(A_t p^2 + B_t p + C_t)}{(A_t + Y_i)p^2 + (B_t + D_t Y_i)p + (C_t + E_t Y_i)}, \\
&\text{where} \\
&X_1 = \zeta, \qquad Y_1 = \zeta, \\
&X_2 = \frac{\zeta}{3}, \qquad Y_2 = \frac{\zeta}{3},
\end{aligned}
\right\} \tag{3.14}
$$

$$\left.\begin{aligned} x_3 &= \frac{2Z_0}{\zeta + 3Z_0}, & Y_3 &= \frac{3Z_0}{\zeta + 3Z_0}, \\ x_4 &= \frac{2Z_0}{\zeta + 3Z_0}, & Y_4 &= \frac{3Z_0}{\zeta + 3Z_0}, \\ x_5 &= 1, & Y_5 &= \frac{\zeta}{2}, \end{aligned}\right\}$$

in which A_t, B_t, C_t, D_t, E_t are the constants given in Eq.s (3.8), and we make assumption that $\zeta = \zeta_j$ in this equations. Moreover, M_6 and α_6 in Eq.s (3.13) are expressed as follows:

$$M_6 = \frac{2}{\zeta_c C}, \qquad \alpha_6 = \frac{1}{\zeta_c C}. \tag{3.15}$$

The voltage equations for each node of the flow graph Fig. 3.18(b) are given as follows:

$$\left.\begin{aligned} v_1(t) &= v_{11}(t - T_j), \\ v_2(t) &= v_{12}(t - T_j), \\ v_3(t) &= v_{13}(t - T), \\ v_4(t) &= v_{14}(t - T), \\ v_5(t) &= v_{15}(t - T_c), \\ v_6(t) &= v_{16}(t - T_c), \\ g_{1j}(t) &= \frac{1}{2}\{i(t) + i(t-\Delta t)\varepsilon^{-\alpha_1 j \Delta t}\}\Delta t + g_{1j}(t-\Delta t)\varepsilon^{-\alpha_1 j \Delta t}, \\ g_{2j}(t) &= \frac{1}{2}\{i(t) + i(t-\Delta t)\varepsilon^{-\alpha_2 j \Delta t}\}\Delta t + g_{2j}(t-\Delta t)\varepsilon^{-\alpha_2 j \Delta t}, \\ g_{3j}(t) &= \frac{1}{2}\{v_2(t) + v_2(t-\Delta t)\varepsilon^{-\alpha_3 j \Delta t}\}\Delta t + g_{3j}(t-\Delta t)\varepsilon^{-\alpha_3 j \Delta t}, \end{aligned}\right\} j = 1, 2$$

$$
\left.
\begin{aligned}
g_{4j}(t) &= \frac{1}{2}\{v_2(t) + v_2(t-\Delta t)\varepsilon^{-\alpha_{4j}\Delta t}\}\Delta t + g_{4j}(t-\Delta t)\varepsilon^{-\alpha_{4j}\Delta t}, \\
g_{5j}(t) &= \frac{1}{2}\{v_4(t) + v_4(t-\Delta t)\varepsilon^{-\alpha_{5j}\Delta t}\}\Delta t + g_{5j}(t-\Delta t)\varepsilon^{-\alpha_{5j}\Delta t}
\end{aligned}
\right\}
$$

$$
\begin{aligned}
v_7(t) &= M_1\{i(t) + A_{11}g_{11}(t) + A_{12}g_{12}(t)\} \\
&\quad + M_3\{v_2(t) + A_{31}g_{31}(t) + A_{32}g_{32}(t)\}, \qquad 0 \le t < t_0, \\
v_7(t) &= M_2\{i(t) + A_{21}g_{21}(t) + A_{22}g_{22}(t)\} \\
&\quad + M_4\{v_2(t) + A_{41}g_{41}(t) + A_{42}g_{42}(t)\} \\
&\quad + M_5\{v_4(t) + A_{51}g_{51}(t) + A_{52}g_{52}(t)\}, \qquad t \ge t_0,
\end{aligned}
$$

$$
\left.
\begin{aligned}
g_{6j}(t) &= \frac{1}{2}\{v_1(t) + v_1(t-\Delta t)\varepsilon^{-\alpha_{6j}\Delta t}\}\Delta t + g_{6j}(t-\Delta t)\varepsilon^{-\alpha_{6j}\Delta t}, \quad j=1,2 \\
v_8(t) &= M_6\{v_1(t) + A_{61}g_{61}(t) + A_{62}g_{62}(t)\}, \\
v_9(t) &= F_5 v_3(t) + F_6 v_6(t), \\
g_7(t) &= \frac{1}{2}\{v_5(t) + v_5(t-\Delta t)\varepsilon^{-\alpha_7\Delta t}\}\Delta t + g_7(t-\Delta t)\varepsilon^{-\alpha_7\Delta t}, \\
v_{10}(t) &= M_7 g_7(t), \\
v_{11}(t) &= v_7(t) - v_2(t), \\
v_{12}(t) &= v_8(t) - v_1(t),
\end{aligned}
\right\} \quad (3.16)
$$

$$v_{17}(t) = 0, \qquad 0 \le t < t_o,$$

$$v_{13}(t) = v_7(t) - v_4(t), \qquad t \ge t_o,$$

$$v_{14}(t) = v_7(t) - v_3(t),$$

$$v_{15}(t) = v_7(t) - v_6(t),$$

$$v_{16}(t) = v_{10}(t) - v_5(t),$$

where

$$i(t) = I_o I_{oo} (\varepsilon^{-a_o t} - \varepsilon^{-b_o t}).$$

In the above equation of $i(t)$, I_o is the peak value of the lightning stroke current, and I_{oo} is the constant given by $1/(\varepsilon^{-a_o t_o} - \varepsilon^{-b_o t_o})$, and t_o is the peak time.

In digital calculation by Eq.s (3.16), in early time we obtain the value of $v_7(t)$ from the 12th equation at $0 \le t < t_o$, and after the instant $t = t_o$ when the value of $v_7(t)$ rises above the flashover voltage of the insulator chain, where we use the v-t characteristic curve of the chain of ten suspention type insulator, we obtain the value of $v_7(t)$ from the 13th equation at $t \ge t_o$.

Next to obtain the value of the node voltage $v_7(t)$, at which the arrester is set up, we can use the calculated value by Eq.s (3.16) while $v_7(t)$ does not rise above the discharge starting voltage of the arrester, and after $v_7(t)$ exceed the discharge voltage we can calculate the value of $v_7(t)$ by using

the method introduced in Section 2.5. We use the v-i and z-i characteristic curves of the arrester whose rated voltage is 196kV and nominal discharge current is 10kA given in JEC-156. The equation of this v-i characteristic curve is expressed by

$$v = 479.5\, i^{0.136} \quad \text{(kV)} \tag{3.17}$$

Moreover, the values of another constants availed in computation are shown in Table 3.6, which are given in the Reference (3).

3.5.2 Calculated Results and Discussions

The calculated transient voltages at tower which is struck by lightning, the neighborhood tower, and the both ends of the cable are shown in each figure listed below.

Fig. 3.19(a)

$i(t)$: I_0=100kA($1\times40\mu s$), $R_g=10\Omega$; with arrester.

Fig. 3.19(b)

$i(t)$: I_0=100kA($1\times40\mu s$), $R_g=10\Omega$; without arrester.

Fig. 3.20(a)

$i(t)$: I_0 = 100 kA (2 × 40 μs), R_f = 10 Ω ; with arrester.

Fig. 3.20(b)

$i(t)$: I_0 = 100 kA (2 × 40 μs), R_f = 10 Ω ; without arrester.

Fig. 3.21(a)

$i(t)$: I_0 = 80 kA (1 × 40 μs), R_f = 20 Ω ; with arrester.

Fig. 3.21(b)

$i(t)$: I_0 = 80 kA (1 × 40 μs), R_f = 20 Ω ; without arrester.

Fig. 3.22(a)

$i(t)$: I_0 = 80 kA (2 × 40 μs), R_f = 20 Ω ; with arrester.

Fig. 3.22(b)

$i(t)$: I_0 = 80 kA (2 × 40 μs), R_f = 20 Ω ; without arrester.

Moreover the computation of the case of

$$i(t) : I_0 = 100 \text{ kA } (1 \times 40\ \mu s\ ,\ 2 \times 40\ \mu s),\ R_f = 20\ \Omega\ ,$$

and

$$i(t) : I_0 = 80 \text{ kA } (1 \times 40\ \mu s\ ,\ 2 \times 40\ \mu s),\ R_f = 10\ \Omega\ ,$$

are carried out, though we don't illustrate here.

The maximum voltages at the both ends of the cable got from

each figure are shown in Table 3.7. And in this table, the maximum values of the case where the arrester is not set up, are the ones which are obtained by assuming that any insulation breakdown does not occur in the cable or at any other point.

In Cases 1 and 2 of Table 3.7, the maximum voltage arrive at about 1700kV when the arrester is not fitted up, but those are put down under about 700kV $\sim$ 800kV in the case where the arrester is set up, and therefore the cable can be protected from the insulation breakdown. And we can see the similar fact for another cases. But in Cases 3 and 4, there is the danger that the arrester will be damaged because the junction point voltages a little exceed the impulse voltage pressure resisting 750kV of the arrester. Thus, we can see that the value of R_4 has a great influence on every transition point voltage, on the contrary the wave front duration of the lightning stroke current has not so great influence on them. But the possibilities of back flashover differ fairly according to whether the wave front duration is 1 μs or 2 μs.

As mentioned above, in this section we can see that the value of the transient voltage at each transition point can be calculated simply by the new method in the case where the circuit composition changes in progress of transient phenomena, and moreover in the case where the circuit has a nonlinear element as an arrester. And it is thought that our calculation and calculated results give many available data for the lightning-proof design of transmission or distribution systems.

Table 3.6 Values of constants used in computations in Section 3.5.

Lightning stroke current	$i(t): I_o = 100\,kA\,(1 \times 40\,\mu s)$
Stroke channel impedance	$Z_o = 400\ \Omega$
Surge impedance of overhead line and ground wire	$Z = Z_g = 500\ \Omega$
Surge impedance of cable	$Z_c = 20\ \Omega$
Surge propagation time on overhead line and ground wire	$T = T_g = 1.0\ \mu s$
Surge propagation time on cable	$T_c = 2.0\ \mu s$
Equivalent capacitance of transformer	$C = 5000\ pF$
Time interval	$\Delta t = 0.1\ \mu s$
Equivalent circuit constant of tower	$R_T = 100\ \Omega$, $R_E = 25\ \Omega$, $R_G = 10\ \Omega$ $L_T = 10\ \mu H$, $L_E = 25\ \mu H$

Table 3.7 Maximum voltages at beginning and final end of cable.

			Maxium voltage (without arrester) $(\frac{V}{I_o})$		Maxium voltage (with arrester) $(\frac{V}{I_o})$	
Case	i(t)	R_G (Ω)	Beginning end	Final end	Beginning end	Final end
1	100kA(1x40μs)	10	1709	1706	705	756
2	100kA(2x40μs)	10	1702	1708	724	882
3	100kA(1x40μs)	20	2747	2833	754	881
4	100kA(2x40μs)	20	2719	2823	755	890
5	80kA(1x40μs)	10	1.393	1378	689	808
6	80kA(2x40μs)	10	dont flashover		dont flashover	
7	80kA(1x40μs)	20	2218	2280	728	830
8	80kA(2x40μs)	20	2188	2272	749	940

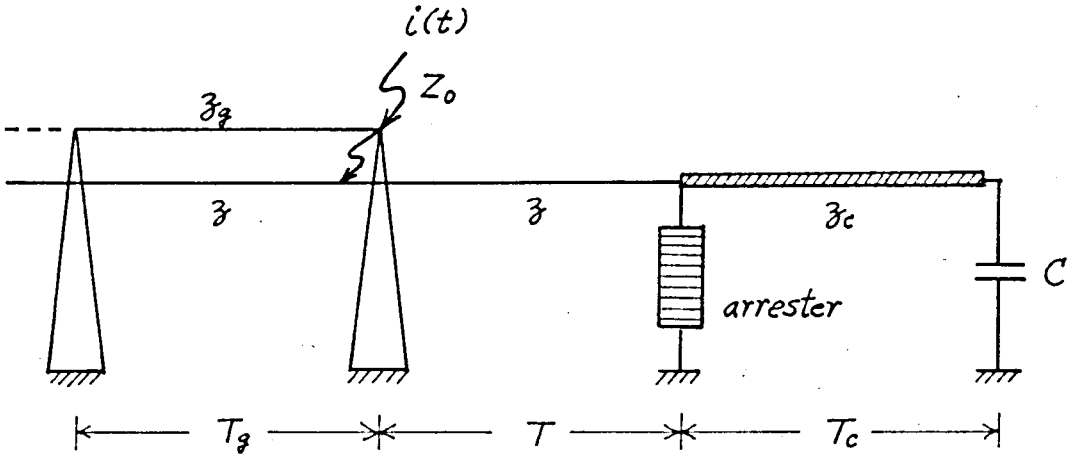

(a) Power system.

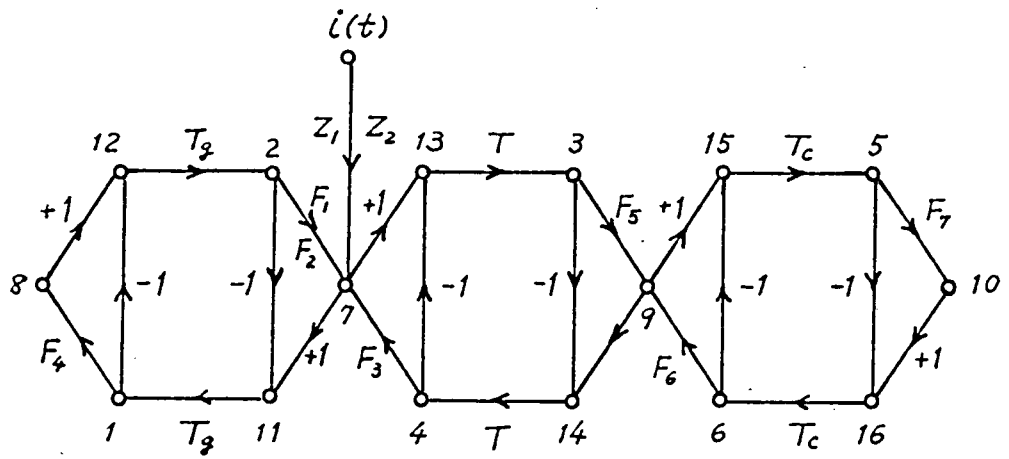

(b) Flow graph.

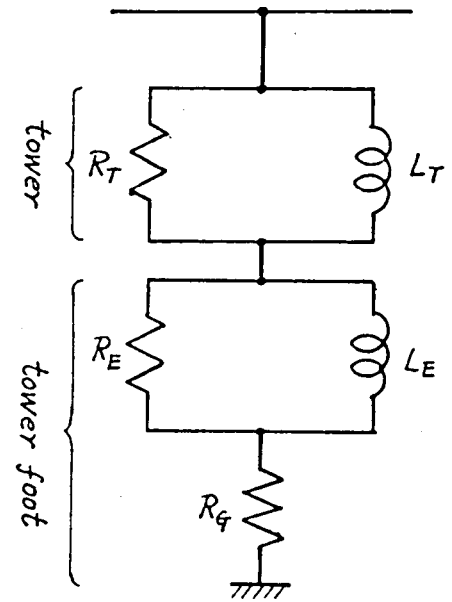

(c) Equivalent circuit of tower.

Fig. 3.18 Illustration of overhead line-cable system with arrester at junction point.

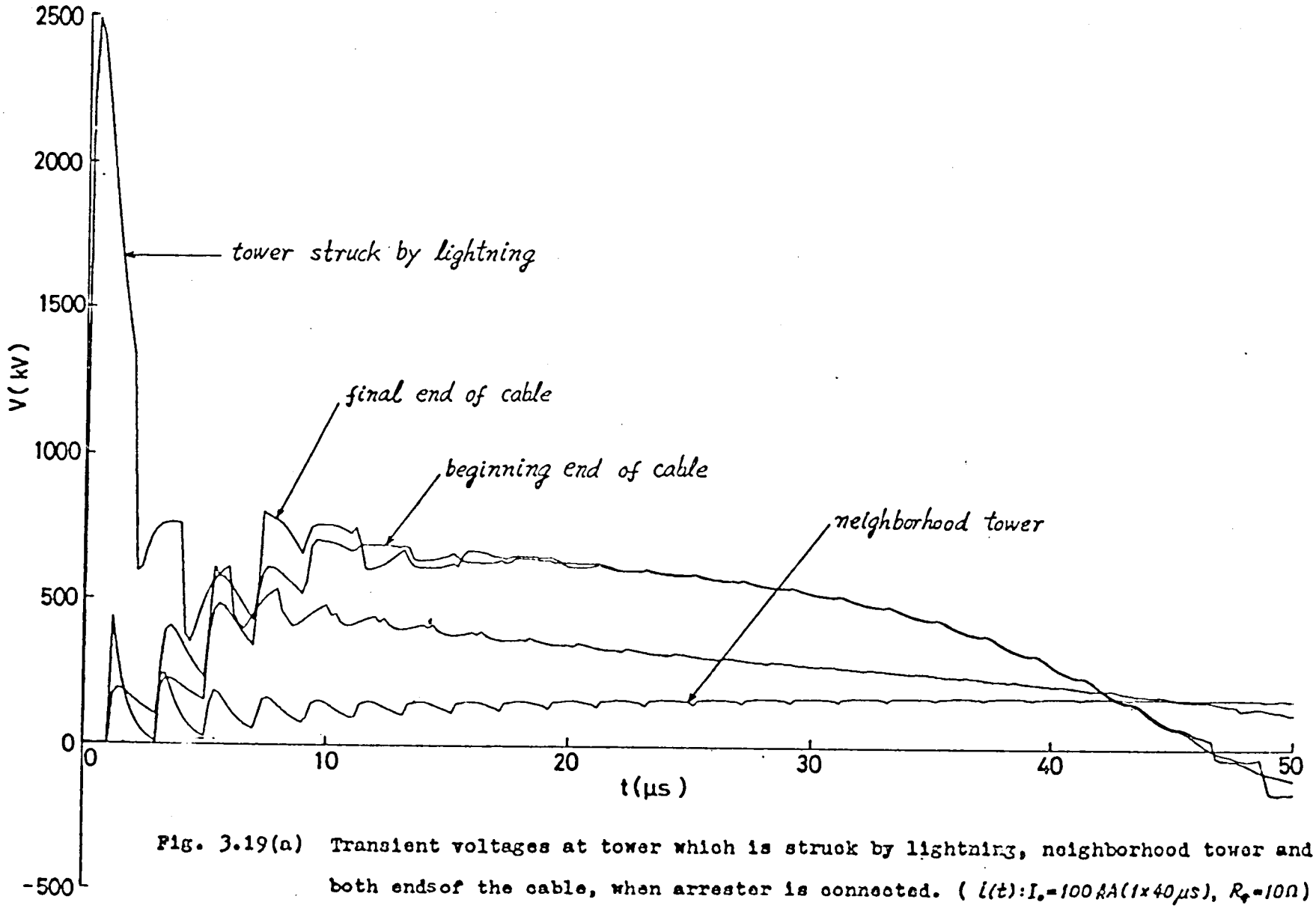

Fig. 3.19(a) Transient voltages at tower which is struck by lightning, neighborhood tower and both ends of the cable, when arrester is connected. ($i(t): I_0 = 100\,kA\,(1\times40\,\mu s)$, $R_f = 10\Omega$)

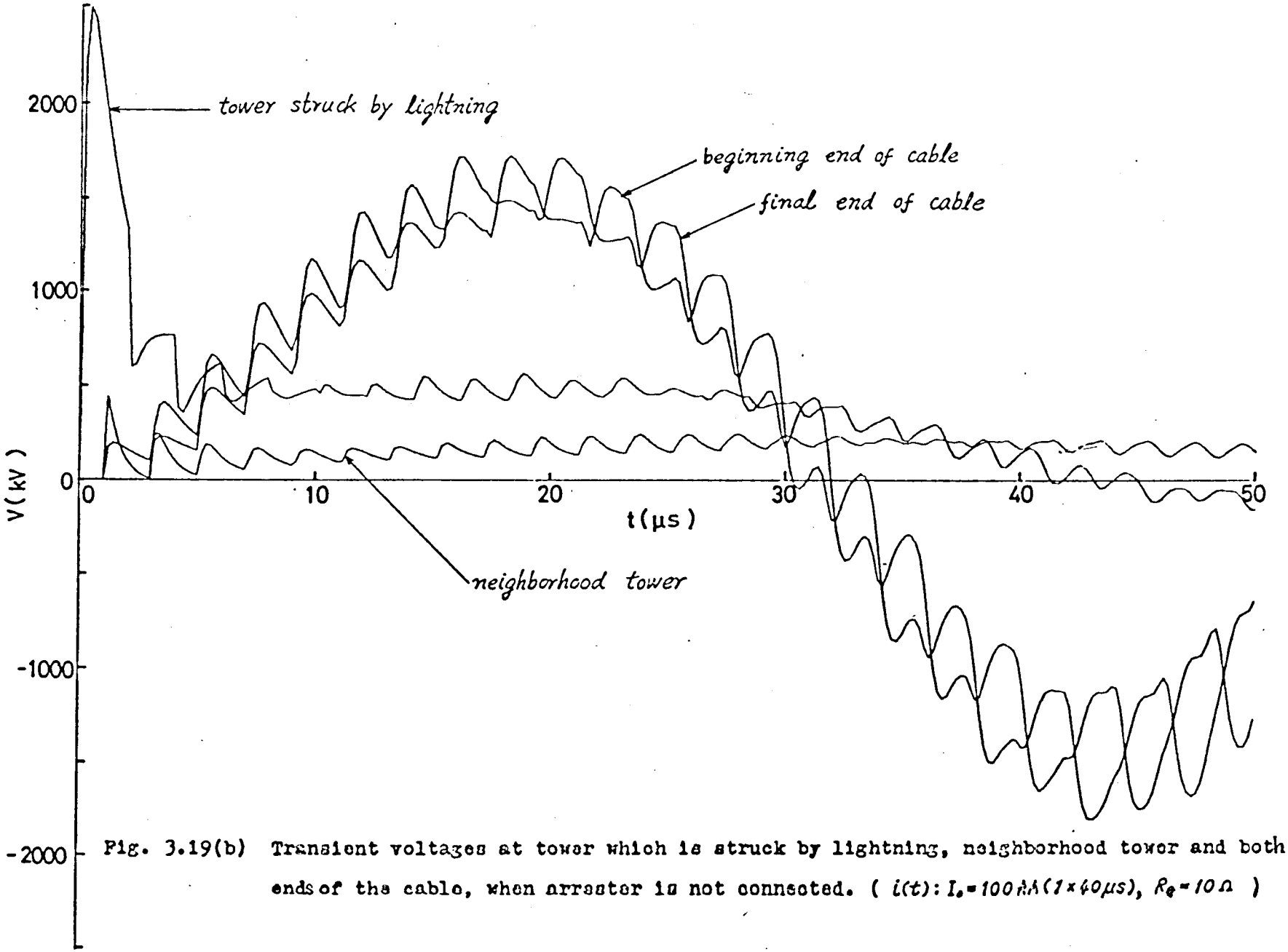

Fig. 3.19(b) Transient voltages at tower which is struck by lightning, neighborhood tower and both ends of the cable, when arrester is not connected. ($i(t)$: $I_0 = 100\,kA\,(1\times40\,\mu s)$, $R_g = 10\,\Omega$)

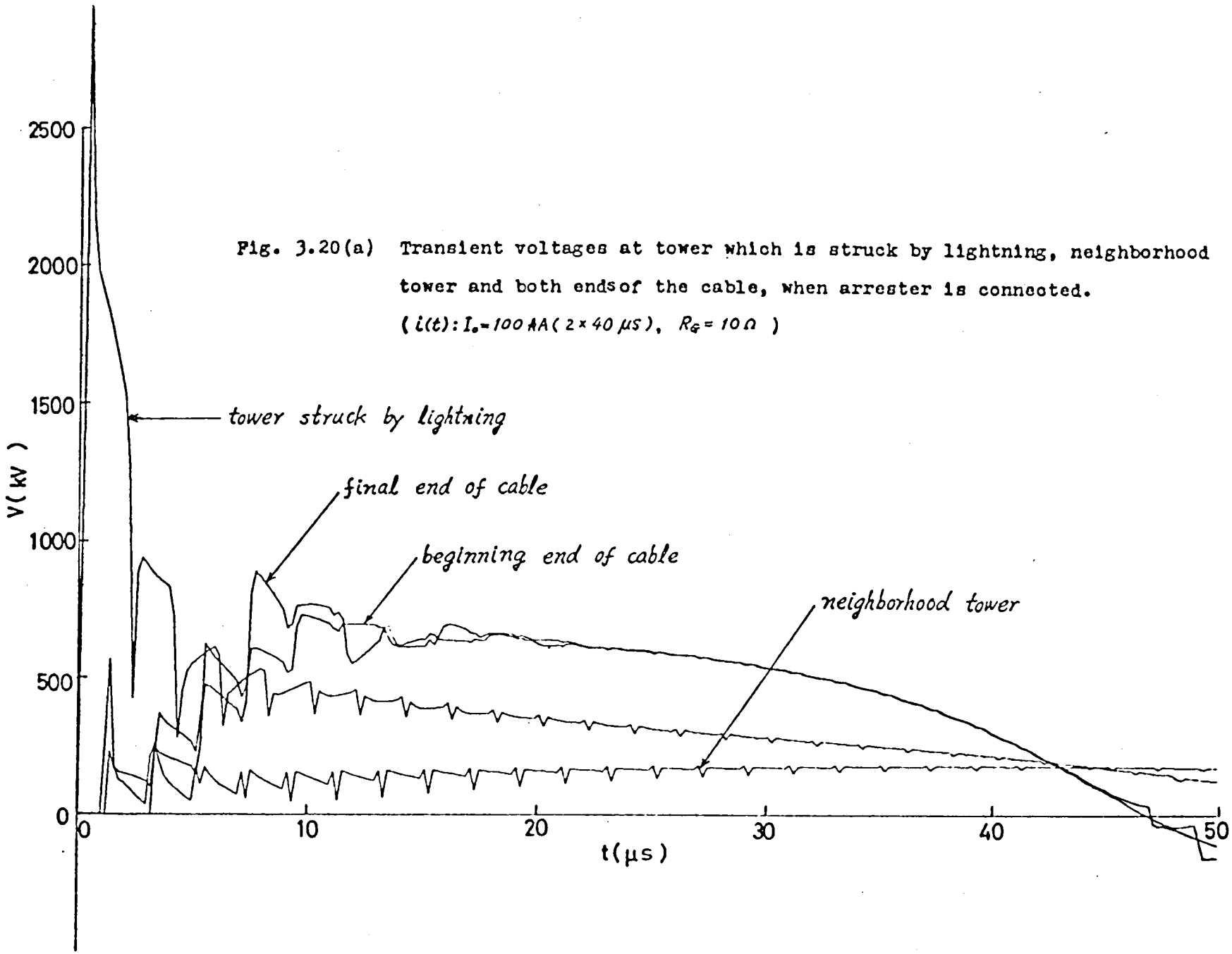

Fig. 3.20(a) Transient voltages at tower which is struck by lightning, neighborhood tower and both ends of the cable, when arrester is connected.
($i(t): I_0 = 100\,kA\,(2 \times 40\,\mu s)$, $R_G = 10\,\Omega$)

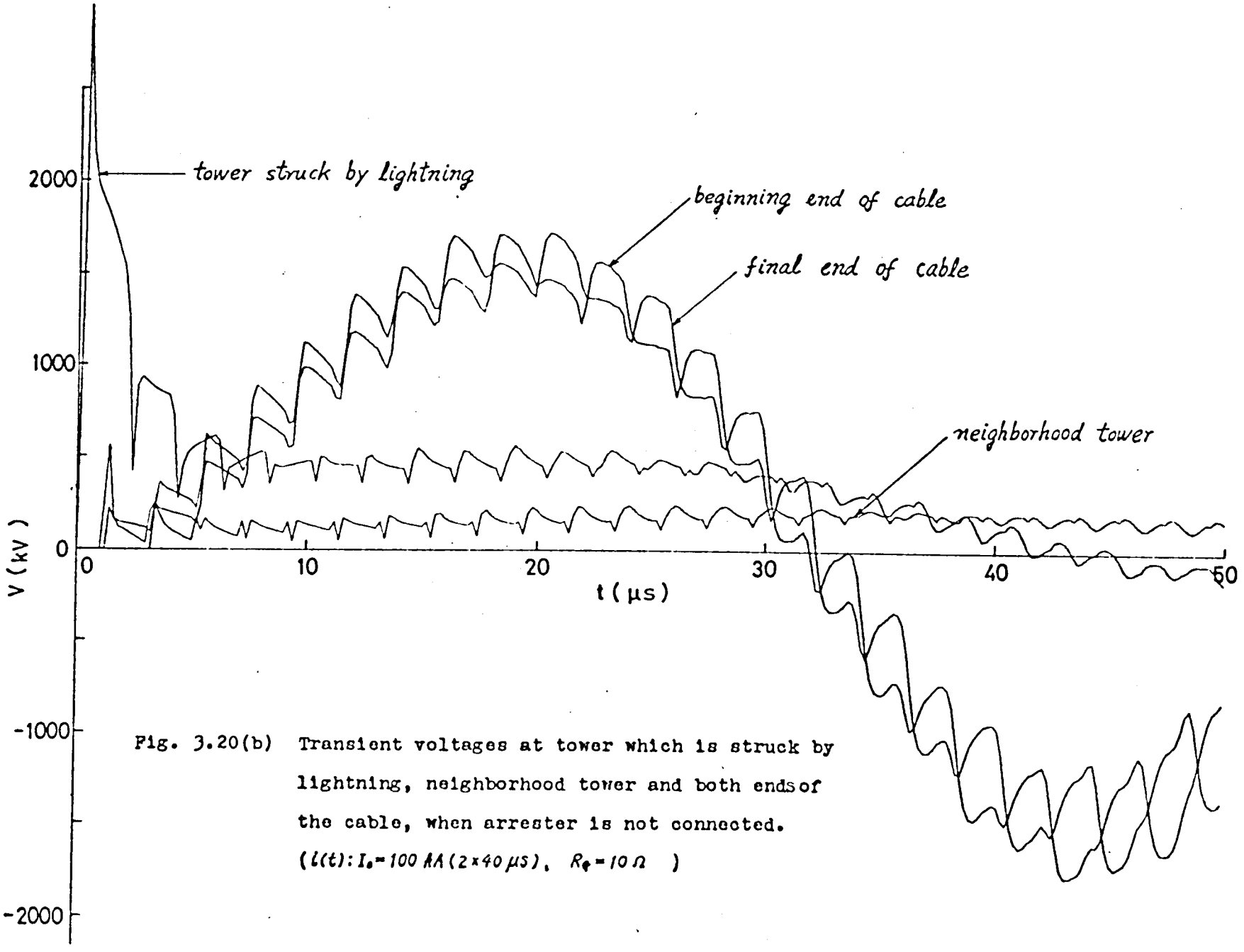

Fig. 3.20(b) Transient voltages at tower which is struck by lightning, neighborhood tower and both ends of the cable, when arrester is not connected.
($i(t): I_0 = 100\,kA\,(2\times40\,\mu s)$, $R_f = 10\,\Omega$)

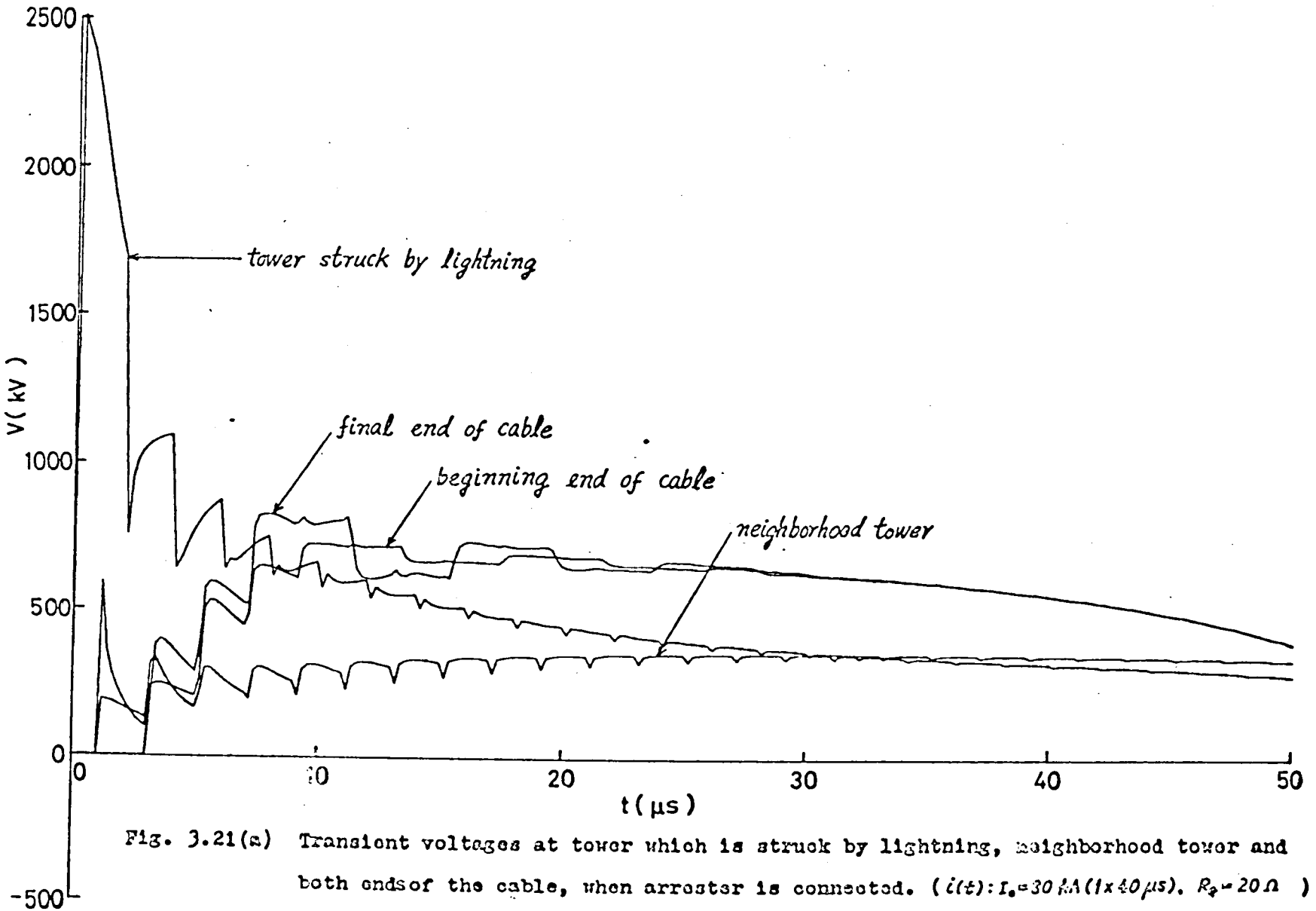

Fig. 3.21(a) Transient voltages at tower which is struck by lightning, neighborhood tower and both ends of the cable, when arrester is connected. ($i(t): I_0 = 30\,kA\,(1\times40\,\mu s)$, $R_g = 20\,\Omega$)

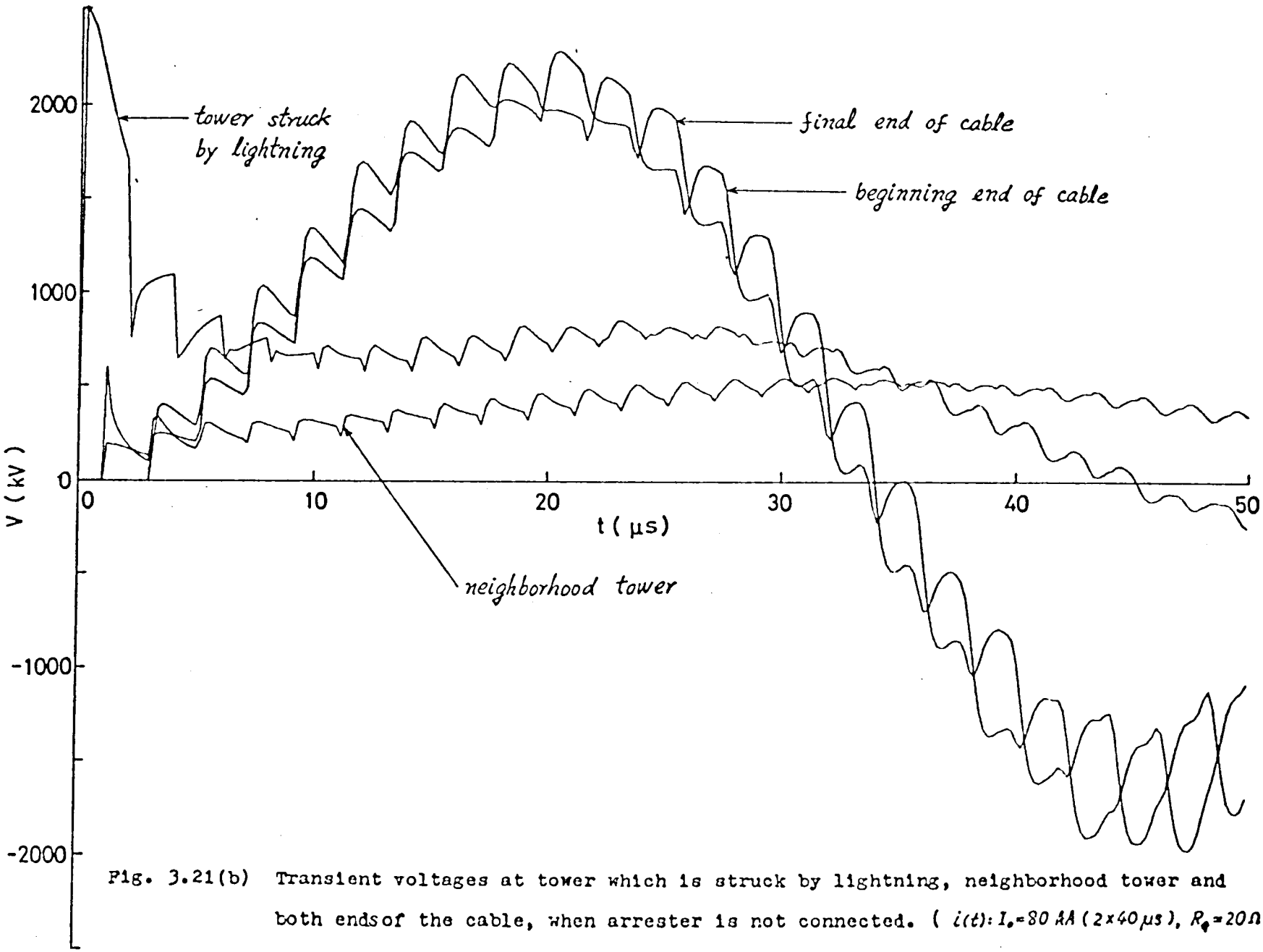

Fig. 3.21(b) Transient voltages at tower which is struck by lightning, neighborhood tower and both ends of the cable, when arrester is not connected. ($i(t): I_0 = 80\,kA\ (2\times40\,\mu s),\ R_f = 20\,\Omega$)

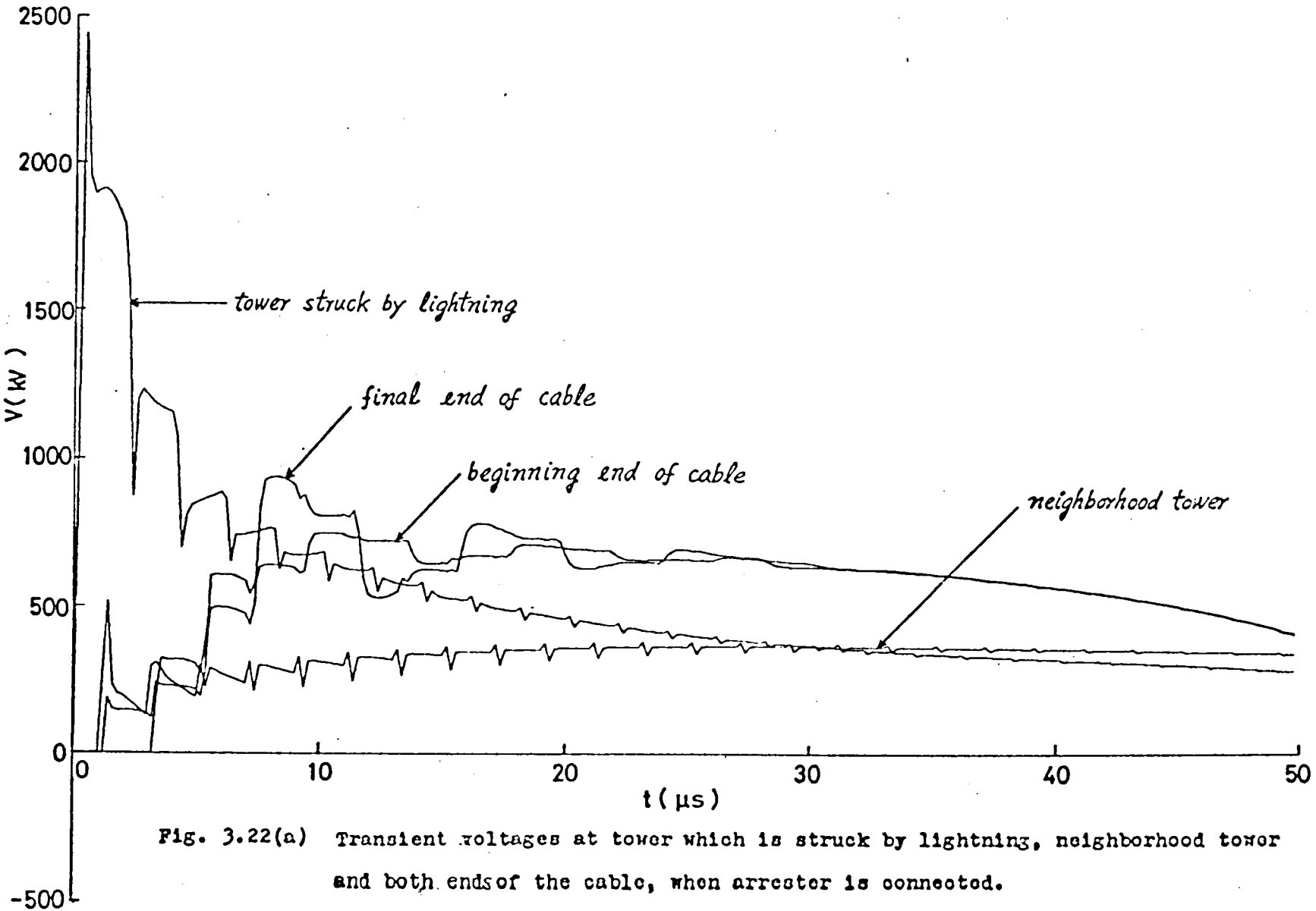

Fig. 3.22(a) Transient voltages at tower which is struck by lightning, neighborhood tower and both ends of the cable, when arrester is connected.
($i(t): I_0 = 80\,kA\,(2\times40\,\mu s)$, $R_g = 20\,\Omega$)

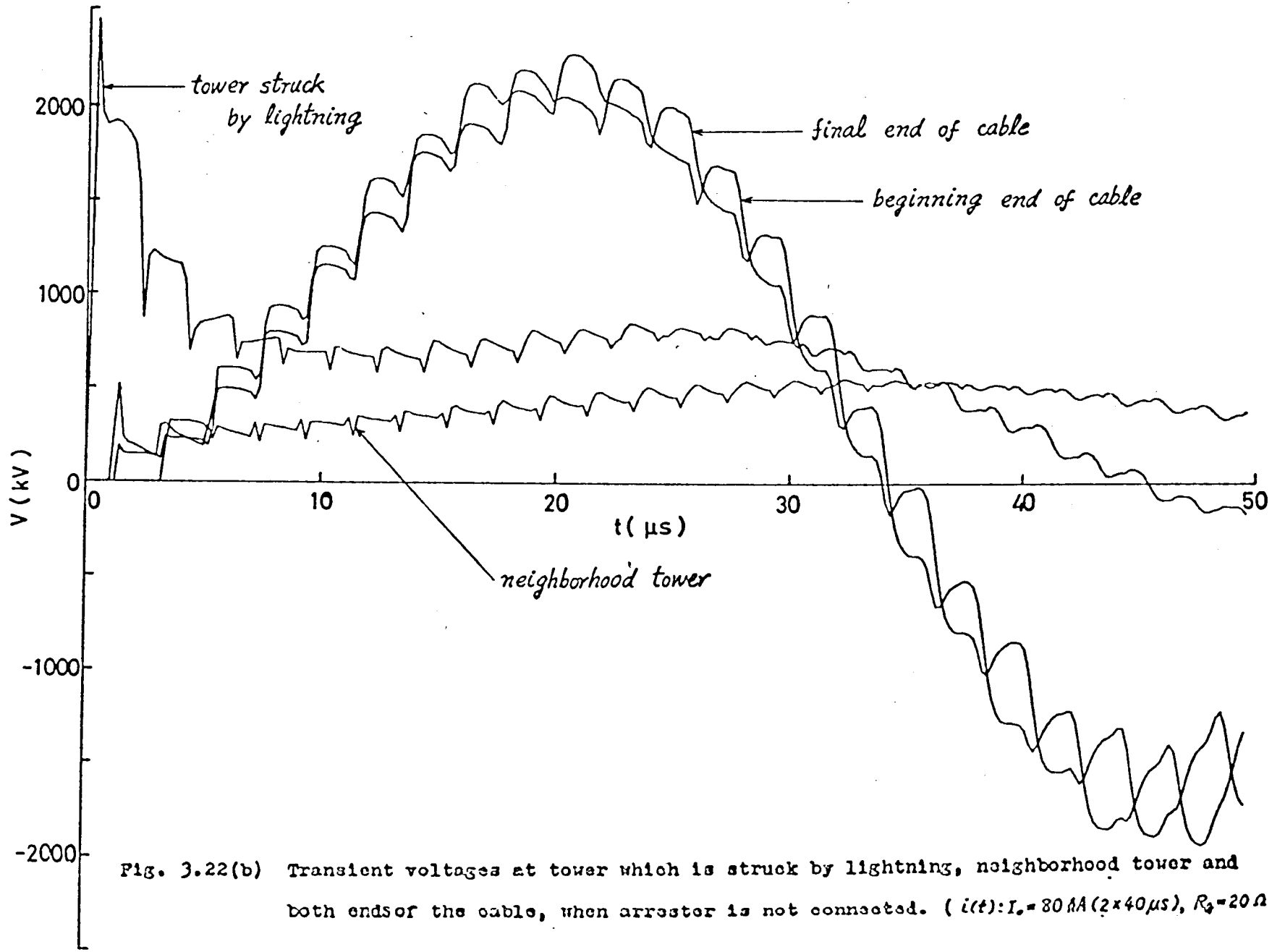

Fig. 3.22(b) Transient voltages at tower which is struck by lightning, neighborhood tower and both ends of the cable, when arrester is not connected. ($i(t): I_0 = 80\,kA\,(2\times40\,\mu s)$, $R_g = 20\,\Omega$)

CHAPTER 4

NUMERICAL ANALYSIS OF LINE EQUATIONS CONSIDERING CORONA LOSS ON SINGLE-CONDUCTOR SYSTEMS (I) —— METHODS 1 AND 2

4.1 Introduction

The voltages of lightning surges on transmission systems often exceed the critical corona voltages of the line conductors, and in such cases, the waveforms are distorted and the peak values are attenuated not only due to the skin effects of the conductor and the ground return but also the corona losses on the conductor.

A precise analysis of the distortion and attenuation of traveling waves caused by the corona losses is very important for the studies on a variety of surge problems in power transmission systems, e.g., prediction of the occurrence of flashback on transmission towers needed for the lightning-proof design of transmission lines and for the protection of elec-

tric equipment in power plants and substations against lightning.

Several theoretical investigations have been reported on the problem of attenuation or distortion of traveling waves due to corona losses such as the leakage-loss theory and the one proposed by Skilling and Dykes.[31] According to the latter theory, the traveling waves are distorted by the increase in distributed capacitance. Under the assumption that the quadratic characteristic equation developed by Peek for the evaluation of ac corona losses is applicable to impulsive corona losses, they have derived the equation to evaluate the surge distortion due to corona losses. This equation has been investigated further by Sunde,[32] who has succeeded in qualitatively reasoning the distortion of crest waveforms due to corona losses. However, further exploration seems necessary in order to provide quantitative explanation of a number of field-test results which have been obtained so far.

Moreover the other researchers have proposed the approximate numerical calculation of the attenuation and distortion of traveling waves due to corona losses.[33],[34] However essentially this problem involves the solution of a set of nonlinear partial differential equations. Because of inherent difficulties involved, no approach has been completely successful.

During the past decade, in the author's laboratory, they have analysed the surge attenuation and distortion due to corona losses by using a surge analyzer specially designed to include the effect of corona losses.[35]~[38]

In performing the analysis by the surge analyzer, a number of peripheral devices such as an impulse generator and instrumenting devices of various types are necessary. So the computation by the analyzer is very tedious and time-consuming and suffers from the shortcoming that the analyzer itself inherently involves some losses.

This chapter, and the following ones are concerned with the numerical computation associated with the solution of the nonlinear surge equations including the effect of corona losses for traveling waves on single- and two-conductor systems. Three methods of numerical calculation are proposed, each of which has been employed to facilitate comparison with the experimental results made on an artificial transmission line by Fujitaka and Aso.[39] It has been found that application of the methods of numerical calculation proposed in this paper makes it possible to estimate the corona loss constants of traveling waves.

In this chapter, the author analyzes approximately the line equations for traveling waves on single-conductor systems by Method 1 or 2,[40]~[42] and in Chapter 5 he does the same equations by Method 3,[43],[44] and in Chapter 6 he treats the line equations for traveling waves on two-conductor systems[45],[46] by means of Method 3.

4.2 Numerical Calculation of Line Equations Considering Corona Loss

4.2.1 Line Equations Considering Corona Loss

In the past, most of the analyses made on the attenuation and distortion of traveling waves due to corona losses were based upon the assumption that the quadratic characteristic equation derived by Peek for the evaluation of ac corona losses is also applicable to traveling waves. Under this assumption, the fundamental line equations of the surge voltage and current on a single-conductor system, when the voltage is above the critical corona voltage, are given by

$$\left.\begin{aligned} -\frac{\partial v}{\partial x} &= L\frac{\partial i}{\partial t}, \\ -\frac{\partial i}{\partial x} &= C\frac{\partial v}{\partial t} + K\frac{(v-v_{co})^2}{v}, \end{aligned}\right\} \qquad (4.1)$$

where

v_{co} : corona critical voltage,

v and i : voltage and current at distant x from sending end,

L and C : inductance and capacitance of line per unit length,

$K = k(f+25) = \sigma_a \sqrt{r/2h} \times 10^{-11}$ (v/m),

$k = \sigma_c \sqrt{r/2h} \times 10^{-11}$ (F/m),

f : frequency (s^{-1}).

r and h : conductor radius and height (m),

$\sigma_a = \sigma_c (f+25)$,

σ_c : corona loss constant.

Since apparently $f \gg 25$ for surges, it is common practice to assume that $f+25 \simeq f = \frac{\partial}{\partial t}$ and that the conductor capacitance is equivalently increased by corona losses. However, our analysis by the surge analyzer[4] has revealed that it is desirable to include not only the increase in distributed capacitance but also the distributed leakage losses. In this connection, the following development will assume that the fundamental surge equations above the critical corona voltage are given by

$$\left.\begin{aligned} -\frac{\partial v}{\partial x} &= L\frac{\partial i}{\partial t}, \\ -\frac{\partial i}{\partial x} &= C\frac{\partial v}{\partial t} + \frac{\partial}{\partial t}(v - v_{c0})^2 + K\frac{(v-v_{c0})^2}{v}. \end{aligned}\right\} \qquad (4.2)$$

Now let us consider the problem of calculating the transient voltage at each point on the line of the length ℓ illustrated in Fig. 4.1, where an impulse voltage having a peak value above the critical corona voltage is impressed on the sending end and

the final one is grounded through the resistance R_l.

This problem requires the solution of the two-point boundary-value problem of nonlinear partial differential equations (4.6) or (4.7), subject to the initial conditions

$$\left.\begin{aligned} v(x,0) &= 0 , \\ i(x,0) &= 0 . \end{aligned}\right\} \tag{4.3}$$

and the boundary conditions

$$v(0,t) = e(t) , \tag{4.4}$$

$$v(l,t) = R_l\, i(l,t) . \tag{4.5}$$

When $v < v_{i0}$ or $\frac{\partial v}{\partial t} < 0$,

$$\left.\begin{aligned} -\frac{\partial v}{\partial x} &= L\frac{\partial i}{\partial t} , \\ -\frac{\partial i}{\partial x} &= C\frac{\partial v}{\partial t} . \end{aligned}\right\} \tag{4.6}$$

When $v \geq v_{i0}$ and $\frac{\partial v}{\partial t} \geq 0$,

$$\left.\begin{aligned} -\frac{\partial v}{\partial x} &= L\frac{\partial i}{\partial t} , \\ -\frac{\partial i}{\partial x} &= C\frac{\partial v}{\partial t} + \frac{\delta}{v}\frac{\partial}{\partial t}(v - v_{i0})^2 + K\frac{(v - v_{i0})^2}{v} . \end{aligned}\right\} \tag{4.7}$$

Up to now, no unified approach has been developed for the numerical solution of partial differential equations. It is necessary to devise a particular method of solution for each problem under consideration. The author has originated the three methods i.e. Methods 1, 2 and 3 for the solution of the aforementioned problems. In this chapter Methods 1 and 2 are described and in the next chapter Method 3 will be presented. The distortion due to the skin effect of traveling waves can be ignored in comparison with that due to corona losses.

4.2.2 Piecewise Linear-Approximation of Line Equations

The first two methods of numerical calculation, viz. Methods 1 and 2, approximate the surge equations by linearization. Although linearization always inevitably involves some errors and the accuracy of calculation becomes worse in comparison with the case without linearization, it is provided with the advantage that all methods employed for the surge analyzer study can be utilized without any modification.

Rearranging the second expression in Eq.s (4.7) we obtain

$$-\frac{\partial i}{\partial x} = C\frac{\partial v}{\partial t} + K v_{co}\frac{\partial}{\partial t}\left(\frac{v}{v_{co}} - 1 - \log\frac{v}{v_{co}}\right) + K v_{co}\left(\frac{v}{v_{co}} - 1\right)^2 \Big/ \left(\frac{v}{v_{co}}\right). \quad (4.8)$$

Let the two $(v/v_{co})-y$ curves given by

$$y = 2\left(\frac{v}{v_{co}} - 1 - \log\frac{v}{v_{co}}\right)$$

and

$$y = \frac{\left(\frac{v}{v_{co}} - 1\right)^2}{\frac{v}{v_{co}}}$$

be approximated by two piecewise linear curves. Also, let H_0 and H_1 be the approximate gradients for the former curve and H_0' and H_1' be those for the latter as shown in Fig. 4.2. If the break-point voltage is denoted by v_{c1}, the system of nonlinear differential equations (4.6) and (4.7) may be piecewise linearized as in the following manner. And we conveniently define modes 0, 1 and 2 as follows. Namely, when $v < v_{co}$ or $\frac{\partial v}{\partial t} < 0$, i.e. for mode 1

$$\left.\begin{aligned} -\frac{\partial v}{\partial x} &= L\frac{\partial i}{\partial t}, \\ -\frac{\partial i}{\partial x} &= C\frac{\partial v}{\partial t}. \end{aligned}\right\} \tag{4.9}$$

When $v_{co} \leq v \leq v_{c1}$ and $\frac{\partial v}{\partial t} \geq 0$, i.e. for mode 2

$$\left.\begin{aligned} -\frac{\partial v}{\partial x} &= L\frac{\partial i}{\partial t}, \\ -\frac{\partial i}{\partial x} &= (C + C_0)\frac{\partial v}{\partial t} + G_0(v - v_{co}). \end{aligned}\right\} \tag{4.10}$$

When $v > v_{c1}$ and $\frac{\partial v}{\partial t} \geq 0$, i.e. for mode 3

$$\left.\begin{aligned} -\frac{\partial v}{\partial x} &= L\frac{\partial i}{\partial t}, \\ -\frac{\partial i}{\partial x} &= (C+C_0+C_1)\frac{\partial v}{\partial t} + G_0(v-v_{c0}) + G_1(v-v_{c1}). \end{aligned}\right\} \qquad (4.11)$$

where

$$\left.\begin{aligned} & C_0 = kH_0, \quad C_1 = k(H_1 - H_0) \\ & : \text{equivalent distributed capacitances,} \\ & G_0 = KH_0', \quad G_1 = K(H_1' - H_0') \\ & : \text{equivalent distributed leakage conductances.} \end{aligned}\right\} \qquad (4.12)$$

4.2.3 Numerical Calculation of Piecewise Linear Approximated Line Equations (1) —— Method 1.

If Eq.s (4.11) is approximated by lumped constants for the infinitesimal distance Δx, the equivalent circuit shown in Fig. 4.3 may result, where

$$\nu = 1, 2, \cdots\cdots, n,$$

v_ν and i_ν : output voltage and current of the ν-th element,

$v_{\nu-1}$ and $i_{\nu-1}$: input voltage and current of the ν-th element or output ones of the $(\nu-1)$-th element,

v_{ci} : voltage at intersection of piecewise rectilinear characteristics,

n : number of total elements.

But, if the value of the line voltage may transiently become both the positive and negative, though it is assumed to be always positive in our case, we must add the inverse-polarity and hysteresis elements to the corona loss ones in Fig. 4.3.

We have the following differential difference equations for the infinitesimal distance Δx for the input and output voltages and currents of the ν-th element in Fig. 4.3. If the ν-th element is in mode 2,

$$\left.\begin{aligned} v_{\nu-1}(t) - v_\nu(t) &= L\Delta x \frac{di_{\nu-1}(t)}{dt}, \\ i_{\nu-1}(t) - i_\nu(t) &= (C + C_0 + C_1)\Delta x \frac{dv_\nu(t)}{dt} \\ &\quad + G_0 \Delta x \{v_\nu(t) - v_{c0}\} + G_1 \Delta x \{v_\nu(t) - v_{c1}\}. \end{aligned}\right\} \tag{4.13}$$

First-order approximation of Eq.s (4.13) for the interval of

time Δt gives the following difference equations

$$\left.\begin{aligned}
&v_{\nu-1}(t)-v_{\nu}(t)=L'\{i_{\nu-1}(t)-i_{\nu-1}(t-\Delta t)\},\\
&i_{\nu-1}(t)-i_{\nu}(t)=(C'+C_0'+C_1')\{v_{\nu}(t)-v_{\nu}(t-\Delta t)\}\\
&\qquad\qquad +G_0'\{v_{\nu}(t)-v_{C0}\}+G_1'\{v_{\nu}(t)-v_{C1}\},\\
&L'=L\,\Delta x/\Delta t, \qquad C'=C\,\Delta x/\Delta t,\\
&C_0'=C_0\,\Delta x/\Delta t, \qquad C_1'=C_1\,\Delta x/\Delta t,\\
&G_0'=G_0\,\Delta x, \qquad G_1'=G_1\,\Delta x.
\end{aligned}\right\} \tag{4.14}$$

Under the assumption that the voltage and current satisfy

$$\left.\begin{aligned}
&i_{\nu}(t)=a_{2\nu}(t)v_{\nu}(t)+b_{2\nu}(t),\\
&v_{\nu}(t)=a_{2\nu-1}(t)i_{\nu-1}(t)+b_{2\nu-1}(t),
\end{aligned}\right\} \tag{4.15}$$

we can establish the following relations among the above coefficients by substituting Eq.s (4.15) into Eq.s (4.14).

$$\left.\begin{aligned}
&a_{2\nu}(t)=1/\{L'+a_{2\nu+1}(t)\},\\
&b_{2\nu}(t)=\{L'i_{\nu}(t-\Delta t)-b_{2\nu+1}(t)\}/\{L'+a_{2\nu+1}(t)\},\\
&a_{2\nu-1}(t)=1/\{C'+C_0'+C_1'+G_0'+G_1'+a_{2\nu}(t)\},\\
&b_{2\nu-1}(t)=\{(C'+C_0'+C_1')v_{\nu}(t-\Delta t)+G_0'v_{C1}+G_1'v_{C1}-b_{2\nu}(t)\}\\
&\qquad\qquad /\{(C'+C_0'+C_1'+G_0'+G_1'+a_{2\nu}(t)\}.
\end{aligned}\right\} \tag{4.16}$$

If the ν-th element is in mode 1, the recurrence formula is reduced to the equation obtained by putting $C_\nu' = G_\nu' = 0$ in Eq.s (4.16); if the element is in mode 0, it becomes the equation obtained by setting

$$C_\nu' = C_\nu' = G_\nu' = G_\nu' = 0 \ .$$

At the final end, Eq. (4.5) gives

$$\left.\begin{aligned} a_{2n}(t) &= 1/R_L \ , \\ b_{2n}(t) &= 0 \ . \end{aligned}\right\} \qquad (4.17)$$

Using Eq.s (4.16) and (4.17), the values of $a_{2n-1}(t), b_{2n-1}(t), \cdots\cdots, a_0(t)$ and $b_0(t)$ can be calculated. Once these values are obtained, $i_0(t), v_1(t), i_1(t), \cdots\cdots\cdots, v_n(t)$ and $i_n(t)$ can be computed successively be using the relation $v_0(t) = e(t)$ in Eq.s (4.4) and (4.15). Lastly, a digital computer flow-chart for calculating the values of voltages at the final end, is drawn in Fig. 4.4.

4.2.4 Numerical Calculation of Piecewise Linear-Approximated Line Equations (2) —— Method 2.

Method 2 is a improvement of Method 1, and has the same computing algorithm as Method 3 which will be introduced in the next chapter. Method 3 is the method to get the numerical solution of nonlinear partial differencial equations (4.6) and (4.7), and on the other hand, Method 2 is the one to seek for the solution of piecewise linear-approximated partial differential equations (4.9), (4.10) and (4.11). However, the procedure of these two methods is almost the same as each other, and therefore the detailed computation procedure will be described in the next chapter, and so, here we will show only the last results.

By applying the same treatment as the one, which will be developed for Method 3 in the next chapter, to Eq.s (4.9), (4.10) and (4.11), we have a set of difference equations.

$$i_{p-1}(t) = \begin{cases} i_{p-1}(t-\Delta t) + \dfrac{1}{L}\dfrac{\Delta t}{\Delta x}\{v_{p-1}(t) - v_p(t)\}, & \text{for } i_{p-1}(t-\Delta t) \neq 0, \quad (4.18) \\ i_{p-1}(t-\Delta t) + \dfrac{1}{2L}\dfrac{\Delta t}{\Delta x}\{v_{p-1}(t) - v_p(t)\}, & \text{for } i_{p-1}(t-\Delta t) = 0, \quad (4.19) \end{cases}$$

$$v_p(t+\Delta t) = \begin{cases} v_p(t) + \dfrac{1}{C}\dfrac{\Delta t}{\Delta x}\{i_{p-1}(t) - i_p(t)\}, & \text{for } v_p(t) < v_{c0} \text{ or } v_p(t) < v_p(t-\Delta t), \end{cases} \tag{4.20}$$

$$v_p(t+\Delta t) = \begin{cases} v_p(t) + \dfrac{1}{C+C_0}\dfrac{\Delta t}{\Delta x}\{i_{p-1}(t) - i_p(t)\} \\ \quad + \dfrac{G_0}{C+C_0}\Delta t\{v_p(t) - v_{c0}\}, \\ \text{for } v_{c0} \le v_p(t) \le v_{c1} \text{ or } v_p(t) \ge v_p(t-\Delta t). \end{cases} \tag{4.21}$$

$$v_p(t+\Delta t) = \begin{cases} v_p(t) + \dfrac{1}{C+C_0+C_1}\dfrac{\Delta t}{\Delta x}\{i_{p-1}(t) - i_p(t)\} \\ \quad + \dfrac{G_0}{C+C_0+C_1}\Delta t\{v_p(t) - v_{c0}\} \\ \quad + \dfrac{G_1}{C+C_0+C_1}\Delta t\{v_p(t) - v_{c1}\}, \\ \text{for } v_p(t) > v_{c1} \text{ and } v_p(t) \ge v_p(t-\Delta t). \end{cases} \tag{4.22}$$

The voltage and current at each point and instant are numerically calculated by applying the same procedure as in Method 3 to Eq.s (4.18) through (4.22).

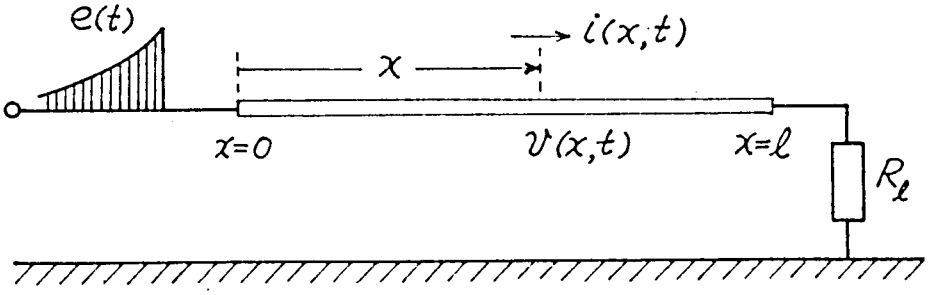

Fig. 4.1 A Single-conductor system

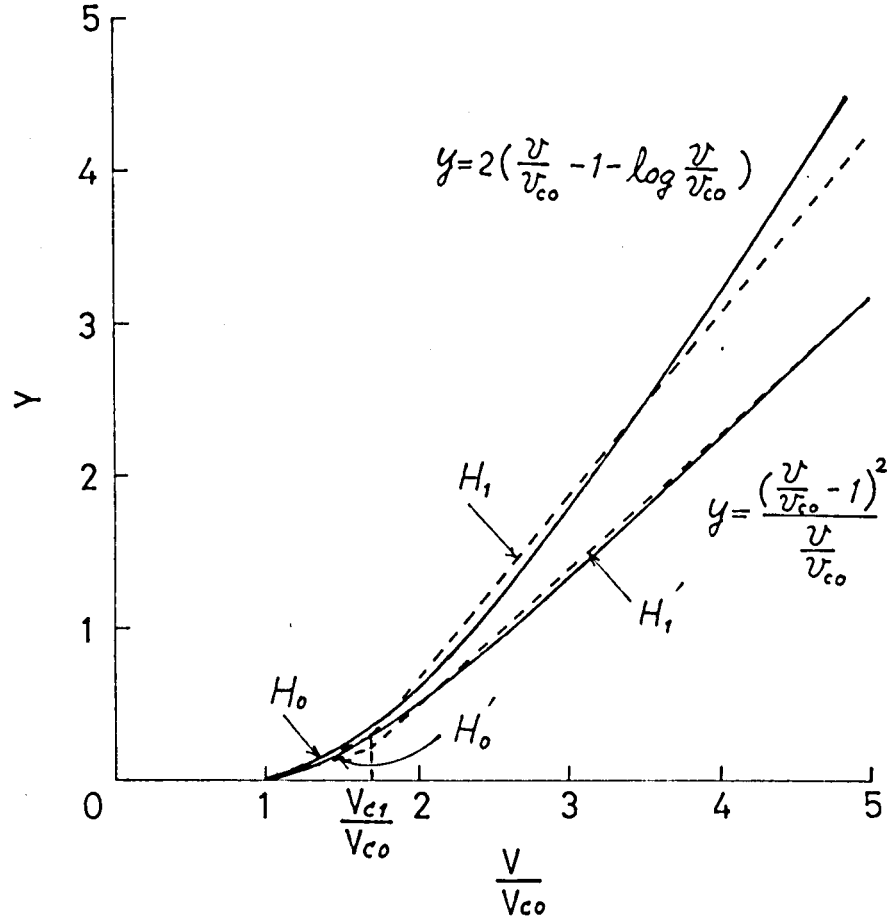

Fig. 4.2 Two (v/v_{co})-y curves and those piecewise linear-approximations.

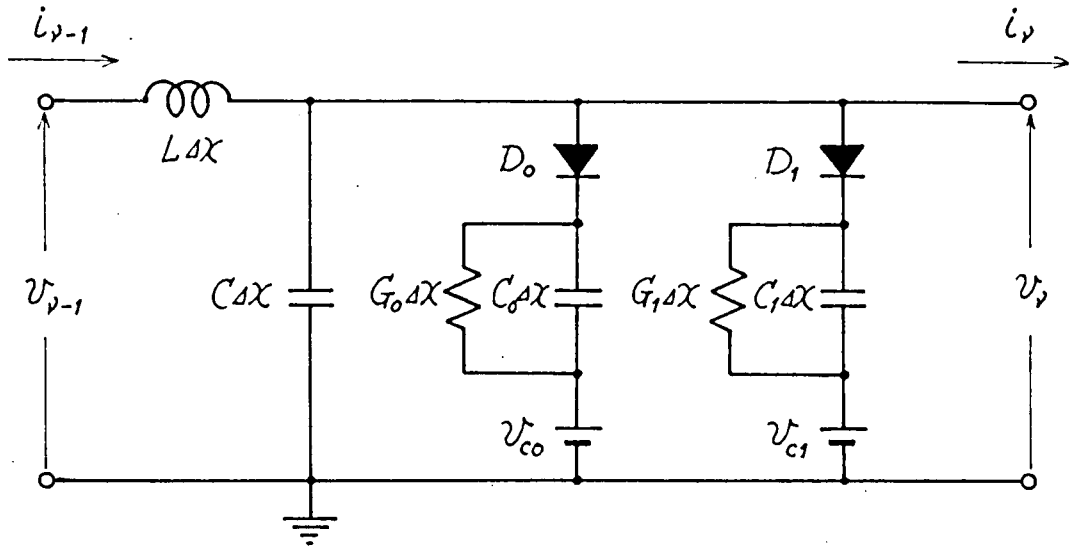

Fig. 4.3 The ν-th element of an approximate equivalent circuit of a single-conductor systems with corona loss elements.

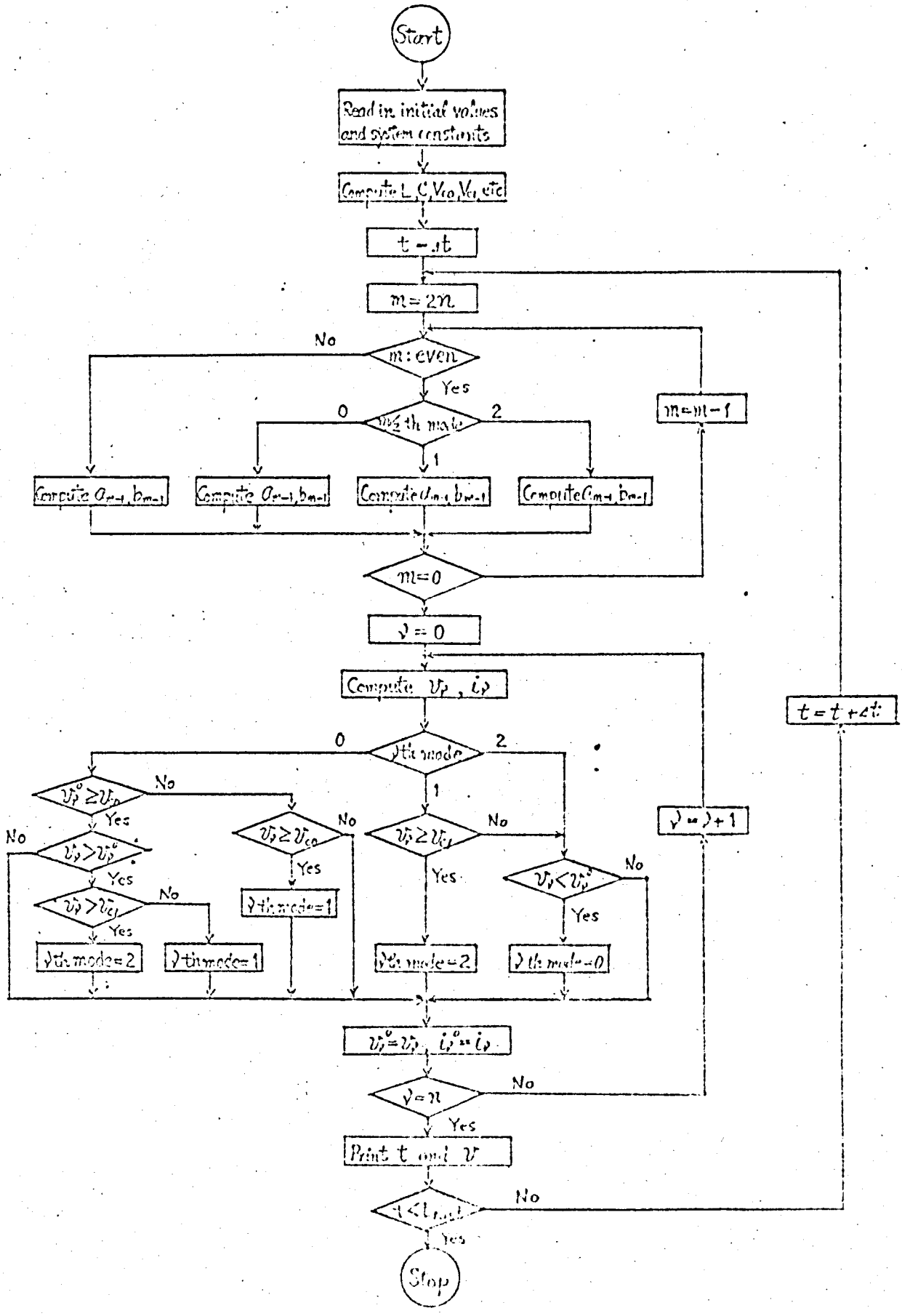

Fig. 4.4 Digital computer flow-chart.

4.3 Numerical Investigation

4.3.1 Numerical Conditions

In this section, the numerical values of the system constants given in the Reference (39) are used in the computations, since we intend to obtain the optimum values of the corona loss constants σ_c and σ_q by comparing the results, which are obtained by the digital computation method described in the previous section, with the experimental ones given by Aso and Fujitaka.[39]

Table 4.1 shows the values of the constants used in the calculations. The value of v_{co} is computed from the following equation:

$$v_{co} = m_o m_1 \delta g_o r \times 10^{-11} / (18C) \qquad (4.23)$$

where

m_o : surface coefficient of conductor ($\simeq$ 0.96),

m_1 : weather factor ($\simeq$ 1),

δ : relative density of air ($\simeq$ 1),

g_o : insulation breakdown strength of air ($\simeq$ 2980kV/m).

The impressed voltage $e(t)$ has been chosen to be a rectangular-crest and exponential-peak surge, viz. $e(t) = E_o \exp(-t/\tau)$,

in order to be coincident with that employed in the experiment. Moreover, $v_{c1}=1.7\,v_{c0}$ is adopted by considering the peak value of the impressed impulse voltages and the shape of two (v/v_{c0})-y curves. And the computation is carried out on the assumption that K and λ and hence σ_q and σ_c are independent of each other. Since the equivalent frequency f with respect to the traveling wave is uncertain, our treatment may be considered as pertinent.

4.3.2 Calculated Results and Discussions

The computations have been carried out according to Method 1. In Fig. 4.5 are plotted the digital calculation results of the transient voltages at the final end, which are grounded with the surge impedance of the line, about the various values of σ_c and σ_q. Also, Fig. 4.5(a) show the final end voltage waveforms in respect to the positive applied impulses, whose wave tail time constant τ is 20 μs and Fig. 4.5(b) show those corresponding to the negative ones.

From these figures, we can see that the waveforms similar to the actual corona distortion of the surges can be obtained. However, as previously described, because of the use of piece-wise linear approximation for the two (v/v_{c0})-y curves in our computation, it is unavoidable that the step shapes appear at the vicinity of the break-point voltage v_{c1} in the voltage

in the voltage waveforms. Furthermore, from Fig. 4.5 it may be said that the time lag of wavefront increases if the value of σ_c does, and on the other hand, the attenuation of the crest increases if the value of σ_q does. These facts will be explained again in Article 5.3.2 more detailedly. Making use of the overall tendency such as above for the waveforms resulting from different combinations of σ_c and σ_q, the waveforms obtained by the experiment have been surrounded by those for different combinations of σ_c and σ_q; this surrounded region has been narrowed gradually to estimate the optimum values of σ_c and σ_q as shown in Fig. 4.5. Finally, we could obtain the optimum values of σ_c and σ_q as shown in Table 4.2.

Next, some examples calculated with the estimated values of σ_c and σ_q given in Table 4.2, are shown by the solid lines in Fig. 4.6. For comparison, the corresponding experimental waveforms by Aso and Fujitaka are also shown by the dotted lines in the same figure. It will be seen that the computed results of the attenuation of the peak value and the distortion of the waveform are in good agreement with the experimental ones. However, in Fig. 4.6, the computed and experimental waveforms are plotted such that both coincide at the instant when the critical corona voltage (calculated value) is reached, because the experimental wavetoes slope somewhat larger than the computed ones. Moreover, the calculated waveforms have had larger distortion than the experimantal results immediately after the arrival of the corona voltage, due to the fact that the slope of the first line segment is larger than the slope of the

actual (v/v_{co})-y curve. As previously described, since the piecewise rectilinear approximation is used, the step phenomena at the vicinity of the break-point voltage are unavoidable.

The author execute the same calculation by using Method 2. But the calculated results shall be omitted, since it is almost the same with the one which is obtained by Method 1.

4.3.3 Comparison With the Computed Results by Surge Analyzer

The author have already estimated the other optimum values of σ_c and σ_q for the surge (wave tail time constant $\tau \simeq 20\,\mu s$) by surge analyzer. They were

$$\sigma_c \simeq 40, \quad \sigma_q \simeq 4.5 \times 10^6 \quad : \text{positive surge},$$

$$\sigma_c \simeq 20, \quad \sigma_q \simeq 5.5 \times 10^6 \quad : \text{negative surge}.$$

Comparing the estimated values by digital computer with those by surge analyzer, we can see that the value of σ_q considerably differs. Fig. 4.7 shows one computed result of the final end voltage by surge analyzer and that by digital computer under the same conditions. From the figure it can be seen that the peak value of voltage waveform computed by surge analyzer is more attenuated than that of digital computer.

It is due to the fact that the resistance losses of the inductance coils are unavoidable in the surge analyzer. Therefore, it seems to be natural that the difference arises between the two estimated values of σ_4.

4.3.4 Comparison of the Results Obtained by Methods 1 and 2

In this section, let us compare Method 1 and Method 2. In Method 1, the coefficients between the voltage and current at each point on the line and at each instant are calculated backwards from the ones at the final end to satisfy the terminal condition. The values of the voltages and currents then are calculated progressively from the ones of sending end. In successfully applying Method 1 to the analysis of line equation, for example the line length must be devided into 40 sections (viz. Δx = 51.7m) and Δt must be of the order of 0.005μs, and then the computation needs very long time.

Method 2 is a revision of Method 1. In Method 2 the voltage and current are calculated progressively from the ones of the sending end in such a way that they also satisfy the terminal condition at the final end. By means of Method 2, the numerical solution can be converged, if we adopt Δt = 0.05 ~ 0.1μs when ΔX = 51.7m. Therefore, using this method a great saving of computing time can be realized and the time decrease to the

order of 1/20 to 1/40 of the one consumed in the above mentioned successful calculation by Method 1.

Table 4.1 Values of main quantities availed in computations.

Line length	$\ell = 2067$ m
Hight of conductor	$h = 3.1$ m
Radius of conductor	$r = 1.15 \times 10^{-3}$ m
Length of subdivisions	$\Delta x = 51.7$ m
Time interval	$\Delta t = 0.005$ μs
Receiving-end resistors	$R_\ell = 516$ Ω
Inductance of conductor	$L = 1.72$ μH/m
Capacitance of conductor	$C = 6.47$ μμF/m
Number of equivalent circuit elements	$n = 40$
Critical corona voltage	$v_{co} = 28.3$ kV
Break point voltage	$v_{ci} = 48.1$ kV

Table 4.2 Optimum values of σ_c and σ_G for positive and negative surges.

Wave tail time constant τ	Positive surge		Negative surge	
	σ_c	σ_G	σ_c	σ_G
5 μs	32	30×10	17	18×10^6
20 μs	32	18×10	17	18×10^6
80 μs	25	27×10	12	27×10^6

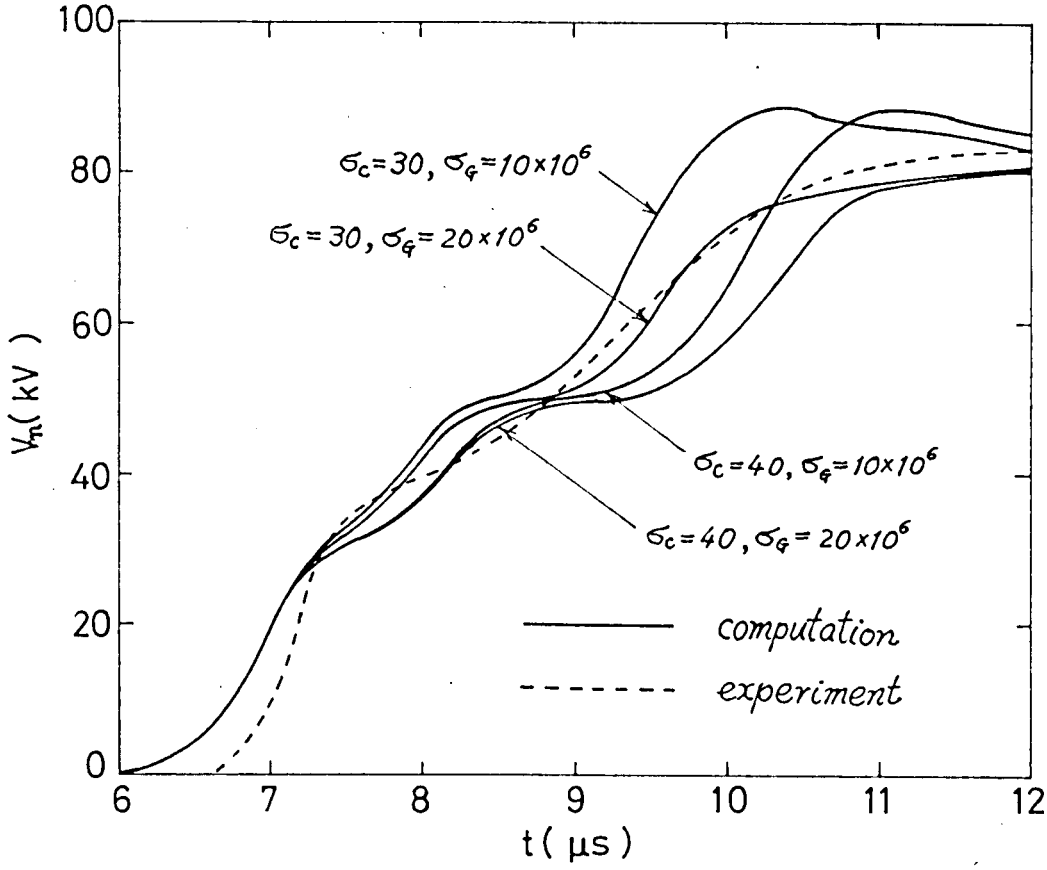

a. E_0= 95 kV (τ= 20 μs)

Fig. 4.5 Examples of calculated voltage waveforms and the corresponding experimental ones.

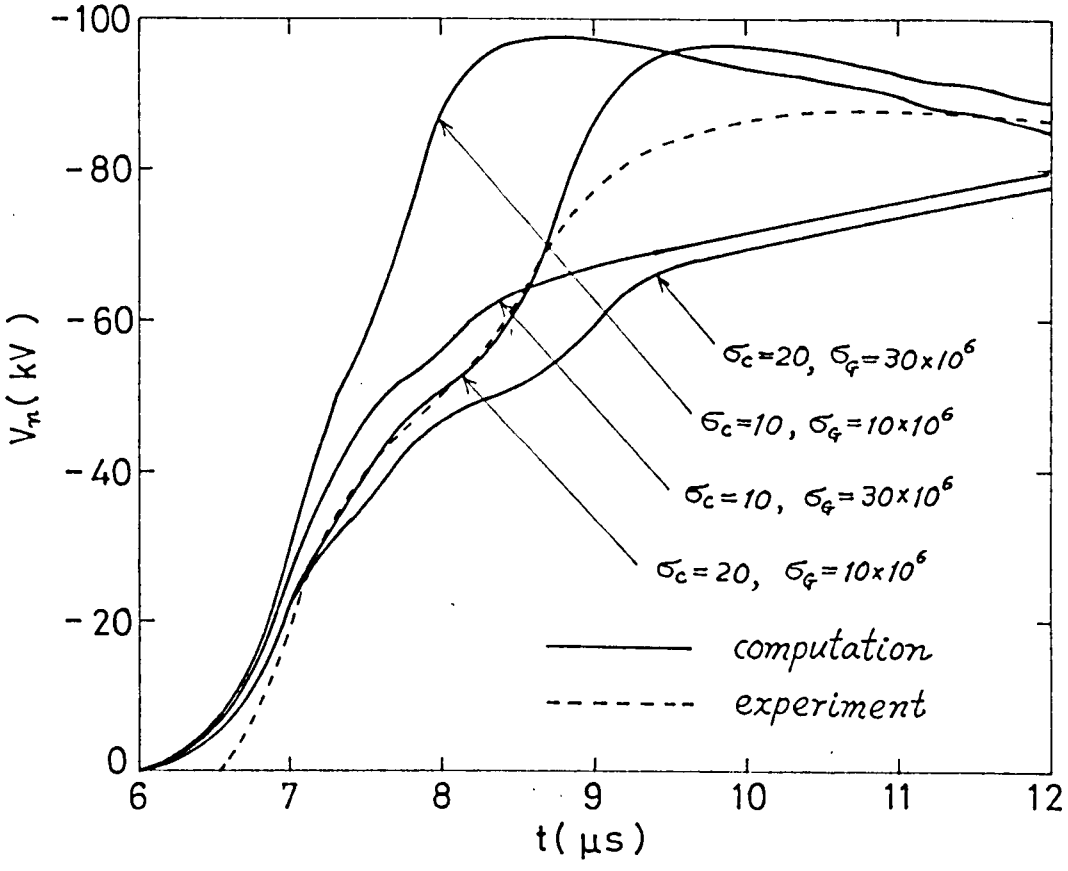

b. E_o = -104 kV (τ = 20 μs)

Fig. 4.5 Examples of calculated voltage waveforms and the corresponding experimental ones.

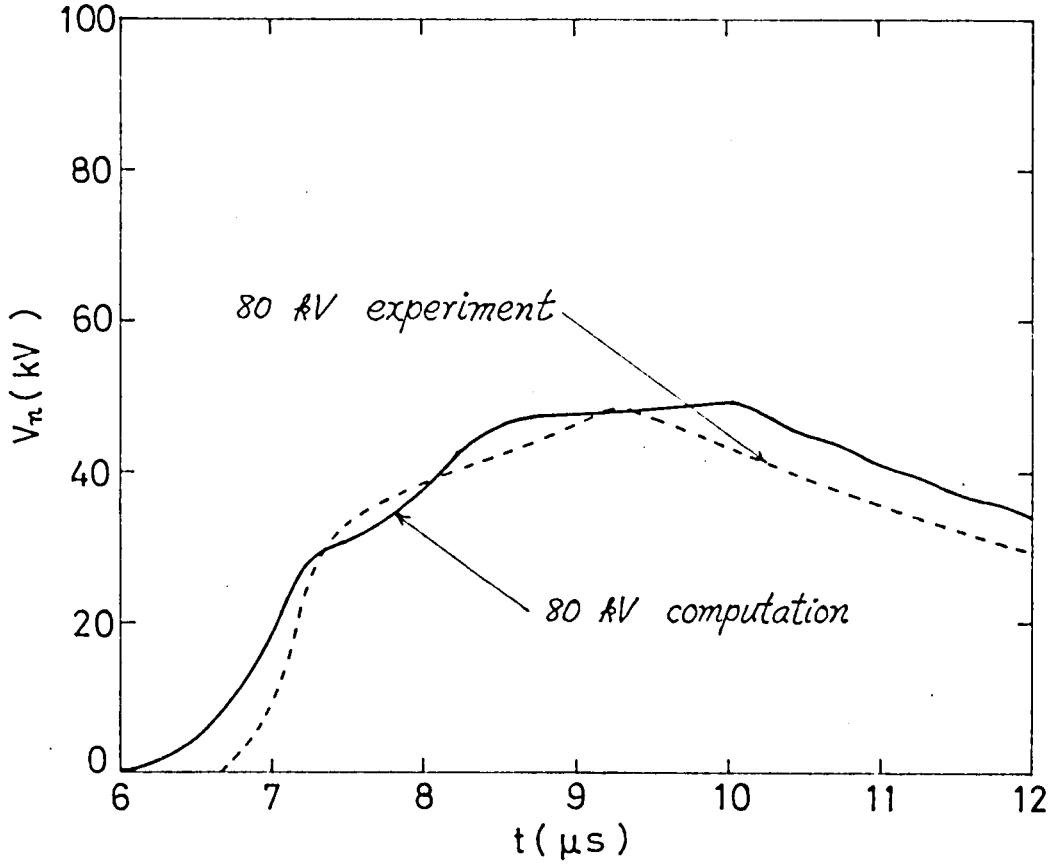

a-1. $E_0 = 80$ kV ($\tau = 5$ μs)

Fig. 4.6 Comparison of computed and experimental examples of final end voltages.

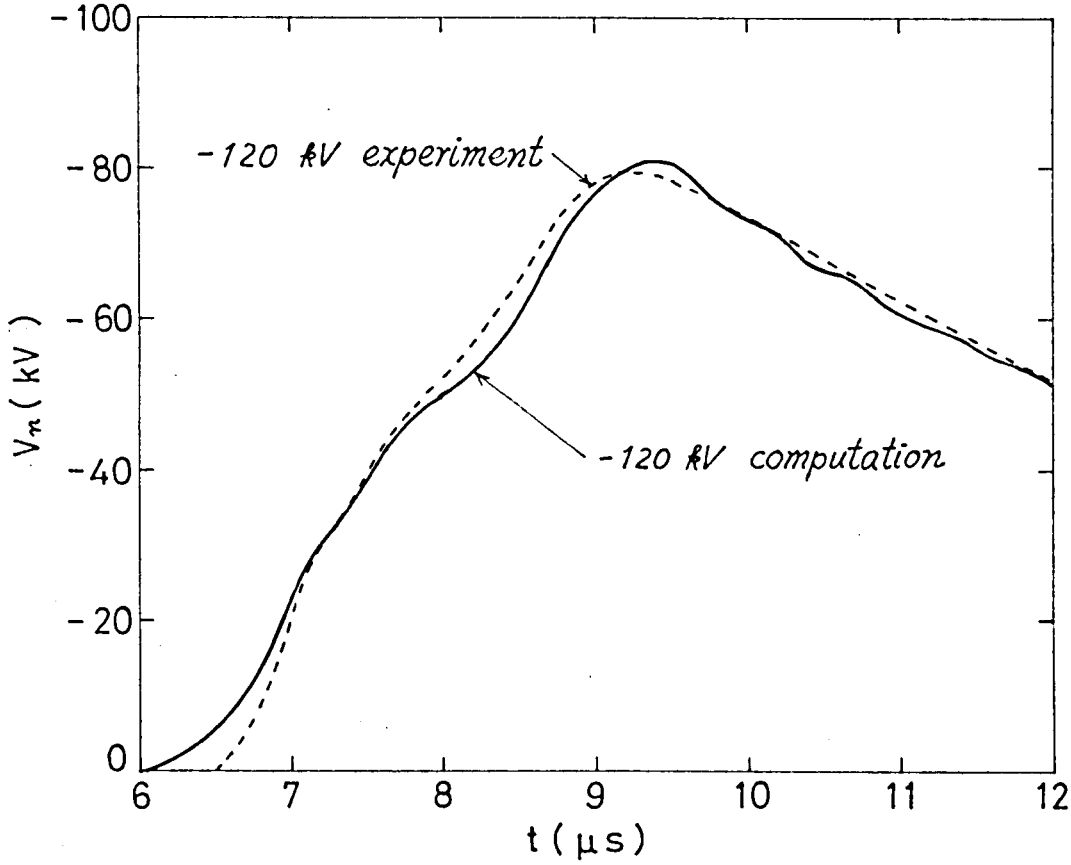

b-1. $E_o = -120$ kV ($\tau = 5$ μs)

Fig. 4.6 Comparison of computed and experimental examples of final end voltages.

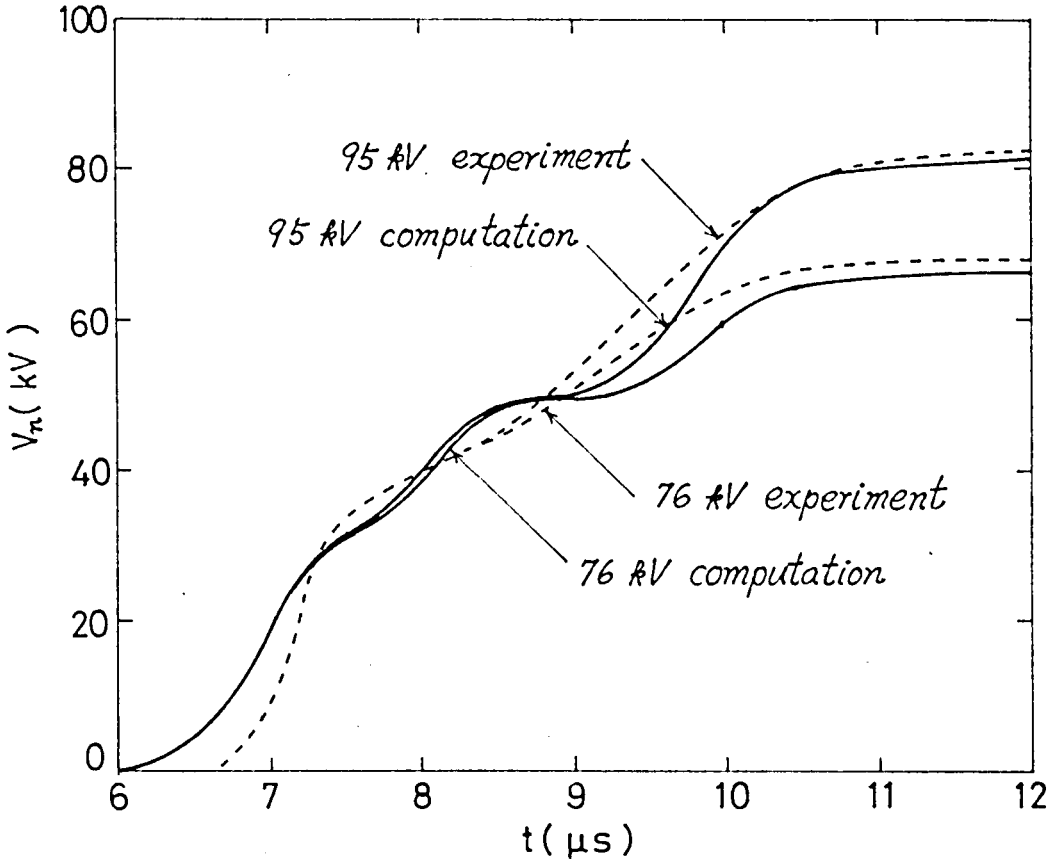

a-2. E_0 = 95 kV, 76 kV (τ = 20 μs)

Fig. 4.6 Comparison of computed and experimental examples of final end voltages.

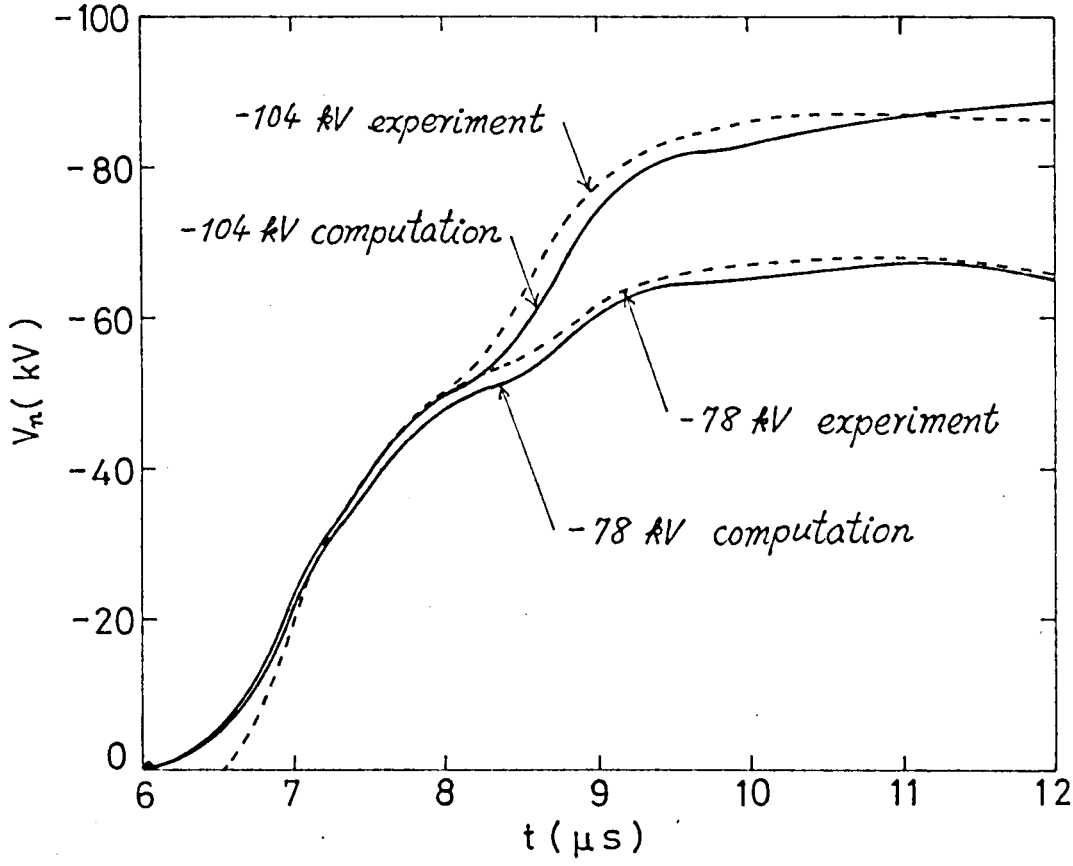

b-2. E_o = -104 kV, -78 kV (τ = 20μs)

Fig. 4.6 Comparison of computed and experimental examples of final end voltages.

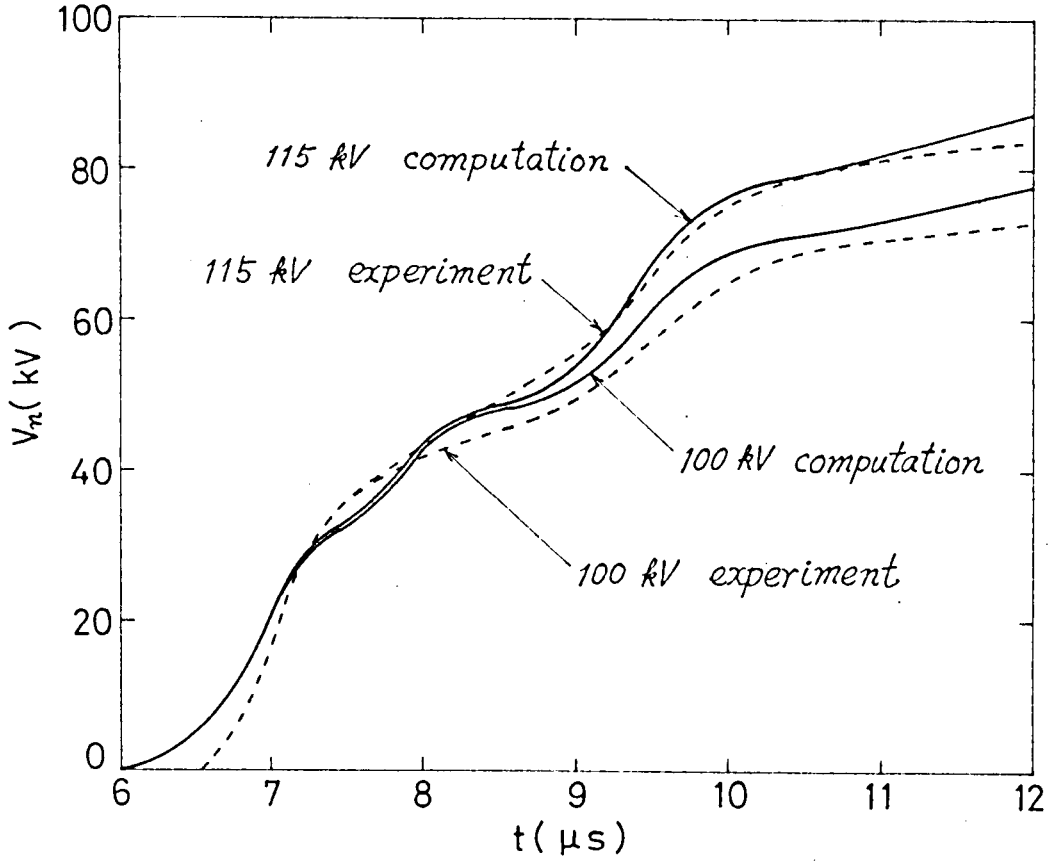

a-3. E_0=115 kV, 100 kV (τ=80 μs)

Fig. 4.6 Comparison of computed and experimental examples of final end voltages.

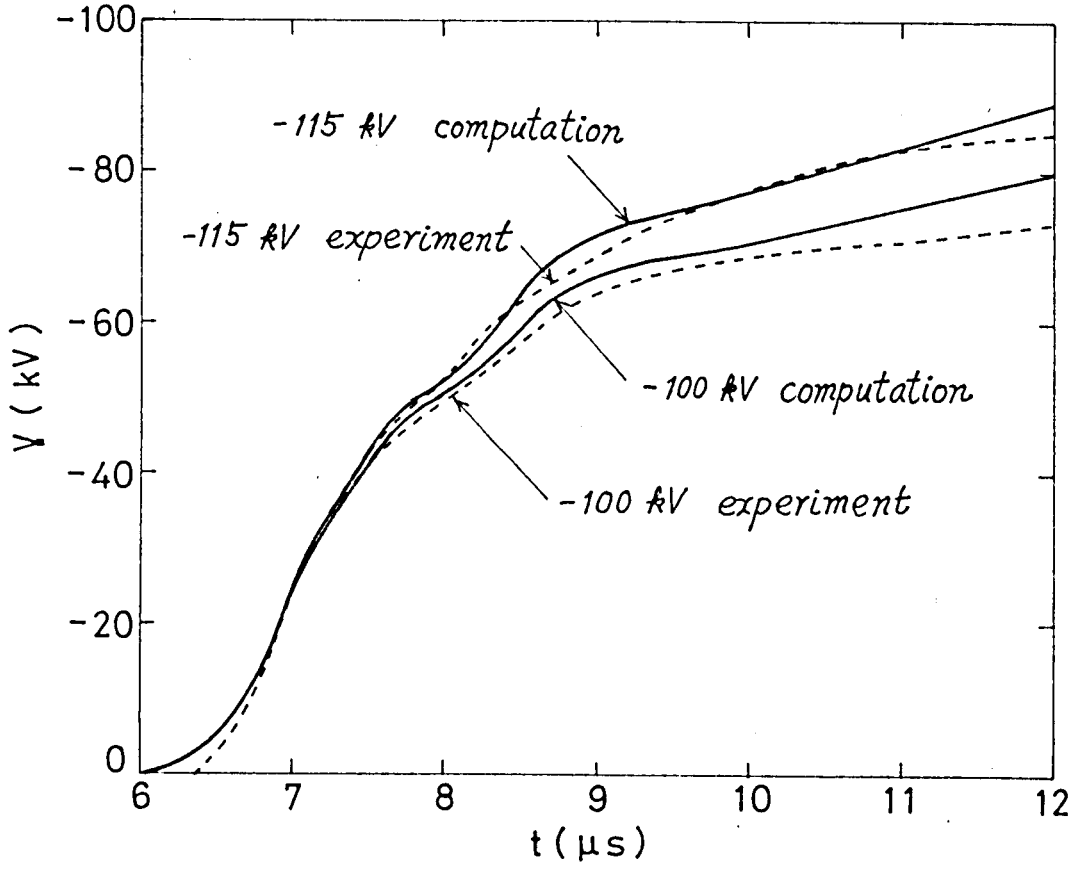

b-3. E = -115 kV, -100 kV (τ=80μs)

Fig. 4.6 Comparison of computed and experimental examples of final end voltages.

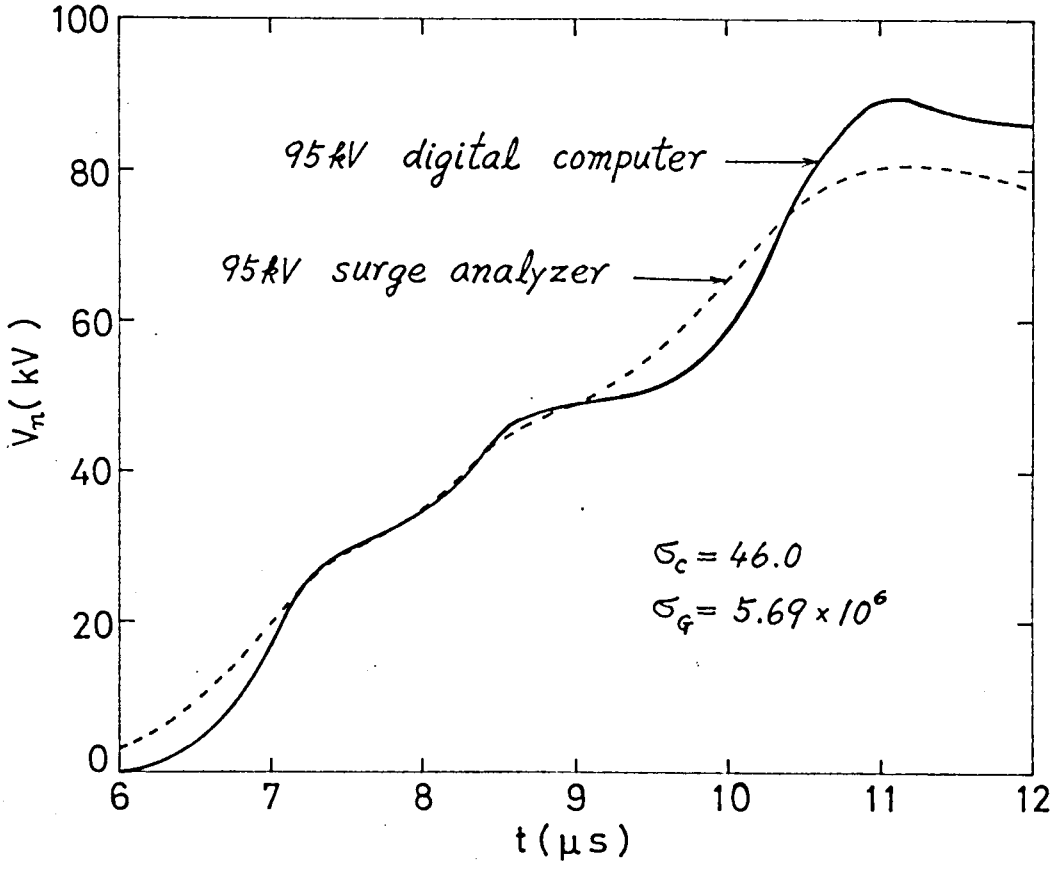

Fig. 4.7 Comparison of computed results by digital computer and by surge analyzer.

CHAPTER 5

NUMERICAL ANALYSIS OF LINE EQUATIONS CONSIDERING CORONA LOSS ON SINGLE-CONDUCTOR SYSTEMS (II) —— METHOD 3

5.1 Introduction

In the preceding chapter, the author introduced the two kinds of method (Methods 1 and 2) for analyzing the piecewise linear-approximated surge equations, which are derived from the nonlinear line equations including the effect of corona losses on traveling waves on single-conductor systems.

However, as noticed in Article 4.3.2, with respect to the computed results by Methods 1 and 2, the step phenomena in the neighborhood of the break-point voltage are unavoidable. By this reason, the calculated voltage waveforms are a little different from the experimental ones. Therefore, some errors in the values of corona loss constants, which are estimated by comparing the computed waveforms with the empirical ones, come into existence.

In order to take away this defect, the author originated the third numerical calculating method (Method 3), which can digitally solve the original nonlinear equations without piecewise linearization. In this chapter, by using Method 3, the author solves the same problems as in the preceding chapter, and again he estimates the values of corona loss constants and corrects the ones obtained by Method 1 or 2. The voltage waveforms computed by Method 3, don't present the above-mentioned step phenomena, and furthermore those are in good agreement with the experimental ones.

5.2 Numerical Calculation of Line

5.2.1 Line Equations Considering Corona Loss

Here, let us rewrite the equations which are introduced in Article 4.2.1. Namely, the initial conditions are

$$\left.\begin{aligned} v(x,0) &= 0 , \\ i(x,0) &= 0 , \end{aligned}\right\} \tag{5.1}$$

and the boundary conditions are

$$v(0,t) = e(t) , \tag{5.2}$$

$$v(l,t) = R_l\, i(l,t) . \tag{5.3}$$

A original nonlinear line equations to be solved are, when $v < v_{co}$ or $\frac{\partial v}{\partial t} < 0$,

$$\left.\begin{aligned} -\frac{\partial v}{\partial x} &= L\frac{\partial i}{\partial t} , \\ -\frac{\partial i}{\partial x} &= C\frac{\partial v}{\partial t} , \end{aligned}\right\} \tag{5.4}$$

and when $v \geq v_{co}$ and $\frac{\partial v}{\partial t} \geq 0$,

$$
\left.
\begin{aligned}
-\frac{\partial v}{\partial x} &= L\frac{\partial i}{\partial t}\,, \\
-\frac{\partial i}{\partial x} &= C\frac{\partial v}{\partial t} + \frac{\alpha}{v}\frac{\partial}{\partial t}(v-v_{c0})^2 + K\frac{(v-v_{c0})^2}{v}\,.
\end{aligned}
\right\} \qquad (5.5)
$$

5.2.2 Numerical Calculation of Original Line Equations

Here we present a method of numerical calculation which, in contrast with the linear approximation approach in the preceding chapter, solves the nonlinear equations without linearization. Let us consider the case where the surge equations (5.4) are valid in the voltage level below the critical corona voltage. If Eq.s (5.4) are approximated by lumped constants for the infinitesimal distance Δx, the equivalent circuit shown in Fig. 5.1 may result. The differential difference equations for the voltage and current in the equivalent circuit of Fig. 5.1 are given by

$$
\left.
\begin{aligned}
v_{p-1}(t) - v_p(t) &= L\Delta x\frac{d i_{p-1}(t)}{dt}\,, \\
i_{p-1}(t) - i_p(t) &= C\Delta x\frac{d v_p(t)}{dt}\,.
\end{aligned}
\right\} \qquad (5.6)
$$

Rewriting Eq.s (5.6) in terms of the difference equation which

employs first-order approximation for the time interval Δt, we have the following equations:

When $i_{p,l}(t-\Delta t) \neq 0$,

$$i_{p-1}(t) = i_{p,l}(t-\Delta t) + \frac{1}{l}\frac{\Delta t}{\Delta x}\{v_{p-1}(t) - v_p(t)\}. \tag{5.7}$$

When $v_p(t) < v_{co}$ or $v_p(t) < v_p(t-\Delta t)$,

$$v_p(t+\Delta t) = v_p(t) + \frac{1}{C}\frac{\Delta t}{\Delta x}\{i_{p-1}(t) - i_p(t)\}. \tag{5.8}$$

When $i_{p-1}(t-\Delta t) = 0$, we obtain

$$i_{p-1}(t) = i_{p-1}(t-\Delta t) + \frac{1}{2L}\frac{\Delta t}{\Delta x}\{v_{p-1}(t) - v_p(t)\}, \tag{5.9}$$

by making second-order approximation for the purpose of improving the accuracy of approximation.

When corona discharge occurs, that is, Eq.s (5.5) are valid, the first equation is the same as the one of Eq.s (5.4) and so no modification is necessary for Eq.s (5.7) and (5.9). On the other hand, the second equation needs to be modified as follows:

$$-\frac{\partial i}{\partial x} = \left(C + 2K - 2K\frac{v_{co}}{v}\right)\frac{\partial v}{\partial t} + K\left(v - 2v_{co} + \frac{v_{co}^2}{v}\right).$$

The difference equation for the above equation can be obtained by the procedure employed previously to derive Eq. (5.8) from Eq.s (5.6). Namely, when $v_p(t) \geq v_{co}$ and $v_p(t) \geq v_p(t-\Delta t)$,

$$v_p(t+\Delta t) = v_p(t) + \Delta t / \{C + 2k - 2k v_{co}/v_p(t)\} \cdot [\{i_{p-1}(t) - i_p(t)\}/\Delta x - K\{v_p(t) - 2v_{co} + v_{co}^2/v_p(t)\}]. \tag{5.10}$$

Arranging the upper equations, we get

$$i_{p-1}(t) = \begin{cases} i_{p-1}(t-\Delta t) + \frac{1}{L}\frac{\Delta t}{\Delta x}\{v_{p-1}(t) - v_p(t)\}, & \text{for } i_{p-1}(t-\Delta t) \neq 0, \end{cases} \tag{5.11}$$

$$\begin{cases} i_{p-1}(t-\Delta t) + \frac{1}{2L}\frac{\Delta t}{\Delta x}\{v_{p-1}(t) - v_p(t)\}, & \text{for } i_{p-1}(t-\Delta t) \neq 0, \end{cases} \tag{5.12}$$

$$v_p(t+\Delta t) = \begin{cases} v_p(t) + \frac{1}{C}\frac{\Delta t}{\Delta x}\{i_{p-1}(t) - i_p(t)\}, & \text{for } v_p(t) < v_{co} \text{ or } v_p(t) < v_p(t-\Delta t), \end{cases} \tag{5.13}$$

$$\begin{cases} v_p(t) + \frac{\Delta t}{\{C + 2k - 2k v_{co}/v_p(t)\}} \cdot \left[\frac{i_{p-1}(t) - i_p(t)}{\Delta x} - K\{v_p(t) - 2v_{co} + v_{co}^2/v_p(t)\}\right], & \text{for } v_p(t) > v_{co} \text{ and } v_p(t) \geq v_p(t-\Delta t), \end{cases} \tag{5.14}$$

where in Eq.s (5.6) to (5.14)

$$j = 1, 2, \text{-----}, n.$$

The computational algorithm explained above may be summarized as follows.

(i) Read in the following initial conditions given by Eq.s (5.1):

$$v_j(0) = \begin{cases} e(0), & j = 0 \\ 0, & j = 1, 2, \text{----}, n, \end{cases}$$

$$i_j(0) = 0, \quad j = 0, 1, \text{----}, n.$$

(ii) Calculate the voltage at $t+\Delta t$, i.e. $v_j(t+\Delta t)$ $(j = 1, 2, \text{----}, n)$ by using Eq.s (5.13) or (5.14). Also, compute

$$v_0(t+\Delta t) = e(t+\Delta t)$$

by using the boundary condition given in Eq. (5.2).

(iii) Using $v_j(t+\Delta t)$ $(j = 1, 2, \text{----}, n)$ determined in (ii) and Eq. (5.11) or (5.12), evaluate $i_{j-1}(t+\Delta t)$ $(j = 1, 2, \text{----}, n)$. Similarly from the boundary condition Eq. (5.3), calculate $i_n(t+\Delta t)$ by

$$i_n(t+\Delta t) = v_n(t+\Delta t)/R_s \ .$$

(iv) Perform Steps (ii) and (iii) repeatedly for every time interval to compute the voltage and current at each instant.

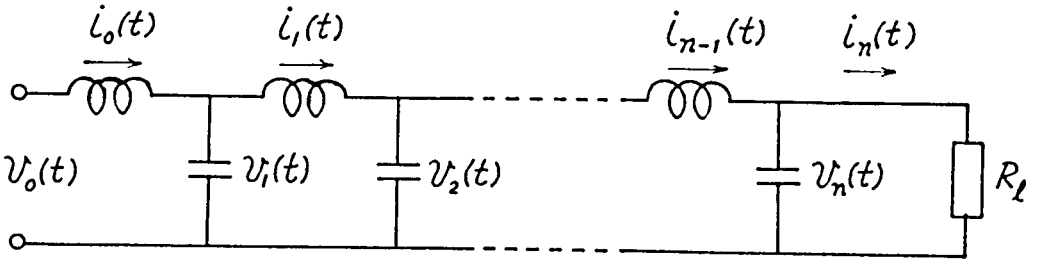

Fig. 5.1 Equivalent lumped constant circuit for voltage lower than corona onset level.

5.3 Numerical Investigation

5.3.1 Numerical Conditions

In this section, the results obtained by the proposed computational algorithms are compared with the experimental results reported by Fujitaka and Aso.[39] The objective here is to estimate properly the corona loss constants σ_c and σ_q by using the constants given in Reference (39).

Table 5.1 lists the constants used for the numerical estimation of the corona loss constants. It has been assumed that the critical corona voltage V_{co} can be calculated by Eq.(4.23).

As same as in the preceding chapter, the impressed voltage $e(t)$ has been chosen to be a rectangular-crest and exponential-tail surge, viz. $e(t)=E_0\exp(-t/\tau)$, in order to be coincident with that employed in the experiment, and it has also been assumed that K and K, hence σ_c and σ_q, are independent of each other.

5.3.2 Calculated Results and Discussions

The constants defined in the preceding section have been used to calculate the voltage waveform at the final end of the line and to estimate the corona loss constants.

In the preceding chapter we have already estimated the

corona loss constants on the basis of Methods 1 and 2. Since Method 3 using the nonlinear surge equations seems to provide improved computational accuracy, it is meaningful to estimate the corona loss constants once again and to correct the previous constants obtained by Methods 1 and 2.

Fig. 5.2 represents the waveform at the final end when a positive surge with E = 95kV and τ = 20μs is impressed where σ_q is fixed but σ_c is varied. Fig. 5.3 shows the waveform when σ_c is fixed but σ_q is varied. From the figures it is seen that σ_c causes a delay in the crest and σ_q attenuates the crest.

With the same procedure as explained in Article 4.3.2 (see Fig. 5.4) the author estimates the optimum values of σ_c and σ_q. The result is listed in Table 5.2.

Fig.s 5.5 (a-1) to (a-3) and (b-1) to (b-3) show the voltage waveforms at the final end for positive and negative surges, respectively, calculated by using the estimated values obtained above. In order to facilitate comparison, the experimental waveforms reported by Fujitaka and Aso also are shown by the dashed lines in the same figures. It is seen that the distortion of the waveforms and the attenuation of the crest obtained by calculation agree well with those by experiment.

But for short-tail surges with the tail time constant τ of 5μs, the calculated values differ slightly from the experimental ones. This difference is inevitable because these surges are more distorted and attenuated by the skin effect than those with the tail time constant τ of 20μs or 80μs. The origin of time scale in these figures corresponds to the instant when an

impulsive voltage is impressed at the sending end. Since it is almost impossible to make coincident the experimental and calculated waveforms at wave toes below the critical corona voltage, the two groups of waveforms are made coincident at the instant when the corona voltage (calculated value) is reached. Since the distortion of waveforms due to the skin effect is ignored in this paper, the surge must build up with the right angle in the portion below the corona voltage. In actual situations, however, because of the fact that Δx and Δt cannot be made infinitesimal during the simulation on a digital computer and so the line must be approximated by a cascaded series of equivalent lumped constant circuits, the surge does not build up with the right angle but is distorted at wave toe below the corona voltage.

Fig. 5.6 shows the voltage waveforms at the distances of 1/4, 1/2, and 3/4 line length ℓ in the case, where $E_0 = -104$kV and $\tau = 20\mu s$. From the figure we can see the situation of the surge attenuation and distortion along the line.

Table 5.1 Values of main quantities availed in computations.

Line length	$\ell = 2067\ m$
Hight of conductor	$h = 3.1\ m$
Radius of conductor	$r = 1.15 \times 10^{-3}\ m$
Length of subdivisions	$\Delta x = 25.8\ m$
Time interval	$\Delta t = 0.025\ \mu s$
Final end resistors	$R_\ell = 516\ \Omega$
Inductance of conductor	$L = 1.72\ \mu H/m$
Capacitance of conductor	$C = 6.47\ \mu\mu F/m$
Number of equivalent circuit elements	$n = 80$
Critical corona voltage	$V_{co} = 28.3\ kV$

Table 5.2 Optimum values of σ_c and σ_G for positive and negative surges.

Wave tail time constant τ	Positive surge		Negative surge	
	σ_c	σ_G	σ_c	σ_G
5 μs	32	20×10^6	15	20×10^6
20 μs	32	16×10^6	15	16×10^6
80 μs	32	30×10^6	15	30×10^6

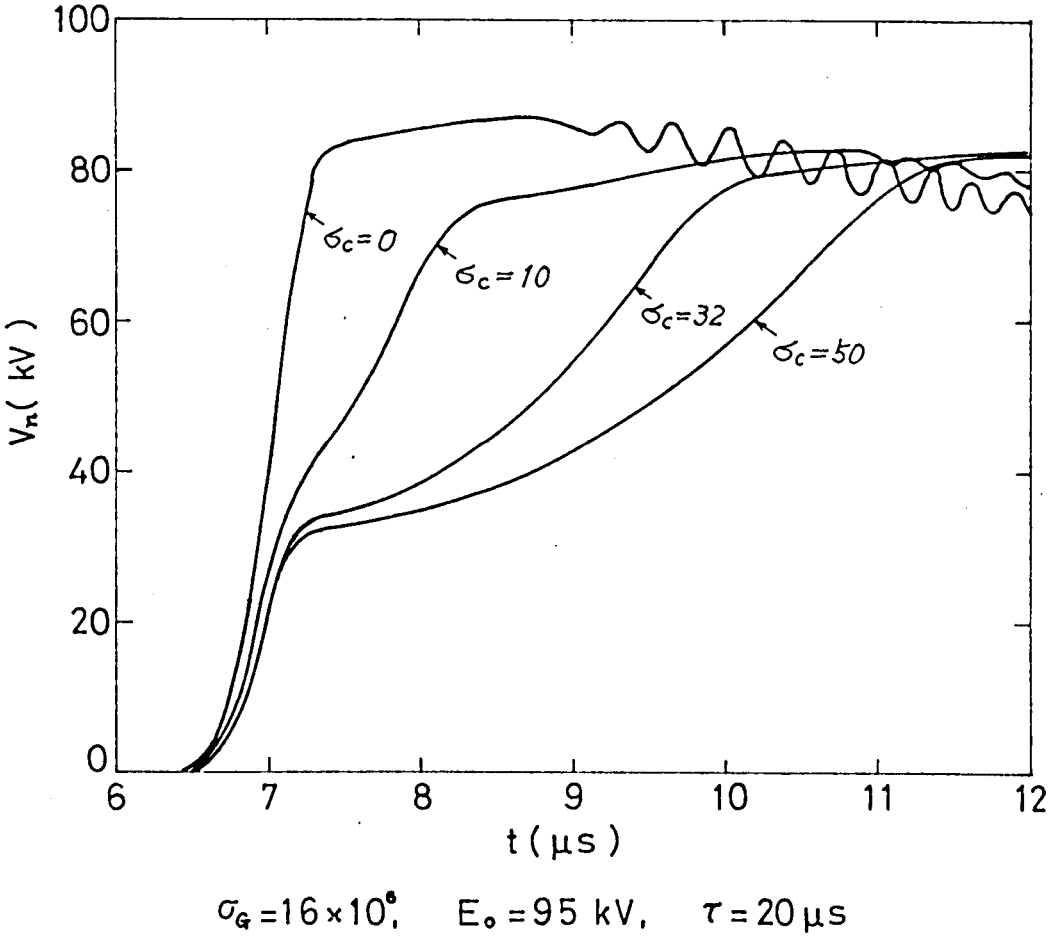

Fig. 5.2 Example (1) of calculated waveforms of the line end voltage.

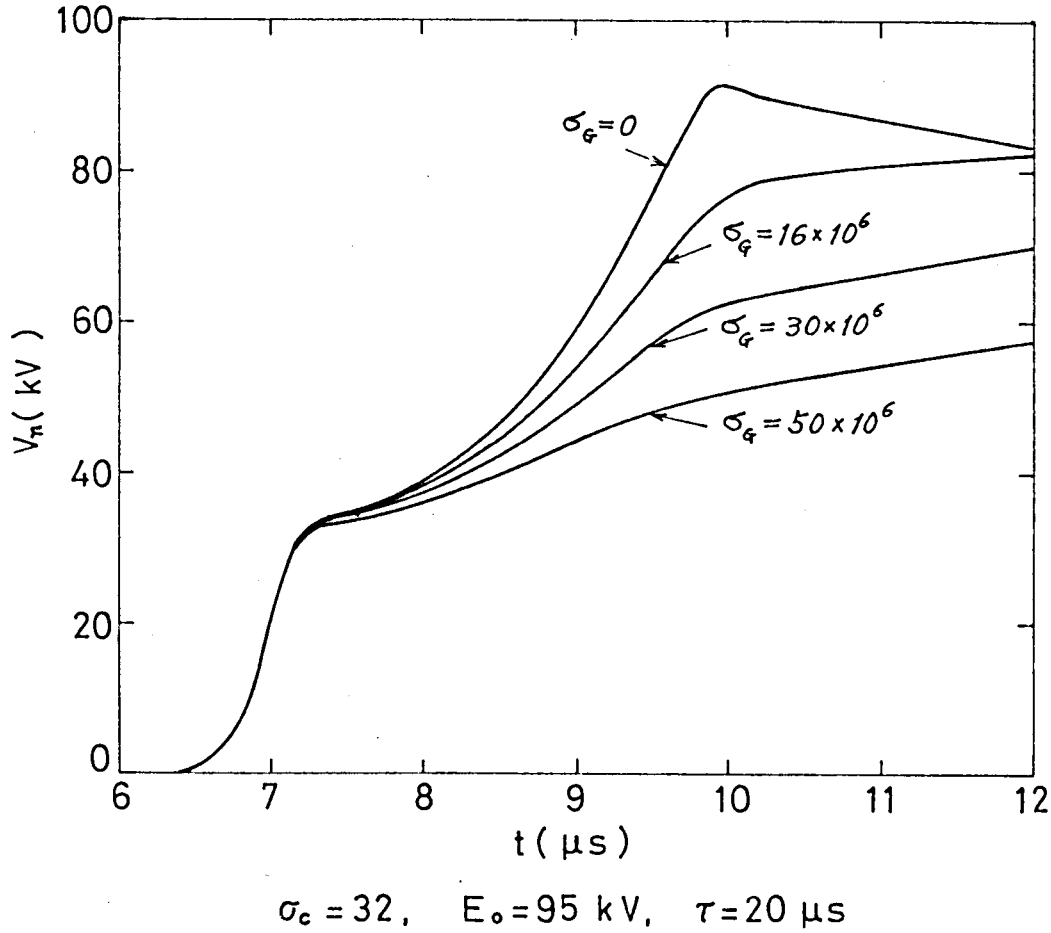

Fig. 5.3 Example (2) of calculated waveforms of the line end voltage.

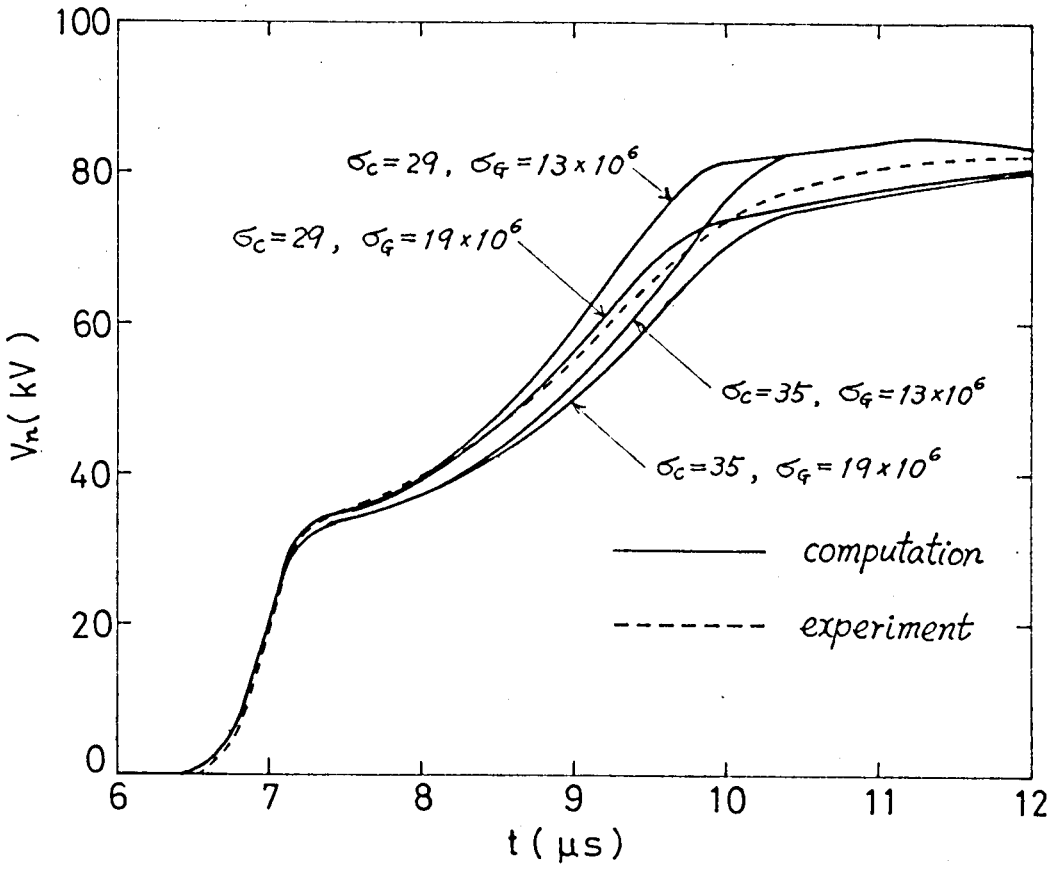

a. $E_0 = 95$ kV ($\tau = 20\,\mu s$)

Fig. 5.4 Examples of calculated voltage waveforms and the corresponding experimental ones.

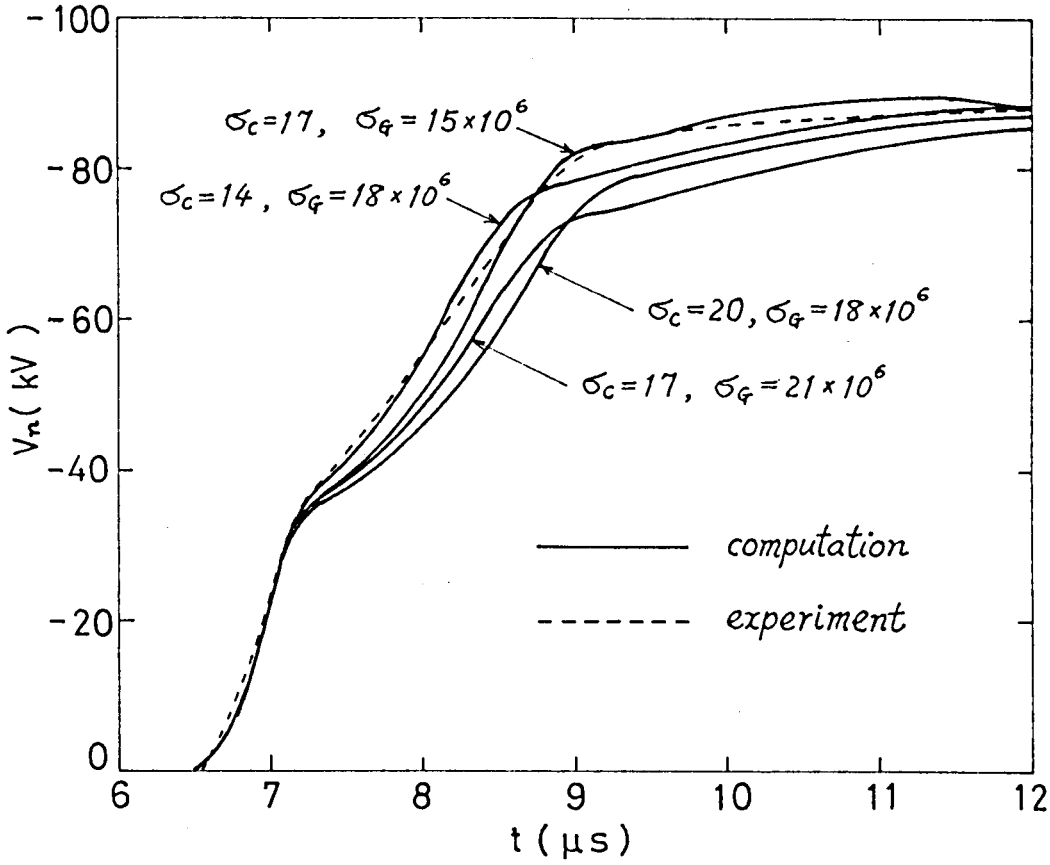

b. $E_o = -104$ kV ($\tau = 20\mu s$)

Fig. 5.4 Examples of calculated voltage waveforms and the corresponding experimental ones.

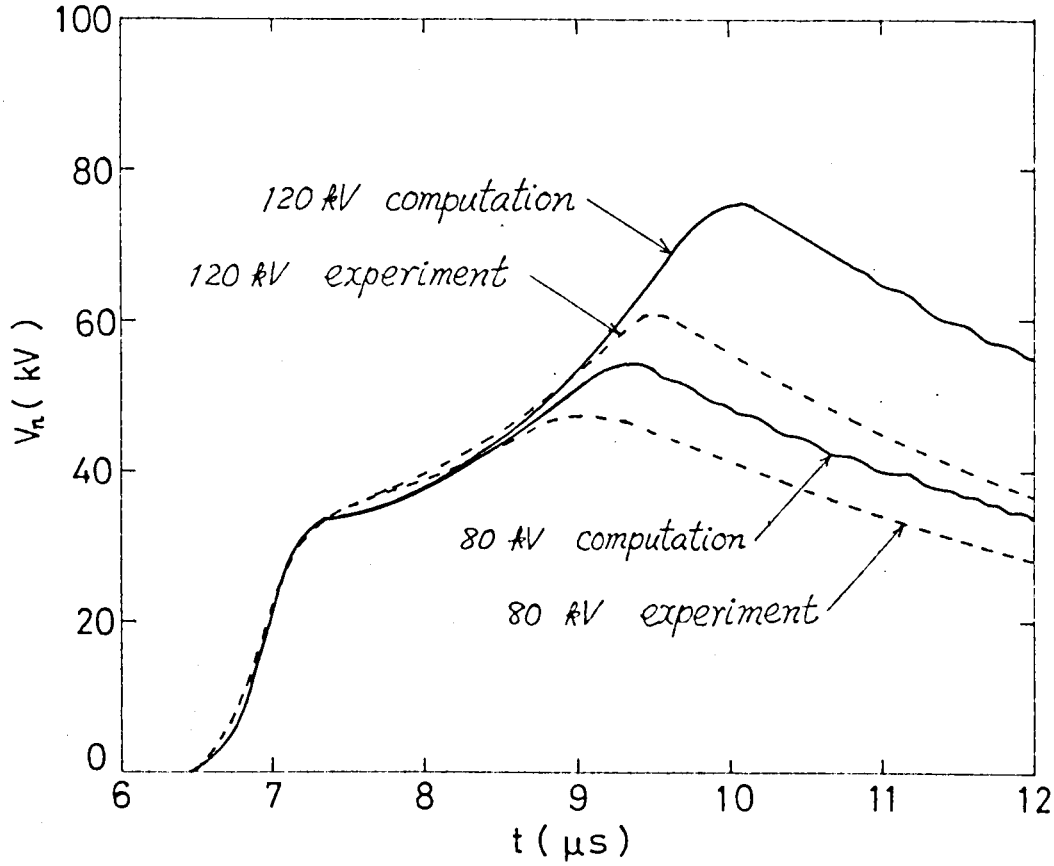

a-1. $E_0 = 120$ kV, 80 kV ($\tau = 5$ μs)

Fig. 5.5 Comparison of calculated and experimental examples of final end voltages.

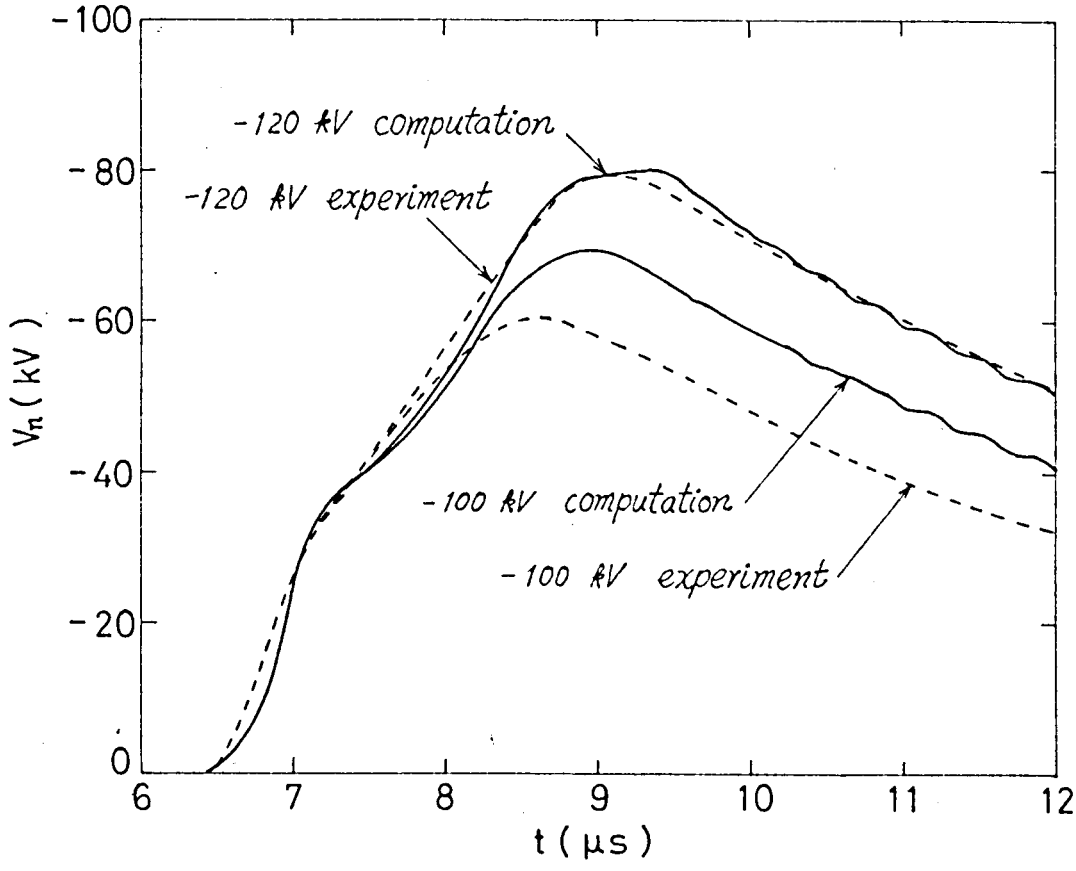

b-1. $E_0 = -120$ kV, -100 kV ($\tau = 5$ μs)

Fig. 5.5 Comparison of calculated and experimental examples of final end voltages.

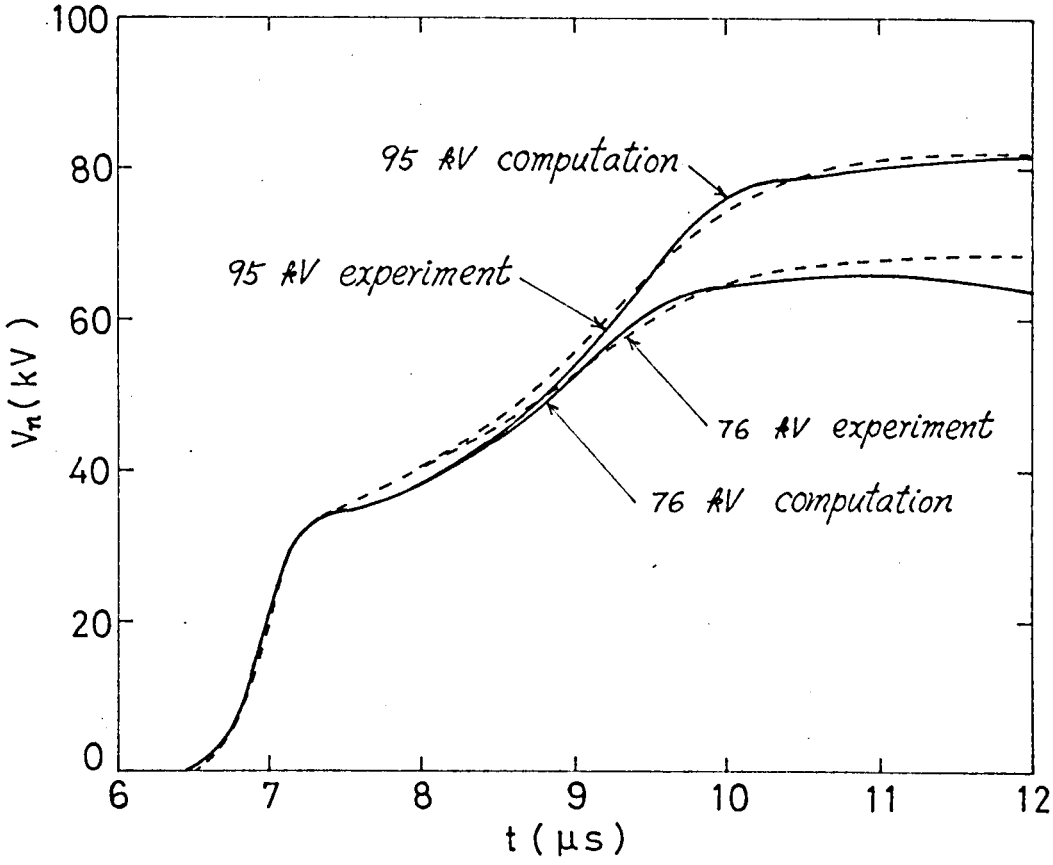

a-2. $E_0 = 95$ kV, 76 kV ($\tau = 20\mu s$)

Fig. 5.5 Comparison of calculated and experimental examples of final end voltages.

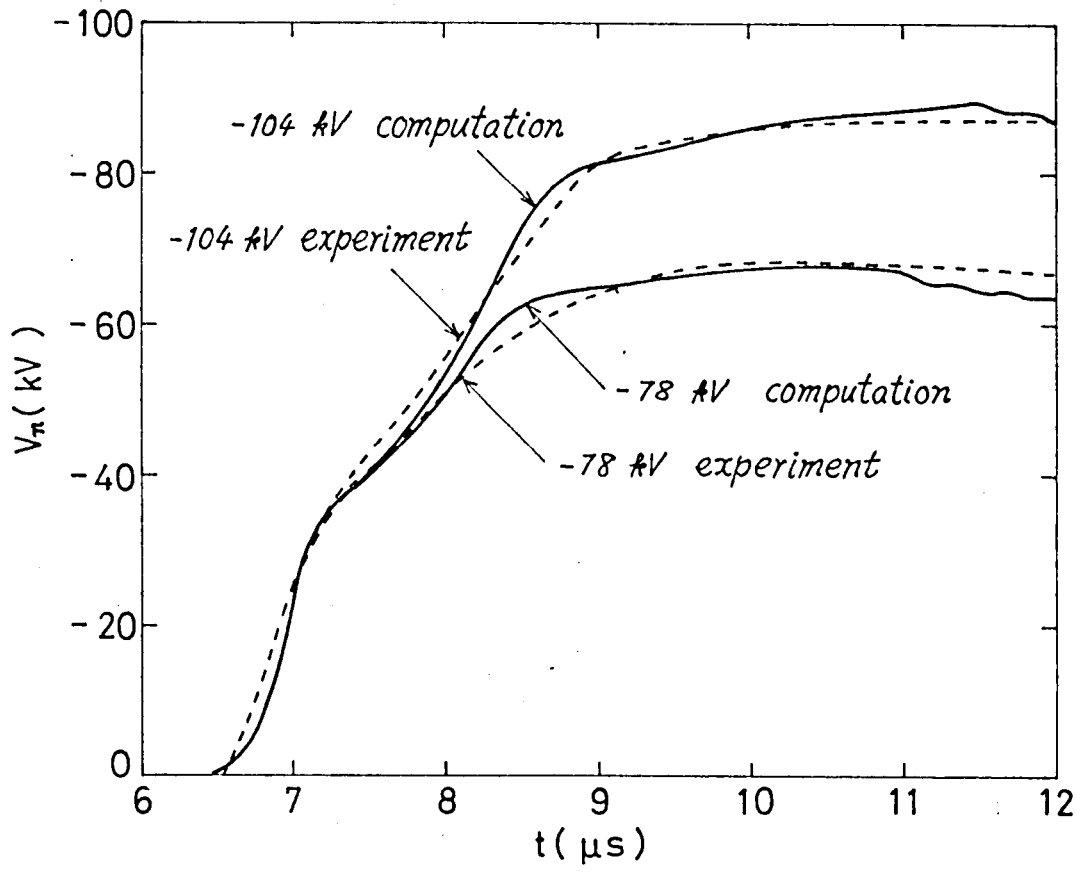

b-2. $E_0 = -104$ kV, -78 kV ($\tau = 20\,\mu s$)

Fig. 5.5 Comparison of calculated and experimental examples of final end voltages.

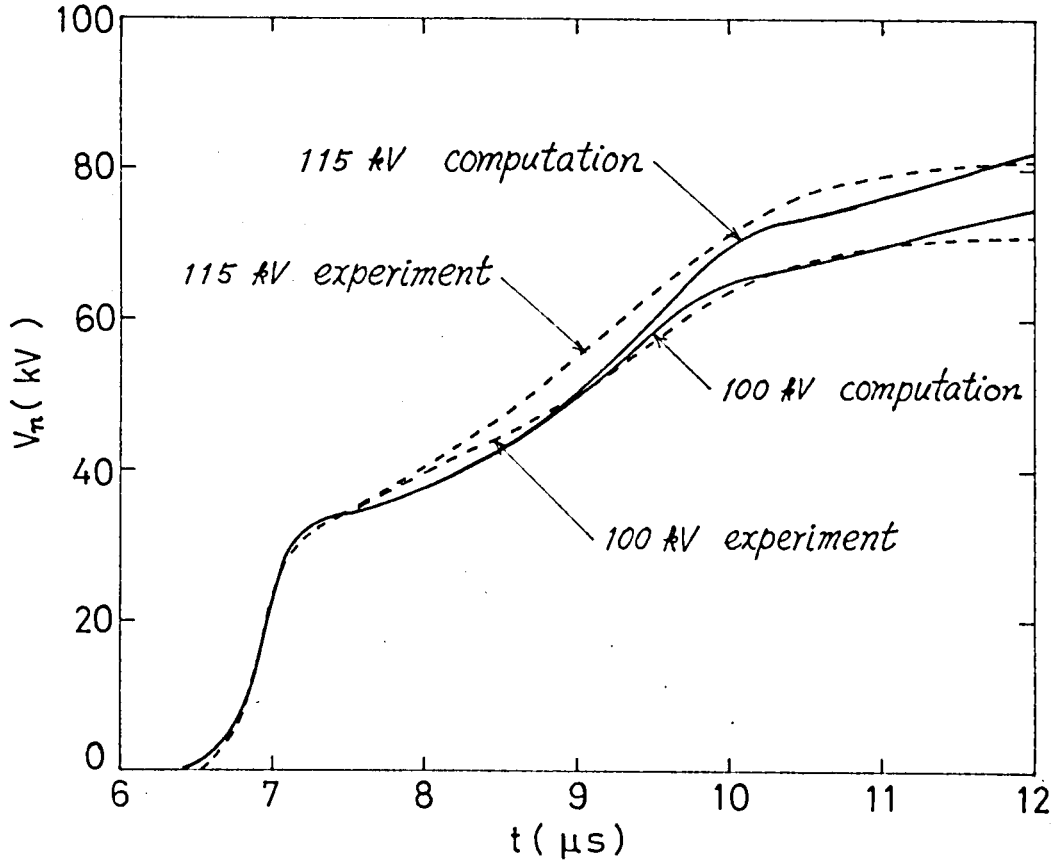

a-3. E_o = 115 kV, 100 kV (τ = 80μs)

Fig. 5.5 Comparison of calculated and experimental examples of final end voltages.

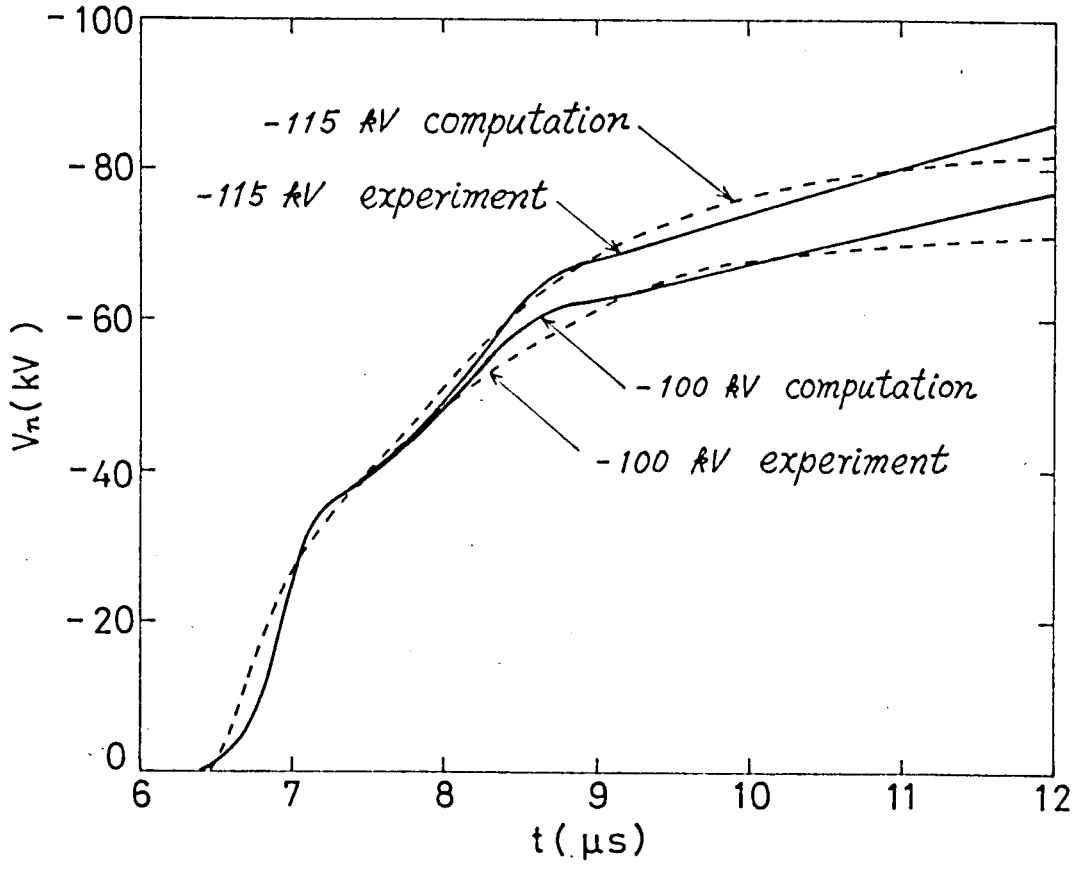

b-3. $E_0 = -115$ kV, -100 kV ($\tau = 80\mu s$)

Fig. 5.5 Comparison of calculated and experimental examples of final end voltages.

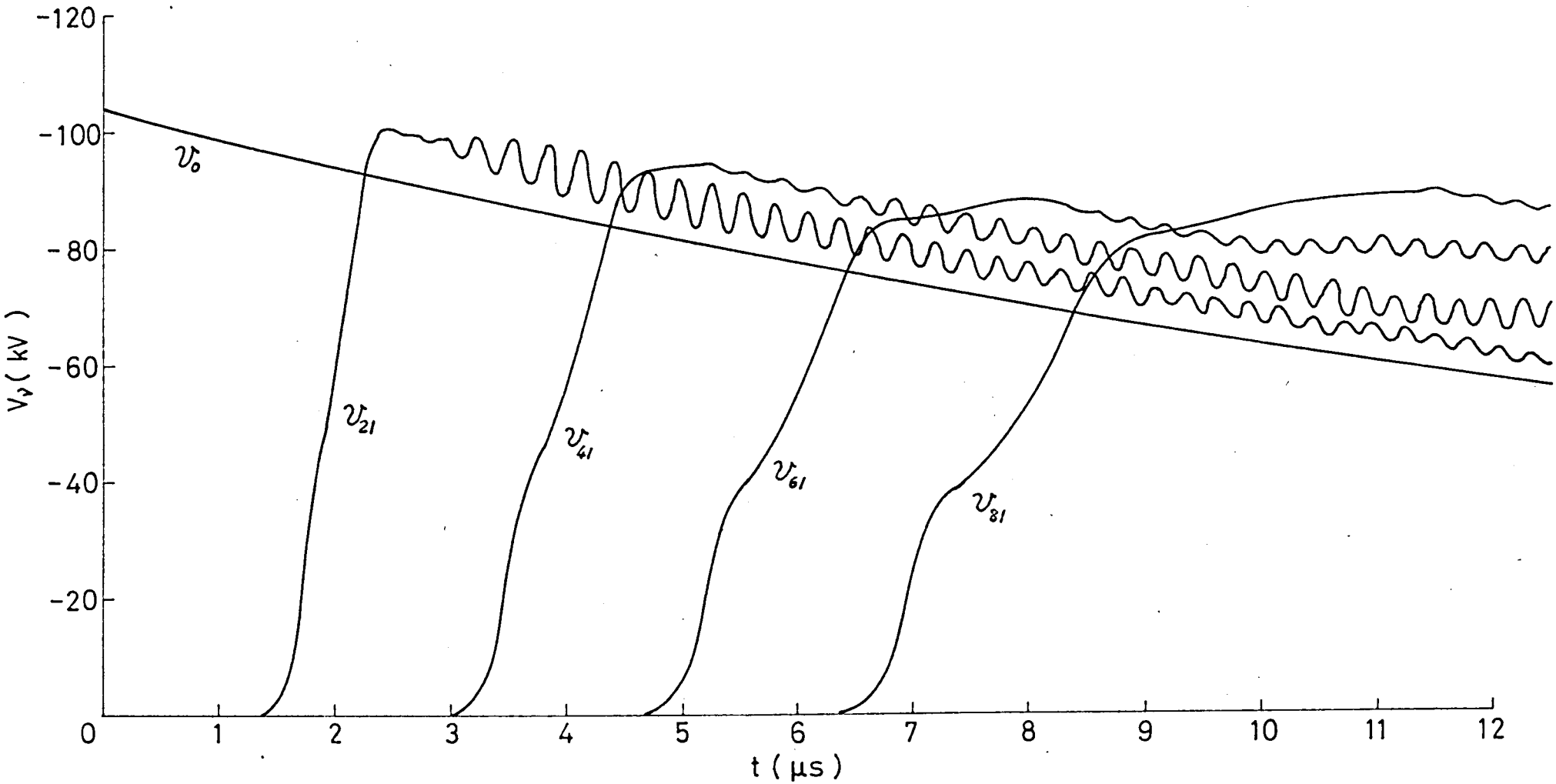

Fig. 5.6 Calculated voltage waveforms at the distances of 1/4, 1/2 and 3/4 line length.
($E_0 = -104$ kV, $\tau = 20\,\mu s$)

5.4 Comparison of the Results Obtained by Methods 1, 2 and 3

Although the computational algorithms of Methods 1 and 2 have been detailed in the preceding chapter, here it seems appropriate to outline the three methods. In Method 1, the coefficient between the voltage and current at each point on the line at each instant is calculated backwards from the final end operating condition, and then the voltage and current are calculated progressively from the sending end, as having been already tried for the estimation of σ_c and σ_g in the preceding chapter. These values are listed in Table 4.2 and agree fairly well with those listed in Table 5.2. The errors between the two sets of values remain within the order of 10%.

In Method 1, the total length of the line was divided into a total of $n = 40$ subintervals. In order for the solution to converge, however, the interval of time must have been of the order of $\Delta t = 0.005\,\mu s$ and therefore the computation becomes very time-consuming.

Method 2 is a revision of Method 1. The voltage and current are calculated progressively from the sending end in such a way that they also satisfy the terminal condition at the final end. This method allows the convergence of solution with $\Delta t = 0.05$ to $0.1\,\mu s$ when $\Delta x = 51.7$m. A great saving of computing time has been realized by the factor of 20 to 40 times in comparison with Method 1.

Method 3 is an extended version of the computing algorithm of Method 2 to the nonlinear case. The computing time requirement is of the same order of that of Method 2. Figure 5.7 represents the examples computed by the three methods for the surge with $E = 95$kV and $\tau = 20\mu s$ and with the calculating condition of $\Delta x = 51.7$m and $\Delta t = 0.005\mu s$. The results computed by Method 1 agree very well with those by Method 2. Since the two methods employ piecewise linearization of nonlinear characteristics, it is inevitable that the results involve step performance in the neighborhood of the break-point voltage. In this respect, Method 3 is superior to Methods 1 and 2 and can provide the waveforms whose distortion characteristics resemble successfully the corresponding experimental result.

With respect to Methods 2 and 3, the computed results with $\Delta t = 0.05\mu s$ are also shown in Fig. 5.7. It is seen that no appreciable difference exists if Δt is increased from $0.005\mu s$ to $0.05\mu s$. As mentioned previously, in estimating the corona loss constants based upon Method 3, we have chosen $n = 80$, i.e. $\Delta x = 25.8$m and $\Delta t = 0.025\mu s$ in order to obtain as realistic waveform as possible in the building-up portion of the surge. This stems from the fact that when solution has converged with a specific pair of Δx and Δt, Δt must be varied almost in proportion to Δx if Δx is varied. In the present example, no appreciable difference is observed if Δt is varied to $0.05\mu s$.

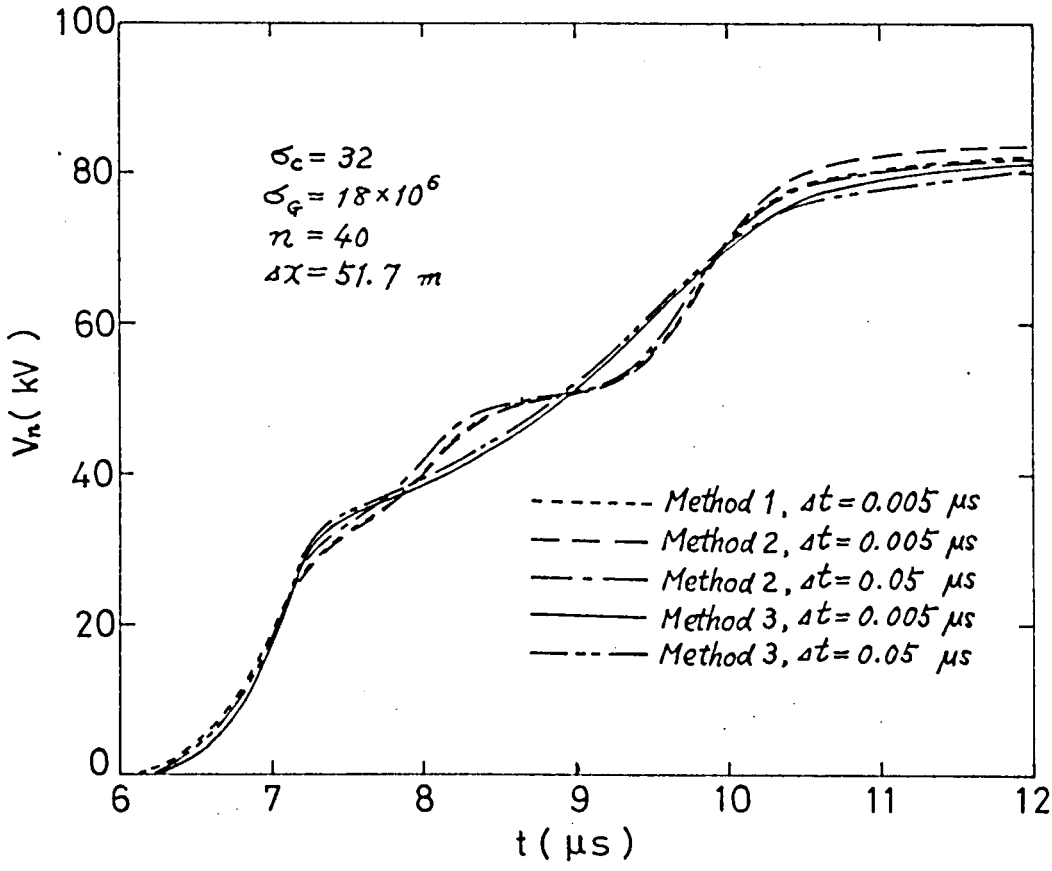

Fig. 5.7 Comparison of final end voltage waveforms calculated by Methods 1, 2 and 3.

CHAPTER 6

NUMERICAL ANALYSIS OF LINE EQUATIONS CONSIDERING CORONA LOSS ON TWO-CONDUCTOR SYSTEMS

6.1 Introduction

In Chapter 4 and Chapter 5, the author has already introduced the numerical calculation of attenuation and distortion of the surge on a single conductor due to corona loss and estimated the optimum values of the corona loss constants for the surges by comparing the computed results with the experimental ones obtained by Fujitaka and Aso[39] on the mimic experimental transmission line.

However, in view of the fact that multi-conductor systems are used in actual power systems, we should make effort to apply the analysis for single-conductor systems to multi-conductor systems.

Now, in this chapter, the author apply the numerical calculation of the line equations of the single-conductor system

to the ones of the two-conductor systems[42],[43] as example of the multi-conductor systems, and analyze the surges along the two-conductor systems by digital computer with the aid of values of the corona loss constants which have been obtained in Chapter 5 for the single-conductor systems. Next he compares the computed results with the experimental ones, which are obtained by Fujitaka and Aso on the mimic two-conductor line under the various sending end and final conditions.

6.2 Numerical Analysis of Line Equations of Two-Conductor Systems Considering Corona Loss

6.2.1 Line Equations of Two-Conductor Systems Considering Corona Loss

In Chapter 4 already we have given the line equations for single-conductor systems considering corona loss. So, here, let us assume the line equations for the two-conductor systems having line voltages over the corona voltage as follows:

$$
\left.
\begin{aligned}
-\frac{\partial v_1}{\partial x} &= L_{11}\frac{\partial i_1}{\partial t} + L_{12}\frac{\partial i_2}{\partial t} \\
-\frac{\partial v_2}{\partial x} &= L_{21}\frac{\partial i_1}{\partial t} + L_{22}\frac{\partial i_2}{\partial t} \\
-\frac{\partial i_1}{\partial x} &= C_{11}\frac{\partial v_1}{\partial t} + C_{12}\frac{\partial v_2}{\partial t} + \frac{K_1}{v_1}\frac{\partial}{\partial t}(v_1 - v_{10})^2 + K_1\frac{(v_1 - v_{10})^2}{v_1} \\
-\frac{\partial i_2}{\partial x} &= C_{21}\frac{\partial v_1}{\partial t} + C_{22}\frac{\partial v_2}{\partial t} + \frac{K_2}{v_2}\frac{\partial}{\partial t}(v_2 - v_{20})^2 + K_2\frac{(v_2 - v_{20})^2}{v_2}
\end{aligned}
\right\} \qquad (6.1)
$$

where

v_j and i_j $(j = 1, 2)$: current and voltage of the j-th conductor at distance x from initial point,

$[L] = \begin{bmatrix} L_{11} & L_{12} \\ L_{21} & L_{22} \end{bmatrix}$: inductance matrix of lines per unit length,

$[C] = \begin{bmatrix} C_{11} & C_{12} \\ C_{21} & C_{22} \end{bmatrix}$: capacitance matrix of lines per unit length, (6.2)

v_{j0} $(j=1,2)$: corona voltage of the j-th line,

$K_j = \dot{K}_j(f+25) = \sigma_c \sqrt{r_j / 2h_j} \times 10^{-11}$ $(j=1,2)$ [V/m],

$\dot{K}_j = \sigma_c \sqrt{r_j / 2h_j} \times 10^{-11}$ $(j=1,2)$ [F/m],

f : frequency [s^{-1}],

r_j and h_j $(j=1,2)$: radius and height of the j-th conductor (m),

$\sigma_c = \sigma_c(f+25)$,

σ_c : corona loss constant.

In these equations we assume that corona discharge rises only between every conductor and ground, and we neglect the corona discharge between conductors.

Next we consider the problem of seeking the voltage at each point on the line, when the impulse voltage, whose crest value exceed the corona voltage, is applied on the sending end of the transmission line, whose length is ℓ and which is grounded by the resistance $[\gamma_f]$ at the final end as shown in Fig. 6.1.

It is a two-point boundary-value problem of solving the nonlinear partial differential Eq.s (6.1) under the following initial conditions,

$$\left.\begin{aligned} [v(x,0)] &= [0] \,, \\ [i(x,0)] &= [0] \,, \end{aligned}\right\} \tag{6.3}$$

and the boundary conditions,

$$[v(0,t)] = [e(t)] \,, \tag{6.4}$$

$$[v(\ell,t)] = [\gamma_l][i(\ell,t)] \,. \tag{6.5}$$

But we should take care that Eq.s (6.1) are available only if both v_1 and v_2 are over the corona voltage, and when v_1 or v_2 is under the corona voltage, we must remove the corona loss terms from Eq.s (6.1).

The auther has found the three methods, which can solve numerically the line equations at single-conductor systems as mentioned in Chapters 4 and 5. Methods 1 and 2 are the ones to solve the approximate piecewise linear equations of the original nonlinear equations, and Method 3 is the one to do Eq.s (6.1) as it is. In this paper we shall solve this problem by Method 3, which is thought most accurate among the three methods. Moreover, we neglect the surge distortion due to the skin effect in this calculation, because it is considered to be fairly small compared with that of the corona discharge.

6.2.2 Numerical Calculation of Line Equations of Two-conductor Systems

In this section we show the calculating method of Eq.s (6.1) by digital computer. Now, from Eq.s (6.1) we can introduce the following difference equations concerning x and t after the same procedure as in the case of single conductor system. Namely, when $i_{1,\nu-1}(t-\Delta t)\neq 0$ or $i_{2,\nu-1}(t-\Delta t)\neq 0$,

$$\begin{bmatrix} i_{1,\nu-1}(t) \\ i_{2,\nu-1}(t) \end{bmatrix} = \begin{bmatrix} i_{1,\nu-1}(t-\Delta t) \\ i_{2,\nu-1}(t-\Delta t) \end{bmatrix} + \begin{bmatrix} L'_{11} & L'_{12} \\ L'_{21} & L'_{21} \end{bmatrix}^{-1} \begin{bmatrix} v_{1,\nu-1}(t)-v_{1,\nu}(t) \\ v_{2,\nu-1}(t)-v_{2,\nu}(t) \end{bmatrix}, \tag{6.6}$$

when $i_{1,\nu-1}(t-\Delta t)=0$ and $i_{2,\nu-1}(t-\Delta t)=0$,

$$\begin{bmatrix} i_{1,\nu-1}(t) \\ i_{2,\nu-1}(t) \end{bmatrix} = \begin{bmatrix} i_{1,\nu-1}(t-\Delta t) \\ i_{2,\nu-1}(t-\Delta t) \end{bmatrix} + \frac{1}{2} \begin{bmatrix} L'_{11} & L'_{12} \\ L'_{21} & L'_{22} \end{bmatrix}^{-1} \begin{bmatrix} v_{1,\nu-1}(t)-v_{1,\nu}(t) \\ v_{2,\nu-1}(t)-v_{2,\nu}(t) \end{bmatrix}, \tag{6.7}$$

where

$$\begin{bmatrix} L'_{11} & L'_{21} \\ L'_{12} & L'_{22} \end{bmatrix} = \frac{\Delta x}{\Delta t} \begin{bmatrix} L_{11} & L_{21} \\ L_{12} & L_{22} \end{bmatrix},$$

$\nu = 1, 2, \cdots\cdots\cdots, n,$

$v_{j\nu}$, $i_{j\nu}$ $(j=1,2)$: voltage and current of the ν-th element of the j-th conductor, (6.8)

Δx : lumped distance of the ν-th element,

Δt : time interval,

n : number of total elements.

Next, from the lower two equations of the Eq.s (6.1), we can arrive at the following equations, when

$$\left.\begin{aligned}&\begin{cases} v_{1\nu}(t) < v_{10}, \\ v_{2\nu}(t) < v_{20}, \end{cases} \quad or \quad \begin{cases} v_{1\nu}(t) < v_{1\nu}(t-\Delta t), \\ v_{2\nu}(t) < v_{2\nu}(t-\Delta t), \end{cases} \\ &\begin{bmatrix} v_{1\nu}(t+\Delta t) \\ v_{2\nu}(t+\Delta t) \end{bmatrix} = \begin{bmatrix} v_{1\nu}(t) \\ v_{2\nu}(t) \end{bmatrix} + \begin{bmatrix} C'_{11} & C'_{12} \\ C'_{21} & C'_{22} \end{bmatrix}^{-1} \begin{bmatrix} i_{1,\nu-1}(t) - i_{1\nu}(t) \\ i_{2,\nu-1}(t) - i_{2\nu}(t) \end{bmatrix}, \end{aligned}\right\} \tag{6.9}$$

when

$$\left.\begin{aligned}&\begin{cases} v_{1\nu}(t) \geq v_{10}, \\ v_{1\nu}(t) \geq v_{1\nu}(t-\Delta t), \\ v_{2\nu}(t) < v_{20}, \end{cases} \quad or \quad \begin{cases} v_{1\nu}(t) \geq v_{10}, \\ v_{1\nu}(t) \geq v_{1\nu}(t-\Delta t), \\ v_{2\nu}(t) < v_{2\nu}(t-\Delta t), \end{cases} \\ &\begin{bmatrix} v_{1\nu}(t+\Delta t) \\ v_{2\nu}(t+\Delta t) \end{bmatrix} = \begin{bmatrix} v_{1\nu}(t) \\ v_{2\nu}(t) \end{bmatrix} + \begin{bmatrix} C'_{11} + 2K'_1\{1 - v_{10}/v_{1\nu}(t)\} & C'_{12} \\ C'_{21} & C'_{22} \end{bmatrix}^{-1} \\ &\qquad \times \begin{bmatrix} i_{1,\nu-1}(t) - i_{1\nu}(t) - K_1 \Delta x \{v_{1\nu}(t) - 2v_{10} + v_{10}^2/v_{1\nu}(t)\} \\ i_{2,\nu-1}(t) - i_{2\nu}(t) \end{bmatrix}, \end{aligned}\right\} \tag{6.10}$$

when

$$\left\{\begin{array}{l} v_{1\nu}(t) < v_{10}, \\ v_{2\nu}(t) \geq v_{20}, \\ v_{2\nu}(t) \geq v_{2\nu}(t-\Delta t), \end{array}\right. \quad or \quad \left\{\begin{array}{l} v_{1\nu}(t) < v_{1\nu}(t-\Delta t), \\ v_{2\nu}(t) \geq v_{20}, \\ v_{2\nu}(t) \geq v_{2\nu}(t-\Delta t), \end{array}\right.$$

$$\left.\begin{array}{l} \begin{bmatrix} v_{1\nu}(t+\Delta t) \\ v_{2\nu}(t+\Delta t) \end{bmatrix} = \begin{bmatrix} v_{1\nu}(t) \\ v_{2\nu}(t) \end{bmatrix} + \begin{bmatrix} C_{11}' & C_{12}' \\ C_{21}' & C_{22}' + 2\hat{K}_2'\{1 - v_{20}/v_{2\nu}(t)\} \end{bmatrix}^{-1} \\ \qquad \times \begin{bmatrix} i_{1,\nu-1}(t) - i_{1\nu}(t) \\ i_{2,\nu-1}(t) - i_{2\nu}(t) - K_2\Delta x\{v_{2\nu}(t) - 2v_{20} + v_{20}^2/v_{2\nu}(t)\} \end{bmatrix}, \end{array}\right\} \quad (6.11)$$

when

$$\left\{\begin{array}{l} v_{1\nu}(t) \geq v_{10}, \\ v_{1\nu}(t) \geq v_{1\nu}(t-\Delta t), \\ v_{2\nu}(t) \geq v_{20}, \\ v_{2\nu}(t) \geq v_{2\nu}(t-\Delta t), \end{array}\right.$$

$$\left.\begin{array}{l} \begin{bmatrix} v_{1\nu}(t+\Delta t) \\ v_{2\nu}(t+\Delta t) \end{bmatrix} = \begin{bmatrix} v_{1\nu}(t) \\ v_{2\nu}(t) \end{bmatrix} + \begin{bmatrix} C_{11}' + 2\hat{K}_1'\{1 - v_{10}/v_{1\nu}(t)\} & C_{12}' \\ C_{21}' & C_{22}' + 2\hat{K}_2'\{1 - v_{20}/v_{2\nu}(t)\} \end{bmatrix}^{-1} \\ \qquad \times \begin{bmatrix} i_{1,\nu-1}(t) - i_{1\nu}(t) - K_1\Delta x\{v_{1\nu}(t) - 2v_{10} + v_{10}^2/v_{1\nu}(t)\} \\ i_{2,\nu-1}(t) - i_{2\nu}(t) - K_2\Delta x\{v_{2\nu}(t) - 2v_{20} + v_{20}^2/v_{2\nu}(t)\} \end{bmatrix}, \end{array}\right\} \quad (6.12)$$

where

$$\left.\begin{aligned} &\nu = 1, 2, \cdots\cdots, n, \\ &\begin{bmatrix} C'_{11} & C'_{12} \\ C'_{21} & C'_{22} \end{bmatrix} = \frac{\Delta x}{\Delta t} \begin{bmatrix} C_{11} & C_{12} \\ C_{21} & C_{22} \end{bmatrix}, \\ &k'_j = \frac{\Delta x}{\Delta t} k_j \quad (j = 1, 2). \end{aligned}\right\} \tag{6.13}$$

Using Eq.s (6.3) to (6.13), we can calculate the final end voltages according to the following process.

(i) Store the initial values of voltages and currents given by Eq.s (6.3).

$$[v_\nu(0)] = \begin{cases} [e(0)], & \nu = 0 \\ [0], & \nu = 1, 2, \cdots\cdots, n, \end{cases}$$

$$[i_\nu(0)] = [0], \quad \nu = 0, 1, \cdots\cdots, n.$$

(ii) Calculate the voltages after the time Δt, namely $[v_\nu(t+\Delta t)]$ $(\nu = 1, 2, \cdots\cdots, n)$ from Eq.s (6.9) to (6.12). On the other hand, we can obtain the values of $[v_0(t+\Delta t)]$ from the boundary condition Eq.s (6.4), as follows:

$$[v_0(t+\Delta t)] = [e(t+\Delta t)].$$

(iii) Calculate the values of $[i_{\nu-1}(t+\Delta t)]$ $(\nu = 1, 2, \cdots\cdots, n)$ from Eq.s (6.9) or (6.10), using the values of $[v_\nu(t+\Delta t)]$

$(\gamma = 0, 1, \cdots\cdots, n)$ which we obtained in (ii). While, from Eq.s (6.5), we can compute the values of $[i_n(t+\Delta t)]$ as follows:

$$[i_n(t+\Delta t)] = [\beta_n]^{-1}[v_n(t+\Delta t)].$$

(iv) After repeating the processes (ii) and (iii) mentioned above, we can get the values of voltages and currents at any point at any time.

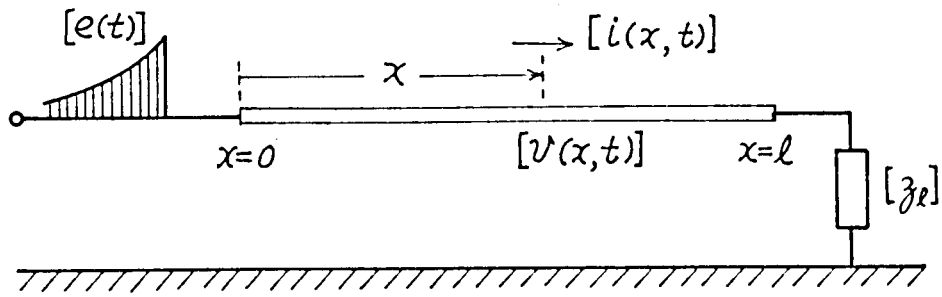

Fig. 6.1 Two-conductor systems.

6.3 Numerical Investigation

6.3.1 Numerical Conditions

In this section, the numerical values of the system constants given in the Reference (39) are used in the computations, since we intend to compare the results, which are obtained by the digital computation method described in the foregoing section, with the experimental ones obtained by Fujitaka and Aso. Further we use the values of the corona loss constants σ_c and σ_g which was obtained in the single-conductor system.

Table 6.1 shows the values of the constants used in the calculations. And we assume the form of the applied impulse voltage as follows:

$$e(t) = E_0 \exp(-t/\tau), \tag{6.14}$$

in order to coincide it with the experimental one. Then, we perform the numerical calculations for the cases of the three sending end conditions corresponding to the experimental ones, namely the case where impulse voltage is impressed on one conductor and the other one is grounded at multiple points, the case where voltage is applied to one conductor and the other one floats, and the case where voltage is impressed to both conductors simultaneously.

The elements of the voltage matrix in the right side of Eq. (6.4) vary corresponding to the three sending end conditions as

below.

First, when impulse voltage is applied to one conductor and the other one is grounded at multiple points, Eq. (6.4) is expressed as follows:

$$\begin{bmatrix} v_1(0,t) \\ v_2(0,t) \end{bmatrix} = \begin{bmatrix} e(t) \\ 0 \end{bmatrix}. \tag{6.15}$$

Next, when voltage is applied to one conductor and the other one floats, Eq. (6.4) becomes

$$\begin{bmatrix} v_1(0,t) \\ v_2(0,t) \end{bmatrix} = \begin{bmatrix} e(t) \\ \frac{z'}{z} e(t) \end{bmatrix}, \tag{6.16}$$

where

z : self surge impedance,

z' : mutual surge impedance,

Lastly, when voltage is applied to both conductors simultaneously, Eq. (6.4) is expressed by the following equation.

$$\begin{bmatrix} v_1(0,t) \\ v_2(0,t) \end{bmatrix} = \begin{bmatrix} e(t) \\ e(t) \end{bmatrix}. \tag{6.17}$$

For the first sending end condition, we give the three kinds of final end conditions that the applied conductor is open-circuited, that it is grounded through the matching resistance and that it is grounded through a resister. To the second sending end conditions, we apply the two kinds of final end ones that the two conductors are open-circuited and they are grounded together through the matching circuit. With respect to the last sending end condition we select the final end condition that both conductors are grounded through the matching circuit.

Now, when the applied conductor is open-circuited at the final end, Eq. (6.5) becomes

$$\left.\begin{aligned} i_1(l,t) &= 0\,, \\ v_2(l,t) &= 0\,. \end{aligned}\right\} \tag{6.18}$$

When the applied conductor is grounded through the matching resistance β at the final end, Eq. (6.5) becomes

$$\left.\begin{aligned} v_1(l,t) &= \beta\, i_1(l,t)\,, \\ v_2(l,t) &= 0\,. \end{aligned}\right\} \tag{6.19}$$

When the applied conductor is grounded through the resistance R at the final end, Eq. (6.5) becomes as

$$\left.\begin{aligned} v_1(l,t) &= R\,i_1(l,t), \\ v_2(l,t) &= 0. \end{aligned}\right\} \tag{6.20}$$

When the two conductors are open-circuited at the final end, Eq. (6.5) is expressed as

$$\left.\begin{aligned} i_1(l,t) &= 0, \\ i_2(l,t) &= 0. \end{aligned}\right\} \tag{6.21}$$

When the two conductors are grounded through the matching circuit at the final end, Eq. (6.5) is expressed as

$$\begin{bmatrix} v_1(l,t) \\ v_2(l,t) \end{bmatrix} = \begin{bmatrix} z & z' \\ z' & z \end{bmatrix} \begin{bmatrix} i_1(l,t) \\ i_2(l,t) \end{bmatrix}. \tag{6.22}$$

Next, we will show the calculating method of corona voltage on two-conductor systems. The relation among voltages v_1 and v_2 of two conductors and electric charges q_1 and q_2 on the conductors per unit length is expressed by the following equation.

$$\begin{bmatrix} q_1 \\ q_2 \end{bmatrix} = \begin{bmatrix} C_{11} & C_{12} \\ C_{21} & C_{22} \end{bmatrix} \begin{bmatrix} v_1 \\ v_2 \end{bmatrix}. \tag{6.23}$$

On the other hand, the surface potential gradient g of the j-th conductor is given by

$$g = 9 \times 10^9 \frac{2 q_j}{r_j} . \tag{6.24}$$

Substituting Eq. (6.24) in Eq. (6.23), we have

$$\left.\begin{aligned} \frac{10^{-9}}{18} r_1 g &= C_{11} v_1 + C_{12} v_2 , \\ \frac{10^{-9}}{18} r_2 g &= C_{21} v_1 + C_{22} v_2 . \end{aligned}\right\} \tag{6.25}$$

As the potential of the j-th conductor reaches the critical voltage v_{j0} when its surface potential gradient g rise till the insulation breakdown strength g_0 of air, we can obtain the corona voltage from Eq. (6.25) as follows.

Since $v_2 = 0$ when impulse voltage is impressed on one conductor and the other one is grounded at many points, we have

$$v_{10} = \frac{10^{-9}}{18} r_1 g_0 / C_{11} . \tag{6.26}$$

Considering the quality of the conductor surface, weather and relative density of air, Eq. (6.26) is changed as follows:

$$v_{10} = \frac{10^{-9}}{18} m_0 m_1 \delta r_1 g_0 / C_{11} = 27.1 \text{ kV} . \tag{6.27}$$

where m_0, m_1, δ and g_0 were defined in Eq. (4.23).

Since $g_2 = 0$ when voltage is applied to one conductor and the other one floats, we have

$$v_{10} = \frac{10^{-9}}{18} m_0 m_1 \delta r_1 g_0 / (C_{11} - \frac{C_{12}^2}{C_{22}}) = 28.3 \text{ kV}. \tag{6.28}$$

Since $v_1 = v_2$ and $g_1 = g_2$ when voltage is impressed on both two conductors, we get the next equations.

$$v_{10} = v_{20} = \frac{10^{-9}}{18} m_0 m_1 \delta r_1 g_0 / (C_{11} + C_{12}) = 34.1 \text{ kV}. \tag{6.29}$$

6.3.2 Comparison of Calculated and Experimental Examples

In this section, the numerical calculations for two-conductor system are carried out by using the values of σ_c and σ_g given in Table 6.2, which were estimated in the single conductor system as described in Chapter 5, and then the calculated waveforms of final end voltages are compared with the experimental ones. Now, in Fig. 6.2 ~ Fig. 6.4 are plotted the digital calculation results of the transient voltages at the final end in the case, where at the sending end the impulse voltages are

applied to one conductor and at the receiving end it is open-circuited or grounded through matching resistance or 201Ω-resistor, and the other conductor is grounded at the multiple points. Here the following three kinds of impulse voltages

$$E_0 = \pm 230\text{kV}, \qquad \tau = 5\,\mu s,$$

$$E_0 = \pm 180\text{kV}, \qquad \tau = 5\,\mu s,$$

$$E_0 = -\ 80\text{kV}, \qquad \tau = 20\,\mu s$$

are utilized as the numerical examples. For comparison, the corresponding experimental waveforms by Fujitaka and Aso are also shown in the right side of the same figure. It will be seen that the attenuation of the crest and the distortion of the waveform by computation are in good agreement with the experimental ones. Therefore, we can see that the value of the corona loss constants σ_c and σ_q which have been estimated in the single-conductor system are adequate values.

Next Fig. 6.5 shows the voltage waveforms of the final end in the case, where the voltage

$$E_0 = 230\text{kV}, \qquad \tau = 5\,\mu s$$

is applied on one conductor and the other one floats at the sending end, and the two conductors are matched with surge impedance matrix, and they are open-circuited at the final end. It will

be seen that the computed results of the waveforms on the applied conductor show the same tendency as the experimental result. But it is thought unavoidable that the computed waveforms on the other conductor is somewhat different from the experimental ones in the rising portion, since the skin effect is neglected in computation.

Lastly, in Fig. 6.6 the waveforms of the final end voltages are plotted in the case, where the following voltages

$$E_0 = \pm 240\text{kV}, \qquad \tau = 5\ \mu s,$$

$$E_0 = \pm 115\text{kV}, \qquad \tau = 5\ \mu s$$

are applied to both conductors, which are bound at the sending end and grounded through the matching circuit at the final end. From figures we can see that the calculated waveforms differs quantitatively a little from the experimental ones, because the latters are considerably distorted by the skin effect, which apears more strongly when the impulse is applied to both conductors simultaneously than when it is done to only one conductor.

Moreover, from another view of Fig. 6.2 or Fig. 6.3, we can see that the open-circuited end voltages rise till almost twice of the matching end voltages of the sharp wave front below the corona voltage, however the former voltages exceeding the corona one are more distorted and attenuated than the latter ones, since in the former case the corona loss on the conductor

increases, as the same polality reflection wave is put upon the incoming wave.

Next, Fig. 6.4 shows the calculated and experimental data in the case when the conductor is grounded through the resistance, which is about 2/5 of the line surge impedance, at the final end. From this figure, it is made sure that the end voltage exceed the one, which is calculated with respect to $2R/(3+R)$, in contrast with the above examples, as the corona loss along conductor decreases because the inverse polality reflection wave is superposed upon the incoming wave.

Table 6.1 Values of main quantities availed in computation.

Line length	$\ell = 2067\ m$
Hight of conductors	$h = 3.1\ m$
Radius of conductors	$r = 1.15 \times 10^{-3}\ m$
Length of subdivisions	$\Delta x = 25.8\ m$
Time interval	$\Delta t = 0.025\ \mu s$
Self-surge impedance of line	$z = 516\ \Omega$
Mutual-surge impedance of line	$z' = 107\ \Omega$
Self-inductance of conductor	$L_{11} = L_{22} = 1.72\ \mu H$
Mutual-inductance of conductor	$L_{12} = L_{21} = 0.356\ \mu H$
Self-capacitance of conductor	$C_{11} = C_{22} = 6.72\ \mu\mu F$
Mutual-capacitance of conductor	$C_{12} = C_{21} = -1.40\ \mu\mu F$
Number of equivalent circuit elements	$n = 80$

Table 6.2 Optimum values of σ_c and σ_G for positive and negative surges.

Wave tail time constants τ	Positive surge		Negative surge	
	σ_c	σ_G	σ_c	σ_G
5 μs	32	20×10^6	15	20×10^6
20 μs	32	16×10^6	15	16×10^6
80 μs	32	30×10^6	15	30×10^6

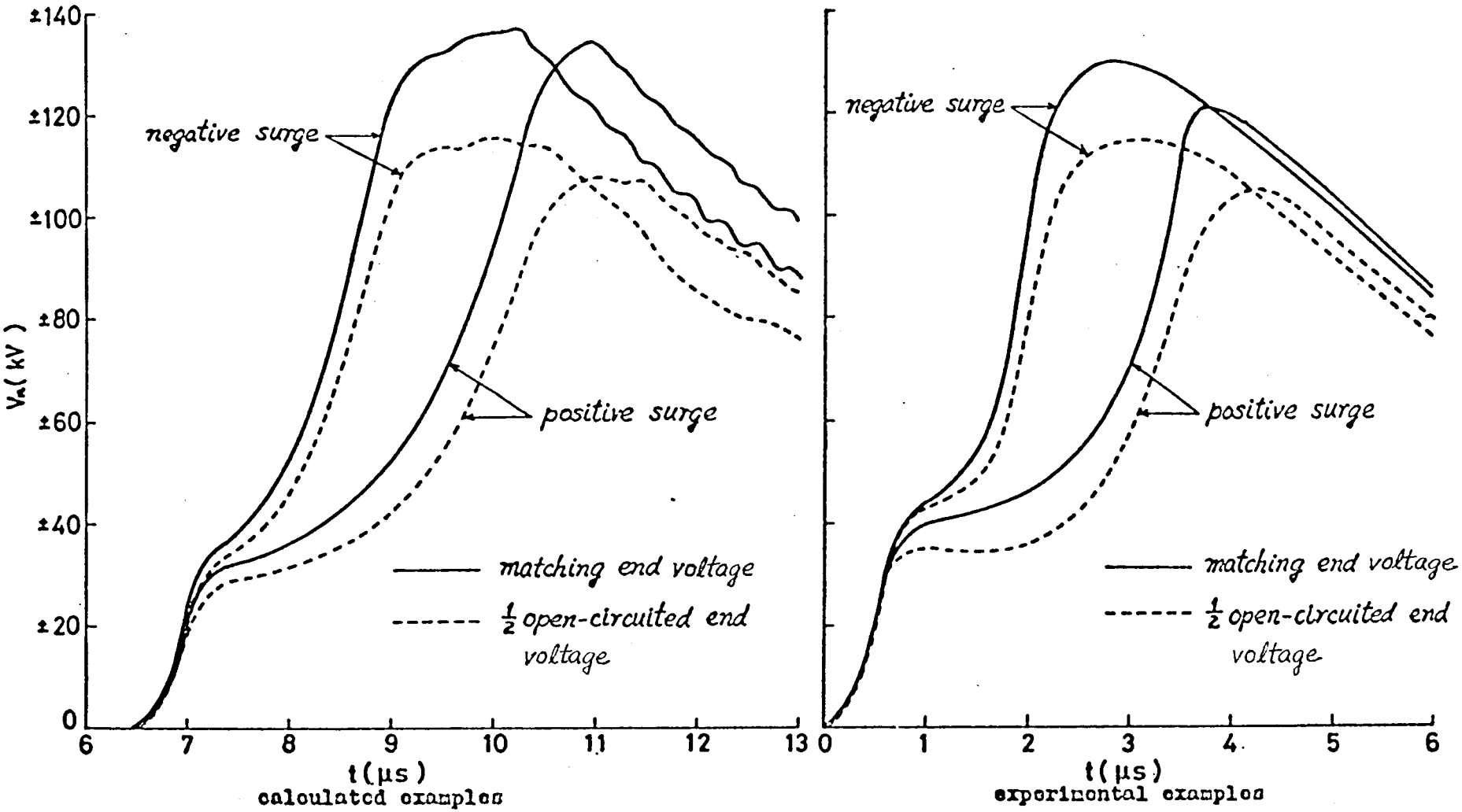

Fig. 6.2 Final end voltage waveforms when the impulse voltage ($E_0 = \pm 230$ kV, $\tau = 5\mu s$) is applied to one conductor and the other one is grounded at the multiple points.

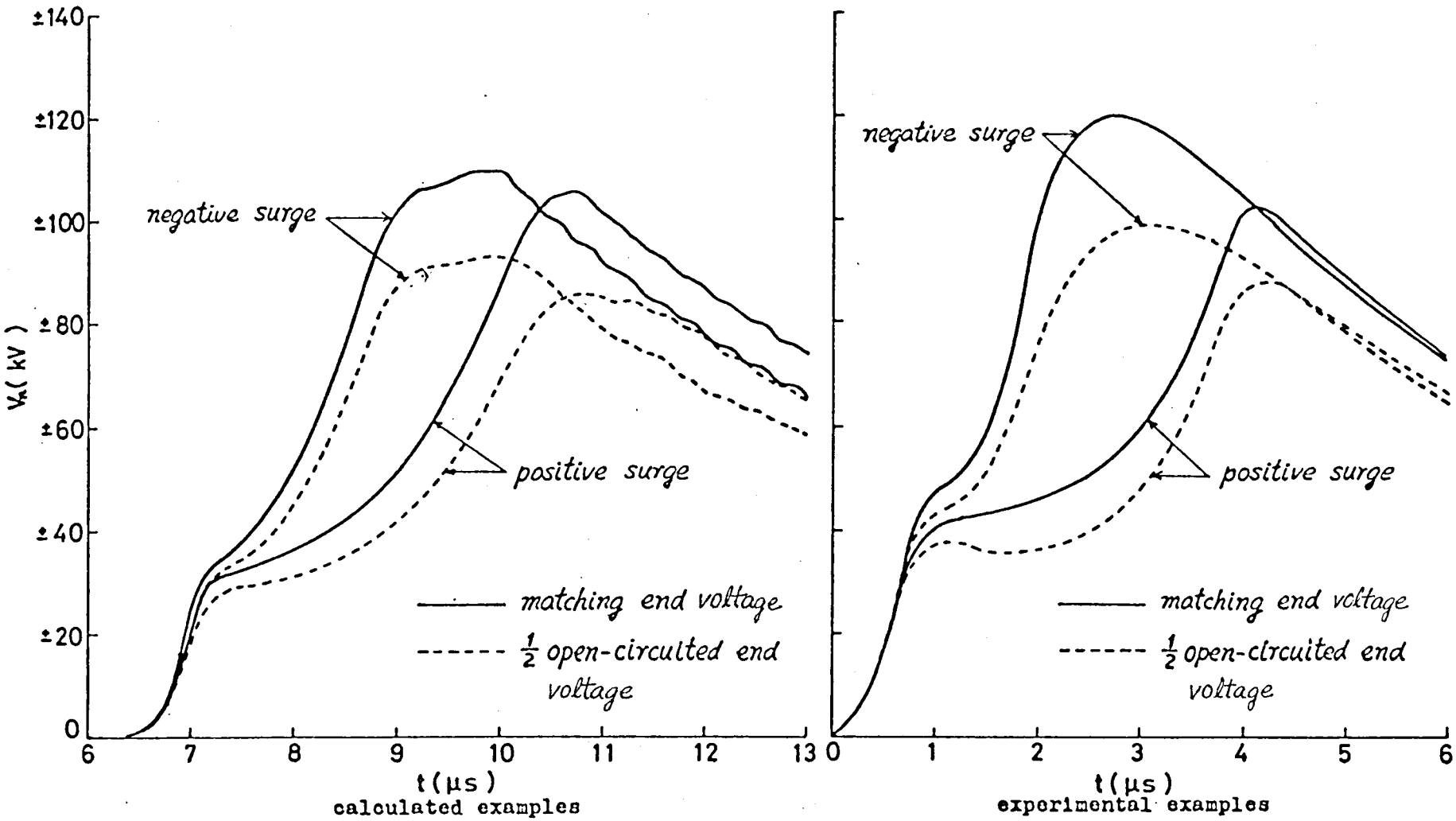

Fig. 6.3 Final end voltage waveforms when the impulse voltage (E_0=±180 kV, τ=5μs) is applied to one conductor and the other one is grounded at the multiple points.

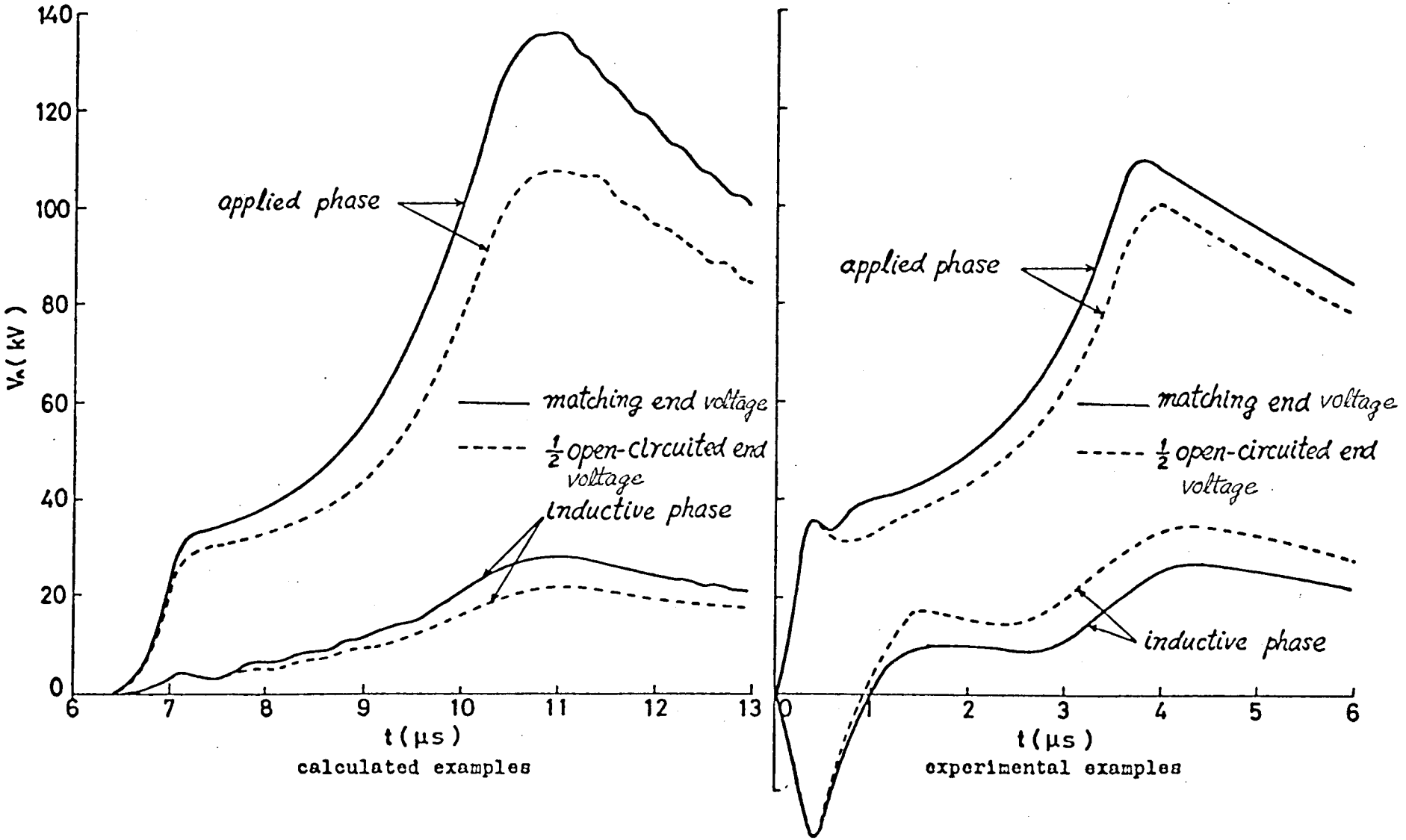

Fig. 6.5 Final end voltage waveforms when the impulse voltage (E_0=230 kV, τ=5μs) is applied to one conductor and the other one is floated.

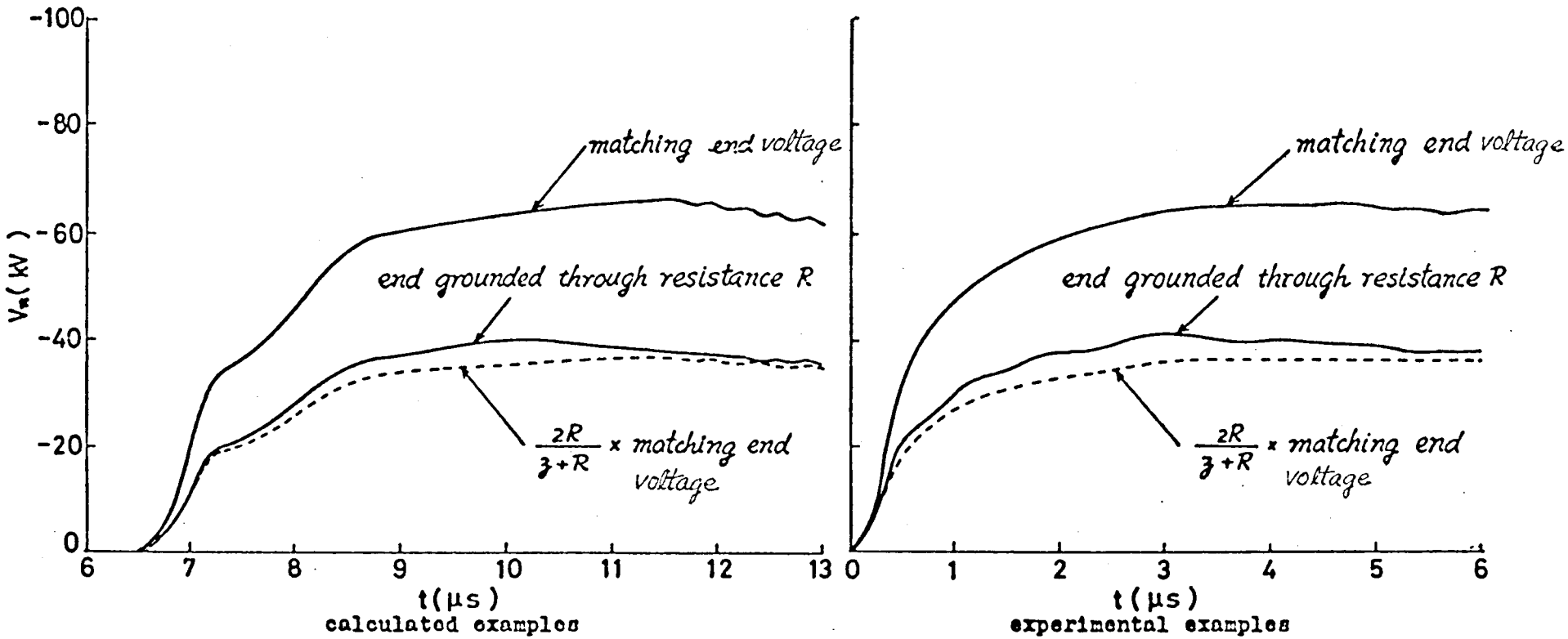

Fig. 6.4 Final end voltage waveforms when the impulse voltage (E_0=-80kV, τ=5μs) is applied to one conductor and the other one is grounded at the multiple points.

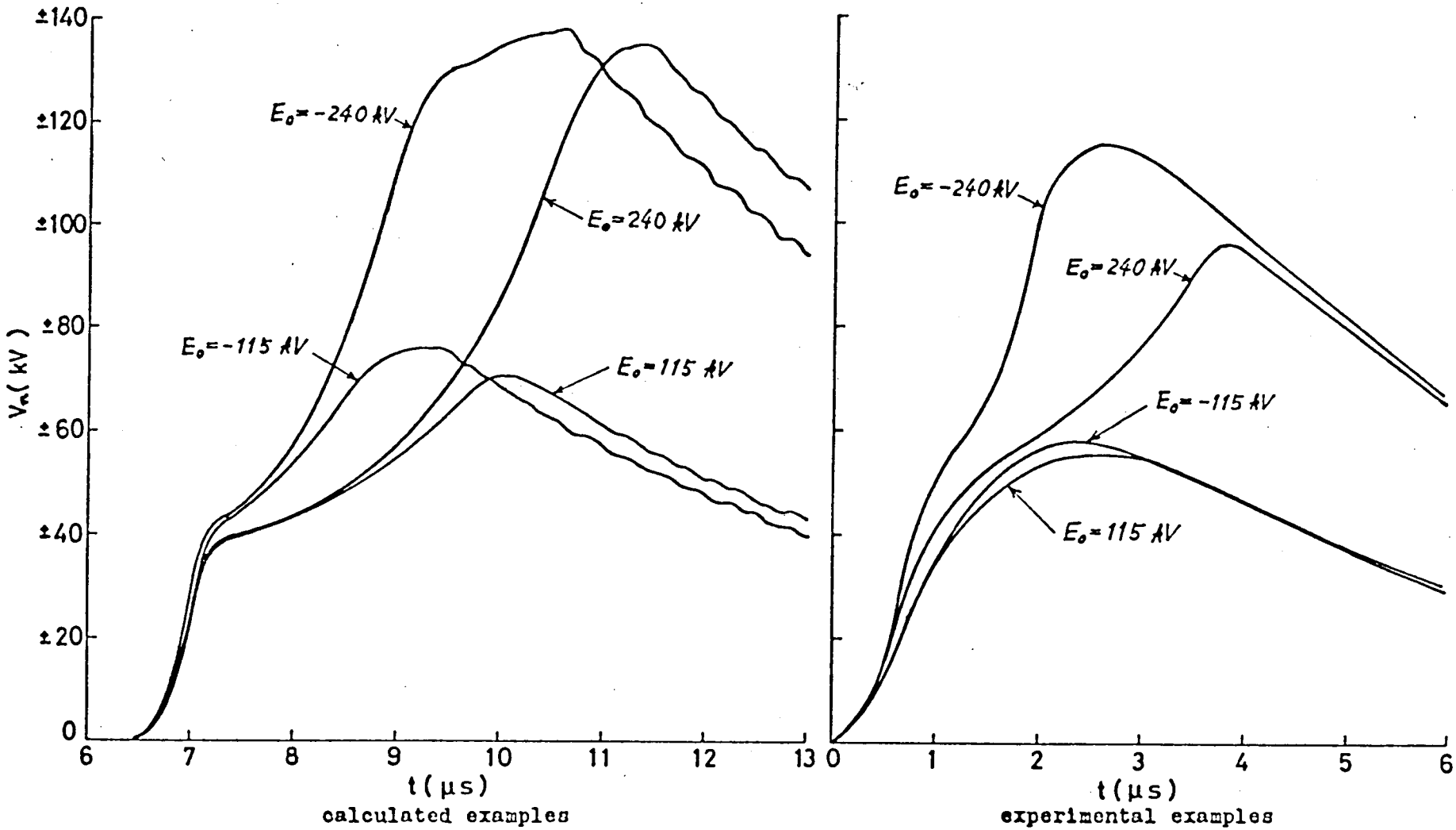

Fig. 6.6 Final end voltage waveforms when the impulse voltages ($E_0 = \pm 240$ kV, ± 115 kV, $\tau = 5\mu s$) are applied to both conductors simultaneously.

CHAPTER 7

SUMMARY

At the conclusion of the report, the author summarizes the main results of his studies, which he has described in Chapters 1 to 6, in the following.

Chapter 1. Numerical Analysis of Surges on Transmission Systems of Overhead Line-Cable Considering the Distortion Due to Skin Effect:

1. In the case considering the wave front distortion by the skin effect of the line and the cable conductors and the ground return, the theoretical exact solutions of the traveling waves on the transmission systems of overhead line-cable have been obtained by using the convolution integral and the numerical calculation of the solutions has been introduced.

2. As the model of the transmission system of overhead line-submarine cable, the author has picked out the 22kV Tonosho Transmission Line of the Chyugoku Electric Power

Company, and using the above-mentioned calculating method, he has analyzed the cable abnormal voltages in the case, where it is assumed that the lightning strikes at the tower near the junction point of overhead line and cable and then immediately the single- or three-phase back flashover along the insulator chain occurs. Namely he has evaluated the transient voltage rises of the both ends of the rubber and paper insulated cable in both cases that the skin effect is considered and not considered. Then he has discussed the influences of skin effect, line length and cable length on the transient voltage rises of the rubber and paper insulated cable ends. Moreover he has ascertained the possibility of the occurrence of the insulation breakdown fault, which had been occurred in the above-mentioned cable.

3. The same digital calculating method as Item 1 has been introduced for the case that the equivalent circuit of the tower considering tower impedance and the tower foot impedance with counterpoise is used, and after the calculation for the same case as Item 2, the transient voltage rises of the cable have been evaluated. From the calculated results, it has been made clear that the influences of the total tower impedance and especially the tower foot impedance with counterpoise on the surge performances are considerably remarkable, and accordingly that not the stationaly grounding resistance but the circuit considering tower and tower foot impedance should be used as the equivalent circuit of the tower.

Chapter 2. Numerical Calculation of Surges in Electric Power Networks Utilizing Convolution Integral:

4. The author has introduced a new digital analysis of the surge problems in power networks with no -loss lines, which utilizes the computation principle of the low speed electronic surge analyzer. Hitherto the digital analysis of the traveling waves in the networks, which have many transition points containing the lumped inductance and capacitance, has been very difficult. However it has been made possible that we can easily calculate the refracted and reflected voltages at the transition points by using the above-mentioned analyzing method and accordingly the transient voltages, at the *specified* points in the network, approximately but with high accuracy.

5. From the above-mentioned calculation for no -loss line the author has derived the computing method for the cases, where the surge distortion due to skin effect is considered, the circuit composition changes in progress of transient phenomena and the nonlinear element as a lightning arrester is connected at the transition point.

Chapter 3. Application of Numerical Calculation Derived in Chapter 2 to Surge Performance in Various Electric Power Networks

6. In this chapter the author has applied the method, which had been introduced in Chapter 2, to the analysis of the surge performances on the four examples of the practical systems. As the first example, he has analyzed the surges on a overhead distribution system having the distributed pole transformers. From the calculated results,it has been ascertained that the initial slopes of the primary terminal voltage wave forms, in the case where the value of equivalent capacitance of the transformer is small, are sharper than the ones in the case where it is large,and the final values of the primary terminal voltages in the former case are higher than the ones in the latter case,and on the contrary the value of the grounding resistance of the transformer has not so much influences on the primary terminal voltages.

7. As the second example, the surge performances on the transmission systems due to lightning stroke on overhead ground wire have been analyzed. Then the author has clarified that the larger the tower foot impedance with counterpoise becomes, the longer the wave front duration of lightning stroke current becomes or the shorter the span length becomes, the larger the possibility of back flashover at the 1st tower becomes. And in the case of the opposite tendency to the above-mentioned, it is supposed that when the back flashover may occur at the lightning stroke point, it will not occur at the tower, too. In providing the counterpoise to decrease the grounding resistance of tower foot for the purpose of preventing the back flashover

along the insulator chain at the tower, it is necessary to reduce the values of the equivalent transient impedance of tower foot as well as the values of the stationary grounding resistance, since the value of the transient impedance has the great influences on the tower voltage rise.

8. As the third example, the author has treated again the surge performances on the overhead line-cable system, which has been discussed in Chapter 1, by the new calculation presented in Chapter 2. And by comparing the results calculated by the new calculation with the one by the accurate solutions which have been got in Chapter 1, he has shown that the method has high accuracy and needs only a little computation time. Moreover he has shown that the calculation can be applied to the case where the surge distortion due to the skin effect is considered.

9. As the fourth example, the performances of traveling waves have been pursued when one tower in the overhead line-cable system, with whose junction point a lightning arrester is fitted up, had been struck by lightning. Then the author has indicated that the new calculation can be applied to the case where the nonlinear element as an arrester is connected at the transition point and also to the case where the circuit composition changes in progress of transient phenomena as the one where the back flashover along the insulator chain at the tower occurs. Moreover he has calculated the values of the junction

point transient voltage in both cases where the arrester is set up and is not set up.

Chapter 4. Numerical Analysis of Line Equations Considering Corona Loss on Single-Conductor Systems (I) —— Methods 1 and 2

10. First the author has separated the two sets of the fundamental nonlinear line equations into the three sets of the piecewise linearized simultaneous partial differential equations. Then he has introduced one analyzing method of the approximate linear equations (Method 1), by which the coefficients giving the relations between the voltages and currents at each point on the line and at each instant are numerically calculated backwards from the ones at the final end so as to satisfy the terminal condition,and then the values of the voltages and currents are computed progressively from the ones of sending end.

11. Next the author has introduced another simpler method (Method 2) than Method 1, by which from start the values of voltages and currents can be calculated progressively from the ones of the sending end so as to satisfy the terminal condition at the final end.

12. The various practical computations using Methods 1 and 2 have been carried out by digital computer, and the computed results have been compared with the experimental results,

which had been obtained by Aso and Fujitaka. From the comparison, the optimum values of corona loss constants σ_c and σ_q have been selected for the positive and negative surges. Using these values the author has calculated the transient voltages at the final end and shown that they agree with the experimental ones fairly well.

13. The author has compared the Method 1, Method 2 and the analyzing method by the surge analyzer considering corona loss which had been developed in the author's laboratory, and he has explained the merits and demerits of these methods.

Chapter 5. Numerical Analysis of Line Equations Considering Corona Loss on Single-Conductor Systems (II) —— Method 3

14. In this chapter, a numerical calculation (Method 3) is presented, by which we can solve the nonlinear line equations without piecewise linearization in contrast with the linear approximation approach in Chapter 4, and this method is an improvement of Method 2.

15. Using Method 3 the author has investigated the influences of the values of corona loss constants σ_c and σ_q on the surge performances and then he has estimated these values, which had been already estimated in Chapter 4, over again. And the following points are clarified.

(1) It is appropriate to apply Peek's quadratic characteristic

equation originally developed for ac corona loss to the evaluation of corona loss for impulsive voltages.

(2) The computed wave forms can be made closest to the experimental wave forms if both the increase in the distributed capacitance and the distributed leakage loss are included for the evaluation of impulsive corona loss.

(3) The proposed method can be used quite successfully for the estimation of the corona loss constants for both positive and negative waves.

16. The author has compared Methods 1 and 2 in Chapter 4 with Method 3 in Chapter 5, and he has shown that the calculated results by Method 3 agree best with the experimental results among the three ones by Methods 1, 2 and 3 with respect to the distortion of the wave forms and the attenuation of the crest.

Chapter 6. Numerical Analysis of Line Equations Considering Corona Loss on Two-Conductor Systems

18. The author has applied the numerical calculation of the line equations for the single-conductor system, which has been introduced in Chapter 5, to the ones for the two-conductor systems as one example of the multi-conductor systems.

19. The transient voltages at the final end have been calculated by the digital computer with the aid of values of

the corona loss constants α_c and α_z, which had been obtained in Chapter 5 for single-conductor systems. Next he has compared the computed results with the experimental ones for the cases of the three sending end conditions, namely the ones where the impulsive voltage had been impressed on one conductor and the other one had been grounded, the voltage had been applied to one conductor and the other one had floated, and the voltage had impressed to both conductors simultaneously, and the three final end conditions, namely the lines had been open, matched and grounded through the resistance R_L. By comparison it has been ascertained that the computed results of the attenuation of the peak values and distortion of the wave forms are in good agreement with the experimental ones.

20. The calculating expressions of the corona critical voltages in the above-mentioned three conditions have been introduced.

REFERENCES

1. Y. Yamamura and S. Oka: "Distribution of Surge Voltage in the Substations and the New Surge Analogue Computer," J.I.E.E.J., Vol. 78, pp. 206-212, February 1958.
2. H. Kitukawa: "Experimental Investigation of Lightning Protection Design for Power System Connected to Overhead Line through Cables," J.I.E.E.J., Vol. 82, pp. 1353-1362, August 1962.
3. H. Ishihara: "Surge Calculation of Non-linear Circuit by Analog-Computer," J.I.E.E.J., Vol. 86, pp. 264-270, February 1966.
4. H. Ishihara: Research Materials, Kansai Electric Power Co. Technical Research Institute, No. 40, 1006, July 1966.
5. J. Umoto and T. Hara: "Digital Analysis of Surges on Transmission Systems of Overhead Line-Cable Considering Skin Effect," J.I.E.E.J., May 1971.
6. H. Shinozaki: Technical Report, Chyugoku Electric Power Co. Technical Research Institute, No. 29, 1967.
7. J. Umoto and T. Hara: Joint Convention Records of Four Elec. Insts. of Japan, No. 1175, March 1969.
8. J. Umoto and T. Hara: Joint Convention Records of Four

Elec. Insts. of Japan, No. 1176, March 1969.

9. S. Hayashi and J. Umoto: "Surges on Transmission Systems Due to Lightning Stroke on Overhead Ground Wire," J.I.E.E.J., Vol. 84, pp. 1114-1122, July 1964.

10. J. Umoto, T. Hara and K. Fukumori: Convention Records of Kansai Branch of I.E.E.J., G4-8, October 1969.

11. S. Hayashi: "Surges on Transmission Systems," Denki-Shoin, Inc., Kyoto, Japan 1955.

12. L.V. Bewley: "Traveling Waves on Transmission Systems," John Wiley and Sons, Inc., New York, 1951.

13. M. Kido: "Traveling Waves on Transmission Systems with the Ground Wire," J.I.E.E.J., Vol. 80, pp. 1431-1438, October 1960.

14. J. Umoto, H. Yamada and S. Hayashi: "Time Delay Devices for Low-Speed Electronic Surge Analyser," Memoirs of the Faculty of Engineering, Kyoto University, Vol. 29, Part 4, pp. 420-431, October 1967.

15. H. Ishihara: "Surge Calculation Method used Block Diagrams and Z Transform," J.I.E.E.J., Vol. 86, pp. 85-92, January 1966.

16. H. Kimura, E. Yamada and H. Iwasaki: "Analysis of Traveling Waves in Electric Power Network. Applied Wave Form at Impulse Voltage Testing of Transformers," Corona, Inc., Japan, 1963.

17. J. Baba and T. Shibataki: "An Approximate Calculation Method of Transient Phenomena in Power Systems," J.I.E.E.J., Vol. 81, pp. 587-594, April 1961.

18. J. Umoto and T. Hara: "A New Digital Analysis of Surge Performances in Electric Power Networks Utilizing Convolution Integral," J.I.E.E.J., March 1971.

19. J. Umoto and T. Hara: Joint Convention Records of Four Elec. Insts. of Japan, No. 1097, April 1970.

20. J. Umoto and T. Hara: Convention Records of Kansai Branch of I.E.E.J., G4-39, November 1970.

21. J. Umoto, T. Hara and K. Fukumori: Convention Records of Kansai Branch of I.E.E.J., G4-40, November 1970.

22. H. Kinoshita: Technical Report, Kansai Electric Power Co. Technical Research Institute, No. 2, 1957.

23. C.F. Wagner: "A New Approach to the Calculation of the Lightning Performance of Transmission Lines," Trans. A.I.E.E., Vol. 75, pp. 1233-1256, December 1956.

24. Y. Ichihara: "Prevention of Abnormal Voltage and Insulating Co-Operation in Power Station," Electrical Review, Vol. 37, pp. 1306-1311, November, 1970.

25. J.Tomiyama: Paper Reported in Journal of Technical Laboratory of Central Research Institute of Electric Power Industry, No. 64019, 1964.

26. J.A. Giaro: "Critical Overvoltages at the Terminals of a Cable Connected to an Overhead Line Struck by Lightning," C.I.G.R.E., Report, Vol. 3, No. 312, 1958.

27. J. Umoto: Doctoral Thesis

28. A. Tanaka: Technical Report, Kansai Electric Power Co. Technical Research Institute, No. 16, pp. 123-133, 1964.

29. Y. Okamura: Convention Records of Kansai Branch of

I.E.E.J., No. 7-2, November 1966.

30. S. Hayashi, B. Kondo and A. Kishima: Joint Convention Records of Three Elec. Insts. of Japan, No. 385, 1956.

31. H.H. Skilling and P.K. Dykes: "Distortion of Traveling Waves by Corona," Trans. A.I.E.E., Vol. 56, pp. 850-857, 1937.

32. E.D. Sunde: "Earth Conduction Effects in Transmission Systems," D. Van Nostrand Co., INC., New York, 1949.

33. C.F. Wagner: "A New Approach to the Calculation of the Lightning Performance of Transmission Lines," Trans. A.I.E.E., Vol. 75, pp. 1233-1256, December 1956.

34. S. Hayashi: Joint Convention Records of Four Elec. Insts. of Japan, No. 424, 1957.

35. S. Hayashi: Joint Convention Records of Four Elec. Insts. of Japan, No. 565, 1958.

36. S. Hayashi and J. Umoto: Convention Records of Kansai Branch of I.E.E.J., No. 98, 1958.

37. S. Hayashi, J. Umoto and E. Nakamura: Convention Records of Kansai Branch of I.E.E.J., No. 9-9, 1964.

38. S. Hayashi, J. Umoto and E. Nakamura: "Surge Analyser to Analyse Attenuation and Distortion of Surges on Single-Conductor Systems Caused by Corona Loss," J.I.E.E.J., Vol. 86, pp. 108-114, January 1966.

39. T. Aso and S. Fujitaka: "On the Corona Distortion of High-Voltage Surges in Power Transmission Lines," J.I.E.E.J., Vol. 74, pp. 1211-1217, October 1954.

40. S. Hayashi, J. Umoto and E. Nakamura: "A Numerical

Analysis of Line Equations Considering Corona Loss on a Single-Conductor Systems and Its Application," Memoirs of the Faculty of Engineering, Kyoto University, Vol. 28, Part 2, pp. 183-197, April 1966.

41. J. Umoto and T. Hara: Joint Convention Records of Four Elec. Insts. of Japan, No. 951, May 1968.

42. J. Umoto and T. Hara: "A Numerical Analysis of Line Equations Considering Corona Loss on Single-Conductor System," Memoirs of the Faculty of Engineering, Kyoto University, Vol. 30, Part 2, pp. 153-164, April 1968.

43. J. Umoto and T. Hara: Convention Records of Kansai Branch of I.E.E.J., 1A-2, November 1968.

44. J. Umoto and T. Hara: "Numerical Analysis of Line Equations Considering Corona Loss on Single-Conductor System," J.I.E.E.J., Vol. 89, pp. 909-916, May 1969.

45. J. Umoto and T. Hara: Convention Records of Four Elec. Insts. of Japan, G4-9, October 1969.

46. J. Umoto and T. Hara: "A New Numerical Analysis of Line Equations Considering Corona Loss on Two-Conductor System," Memoirs of the Faculty of Engineering, Kyoto University, Vol. 32, Part 2, pp. 143-155, April 1970.